Alterations in Myofilament Properties in a Rabbit Coronary Artery Ligation Model of Left Ventricular Dysfunction

A thesis presented for the degree of

Doctor of Philosophy

by

Gayle Wilson

Neuroscience and Biomedical Systems
Institute of Biomedical and Life Sciences
University of Glasgow

June 1998

"The outcome of any serious research can only be to make two questions grow where only one grew before"

-Thorstein Veblen, 1857-1929, *The Place of Science in Modern Civilization.*

Acknowledgements

There are many people whom I would like to thank for their help throughout the duration of my PhD and writing of this thesis:

I would like to thank my supervisor, Dr. David Miller, for his support and guidance throughout my time in his lab.

Dr. Niall MacFarlane for providing (doughnuts!) assistance and supervision when the boss wasn't available and his patience in teaching me surgical techniques.

The Medical Research Council for awarding the necessary funding for this study.

The staff of the Medical Cardiology Unit at the Royal Infirmary for their surgical expertise, without which there would be no rabbit model to work with.

Fellow labmates and technicians (both new and old! - and too many to mention in full) for their help and friendship over the last few years.

My flatmates Dave, Andy and Liz for the fun, friendship and trials of writing-up that we have shared over the last few years. Life in Woodlands Drive was certainly (never sober) entertaining - except for despot and the cockroaches!.

A special thanks goes to Gavin for his unending patience, encouragement and amusing distractions! It takes a braver person than I to choose to live with someone who is writing-up! I would also like to thank him for handing out very much needed cash subs during my financially distraught writing-up period.

Finally, my parents for their continued support throughout my PhD (and indeed throughout my university career - not least for keeping me out of trouble with the bank manager!), without their help and encouragement I would not have made it this far.

Contents

Chapter 2 - Methods

List of Figures

List of Tables

Declaration

The work reported in this thesis is my own and original work, except where otherwise stated and has not been submitted for any other degree.

List of Publications

MACFARLANE, N.G., MILLER, D.J., OKABE, E., TAKAHASHI, S. & WILSON, G. Effects of Reactive Oxygen Species on Myofilament Function in a Rabbit Coronary Artery Ligation Model of Heart Failure. (submitted for publication)

WILSON, G., MACFARLANE, N.G. & MILLER, D.J. (1997) Oscillatory work absorbed by chemically skinned ventricular trabeculae is reduced in a coronary artery ligation model of left ventricular dysfunction in the rabbit. *Journal of Physiology,* **501**, P138-139.

WILSON, G., MACFARLANE, N.G. & MILLER, D.J. (1996) Sinusoidal analysis of muscle mechanics in failing myocardium. *Journal of Molecular and Cellular Cardiology*, **28**, A228.

MACFARLANE, N.G., WILSON, G. & MILLER, D.J. (1996) The response of failed myocardium to reactive oxygen species differs from that of normal myocardium. *Journal of Molecular and Cellular Cardiology*, **28**, A229.

MACFARLANE, N.G., WILSON, G., DENVIR, M. & MILLER, D.J. (1996) Altered response of failed myocardium to reactive oxygen species. *Circulation*, **94**, P710 (4151).

MACFARLANE, N.G., WILSON, G. & MILLER, D.J. (1995) Altered rabbit myocardial crossbridge kinetics by oxidative species during maximal Ca-activation in isolated trabeculae. *Journal of Physiology*, **489**, P144.

WILSON, G., MACFARLANE, N.G. & MILLER, D.J. (1997) Reduced oscillatory work in chemically skinned ventricular trabeculae from a coronary artery ligation model of left ventricular dysfunction in the rabbit. (published at Heart Failure '97, Cologne, 1997)

Abbreviations

ADP	Adenosine diphosphate
ATP	Adenosine triphosphate
AV	Atrioventricular
$[Ca^{2+}]_i$	Intracellular calcium concentration
CHF	Congestive heart failure
CICR	Calcium-induced calcium release
CK	Creatine kinase
C_{max}	Maximum calcium-activated tension
CrP	Creatine phosphate
DIC	Differential interference contrast
EGTA	Ethyleneglycol bis(β-aminoethyl ether) N,N,N',N' tetraacetic acid
f_{min}	Frequency of minimum stiffness
H_2O_2	Hydrogen peroxide
HDTA	Hexamethylene N,N,N',N' -diamine tetraacetic acid.
HMM	Heavy meromyosin
HOCl	Hypochlorous acid
LMM	Light meromyosin
LV	Left ventricle
LVD	Left ventricular dysfunction
MLC_1	Myosin light chain 1 (essential / alkali light chain)
MLC_2	Myosin light chain 2 (regulatory /phosphorylatable light chain)
NZW	New Zealand White
O_2^-	Superoxide
OCl^-	Hypochlorite anion
P_i	Inorganic phosphate

ROS..... Reactive oxygen species

RV..... Right ventricle

S1..... Myosin subfragment 1

S2..... Myosin subfragment 2

SL..... Sarcomere length

SR..... Sarcoplasmic reticulum

TnC..... Ca^{2+}-binding troponin subunit

TnT..... Tropomyosin-binding troponin subunit

TnI..... Inhibitory troponin subunit

Tm..... Tropomyosin

XB..... Crossbridge

Symbols

ϕ..... Phase shift value.

Summary

The work reported in this thesis examines alterations in the properties of the myofilaments in a rabbit coronary artery ligation model of heart failure. Heart failure is characterised by abnormalities of myocardial systolic and diastolic function. While much research in this field focuses on alterations in Ca^{2+} handling by the sarcoplasmic reticulum, fewer studies have purely examined alterations in the properties of the myofilaments, particularly so in this model of heart failure. This particular model has clinical relevance in that it produces a well defined region of infarcted tissue which induces ventricular remodelling in a similar way to that seen after infarction in the human.

Treatment of ventricular trabeculae with the non-ionic detergent Triton X-100, results in the complete disruption of surface and intracellular membrane diffusion barriers, but leaves the myofilaments functionally intact. After this chemical 'skinning', the bathing solution essentially becomes an extension of the intracellular environment. Therefore, chemical interventions that produce an alteration in the mechanical activity of the preparation can be directly attributed to an effect on the myofilaments. The technique of applying small sinusoidal length changes to chemically-skinned trabeculae is ideal for examining both resting and dynamic properties of the myocardium as it allows both mechanical and chemical perturbations to be applied and studied simultaneously.

Chapter 3 reports upon the alterations in the contractile activity of the myofilaments found in this model of heart failure using the technique of sinusoidal analysis. The results presented show that there is a significant decrease in the intrinsic cycling rate of the crossbridges (as indicated by a reduction in f_{min}, the frequency at which dynamic stiffness is lowest), without a decrease in maximal force generation or Ca^{2+}-sensitivity of the muscle.

Chapter 4 reports the alterations in the maximal work and power generating capacity of the myocardium found to be associated with heart failure using the

sinusoidal analysis method. One of the advantages of using this technique to assess these parameters, is that it also allows the negative (absorptive) work and power generating capacity of the crossbridges to be examined. Other traditionally used techniques such as the 'slack' test, which examines unloaded shortening conditions, do not provide any information about the work required to be put into the system, termed 'negative' work, for re-lengthening of the muscle. The results presented show that the maximal positive work and power generating capacity of the myocardium are significantly reduced in this model of failure. There is also a small reduction in the amount of (negative) work and power that is absorbed by the muscle, and is therefore potentially available for useful work.

Chapter 5 reports the alterations in the relaxation properties of the myocardium in this model of heart failure using an 'EGTA'-jump protocol. This technique employed accelerating the speed of relaxation of chemically-skinned trabeculae by increasing the applied [EGTA] gradient in an attempt to reach the point where the rate of change of $[Ca^{2+}]$ around the myofilaments was no longer rate limiting. Beyond this point, it could be assumed that any difference in the maximal rate of relaxation associated with heart failure could be attributed to alterations in the mechanical properties of the myofilaments then governing relaxation. The results presented show that the maximal rate of relaxation is significantly reduced in the ligated animals when compared with controls. The relaxation transients were closely fitted with a single exponential function. It was concluded that diffusion difference alone could not account for the slower relaxation seen in preparations from ligated animals.

Chapter 6 investigates the effects of the hypochlorite anion, a reactive oxygen species, on the mechanical functioning of the myocardium. The reason for investigating the effects of this compound is that increased oxidative stress is one detrimental factor to which the myocardium is subjected during the progression of heart failure. The oxidative stress results from an increase in the production of oxygen-derived free radicals and reactive oxygen species and/or a decrease in the

antioxidant capacity of the myocardium. All the parameters mentioned so far were re-examined in tissues acutely exposed to the hypochlorite anion. The results show that exposure to the hypochlorite anion significantly reduced maximum Ca^{2+}-activated force, f_{min}, positive and negative work/power generation and the relaxation rate of both sham and ligated trabeculae, whereas myocardial resting and dynamic stiffness was increased. The contractile proteins of the sham animals demonstrated an increased susceptibility to oxidant damage for all of these parameters just described. The relationship between the frequency of maximum positive and negative work/power generation and fmin was unchanged after hypochlorite anion exposure, though the frequencies at which all of these parameters were observed occurred at a lower frequency than pre-exposure. On examination of the results presented in Chapter 6 for the control animals, with the exception of a decrease in maximal force generation, the alterations in mechanical functioning that occur after free radical exposure closely resemble the changes seen in the mechanical functioning between sham and ligated animals described in the three preceding results chapters. The results presented in this chapter are consistent with the idea that pre-exposure to this reactive oxygen species has occurred in the intact myocardium *in vivo* in the ligated animals used in this study.

Chapter 1

Introduction

1.1 Heart Failure

1.1.1 A brief introduction

The first case of heart failure to be recorded was diagnosed several centuries ago and led to the death of Alexius I, ruler of the Byzantine empire (Lutz, 1988). Throughout the centuries, the diagnosis of the disease increased and several accounts of early treatment have been published. Today, cardiovascular disease remains one of the major causes of mortality in Western society. Indeed, the incidence of heart disease in developed countries has risen dramatically in recent years, for example, there had been a 60% increase in hospital admissions in Scotland for congestive heart failure over the period between 1980-1990 (McMurray *et al,* 1993), and also in the USA, where the number of hospital admissions for heart failure has risen steadily over the last two decades (Ghali *et al,* 1990; Gillum, 1993). Thus, heart failure is a continually growing problem, both medically and financially. In Europe alone, it is estimated that approximately 1% of national health care budgets is spent on individuals with heart failure (Eriksson, 1995; McMurray *et al,* 1993). The incidence and prevalence of heart failure increasing substantially with age, together with the increased life expectancy of the population has mainly accounted for the increasing medical problem. Additionally, surgical and medical interventions improving the prognosis of patients with heart failure as well as prompt therapy increasing post-myocardial infarction survival have increased the financial burden.

1.2 Pathophysiology of Heart Failure

Heart failure is a disease that concerns not only the heart, but also the response of the rest of the body to its impaired function. Indeed, in the past, definitions of heart failure have failed to reflect the complexity of the disease, ignoring the widespread

physiological changes that occur in virtually all of the other major organs of the body, with the exception of the brain. Recently, Poole-Wilson (1985) provides a more comprehensive definition of the disease, taking into account these widespread physiological alterations: " *A clinical syndrome caused by an abnormality of the heart and recognised by a characteristic pattern of haemodynamic, renal, neural and hormonal responses".* The 'syndrome' is commonly the end result of many different disease processes that impair cardiac function (Katz, 1990). In Western society, these main disease processes tend to be coronary heart disease and hypertension, often together. Patients with heart failure tend to have a normal cardiac output at rest, however, this fails to increase with exercise or stress such that vasoconstriction must occur to maintain systemic blood pressure. Hence the involvement of other physiological systems within the body that are required to compensate the heart's inability to meet its demands, such as the sympathetic nervous system and the renin/angiotensin system.

1.3 Morphological Alterations in the Heart During the Development of Failure

During the progression of failure, many morphological changes occur that severely compromise normal cardiac function. Clinically, the most common cause of myocyte depletion occurs as a direct result of myocardial infarction. Myocardial infarction also produces alterations in ventricular architecture such as thinning and lengthening of the infarcted portion and possibly alterations in cellular shape (Nakao *et al,* 1992). Presently, much interest lies in the process of apoptosis as an additional cause of myocyte loss in some forms of cardiac disease. Apoptosis occurs as a result of previous viral infection or toxic damage. In some models of heart failure, apoptosis has been proposed as a mechanism involved in the reduction of cardiac myocyte mass that accompanies the transition from stable compensation to heart failure (*e.g.* Bing, 1994; Li *et al,* 1997).

Cardiac hypertrophy is an adaptive response to preserve normal systolic wall stress as a result of increased workload (Pfeffer & Braunwald, 1991) *i.e.* ventricular wall tension is described by the law of LaPlace:

$$T \propto \frac{r \cdot p}{D} \tag{1.1}$$

where T is the wall tension, r is the radius of the ventricle chamber, p is the transmural pressure and D is the wall thickness. Examining this law, it is obvious that any increase in end- diastolic volume (EDV) and end-diastolic pressure (EDP), as is observed in heart failure, will have profound effects on the wall tension of the chamber and as a consequence wall stress, ultimately leading to the initiation of hypertrophy.

Cardiac hypertrophy is associated with significant changes in contractile properties. With mild to moderate hypertrophy, there is a slowing of contraction and relaxation and hence an overall prolongation of contraction duration (Cooper *et al,* 1981). As the severity of hypertrophy increases, the magnitude of these changes increases, with a concomitant reduction in the cardiac output (Spann *et al,* 1967). These alterations are responsible for the systolic and diastolic contractile defects in hypertrophy that consequently lead to congestive heart failure (Feldman *et al,* 1993). A study by Pouleur and his group on human ventricular function has shown this to be the case (Pouleur *et al,* 1993). They have shown that with time, systolic ejection fraction (EF), defined as: LVEDD-LVESD/LVEDD x 100, where LVEDD is left ventricular end-diastolic dimension and LVESD is left ventricular end-systolic dimension, decreases and the ventricle dilates producing an increase in wall tension. Initially, activation of the Frank-Starling mechanism in response to the increased dilatation of the chamber compensates for the reduced EF, maintaining it at a relatively stable level. However, with progressive dilatation, the heart is no longer able to use the Frank-Starling relationship (Schwinger *et al,* 1994) and consequently the EF begins to fall further and clinical heart failure ensues.

In addition to ventricular remodelling, cellular abnormalities in hypertrophied hearts have been reported (Morgan *et al,* 1987; Hasenfuss *et al,* 1994), which may contribute to the contractile dysfunction observed in failure. A number of different cell types exist within the myocardium, for example, cardiac myocytes, the most abundant of all the cells and a focus of much research, vascular smooth muscle cells, fibroblasts and endothelial cells. Indeed, any alterations that occur in any of these during cardiac remodelling will interfere with normal contractile function. It has already been established that alterations in the structure and function of cardiac myocytes affect cardiac contractility (Scholz *et al,* 1994; Landesberg, 1996).

Alterations in the components of the extracellular matrix have also been reported (Conrad *et al,* 1990; Weber and Brilla, 1991; Chien *et al,* 1991), as well as an increase in the expression of the genes encoding them (Boluyt *et al,* 1994). These include elastin, fibronectin, laminin, desmin and various types of collagen. Changes in the relative amounts of the different types of collagen have already been well documented. The relative proportions of type III to type I collagen are altered in the hypertrophied rat heart (Doering *et al,* 1983) and a similar alteration in the production of collagen can be produced in cultured cardiac fibroblasts exposed to mechanical stretch (Carver *et al,* 1991). Obviously, with alterations in collagen production to a less elastic form, and the increased production of other extracellular matrix components, the compliance of the ventricle will be reduced. This has consequences for both diastolic and systolic function. The ability of the heart to relax, and therefore diastolic function, is clearly compromised. In addition, the 'stiffer' extracellular matrix surrounding the cardiac myocytes reduces their ability to develop force so that systolic function is also compromised.

Myocardial infarction is usually more severe in the sub-endocardial region than in the epicardial region (Savage *et al,* 1988), creating a transmural inhomogeneity. Pathological examination of these sub-endocardial regions of infarct, has revealed that there are small areas of necrosis surrounded by viable myocardial tissue. It therefore appears that not all the myocytes within an infarcted region die

simultaneously (Reimer *et al,* 1977). Additionally, lateral displacement of myocytes, or cell 'slippage' is seen in failure (Schaper & Schaper, 1983; Weber & Brilla, 1991). Alterations in the ultrastructure of the myocardium, such as these, may produce unco-ordinated cell activation, such that the heart fails to function as a syncytium. This would therefore diminish the myocardium's ability to develop force.

The ability to alter the structure of the failing heart is not limited to biophysical factors. Several neurohormonal factors, such as angiotensin II (Lindpaintner & Ganten, 1991), are also capable of influencing myocardial structure, and hence function.

1.4 Animal Models of Heart Failure

Several different animal models, employing different species, have been developed for the study of heart failure. Heart failure may be induced experimentally by pressure loading, volume loading, myocardial infarction or by the creation of disease states within the myocardial tissue itself. Most of these models are useful in evaluating particular aspects of failure, however, no single model can satisfactorily mimic any one of the patterns of heart failure development observed in humans. The different models that have been, and still are being, used in heart failure research will briefly be described here and their value in studying various aspects of the progression of the disease.

Pressure loading has been used to produce right ventricular hypertrophy in species such as the pig (Wyse *et al,* 1983), cat (Anderson *et al,* 1977), rabbit (Sordahl *et al,* 1970), dog (Womble *et al,* 1979) and rat (Mercadier *et al,* 1981). Experimental procedures used to induce pressure overload include aortic constriction, pulmonary banding and experimental hypertension. Models using these methods have proved most useful in studying the pathogenesis of hypertrophy and subcellular failure (Smith & Nuttall, 1985).

Volume loading has been used to examine the electrolyte and hormonal disturbances which are commonly seen in human heart failure. Experimental

procedures used to induce volume loading include surgical techniques that cause aortic valve incompetence, for example in the rat (Mercadier *et al,* 1981) and in the rabbit (Carabello *et al,* 1981).

The induction of myocardial infarction in animals is probably the model most suited for assessing novel heart failure therapy, provided that peripheral reflexes are maintained (Smith & Nuttall, 1985). Coronary artery ligation is the technique employed to induce myocardial infarction, and is the technique used in this study (described in more detail in Methods, section 2.1.2).

Experimental models of cardiomyopathy are useful in studying the subcellular pathological processes associated with heart failure. Some species of animal such as the Syrian hamster are used in selective breeding programmes to produce animals that spontaneously develop heart failure (Gertz, 1973), however, this model may not be applicable to human heart failure because it appears to involve excess catecholamine activity mediated primarily through α-adrenoreceptors (Kagiya *et al,* 1991). Other programmes employed involve the administration of myocardial 'poisons' such as adriamycin (Mettler *et al,* 1977) or the rapid pacing of animals such as dogs, with the resultant development of failure.

These are only a few of the main experimental models used today. However, it is evident that the choice of model is very important to the research and should be selected on the basis of which aspects of heart failure are to be examined.

1.5 Excitation-Contraction Coupling

The body of this thesis will concentrate on the myofilaments and any alterations in their function during the development of failure. However, the picture would not be complete without providing a brief outline of the processes leading up to, and initiating their movement during contraction. The role of the regulatory proteins will be discussed in more detail later in this section.

Regulation of myofilament activation is achieved through activation of the functional units of the muscle by calcium (Ca^{2+}). Each functional unit is comprised of

actin: troponin (Tn): tropomyosin (Tm) in a 7:1:1 ratio (see sections 1.15-1.19 for more details on these proteins). In striated muscle, F-actin is arranged as two strands of monomers coiled around each other with a tropomyosin (Tm) filament lying along each of the two grooves between the strands. The physical presence of Tm prevents any interaction between the thick and thin filaments by sterically blocking the myosin binding regions on actin. This is known as the steric-hindrance model (Huxley, 1973; Parry & Squire, 1973). Tn itself is composed of three subunits: TnC, the Ca^{2+}-binding subunit; TnI, the inhibitory subunit; and TnT, the Tm-binding subunit. During diastole, the $[Ca^{2+}]_i$ is sub-threshold for activation (~0.2μM). Under these conditions, TnI binds to actin-Tm thereby inhibiting the force-generating interactions between myosin and actin.

After the arrival of an action potential triggering the onset of systole, a small amount of Ca^{2+} enters the cell via voltage-operated channels (VOCs) in the sarcolemma. This small rise in $[Ca^{2+}]_i$ is insufficient by itself to activate the myofilaments, but it does induce the release of further Ca^{2+} from the sarcoplasmic reticulum (SR) that is sufficient for activation (~1μM). This phenomenon is known as calcium-induced calcium-release (CICR) (Bianchi, 1968). Ca^{2+} ions are then able to bind to the regulatory site on TnC, inducing a conformational change which is transmitted through the thin filament protein TnI to Tm. This involves a weakening in the interaction between TnI and actin-Tm and a strengthening in the interaction between TnI and TnC. As a consequence, Tm moves into the groove of actin exposing the binding sites for the myosin heads on actin promoting the formation of force-generating crossbridges.

1.6 The Crossbridge Cycle

1.6.1 A brief history

In 1957, work by H.E. Huxley confirmed, by electron microscopy on skeletal muscle fibres, previous observations that striated muscle was indeed comprised of two sets of filaments, actin and myosin. In addition, he provided early evidence for the existence of actin-myosin cross-linkages or 'crossbridges'. He observed, in thin longitudinal strips of muscle, that these projections were observed only in the region of overlap between the two sets of filaments, the A-band, and not in the actin-only containing I-bands. This suggested that the crossbridges were in fact extensions of the myosin filament itself that projected outwards from the main axis of the thick filament to form 'bridges' between the myosin and actin filaments. Work carried out four years earlier by Szent-Gyorgyi that recognised that the actin-binding and ATPase activities of myosin resided in the HMM subfragment, led Huxley to suggest that this HMM portion could in fact correspond to the actin-myosin crossbridges he had observed.

The next major insight into the role of the crossbridges in muscle contraction was due to observations made by Reedy *et al* (1965) using X-ray diffraction and electron microscopy techniques with insect flight muscle. They studied the structure of insect flight muscle fibres while relaxed (+ATP) and during rigor-induced contractures (-ATP). They noted that while the crossbridges were permanently attached, as in rigor, they were tilted at an angle of 45°. However, when relaxed, the crossbridges were no longer observed at this angle, but were now at an angle of 90°. From this they were able to conclude that this change in orientation of the crossbridges must in some way be involved in the muscle's ability to contract. Much work in this area continued, however by 1969 the main conceptual framework behind muscle contraction had been established. Shortening did occur by the sliding of actin and myosin filaments relative to one another, with the myosin crossbridges generating

force through asynchronous cyclical interactions with actin (Huxley, 1969), often termed today as the 'power stroke'. This interaction is also known to be driven by the free energy of ATP hydrolysis and the system's ability to absorb these hydrolysis products (MgADP, phosphate [P_i] and work output) in order for the next cycle to begin.

Observations made from the equatorial reflections of X-ray diffraction experiments have shown that the time course of changes in X-ray pattern during contraction have a substantial lead over the time course of force development (Huxley, 1975). Additionally, results from quick-release experiments on isometrically contracting muscle (Huxley *et al,* 1983) have shown that when a quick-release is applied, sufficient to reduce force to a low value for a short period of time, no corresponding change in equatorial reflection towards the pattern observed in relaxed muscle occurs. Together, these results imply that during the early stages of muscle contraction, and thereafter, there are a substantial proportion of attached myosin heads which are not contributing to force development and generation. These crossbridges are referred to as being 'weakly' bound. However, these experiments did not resemble *in vivo* conditions as they were carried out at low ionic strength rather than physiological ionic strength, because at low ionic strength, the affinity of myosin heads, and myosin-nucleotide states, for actin is greatly increased. Therefore, early experiments examining S1 and HMM and their affinity for actin were routinely carried out at low ionic strength (generally < 50mM). Chalovich and colleagues (1991) sought to determine whether or not these weakly bound crossbridges existed at physiological ionic strength (~200mM), and if they were a necessary pre-requisite for force production. They used the smooth muscle protein caldesmon, a selective inhibitor of the weak crossbridge configuration (Velaz *et al,* 1989), to determine this. They found that inhibition of the attachment of the weakly bound state was indeed sufficient to inhibit active contraction. They were therefore able to conclude that the weakly bound crossbridges were an essential intermediate in the crossbridge cycle in order to generate filament sliding and force. From the binding of caldesmon

fragments to specific sites on actin, they also determined that the weakly bound crossbridges bind to specific sites on the actin filament.

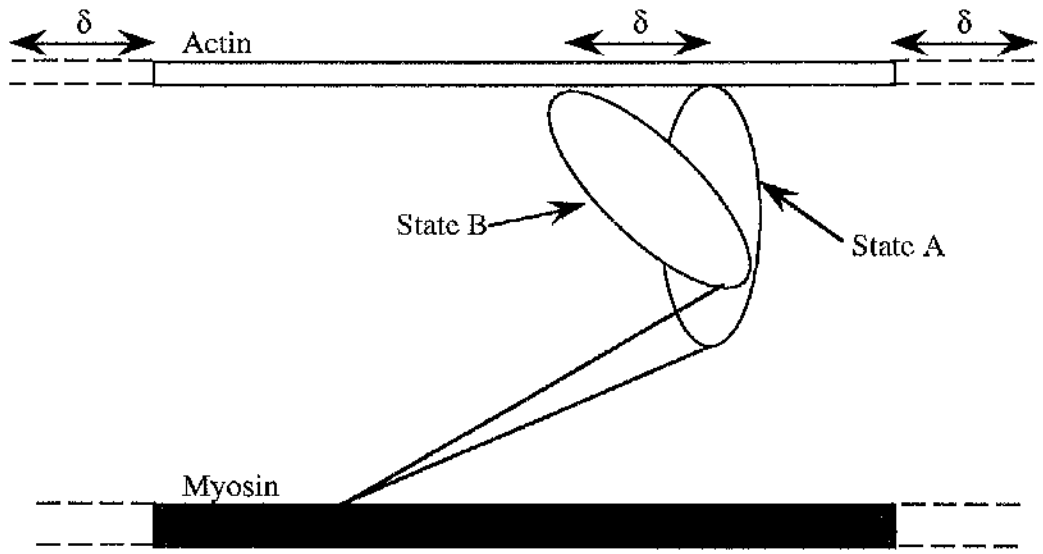

Fig. 1.1. Diagrammatic representation of the two conformational states of the crossbridge. State A denotes the weakly bound configuration, whereas State B denotes the strongly, bound, force generating configuration. δ is the working stroke of the crossbridge (see later text) performed during the power stroke.

It is now generally accepted that crossbridges exist in two main configurations (Fig. 1.1.). The first of these, the weakly bound crossbridge (S1.ATP and S1.ADP-Pi), has a low affinity for actin and cannot significantly contribute to force generation. On the other hand, the strongly bound crossbridge (S1.ADP) has a high affinity for actin and represents the main force generating configuration (see later crossbridge cycle scheme in Fig. 1.3. for details). The progression of the weakly bound state to the strongly bound state, fuelled by the hydrolysis of ATP, represents the power stoke generated by the crossbridges in order to produce filament sliding, and hence force generation.

1.7 The *in vitro* motility assay

More recently, the development of the *in vitro* motility assay has been of great importance in answering many previously unresolved questions concerning the mechanism by which force and movement are produced in muscle. The *in vitro* motility assay is a cell free system in which the movement of purified motor proteins can be assayed by direct observation through the light microscope.

The first partially defined system which measured, reproducibly, the movement of small groups of molecules was devised by Sheetz and Spudich in 1983. They examined actin filament arrays from the alga *Nitella*. Previous attempts at devising a similar system had failed to provide reproducible results (*e.g.* Yano *et al,* 1982). Sheetz and Spudich applied to bundles of actin filaments a suspension of tiny beads to which heavy meromyosin (HMM) was covalently attached. When ATP was present, these beads, which had settled on the actin filaments, moved along actin in a direction that was determined by the polarity of the actin filaments, hence the beads always moved in the same direction on any one filament. Later experiments demonstrated that the speed at which these beads moved was dependent on the type of myosin used (Sheetz *et al,* 1984; Harris & Warshaw, 1993 - see later section 1.8). Collectively, these studies provided further strength to the sliding filament theory of muscle contraction. The 'bead' assay was further developed by Kron and Spudich (1986), using fluorescently labelled actin filaments in solution and detected by video light microscopy. They used a glass surface that was randomly coated with myosin along which, in the presence of ATP, the actin filaments orientated themselves and generated a steady sliding movement in a direction determined again by their structural polarity. A simplification of this technique was employed by Toyashima *et al* in 1987, in which they showed that the sliding movement of actin could be supported by the myosin heads (subfragment 1) alone. This clearly showed that a major amount of movement could be produced by the S1 heads alone, however, it

does not rule out the possibility that the S2 region of myosin could still contribute and therefore increase the movement further, as suggested by Harrington (1971, 1979) and the 1971 Huxley and Simmons model.

Kishino and Yanagida (1988) then took Toyashima's technique one stage further by attaching actin filaments to flexible glass microneedles, using inactivated myosin as a 'glue', and measuring the displacement of the needle, enabling them to measure the force developed by a single actin filament interacting with a myosin or S1-coated substrate.

However, the most recent and sophisticated refinement of the *in vitro* motility assay system has produced the 'optical tweezers' technique (Block *et al,* 1990; Svoboda *et al,* 1993; Finer *et al,* 1994). The resolution of this technique has allowed direct measurement of the force and displacement (with piconewton and nanometre sensitivity respectively) that is invoked when a single myosin molecule interacts with a single suspended actin filament (Finer *et al,* 1994). It was used initially to determine the single molecular mechanics of another motor protein, kinesin, which can support the continuous movement of microtubules over large distances (Svoboda *et al,* 1993). This technique 'traps' a latex bead, which is attached to the actin filament, with a focused laser beam and the displacement of the bead is measured using high resolution photodiode detectors. Additionally, the bead position is proportional to an applied force acting on the bead so that they can measure force as well as displacement. Finer *et al* have used two optical traps so that an actin filament can be held and manipulated through beads attached at each end. Using this technique they determined that the average working distance of a crossbridge under low load was ~11nm (range 8-17nm, in close agreement with the value of 14nm found by Ford *et al* in 1977) and that under isometric conditions, myosin is able to produce an average force of 3-4pN.

1.8 The Lever Arm Hypothesis

In contrast to Huxley's model (1969) that muscle force was developed as a result of a change in orientation of the S1 head part of myosin, in which the two chain coiled-coil helical structure of the myosin rod backbone (see section 1.12 for more detail) had merely a passive role, Huxley and Simmons (1971) proposed that the S2 portion of the myosin rod may function as a series elastic element and may therefore influence force generation (by being the predominant component of series elasticity). They suggested that each crossbridge consisted of an elastic element in series with a second component having both elastic and viscous properties.

Currently, there is much interest in the role of the light chain binding region (LCBR), or 'neck' region of the myosin molecule, in muscle force production. Proteolytic treatment of the S1 region reveals three distinct fragments of differing sizes that are known simply as the 50 kDa, 25 kDa and 20 kDa regions. Actin binding is mediated by the 50 kDa region, the ATPase site spans the 50-25 kDa interface and the 20 kDa (neck) region binds the two light chains (*i.e.* the LCBR). The LCBR has an α-helical structure, around which the two light chains are wrapped offering rigidity to its structure. Based on the 3D-atomic structure of the myosin head, determined by Ivan Rayment and his group (1993), it was suggested that the neck region swings relative to the catalytic domain, thereby acting as a lever arm to amplify small conformational changes in the motor domain. This proposed model has been termed the 'lever-arm hypothesis' and was first demonstrated experimentally using brush border and smooth muscle myosin by Jontes *et al* and Whittaker *et al* in 1995 but has remained controversial. The lever arm hypothesis has sparked interest because it provides a probable site for the series elastic compliance in actomyosin (as suggested by Huxley and Simmons in 1971) but it also suggests a means of mechanical amplification within the myosin motor system. Other groups (Irving *et al,* 1995; Uyeda *et al,* 1996; Anson *et al,* 1996) have attempted to test this model, using

different experimental techniques, the first of these groups using structural and spectroscopic techniques and the latter two using the *in vitro* motility assay to assess the effects of altering the length of the neck region on sliding velocity. By attaching fluorescent probes to specific sites within the LCBR and monitoring any change in orientation, Irving and colleagues have shown that there is tilting of the LCBR during muscle movement, however, the changes in orientation were smaller (~3°) than perhaps expected. Uyeda and colleagues, as well as Anson and co-workers, used the same principle, using molecular biology techniques to alter the length of the neck region of myosin in the slime mould *Dictyostelium discoideum* (which is homologous to skeletal muscle myosin), but different techniques to examine the lever-arm model. They hypothesised that if the neck region of myosin actually does function as a lever-arm, then altering its length should produce a corresponding alteration in the myosin step size.

The former of these groups altered the length of the neck region by either deleting or adding one or both of the LCs to the myosin motor producing three mutants. The first of these had both LCs deleted, the second had its regulatory LC deleted and the third had a repeat of its essential LC attached so that it now possessed three LCs, producing myosin constructs with neck regions of 2, 6 and 13 nm respectively (compared with the wild-type myosin with a neck region of 8.5 nm). They found that there was a linear relationship between the number of LCBRs (*i.e.* the length of the neck region) and sliding velocity.

The latter of these two groups altered the length of the neck region using *Dictyostelium* α-actinin repeats as artificial lever arms, producing lever arms of 6.5 and 13 nm (wild-type again 8.5nm). They also found a clear correlation between *in vitro* sliding velocity and lever arm length.

Collectively, these results strengthen the lever-arm hypothesis, however, their relevance to *in vivo* conditions must be interpreted with caution, since many of these results were conducted under unloaded conditions, a limitation of the *in vitro* motility assay. Using this approach, in combination with the optical tweezers technique (Block

et al, 1990: see introduction section 1.7), which allows simultaneous force and sliding velocity measurement should therefore be more useful in providing insight into motor function *in vivo* (as are the collaborative labs of Warshaw and Trybus). Mutations in the LCBR of myosin are seen in some forms of human cardiac hypertrophy (Poetter *et al,* 1996), hence, results from this type of study will be particularly interesting when examining the decreased contractility and efficiency associated with diseased myocardium.

1.9 The Duty Ratio

The optical tweezers, high resolution, single molecule technique has allowed the examination of the functional differences between motor proteins, and indeed different types of myosin. The differences are understood using the concept of the 'duty ratio', the time that a motor domain spends attached to its filament (recently reviewed by Howard (1997)). This concept was first employed to explain the high force generated by smooth muscle in 1982 by Dillon and Murphy and was calculated as the ratio of the stiffness of active muscle to the stiffness of that of rigor muscle. The following section will detail the concept of the duty ratio for myosin only, unless otherwise mentioned, however, the same scheme can be applied to other molecular motor proteins such as kinesin, in order to make functional comparisons.

Each crossbridge must cycle repetitively between attached and detached states in order to move an actin filament through a distance that is large compared to molecular dimensions (Fig. 1.2.a.). The working stroke of the crossbridge is performed during the attached phase (duration t_{on}), and the recovery stroke returns the crossbridge to its original state during the detached phase (duration t_{off}). The working distance of the crossbridge (illustrated in Fig. 1.2.b.) is defined as the distance the actin binding site of the myosin head moves relative to the neck binding region of the head. The duty ratio, r, is therefore represented by:

$$r = \frac{t_{on}}{t_{on} + t_{off}} = \frac{t_{on}}{t_{total}} \qquad (1.2)$$

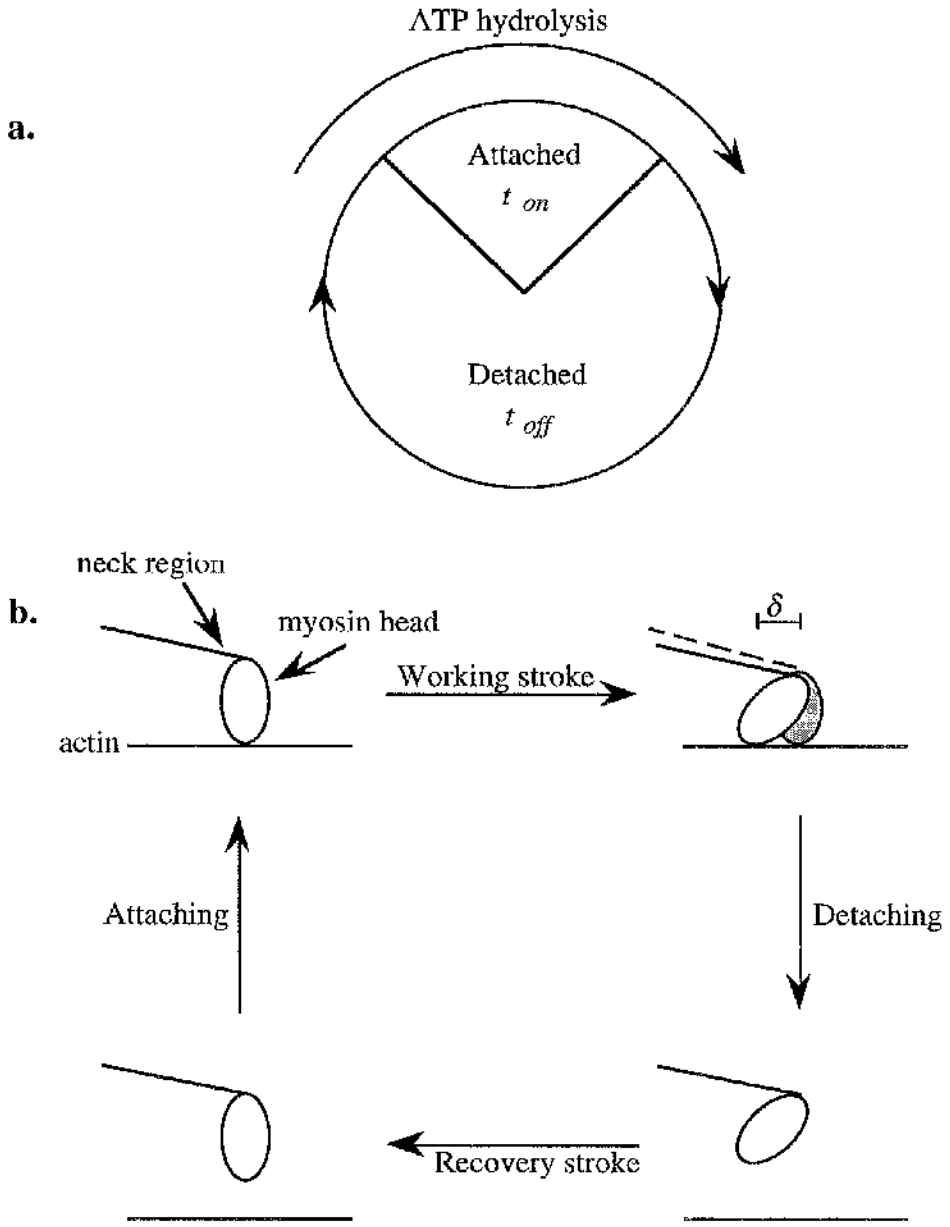

Fig. 1.2. Simplified crossbridge cycle schemes. **a.** the crossbridge cycles between the attached (duration t_{on}) phase, where it performs the 'working stroke', and the detached phase (duration t_{off}), where it undergoes the 'recovery stroke'. **b.** illustrating the working and recovery strokes.δ represents the working distance of a crossbridge. The crossbridge recovers its initial position while detached, avoiding any backwards step, therefore the filament sliding progresses a distance equal toδ during each cycle. The duty ratio is defined as the fraction of time that the crossbridge is bound and in its working phase.

The duty cycle of a crossbridge can in principle be large (~1) if it spends most of its time attached, or small (~0) if it spends most of its time detached, for example, skeletal muscle requires an assembly of at least 10 to 100 crossbridges to move, its duty ratio must be small, ~0.01-0.1, the reciprocal of the minimum number of heads required for continuous motility (Uyeda *et al,* 1990; Leibler & Huse, 1993).

As well as explaining the different functional characteristics of different types of molecular motors, the duty cycle also provides an important link between the chemical speed of a motor (its ATPase rate) and the mechanical speed (its velocity). Assuming that an actin filament, is moving at a constant velocity, v, over a fixed array of myosin heads, analogous to filament sliding in muscle, or as observed in *in vitro* motility assays, and that there are enough myosin heads present to sustain filament sliding, information about the ATPase rate can be determined as follows: if each head remains attached for time t_{on} and moves through the working distance, δ, then

$$v = \frac{\delta}{t_{on}} \tag{1.3}$$

However, the energy required to drive this cycle is supplied by ATP hydrolysis, therefore the total cycle time is given by

$$t_{total} = \frac{1}{V} \tag{1.4}$$

where V is the rate at which each head hydrolyses ATP. Now by substituting these expressions for t_{on} and t_{total} into equation (1.2) another expression for the duty ratio, is obtained:

$$r = \frac{\delta \cdot V}{v} \tag{1.5}$$

This expression assumes that one molecule of ATP is hydrolysed per mechanical cycle. This assumption still remains controversial (see A.F. Huxley, 1992 for discussion of this), as some groups argue that each crossbridge may undergo several

cycles per molecule of ATP hydrolysed (*e.g.* Yanagida *et al*, 1985). Using these concepts just described, allows functional comparisons to be made between different biological motor proteins, which will prove useful in understanding the complexities of biological motor proteins assemblies and how this relates to their function *in vivo*. For example, skeletal muscle must be able to respond rapidly if the load it is pulling on yields. Functionally, a low duty ratio ensures that skeletal muscle can respond in this manner by having a population of 'primed' heads that can rapidly attach after a small shortening, when previously unreachable actin binding sites come within an accessible range.

Howard (1997) proposes that the low duty ratio of myosin arises because of steric, rather than biochemical, constraints. Ferenczi and co-workers (1984) demonstrated that decreasing the [ATP], and therefore increasing the time that a crossbridge spends attached (t_{on}), decreased force by a small amount. However, if there were no steric limitations, an increase in the crossbridge attachment time, according to equation 1.2, should increase the number of attached crossbridges and therefore force generation. Since this doesn't occur, only a small fraction of the crossbridges can be attached, and generating force, at any one time consistent with there being a steric rather than biochemical restraint to binding.

1.10 Mechanical Studies

Since the elucidation of the 'crossbridge cycle', many groups have sought to describe the elementary steps of the cycle using biochemical techniques (Taylor, 1979; Sleep & Smith, 1981; Geeves *et al*, 1984) on isolated muscle proteins, and muscle fibre studies on both intact and chemically-skinned muscle preparations. More recently, biochemical techniques such as the *in vitro* motility assays, involving purified actin and myosin and also other motor proteins such as kinesin (see previous section 1.7) and 'solution studies' have been developed (*e.g.* Yanagida *et al*, 1985) and have proved useful in determining several intermediate states of the cycle (Stein

et al, 1979; Eisenberg & Greene, 1980; Geeves *et al,* 1984). These techniques have severe limitations to the amount of information they can elucidate about contractility, since these techniques cannot provide any information on the force generation of the muscle (with the exception of the recent modification of the motility assay, the optical tweezers technique - detailed section 1.7). However, mechanical perturbation techniques such as sinusoidal analysis (Kawai & Brandt, 1980), pseudo-random binary noise (PRBN - Rossmanith, 1986) and step-length changes (White & Thorson, 1973) on both intact and chemically-skinned preparations have been used to overcome the shortfalls of the biochemical techniques and characterise the elementary steps of the crossbridge cycle. Skinned fibres, in particular, have proved very useful in these studies, allowing both mechanical and chemical perturbations to be applied simultaneously. The process of chemical skinning has been shown, in a study by Saeki and colleagues (1991), not to affect the validity of comparing results with the intact preparation when examining kinetic processes. They compared crossbridge dynamics between intact and skinned ferret trabeculae at 20°C and found that there was no significant difference in kinetic data.

Mechanical studies on cardiac muscle, however, have progressed much slower than those carried out on skeletal muscle due to the different structural integrity of the two muscle types. Results from these kinds of experiments on cardiac muscle have proved more difficult to interpret than those from skeletal muscle because of the series elasticity of intercalated discs and the greater end compliance and parallel elasticity of the myocardium.

Figure 1.3. illustrates the crossbridge cycle based on schemes developed previously (*e.g.* Eisenberg and Hill, 1985: by sinusoidal analysis on skeletal muscle Kawai & Halvorson, 1991; Zhao & Kawai, 1993; Kawai & Zhao, 1993). In this scheme, the following abbreviations are used: A, actin; M, myosin head; T, ATP; D, ADP; and Pi, inorganic phosphate. The cycle is comprised of seven crossbridge states: In *step 1a*, Mg ATP binds to the rigor-like AM state to form a collision complex AM†T, which then isomerises to AM*T in *step 1b* . *step 2* involves the detachment of

the crossbridges to form the 'detached' state. Here, the detached state includes all truly detached states in addition to 'weakly' attached states.

In the weakly attached states, myosin is bound to actin but the crossbridges are not generating any force. Hydrolysis occurs in *step 3* . In *step 4*, the detached crossbridges attach to form the AM^*DP state, which in turn is followed by Pi release in *step 5* to form the AM^*D state. *step 6* is the ADP isomerisation step, in which ADP isomerises to form AMD, followed by the loss of MgADP in *step 0* to form the AM state and the cycle begins again if sufficient ATP is present.

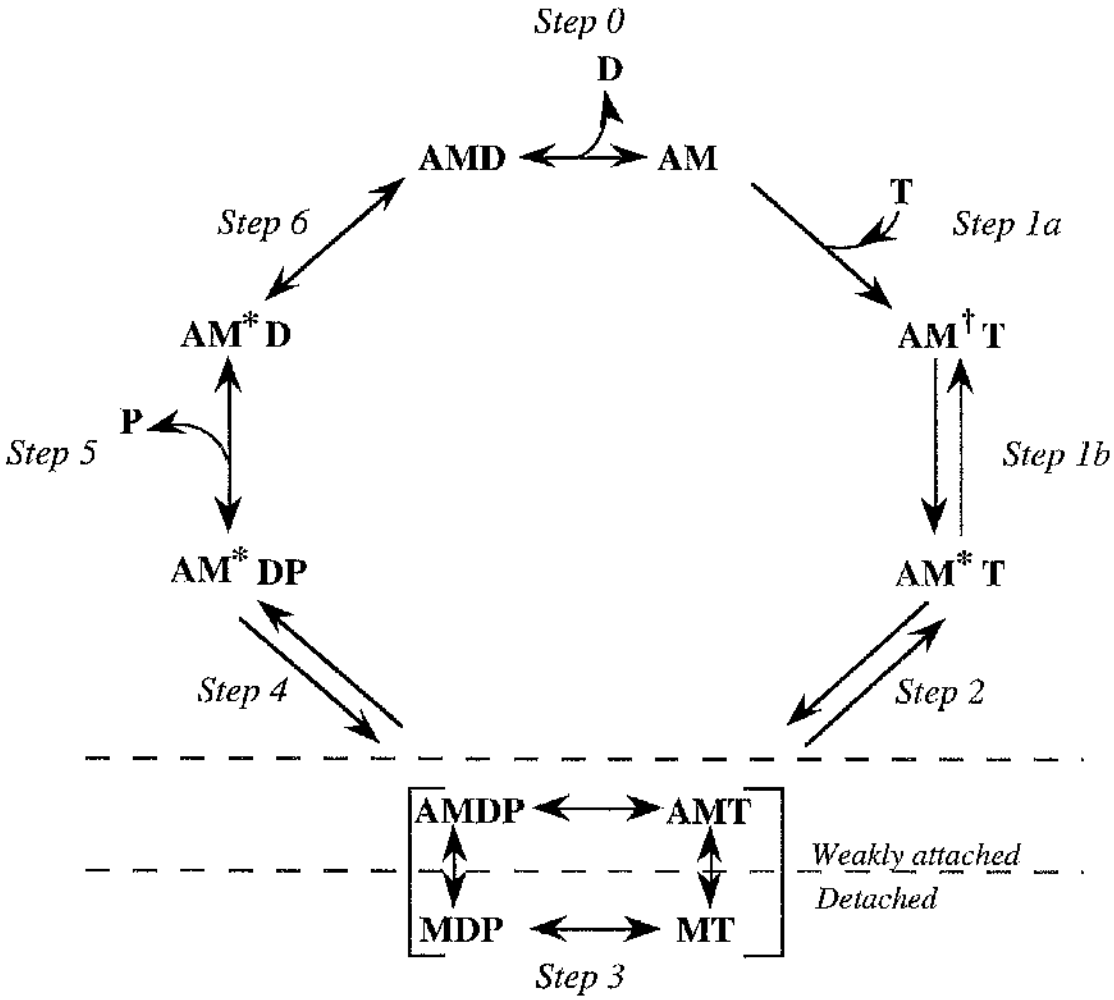

Fig. 1.3. The crossbridge cycle, where A=actin, M=myosin head, T=MgATP, D=MgADP and P=inorganic phosphate (Pi). † and * denotes different conformational states.

1.11 The Myofilaments

The next section reviews the status of the myofilaments themselves, the most direct subject of the present study. Before going into detail about the respective thick and thin filaments and their role in cardiac contraction, their arrangement within the sarcomere, the repeating unit of striated muscle, will first be described. Early observations of muscle fibres using light microscopy (reviewed by Huxley, 1957) revealed cross-striations of alternating bands of high and low refractive index (see Fig. 1.4.a.), which came to be known as the A- (anisotropic) and I- (isotropic) bands respectively. Each I-band is bisected by the Z-line. The region enclosed between two successive Z-lines is termed the sarcomere (Fig. 1.4.b.). Within each A-band there is a centrally located H-zone, that appears as a lighter region. In addition, running within this H-zone, parallel with the Z-lines, there is dense line known as the M-line. The sarcomere is comprised of a system of interdigitating thick and thin filaments, with associated titin and nebulin filaments (see Fig. 1.4.c. for diagrammatic representation) extending between successive Z disks. Nebulin filaments are closely associated with the thin filaments (as are the regulatory proteins- these will be discussed in more detail in sections 1.15-1.19), and both of these insert into the Z disks. Titin filaments (sometimes referred to as connectin), on the other hand, are closely associated with the thick filaments, but extend into the I band as well as inserting into the Z disks. Also associated with the thick filaments are other proteins known as C protein, H protein, M protein and myomesin, however, only a few of these will be discussed in the body of this thesis. Multiple isoforms of the thick and thin filaments exist, however these will be discussed later in the relevant sections.

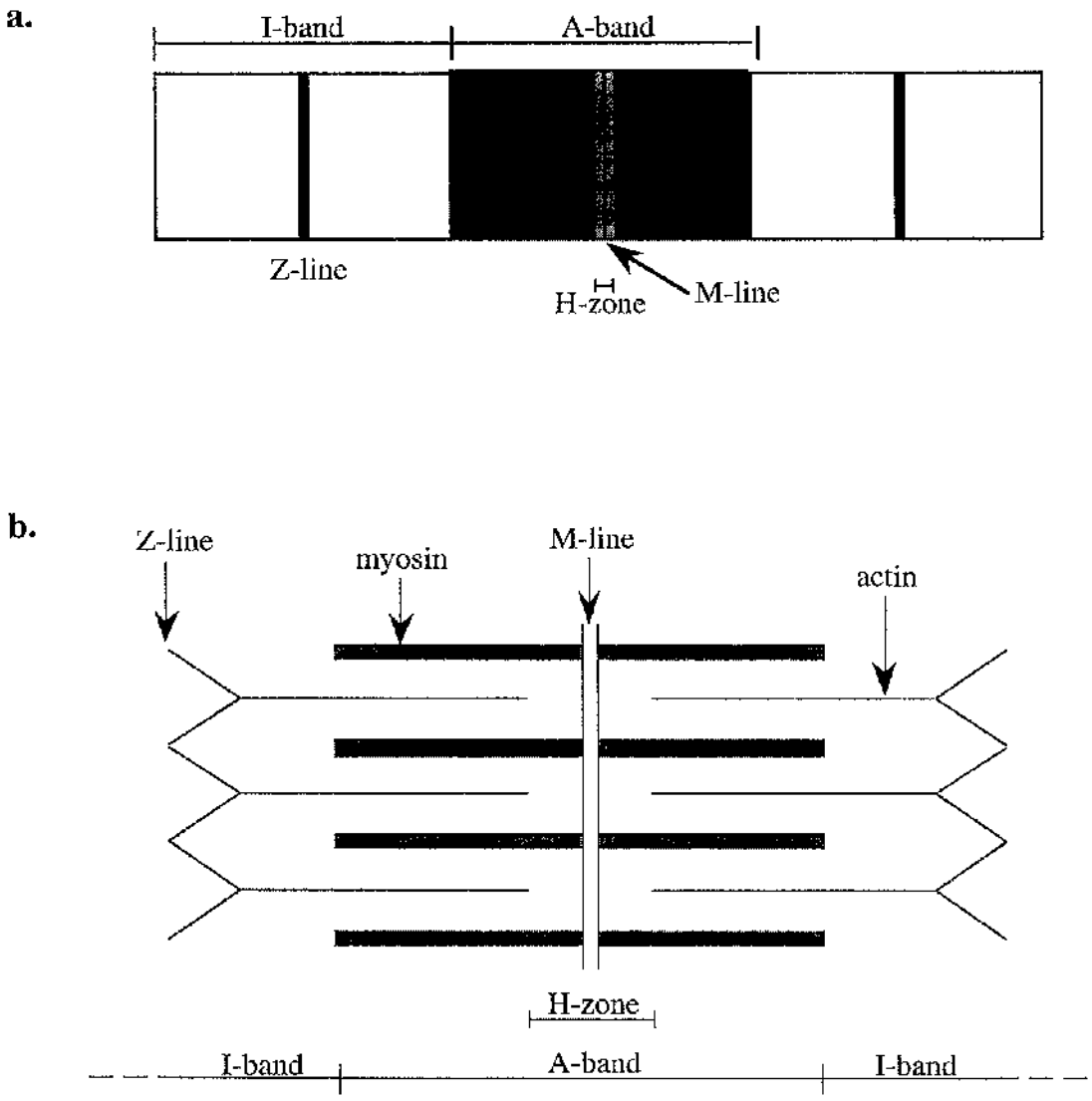

Fig. 1.4. Myofibril structure. (a) Schematic representation of the cross-striation pattern observed under light microscopy. The longitudinal axis of the fibre is horizontal in the figure. (b) Organisation of the thick (myosin) and thin (actin) filaments within the sarcomere. (c) shown overleaf.

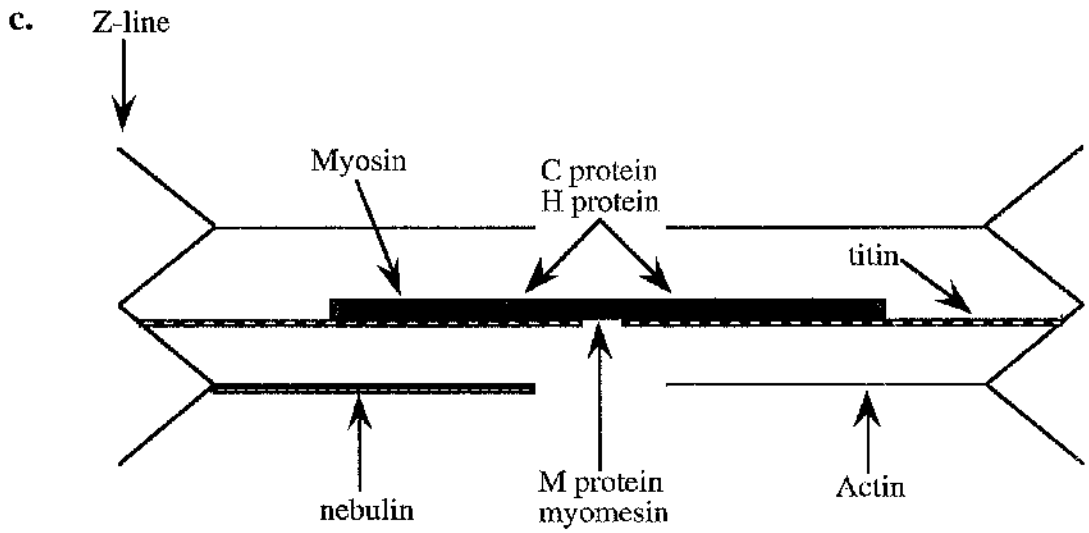

Fig. 1.4. **(cont.)** (c) Close up of myofilament arrangement shown in (b) illustrating the other proteins associated with the thick and thin filaments.

1.12 Myosin - the thick filament

1.12.1 A brief outline

Myosin is an ATPase that converts chemical energy into directed movement, often being referred to as a 'molecular motor'. The molecular diversity of this protein is huge, there being at least eleven families already identified, some of these being further characterised into sub-families, and it is anticipated that more will be discovered as research continues.

Cardiac myosin belongs to the class II myosins and, within this class, several isoforms exist (these will be discussed later). Class II myosins are hexameric molecules, consisting of two heavy chains (MHCs) each with a pair of light chains. The individual light chains are referred to as the 'essential' or 'alkali' light chain (MLC_1) and the 'regulatory' or 'phosphorylatable' light chain (MLC_2). These light chains are associated with the neck region of myosin. The essential light chain lies close to the motor domain of myosin, whereas, the regulatory light chain lies close to the head-myosin rod junction. Each MHC contains a 'head' region. The myosin head corresponds to the motor domain that contains the ATP- and actin-binding sites. This motor domain is connected to the long myosin backbone by a neck region, along which the light chains are associated, as mentioned previously. The main axis of the myosin filament, the myosin rod, is comprised of the two MHCs intertwined to form an α-helical coiled-coil. Proteolytic treatment of the myosin molecule can dissociate the rod from the head region, the latter now being known as myosin subfragment 1 (S1). The backbone region can also be further sub-divided into myosin subfragment 2 (S2), the part that connects the S1 heads to the backbone, and light meromyosin (LMM). The heavy meromyosin (HMM) fragment is comprised of the S1 and S2 regions (see Fig. 1.5.).

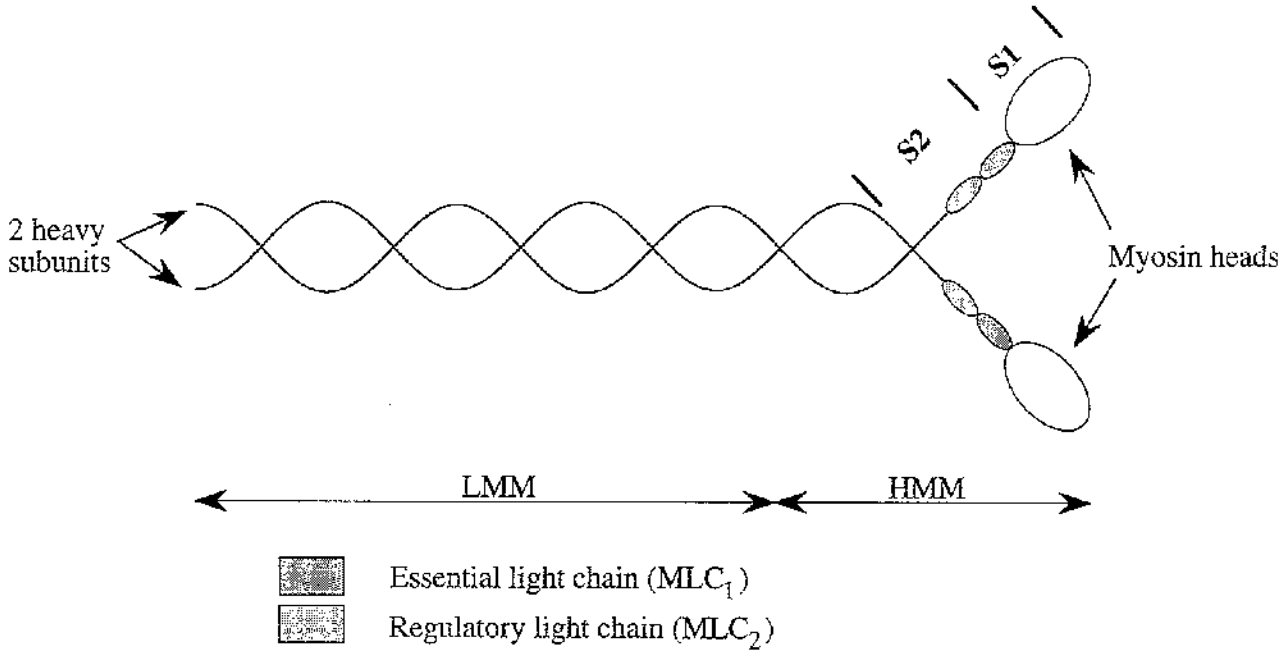

Fig. 1.5. The myosin molecule is approximately 160nm in length with two globular heads (heavy meromyosin subfragment 1) and two heavy chains forming a coiled-coil myosin rod. Each 'neck' region of heavy meromyosin (subfragment 2) is associated with a pair of myosin light chains. (see text for more details).

1.13 Myosin Heavy Chains

At present, nine MHC isoforms have been characterised at the protein and mRNA levels in mammalian muscle. Of these, three isoforms exist in ventricular muscle, known as V_1, V_2 and V_3 (Flink *et al*, 1979; Hoh *et al*, 1979). Although they differ in their MHCs, these isomyosins have the same two pairs of light chains (Hoh *et al*, 1978). V_1 and V_3 are homodimers of two distinct types of heavy chains HC_α and HC_β, while V_2 is a heterodimer (Hoh *et al*, 1979; Everett *et al*, 1982), the heavy chain compositions of these isoenzymes being $(HC_\alpha)_2$, $(HC_\beta)_2$ and $HC_\alpha HC_\beta$, respectively.

With the advent of the *in vitro* motility assay, in which single fluorescently-labelled actin filaments are observed sliding over a myosin coated surface, it may now be possible to characterise, at the molecular level, the force and motion generating capabilities of myosin. Previous studies using this technique (Harris & Warshaw, 1993) have looked at the ability of myosin to move actin filaments under load. They allowed a mixture of two different myosins, with different cycling rates, to move a single actin filament. They observed that by doing this they were able to modulate actin filament velocity by mixing different proportions of each type of myosin. They concluded from these experiments that the two myosin populations interacted mechanically such that the slower myosin imposed an internal load against which the faster cycling crossbridges must act.

This type of mechanical myosin crossbridge interaction is physiologically relevant *in vivo* during the development or response to stress of the myocardium, when two myosin isoforms are simultaneously expressed within the same cell as in hypertrophy (see later). The relative distribution of ventricular isomyosins can be influenced by several factors, for example, thyroid state (Hoh & Egerton, 1979) and hypertrophy (Lompre *et al*, 1979; Mercadier *et al*, 1981). The MHC_α isoform is predominantly found in the atria of the heart, with the exception of mouse and rat

myocardium where it is the predominant form throughout all of the myocardium (Hoh *et al,* 1978). In the rabbit and larger mammals, however, the predominant isoform found in the ventricles is the MHC$_\beta$ (Lompre *et al,* 1984; Swynghedauw, 1986). The V_1 isoform has a much higher actin-activated MgATPase rate, but lower affinity, than the V_3 isoform. This is of functional significance in some disease states in small rodents, such as heart failure and diabetes, where a shift in the relative isoform distribution from V_1 to V_3 can occur as an adaptational response to impaired contractile function (Dillman, 1980; Lompre *et al,* 1979; Mercadier *et al,* 1981).

Myocardial hypertrophy is a basic adaptive response to increased cardiac loading conditions. Immunofluorescence studies of hypertrophic rabbit myocytes indicate that V_1 and V_3 myosin isoforms are simultaneously expressed within a single cell (Samuels *et al,* 1983). Biochemical alterations, such as the shift in myosin isoform from V_1 to V_3, during myocardial hypertrophy permits the affected myocardium to compensate to some degree for its reduced contractility. Compared with V_1, the reduced ATPase catalytic activity of V_3 results in an improved thermomechanic efficiency of cardiac work.

In humans (Mercadier *et al,* 1983) and larger mammals, since V_3 is already the predominant isoform, this isoform shift is not as significant a functional adaptation to impaired contractile function as in other small mammals. However, alterations in human myosin isoforms in cardiac disease have been observed. The human genetically linked cardiac disease state, familial hypertrophic cardiomyopathy, is an autosomal dominant genetic disorder characterised by left ventricular hypertrophy without concomitant chamber dilatation (Maron, 1988). It has been associated with, amongst others, a number of missense mutations (more than forty have been described to date) in the genes of the myosin V_3 isoform (Geisterfer-Lowrance *et al,* 1990; Epstein *et al,* 1992). Most of these occur in the S1 region of myosin, however, a smaller number occur in the proximal S2 region (Sellers & Goodson, 1995; Schwartz *et al,* 1995).

1.14 Actin - the thin filament

The crystal structure of the actin monomer (known as G-actin) was first obtained by Holmes and co-workers (Kabsch *et al,* 1990). The G-actin monomer polymerises to form the double-helical actin filament (now known as F-actin), which is the form associated with the sliding of the myofilaments in muscle. The atomic structure of the actin monomer was fit into a model of the F-actin filament by the same group (Holmes *et al,* 1990) using X-ray diffraction patterns of actin filaments aligned in capillaries as a constraint. The actin monomer is comprised of four subdomains with a tightly bound nucleotide inserted into a central cleft in the molecule. In the filament model, subdomains 3 and 4 form the core of the filament, while subdomains 1 and 2 project towards the periphery. Subdomain 1 has been shown to contain sites for the interaction with the myosin heads (Miller *et al,* 1995) as determined by cross-linking and site-directed mutagenesis. The inner two subdomains are connected to the outer two by only two polypeptide strands. It has been postulated (Schutt *et al,* 1993), that conformational changes within the actin filament may play a role in the generation of force, but, to date, there is no definitive evidence that this conformational change actually occurs. There are, however, reports from a number of studies using spectroscopic probes (for review see Dosremedios & Moens, 1995) that there are changes in the structure of actin upon interaction with myosin, but these changes seem to be small and not associated with force generation.

There are two sarcomeric actin isoforms found in the striated muscle of mammals and birds, α-skeletal actin and α-cardiac actin. The amount of each isoform present, and the respective mRNAs, varies with species, muscle type, development and ageing. For example, in the rat, α-skeletal actin mRNAs account for as much as 50% of the total at birth, but the amount decreases to levels of <10% in the adult. After imposing a chronic haemodynamic load on the rat heart, α-skeletal actins begin to accumulate in the ventricles (Schwartz *et al,* 1986). In humans, however, much less is known about the levels of the different actin mRNAs present during

development, ageing or disease states. It is known that the two actins are co-expressed in human adult cardiac muscle (Gunning *et al,* 1983; Boheler *et al,* 1991). Boheler and co-workers demonstrated that their accumulations are developmentally regulated *i.e.* cardiac actin mRNA is the major isoform of the human foetal heart, whereas skeletal actin predominates in young adult hearts. This is somewhat different from what is seen in other animal species. Furthermore, in contrast to the rat, there is no actin isoform transition associated with cardiac disease states, rather the proportion of the two transcripts are maintained at a relatively constant level in failing and non-failing hearts.

1.15 The Regulatory Proteins

The cyclic interaction of myosin crossbridges with actin in vertebrate striated muscle is regulated by the $[Ca^{2+}]_i$ (Ebashi and Endoh, 1968). Associated with the thin filaments are a group of proteins known as the 'regulatory' proteins, as mentioned briefly in section 1.5. These proteins are tropomyosin (Tm), and troponin C (TnC), TnT and TnI. The Tn-Tm complex acts as this Ca^{2+}-sensitive molecular switch for the activation of actin-myosin interaction, and therefore regulation of muscle contraction. Muscle fibres which lack this Tn-Tm complex have relatively high MgATPase activities that are insensitive to $[Ca^{2+}]$. The addition of Tm either inhibits or enhances this activity, depending on the myosin:actin ratio (Lehrer and Morris, 1982). The addition of purified Tn to these systems inhibits the ATPase at submicromolar $[Ca^{2+}]$s and activates the ATPase at micromolar $[Ca^{2+}]$s (Greaser and Gergely, 1971).

1.16 TnC- the Ca^{2+}-binding subunit

TnC is the subunit of troponin necessary for rendering the actin-myosin interaction Ca^{2+}-sensitive. This has been shown in chemically-skinned muscle preparations from which TnC has been selectively removed, using the Ca^{2+}-buffer EDTA (Zot and Potter, 1982), such that they remain permanently relaxed at all Ca^{2+}

concentrations. Moreover, the subsequent addition of exogenous TnC restores the Ca^{2+}-dependence of the muscle.

TnC is a dumb-bell-shaped protein, with two globular domains connected by a long central helix (Herzberg and James, 1988). Each of these globular domains is comprised of two EF-hand (*i.e.* helix-loop-helix Ca^{2+}-binding sites) Ca^{2+}-binding sites (sites I-IV: Farah and Reinach, 1995). Sites I and II, located at the amino terminal of TnC, are low affinity Ca^{2+}-binding sites ($K \approx 10^5\ M^{-1}$), whereas sites III and IV, in the carboxy-terminal domain, bind Ca^{2+} with a higher affinity ($K \approx 10^7\ M^{-1}$). However, these latter two high affinity sites also competitively bind Mg^{2+} ($K \approx 10^3\ M^{-1}$), which occupies these sites at physiological concentrations in relaxed muscle. Under such conditions, the kinetics of Ca^{2+}-binding to the high affinity sites are too slow (limited by Mg^{2+}- Ca^{2+} exchange) to be able to account for the kinetics of Ca^{2+}-induced force generation and relaxation. Hence it is the empty, low affinity sites I and II which possess the major role in regulation of actomyosin interaction (Johnson *et al,* 1979 and 1994). However, in cTnC, unlike skeletal muscle, site I lacks the crucial sequence requirements for Ca^{2+} binding and is therefore inactive (van Eerd and Takahashi, 1975). This leaves site II as the primary site for regulation of myocardial contraction. The role of the high affinity sites of cTnC (and also sTnC) may therefore be to maintain structural organisation of the folded TnC molecule (Zot and Potter, 1982) since they are permanently occupied by either Mg^{2+} or Ca^{2+} which offer stability to the arrangement. The difference in Ca^{2+} binding to the low affinity sites between cTnC and sTnC may account for the less steep pCa-force relationship seen in cardiac muscle (Johnson *et al,* 1980). The role of TnC type in determining the form of the pCa-force relationship was investigated by various groups using regulatory protein extraction and replacement protocols (Moss *et al,* 1986; Babu *et al,* 1987). As yet there is no evidence for the existence of TnC isoforms (Parmacek & Leiden, 1991), but rather this subunit remains constant during cardiac development.

1.17 TnI- the inhibitory subunit

TnI binds to actin, Tm, TnT and TnC. On its own, purified TnI inhibits the actomyosin ATPase in a Ca^{2+}-independent manner (Greaser and Gergely, 1971). The presence of Tm enhances the actin-binding and inhibitory activity of TnI (Perry *et al,* 1972; Potter and Gergely, 1974). The cardiac TnI isoform (cTnI) is a distinct form of TnI, in that it contains an additional 32-residue amino-terminal domain that is not seen in its skeletal counterpart, or indeed any other type of TnI. Phosphorylation of cTnI in this region, at serine residues 22 and 23, by cAMP-dependent protein kinase (PKA) has important effects on its structure (Dong *et al,* 1997), its interaction with TnC (Dong *et al,* 1997) and the binding of Ca^{2+} to TnC (Robertson *et al,* 1982), as well as the co-operative binding of TnI to actin-Tm (which is unique to the cardiac variant: Al-Hillawi *et al,* 1995). The net outcome of TnI phosphorylation is a decrease in the Ca^{2+}-sensitivity of the myofilaments (Solaro *et al,* 1976) and an increase in the rate of relaxation of the myofilaments, as is seen with β-adrenergic stimulation (Tsein, 1973; Solaro, 1993; Zhang *et al,* 1995).

The near amino-terminal domain binds to the carboxy-terminus of cTnC, in a Ca^{2+}-independent manner, anchoring cTnC to actin and therefore maintaining the TnI-TnC complex in its antiparallel arrangement (Krudy *et al,* 1994). This region also contains phosphorylatable serine residues (at positions 41 and 43) which when phosphorylated, by protein kinase C (PKC), causes a reduction in the maximal activity of the actomyosin ATPase.

In heart failure it has been shown, using chemically-skinned myocardium, that the Ca^{2+}-sensitivity of the myofilaments is decreased in failing hearts (Wolff *et al,* 1996), and that the maximal ATPase activity is reduced (Wattanapermpool *et al,* 1995) when compared with controls (reminiscent of the effects of cTnI phosphorylation). In addition, it was shown that PKA treatment of failing myocardium eliminated this difference in Ca^{2+}-sensitivity. Together these observations suggested that any alterations in cTnI phosphorylation, associated with

heart failure, may contribute to these alterations in cardiac function, most specifically the changes seen in Ca^{2+}-sensitivity. Indeed, decreased cTnI phosphorylation has been demonstrated in failing human (Bodor *et al,* 1997) and canine hearts (Wolff *et al,* 1995). However, these results remain conflicting since other groups (*e.g.* Hajjar *et al,* 1988) have failed to find any differences in Ca^{2+}-sensitivity, as would be expected if cTnI phosphorylation is decreased, between normal and failing hearts.

1.18 TnT- the Tm-binding subunit

TnT is a structurally asymmetric protein, containing a globular carboxy-terminus and an extended amino-terminal 'tail' region. Its carboxy terminus mediates its interactions with TnC and TnI, whereas its amino-terminus binds tropomyosin (Tanokura *et al,* 1983). The TnT subunit is important in conferring Ca^{2+}-sensitivity on the myofibrils and modulating myofibrillar ATPase activity (Tobacman and Lee, 1987). Several isoforms of TnT exist, varying with development and within species (*e.g.* rabbit contains five different isoforms: Anderson and Oakeley, 1988). Alterations in the relative content of these isoforms, and the functional consequences of this, have sparked interest in the last few years because of reports of altered isoform content in human myocardium with end-stage heart failure (Anderson *et al,* 1992, 1995). Alterations have also been reported in a guinea pig model of heart failure (Gulati *et al,* 1994). In human foetal myocardium TnT_3 is the predominant isoform, with a small amount of TnT_4. Adult human non-failing hearts exclusively contain TnT_3, whereas adult failing myocardium possesses a small, but significant, amount of TnT_4, echoing the foetal pattern.

1.19 Tropomyosin

Tropomyosin is a highly extended α-helical coiled-coil protein of ~40nm in length. The continuous Tm strand spans seven actin monomers and forms an indirect connection between Tns, which have the ability to control its position on the actin

filament and therefore regulate muscle activation (steric-hindrance model of muscle contraction). Tm molecules are assembled in a head-to-tail fashion forming a filament that lies in each of the grooves of the actin double helix.

1.20 Titin

The giant protein titin, sometimes referred to as connectin, is a polypeptide found in vertebrate skeletal and cardiac muscle. During the 1980s, electron microscopic studies with titin-specific antibodies demonstrated that titin is an integral part of the myofibril. Single titin molecules were shown to span from the Z disk to the M line (see Fig. 1.4.c.), therefore comprising a third, extensible sarcomeric filament system after the thick and thin filaments. It also appears that after these latter proteins, titin is the third most abundant protein found in muscle (≈10% of the combined protein content: Labeit *et al,* 1997). Titin is now generally assumed to be responsible for the elasticity of relaxed striated muscle, as well as acting as a molecular scaffold for thick filament formation (Maruyama, 1994; Trinick, 1996). Its molecular structure is comprised mainly of tandem repeat domains of the immunoglobulin (Ig) and fibronectin-III (FN3) types, which fold into globular domains (giving titin its beaded rod appearance) together with specialised binding domains and a putative elastic region, referred to as the PEVK domain (as this domain is rich in proline (P), glutamate (E), valine (V) and lysine (K): Labeit and Kolmerer, 1995).

Titin is primarily associated with the thick filaments, and because of this tight association, the A-band portion of titin is functionally stiff under physiological conditions. In contrast to this, the I-band region of titin is elastic (Fürst *et al,* 1988). More recently, Trombitás and colleagues (1997) have shown that connections between titin and the thin filaments can exist, however, these connections are weak enough such that they can be broken by simply the elastic recoil force of the muscle. In addition, epitope retraction techniques (Trombitás *et al,* 1997) have shown that

titin filaments, although they may associate with the thin filaments, remain functionally independent of them.

When titin filaments are extracted from the sarcomere, the stiffness of the relaxed myofibril decreases (for review see Maruyama, 1994). Cardiac muscle has a much higher passive stiffness than its skeletal muscle counterpart. Early studies (Brady, 1968) had attributed the high passive stiffness of cardiac muscle to the low compliance of extracellular matrix constituents such as collagen. However, with the advent of techniques using single myocyte preparations (Fabiato and Fabiato, 1976), and the myocytes still bearing a high passive stiffness, it was obvious that some intracellular component(s) must be contributing to this stiffness (Brady, 1991; Granzier and Irving, 1995). During physiological extensions, titin has now been shown to bear most of the resting force in both skeletal (Granzier and Wang, 1993) and cardiac (Linke *et al,* 1994) muscle.

1.21 Myocardial Relaxation

The period of relaxation in the contractile cycle of the heart is of key interest in cardiac mechanical studies, since it is intimately associated with the filling of the heart, which in turn mediates the contractility of the heart through the Frank-Starling relation. The phase of the contractile cycle of the heart during which relaxation occurs is known clinically as diastole. Diastole is the phase in each cardiac cycle that includes the period of isovolumic relaxation after closure of the aortic valve through mitral valve opening, and the period of left ventricular filling after mitral valve opening until mitral valve closure. In mechanical terms, myocardial relaxation begins when force development or shortening reverses and starts to decline and proceeds until the myocytes return to their original length. There are three physiological mechanisms, whose interplay determines the rate of myocardial relaxation, these are: (i) the rate of removal of the cytoplasmic Ca^{2+} by the SR from the cytosol; (ii) the rate of Ca^{2+} detachment from troponin C; and (iii) the rate of crossbridge detachment from actin.

1.22 Reactive Oxygen Species

Increased levels of oxidative stress is one detrimental factor the myocardium is subject to during the progression of congestive heart failure (CHF). The oxidative stress results from an increase in the production of oxygen-derived free radicals and reactive oxygen species (ROS) and/or an increase in the antioxidant capacity of the myocardium (McMurray *et al,* 1990; Halliwell, 1991; Hill and Singal, 1996). The literature suggests that patients with CHF have increased levels of ROS activity and decreased endogenous antioxidants levels (McMurray *et al*, 1990, Halliwell, 1991). Thus, reactive oxygen species have been postulated to contribute to the depression of contractile function observed during the development of CHF.

Chapter 2

Methods

2.1 Coronary Artery Ligation in the Rabbit

2.1.1 Background

The rabbit coronary artery ligation model is a well characterised and relatively straightforward model of left ventricular dysfunction (LVD). Like man, the rabbit has a poorly developed collateral coronary circulation (Maxwell *et al,* 1987) and therefore, the ligation of a single coronary artery produces a well defined region of myocardial infarction. The model has clinical relevance in that it produces a region of infarcted tissue which induces ventricular remodelling in a similar way to that seen in the human. The severity of LVD produced by the operative procedure depends on how far down the artery the ligature is tied. This reflects the extent of infarction of the left ventricle. The rabbit is of a convenient size to allow instrumentation and echocardiography to be performed with relative ease so that the extent of LVD produced by ligation can be assessed.

2.1.2 Method

Male New Zealand White (NZW) rabbits (2.5-3.5 kg) were pre-medicated with intra-muscular Hypnorm [0.3 $mg \cdot kg^{-1}$ fluanisone (10 $mg \cdot ml^{-1}$): fentanyl citrate (0.315 $mg \cdot ml^{-1}$)]. The anterior and left lateral chest wall was shaved and cleaned with Hibitane and alcohol. The animal was further sedated with intravenous midazolam (0.25-0.5 mg/kg) via the marginal ear vein to allow endotracheal intubation. Endotracheal intubation was performed using a Wisconsin paediatric straight blade (size 1) laryngoscope with the rabbit lying on its back and the head allowed to drape, supported, over the edge of the operating table. The tongue was pulled laterally and the laryngoscope introduced to allow visualisation of the vocal chords. Gentle chrichoid

pressure was applied to allow clearer vision of the vocal chords. The chords were sprayed with 1% xylocaine and after a few minutes, an uncuffed endotracheal tube (size 3-4) was introduced over a soft-tipped plastic coated wire introducer. The endotracheal tube was secured by taping to the operating table and was attached to a small animal pressure-regulated ventilator (SAR-830/P, CWE Inc, Ardmore PA, USA). To check that the tube was correctly positioned, a stethoscope was used upon the chest area to listen for air entry and exit. The animal was ventilated using mild positive end-expiratory pressure (1-2 cm H_2O). Anaesthesia was maintained using an inhaled mixture of 1 $Lmin^{-1}$ O_2, 1 $Lmin^{-1}$ NO_2 and 1% Halothane. No muscle relaxants were administered to allow possible distress to be recognised quickly by the operator. The animal was placed on a pre-warmed table and body temperature maintained by means of a thermostatically controlled heating mat.

The heart was exposed through a left thoracotamy, the pericardium opened and a tie placed through the cardiac apex to allow easier manipulation of the heart. The coronary artery anatomy in the rabbit is somewhat different from that of other species in the left anterior descending artery is small and supplies only a small area of the upper inter-ventricular septum (Flores *et al*, 1984). The left circumflex is dominant and gives off a large left ventricular branch early in its course in the atrioventricular (AV) groove. This left marginal branch is easily seen running over the left ventricle (LV) surface towards the apex and supplies the lower lateral LV wall, the LV apex and occasionally part of the right ventricle (RV) apex. This artery was ligated using 4/0 Ethibond suture with a 4mm curved needle at the midpoint between the AV groove and the cardiac apex. The infarcted region rapidly becomes blue and is easily seen. The size of this infarcted region could be assessed and, if it was not large enough, a second suture was placed more proximal to the first until a satisfactory infarct size was obtained.

Occasionally, the infarct size was so large that cardiac output fell sufficiently to produce a marked reduction in peripheral pulse volume. Intractable ventricular fibrillation would soon follow and the only hope for the animal recovering was to untie the ligature. Such animals rarely survived and are not included in analysis. Animals

were treated with intravenous quinidine (15 mg·kg^{-1}, marginal ear vein) five minutes prior to ligation of the coronary artery, as this has been shown to reduce the incidence of arrythmias with this procedure in rabbits (Connelly *et al,* 1982). Ventricular arrythmias were most commonly observed 10–12 minutes after coronary occlusion and were treated with DC shock (5-10 J) using small, sterilised defibrillation pads applied directly to the myocardial surface using the apical suture to hold the heart away from the chest wall.

Once the animal was haemodynamically and electrically stable, the left lung was examined for regions of lobar collapse. Such non-perfused and non-ventilated regions could be re-inflated by applying constant positive airway pressure. The chest wall was closed using three interrupted 2/0 catgut sutures placed through the chest wall around the ribs adjacent to the wound and drawn firmly together thus splinting the ribs. The skin was closed with continuous Dexon using a subcuticular stitch. An antibiotic was administered at the end of the procedure by intramuscular injection (ampicillin 25 mg/kg). Intravenous fluids were administered at the end of the procedure (15-20 ml normal saline). Analgesia (buprenorphine- 0.2 mg·kg^{-1})was also administered intra-muscularly before the end of the procedure and thereafter the following morning post-procedure. Animals showing signs of distress after this period were given further similar doses of analgesia as required. The animal was then allowed to develop chronic left ventricular dysfunction over a period of 8 weeks.

Sham-operated controls underwent thoracotomy, the pericardium opened, a tie placed through the apex and the heart manipulated in a similar fashion to the ligation animals but without ligation of the coronary artery.

The haemodynamic and morphological adaptation to coronary artery ligation have been well characterised in this model (Denvir *et al,* 1996; Pye *et al,* 1996; Ng *et al,* 1997). The coronary ligation procedure described here increases liver and lung weights (when expressed as a percentage of body weight), left ventricular end-diastolic dimension (assessed by echocardiography) and left ventricular end-diastolic pressure (assessed by invasive haemodynamic monitoring). Ejection fraction (assessed by echocardiography), left ventricular systolic pressure (assessed by invasive

haemodynamic monitoring) and cardiac output (assessed by a thermodilution method) are reduced by the coronary ligation procedure.

The operative procedures just described were carried out by me on some, but not all of the rabbits used in the experiments described in this thesis. In addition, all of the haemodynamic and echocardiographic measurements were performed by Dr. Martin Hicks and Dr. Andre Ng within the Medical Cardiology Unit based at Glasgow Royal Infirmary.

2.2 Isolated Ventricular Trabeculae Experiments

New Zealand White rabbits were killed by a lethal dose of intravenous Euthatal (1.0 ml /1.4 kg). The heart was rapidly removed and placed, still beating, in Ringer's solution (composition: 150 mM NaCl, 5 mM KCl, 1 mM $MgCl_2$, 2 mM $CaCl_2$, 5 mM HEPES at pH 7.0) at 20°C. The heart was then transferred to a petri dish containing Ringer's solution. The right ventricle was opened by a single cut, close to the intraventricular septum, running from the base of the heart to the apex. The Ringer's solution also contained 30 mM 2,3 - butanedione monoxime (BDM). BDM is known to inhibit force generation in cardiac and skeletal muscle (Fryer *et al,* 1988; Gwathmey *et al,* 1991; Backx *et al,* 1994). BDM was included in the Ringer's solution to aid mounting of the preparation by preventing the trabecula from contracting and hence 'curling-up' on itself, which would make it difficult to pass the trabecula through the snares without damage.

Experiments were performed on free running trabeculae, mostly isolated from the right ventricle. Occasionally trabeculae from the left ventricle were used. The left ventricle was consistently found to be less trabeculated than the right, making it difficult to obtain free running trabeculae of suitable dimensions for experimentation. Additionally, and especially in the left ventricle, the size and location of the infarcted region of muscle reduced the availability of suitable, viable trabeculae for experimentation. In most animals the infarct was mainly confined to the left ventricle, however, it was not unusual for the area of infarcted tissue to extend across into the apex region of the right ventricle as well as the left. Obviously, the trabeculae within the infarcted area were non-viable and of no experimental use. Hence, the majority of preparations used were dissected from the base of the ventricle near the tricuspid valve. Preparations were of various sizes, from 1-3mm in length and 70-200μm in diameter

(mean length±sem: 1.34±0.067 vs. 1.54±0.084 mm, and mean diameter: 162.07±6.65 vs. 173.43±7.18 μm, for sham [n=49] and ligated [n=54] animals respectively).

The trabeculae were mounted for isometric force measurement and mechanical perturbation as follows: the preparation was suspended between an Akers AE 875 force transducer and a lever system (Cambridge Technology Inc., Watertown, Mass. USA, Series 300B Lever System). The two ends of the muscle were held by nylon monofilament snares (Fig. 2.1). The snares were held within stainless steel tubing (Goodfellows Metals Ltd, Cambridge; outside diameter 200 μm, internal diameter 100 μm) and were formed by double threading a 3-4 cm length of the stainless steel tube with monofilament (7/0 *i.e.* ~30 μm diameter nylon) so that a loop was formed at the base of the tube. This loop could be tightened by pulling the free ends of the monofilament from the top of the tube. Further pieces of tubing glued to those forming the snares provide additional rigidity in the same plane as the longitudinal axis of the trabecula (as shown in Fig 2.1.).

The compliance of the transducer and lever arm was measured separately by applying weights to the end of the relevant arm in the plane of use. Two or more test weights, ranging up to ~0.01 mN, were used and the compliance measured proved to be linearly related to force. It was assumed to be linear down to the much smaller working forces. The displacement was measured using a microscope with a calibrated eyepiece. The compliance was found to be 4 μm mN^{-1} and 0.76 μm mN^{-1} for the transducer and lever end respectively, assuming a preparation length of 1.40 mm and producing 0.6 mN force. The first resonant frequency of the transducer and its assembly carrying the multi-tube snare was measured with the assembly hanging freely. It was then induced to resonate by firmly tapping the base plate upon which it was standing. The output of the transducer was pre-amplified and digitised on computer, using appropriate software, at 1 kHz. Analysis of the resonant waveforms produced by the assembly indicated that its first resonant frequency was about 240 Hz. This lies at least an order of magnitude above the highest frequency components of relevance in the present study.

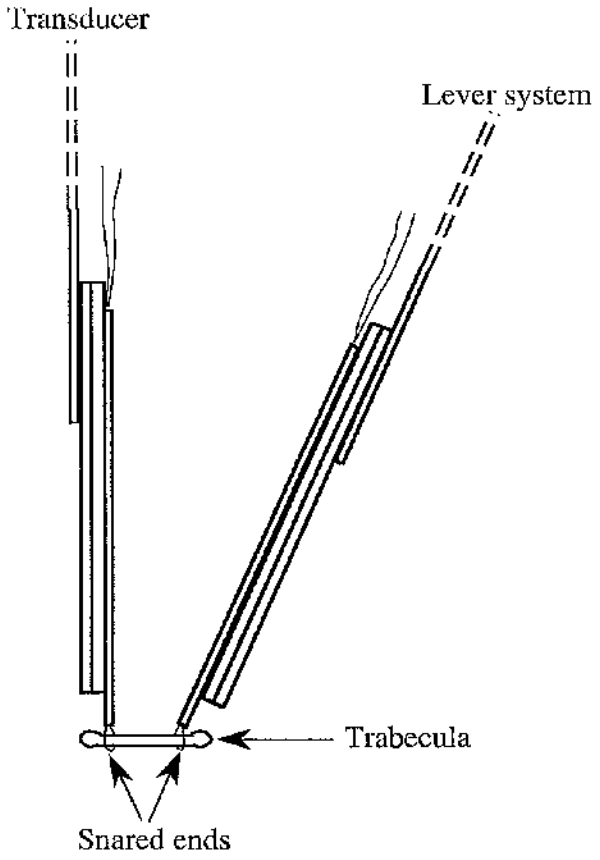

Fig. 2.1. A schematic view of the mounting of a trabecula for sinusoidal analysis. Nylon monofilament snares hold the muscle. Although not illustrated to scale in this figure, the tube diameter is generally about twice that of the preparation. Additional lengths of tube in the same plane as the long axis of the muscle offer rigidity to the whole assembly, while still keeping it thin enough to enter the microscope chamber shown in Fig. 2.2.

The assembly was mounted on a Narashige MM3 micromanipulator. This allowed fine movement in three planes to allow accurate positioning of the muscle within the bath change system and the microscope chamber. In addition, a further micromanipulator supporting the force transducer allowed fine adjustment of the snare separation to set the sarcomere length.

2.3 Measurement of Sarcomere Length

It is important to measure sarcomere length accurately and consistently in experiments such as these, as a number of physiological parameters are influenced by sarcomere length, particularly force production and its Ca^{2+} sensitivity. In preference to the laser diffraction system used in most other laboratories, a modified Vickers M-16 microscope with Differential Interference Contrast (DIC) optics (Smith, 1969) was used to examine the preparation and adjust sarcomere length to the optimal value (*i.e.* 2.1-2.2μM) for force production. The microscope lies supine. Its stage was replaced by a mounting for the transducer assembly and an observation chamber (so that the preparation can be lowered into the optical path of the microscope, Fig. 2.2). The preparation was viewed on a television monitor via a video camera which further enhanced the contrast of the DIC image. A calibrated graticule placed in the video camera mounting tube allowed the accurate measurement of the preparation from the monitor *i.e.* the snare separation was adjusted so that typically fifteen sarcomeres could be counted between two major divisions on the graticule. The length was adjusted until the number of sarcomeres in a given distance was appropriate to give a sarcomere length of 2.1-2.2μm. This observation was repeated at various parts of the preparation to ensure that the sarcomere length was maintained across the preparation. In most preparations the sarcomere pattern was consistent at several regions. There was only a small distortion of sarcomere pattern over a region representing typically less than 1% of preparation length, in the immediate vicinity of the snares, indicating relatively little damage. The distortion usually appears as hypercontracture of the region immediately adjacent to the snare.

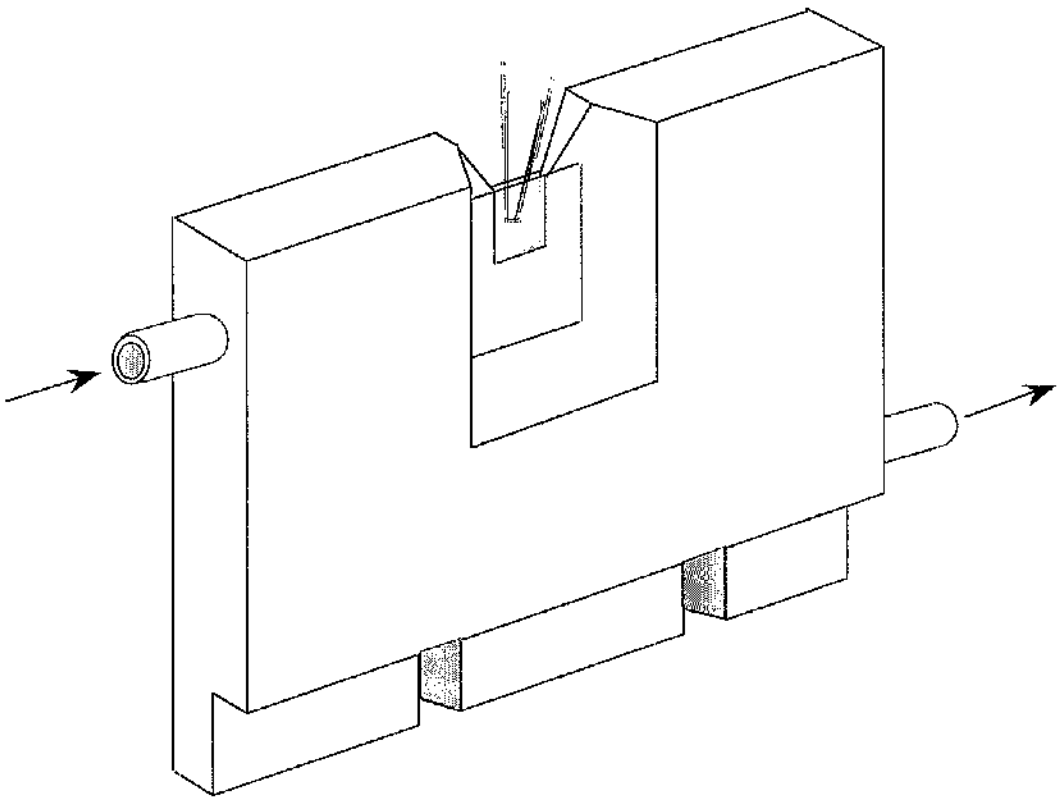

Fig. 2.2. Schematic view of the chamber used in the DIC microscope for sarcomere length measurements. The gap of 1.5 mm between the glass faces (two cover-slips) allows the mounting to gain access to the bath while being narrow enough for the optical requirements of high magnification differential interference contrast.

2.4 Measurement of Preparation Cross-sectional Area and Length

Measurement of the preparation dimensions and length was performed using light microscopy with DIC optics. Once sarcomere length was set at 2.1-2.2μM, the width, depth at various points along the length of the trabecula, and length of the preparation were measured from the calibrated graticule displayed on the TV monitor. The length of the preparation was determined from the distance measured between the snares. The snares form a sharply defined end which run perpendicular to the long axis of the trabecula. The depth of the preparation was measured by focusing backwards and forwards through the preparation and, using a micrometer on the stage, the distance moved by the preparation could be measured to within a few μm. The trabeculae were typically elliptical in cross-section and so, using average major (D) and minor (d) diameters, the cross-sectional area was calculated from the formula for the area of an ellipse *i.e.*

$$area = \frac{(\pi \times D \times d)}{4} \tag{2.1}$$

2.5 Solution Composition

The components and their respective concentrations in experimental solutions are given in detail in Table 2.1. These solutions were made by mixing the appropriate volume of the following stock solutions, which were prepared on a regular basis, and then kept frozen until needed : 1M KCl, 1M $MgCl_2$, 100 mM EGTA, 100 mM CaEGTA, 100 mM HDTA and 500 mM HEPES. The EGTA and HDTA were dissolved by adding twice the molar amounts of KOH, heating to 50-60°C, stirring continuously and allowing to cool, before adding distilled water to bring to the desired volume. CaEGTA stock was prepared in a similar way, except that $CaCO_3$ was added to the EGTA, CO_2 is driven off leaving CaEGTA. ATP and CrP were added in solid form, as disodium salts,

and the solution was then titrated to pH 7.0 with 1M KOH. Solutions with different calcium concentrations were obtained by mixing solutions A and B (Table 2.2). $CaCl_2$ was added to aliquots of solution A (Table 2.1) to achieve pCa 4.00 which, under our standard conditions, ensured maximal activation. The 'calcium-jump' method was employed to ensure rapid and near uniform activation throughout the cross-section of the preparation. This method produces a rapid increase in $[Ca^{2+}]$ by increasing the Ca^{2+} buffer concentration at the same time as the free Ca^{2+} concentration (Miller, 1975; Moisescu, 1976; Ashley & Moisescu, 1977) *i.e.* the preparation is moved to the test pCa solution after prior equilibration in solution C (Table 2.1), which has its ionic balance (0.2 M) maintained by addition of HDTA and KCl.

Soln.	K^+ *	*Mg* †	*ATP*	*CrP*	*Na* ‡	*CaEGTA*	*EGTA*	*HDTA*	*Hepes*	*pCa*
A	140	7	5	15	40	10	-	-	25	4.25§
B	140	7	5	15	40	-	10	-	25	9.03
C	140	7	5	15	40	-	0.2	9.8¶	25	7.29

Table 2.1. Composition of basic solutions (in mM except where stated; pH 7.0).

* Potassium ions added as KCl and KOH. † Magnesium ions added as 1M $MgCl_2$; free Mg^{2+}= 2.1-2.5 mM in solutions A, B and mixtures of these solutions. ‡ Sodium ions from the salts Na_2ATP and Na_2CrP. The $[Ca^{2+}]_{total}$ in all solutions was 0.02 mM due to Ca^{2+} contamination (Smith & Miller, 1982), except solution B where it was 10 mM. § $CaCl_2$ was added to aliquots of solution A to yield "full activating" solution (pCa 4.0). Total chloride concentrations varied from about 110 to 120 mM. ¶ HDTA (9.8 mM) was added to solution C to maintain the equivalent ionic strength, but lower Ca^{2+} buffering power.

Ratio A:B	pCa
1:1	6.22
3:1	5.74
5:1	5.52
8:1	5.31
10:1	5.22
15:1	5.04
25:1	4.83
$10_{activating}$	4.25
$10_{relaxing}$	9.03
$0.2_{relaxing}$	7.29

Table 2.2. pCa values for commonly used ratios of solutions A and B.
In some experiments a range of $[Ca^{2+}]$ was produced by mixing '$10_{activating}$' and '$10_{relaxing}$' solutions. The above shows commonly used ratios of these solutions and their respective pCa values.

2.6 Chemical Skinning

The mounted trabecula was exposed to solution B containing 1% Triton X100 for 30 minutes. The Triton X-100 was then removed by washing the preparation in fresh solution C before beginning the experiment. Treatment with this non-ionic detergent results in the complete disruption of surface and intracellular membrane diffusion barriers, while leaving the myofilaments functionally intact (Miller, Elder & Smith, 1985). After chemical skinning, the bathing solution surrounding the preparation essentially becomes an extension of the intracellular environment. Therefore, any intervention that influences the contractile response of the preparation can be attributed to a direct action on the myofilaments.

2.7 pH Measurement and Buffering

The pH of solutions used in these experiments was accurately measured and tightly buffered. Within our laboratory, separate reference and pH electrodes are used (Ciba Corning Diagnostics Ltd., Essex, England) to give a reliable measure of pH, in response to criticism of general pH measuring technique raised by Illingworth in 1981. The pH of experimental solutions was adjusted using a null point method. The electrodes were allowed to equilibrate in a standard solution (6.08 mM KOH, 197mM KCl and 25mM HEPES) calculated to have the same pH_a (H^+ activity) and ionic strength as the experimental solutions (Harrison *et al*, 1988). HEPES (25mM) was included in all experimental solutions to minimise changes in pH that may occur during contraction (local acidosis principally resulting from hydrolysis of ATP by myofilaments).

2.8 Calculation of Free Metal Concentration and Ionic Strength

EGTA binds metal ions other than Ca^{2+} and, therefore, the affinity constants of EGTA and the other ligands (ATP, CrP and HEPES) in these experimental solutions must be known. In order to calculate free $[Ca^{2+}]$ it is important to take account of the concentration of other ionic species and other experimental variables such as pH and temperature.

The REACT computer program (Smith & Miller, 1985) was used to assess free ion concentrations of experimental solutions. The free metal concentration of the various commonly used mixtures of solutions A and B are given in Table 2.1. Ionic strength was defined using the following equation (see Miller & Smith, 1984):

$$I_e = \frac{1}{2}\Sigma c_j z_j \tag{2.2}$$

where I_e is ionic strength, defined as the total of the ionic equivalents and cj is the concentration of the jth ionic species and z_j is its valency. This expression is found empirically to be a more consistent description of ionic strength for the present media, with several polyvalent anions present, than the more conventional formal ionic strength *i.e.*

$$I_f = \frac{1}{2}\sum c z^2 \tag{2.3}$$

2.9 Automated Solution Change System

A computer-controlled solution change system was employed in all experiments. Solutions were contained within a series of wells (volume 4.65ml) cut into a Perspex block and were continuously stirred by a small stainless steel paddle driven by an electric motor. A solution change was made by lowering the Perspex block, moving it horizontally under the preparation and raising it to immerse the preparation in the required solution. Horizontal and vertical movements of the wells were made by two stepper motors controlled by a 486 PC using in-house software. The speed of these stepper motors was such that, if required, a solution change could be made within 200ms. One of the many advantages of this system is a reduction in 'carry-over' of solution from one bath to the next. Previous checks performed in this laboratory (e.g. Harrison *et al,* 1988) have shown that the emergence of the trabecula through the meniscus of the solution, as the Perspex block is lowered, removes any significant adhering droplets and therefore minimises subsequent contamination of the new experimental solution.

2.10 Data Handling and Analysis

In all experiments the output of the force transducer was displayed on a chart recorder (Gould TA11), after being pre-amplified and filtered at 50Hz (roll off 18 dB decade^{-1}), comfortably above any frequency components relevant to the present experiments. Simultaneously the signal was digitised at appropriate rates, typically 400 points per second during sinusoidal oscillation and 40 points per second at all other times, using MacLab and the commercially available software. Data can then be transferred to Macintosh data handling and graphics programmes such as Igor Pro (ver. 3.3) and MacDraw II, within which they can be scaled and annotated prior to obtaining a hard copy via an Apple Laserwriter.

2.11 Statistical Analysis

Statistical analyses were performed using Microsoft Excel (ver. 5.0a). Collected data are reported as mean±sem, unless otherwise stated. Significance of difference was taken at the 5% level.

2.12 Control of Lever System

The lever system was under the control of a 486 PC clone. In-house software allowed accurate control of the distance moved by the lever and the frequency at which it produced the sinusoidal length changes. The distance moved by the lever tip had previously been calibrated under 400x magnification using a calibrated electron microscope graticule at the microscope, however, the effective magnification was enhanced by viewing on the television monitor.

2.13 Sinusoidal Length Change Experiments

Sinusoidal analysis was used to determine the mechanical behaviour of the Triton-skinned trabeculae. This method, although previously used by others (*e.g.* Steiger & Rüegg, 1969), was first rigorously analysed and described by Kawai and Brandt in 1980. The trabeculae were subjected to small-amplitude (≤ 1% of muscle length), sinusoidal oscillations of length at several frequencies, ranging from 0.125-12.5 Hz. This small length change was used for this protocol to avoid stretching the crossbridges beyond their working stroke (originally elucidated by Huxley and Simmons in 1972 and currently still controversial, but reported by various groups to be between 4 and 20nm e.g. Molloy *et al,* 1995; Ishijima *et al,* 1996; Mehta *et al,* 1997; Guilford *et al,* 1997) which would force them to detach from actin and consequently re-attach, as in stretch-release protocols (e.g. Jung *et al,* 1988; De Winkel *et al,* 1993) which examine the kinetics of crossbridge reattachment. This range of frequencies was chosen since observations made during preliminary protocols noted that the stiffness of the muscle was generally maximum at around 12.5 Hz. The sequence that the frequencies were applied was examined and the order that they were imposed did not affect the mechanical behaviour of the preparations. Therefore, during the sinusoidal perturbation protocol, the imposed frequencies were generally sequentially decreased and then at the end of the run, the frequency was stepped back to the highest frequency . Muscle force (F) and length (l) signals were digitised simultaneously after pre-amplification. This protocol is illustrated in Fig. 2.3., which shows the force and corresponding length outputs obtained when a maximally Ca-activated trabecula is subjected to sinusoidal perturbation over the range of frequencies just described.

The sinusoidal oscillations were applied to both resting and Ca-activated preparations, and in some cases to preparations in ATP withdrawal-induced rigor. The

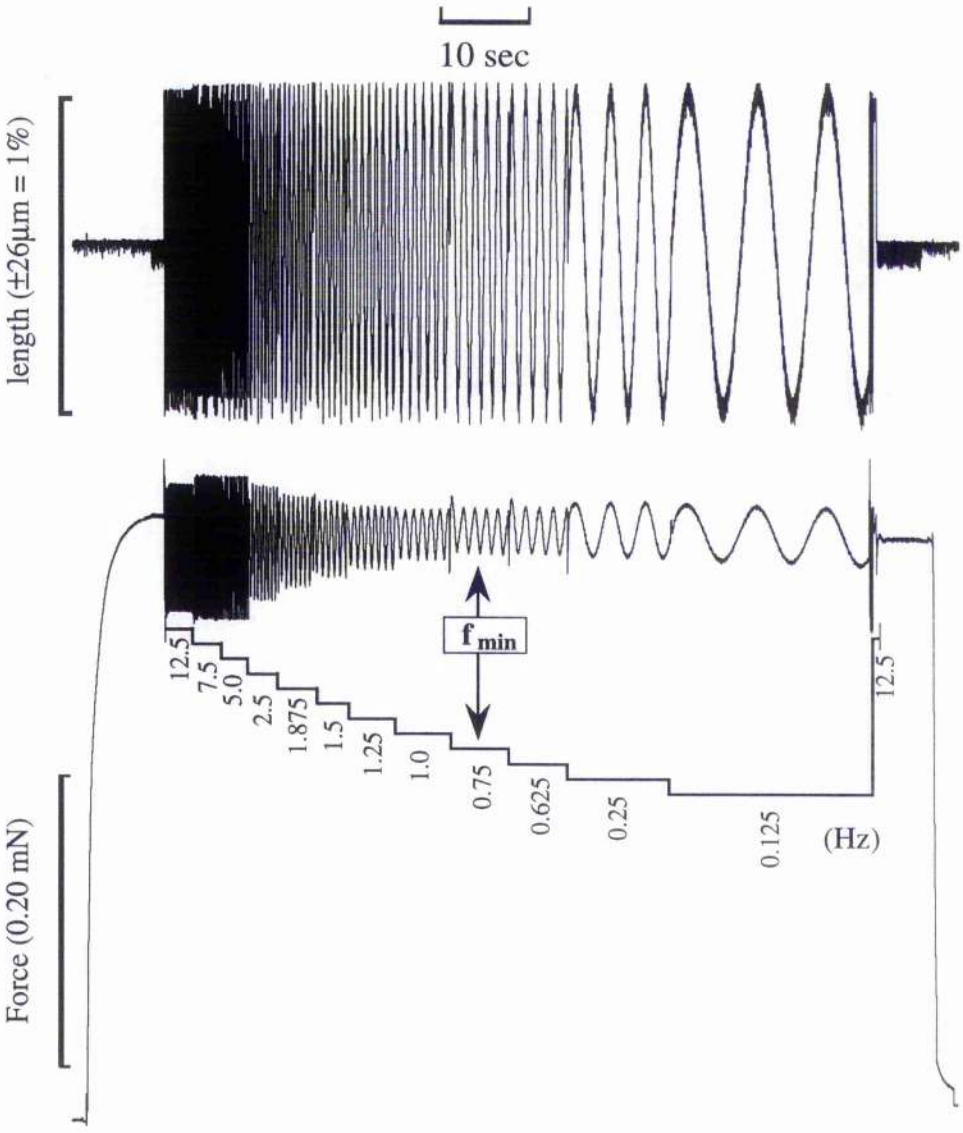

Fig. 2.3. Maximal Ca-activated force (**F**, lower trace) is evoked and muscle length (**l**) oscillated at various frequencies (**f**, upper trace). The stiffness ($\Delta F/\Delta l$) varies with **f** and is minimal at 0.75Hz ($=f_{min}$) in this example.

sinusoidal length signal and corresponding force response of the muscle gave rise to dynamic stiffness and phase data at the discrete frequencies examined.

2.13.1 Muscle stiffness

The ratio ΔF/Δl defines 'instantaneous' muscle stiffness. The amplitude of the force transient was measured at each imposed frequency after the sinusoid had stabilised; this typically occurred within less than one cycle of the waveform, even at the highest frequency (see Fig. 2.4.). Dynamic stiffness can then be plotted as a function of oscillation frequency. In a Ca-activated muscle, this type of plot yields a characteristic minimum in stiffness amplitude at a discrete frequency, termed f_{min} (see Figs. 2.3. and 2.5.). This finding is similar to that obtained by other workers who have used sinusoidal analysis. f_{min} is an index of mean crossbridge cycling rate (Kawai & Brandt, 1980; Rossmanith, 1986: see discussion chapter 3).

Fig. 3.5 (in results, chapter 3), shows that f_{min} was unaffected by altering the level of Ca-activation. Since f_{min} was unaffected by altering Ca-activation levels, the trabeculae were maximally activated throughout experimental protocols, to eliminate any possible influences that sub-maximal activations may have on contractile protein contraction kinetics.

In a resting muscle, dynamic stiffness is essentially frequency-independent (see Chapter 3 results). The stiffness at rest provides information about the passive properties of the muscle and can be attributed to many factors, for example the giant protein titin (Linke *et al,* 1994) connective tissue such as collagen (Doering *et al,* 1983; Kovanen *et al,* 1984) and elastin (Granzier & Irving, 1995), and/or, in the case of disease states, the extent of tissue fibrosis.

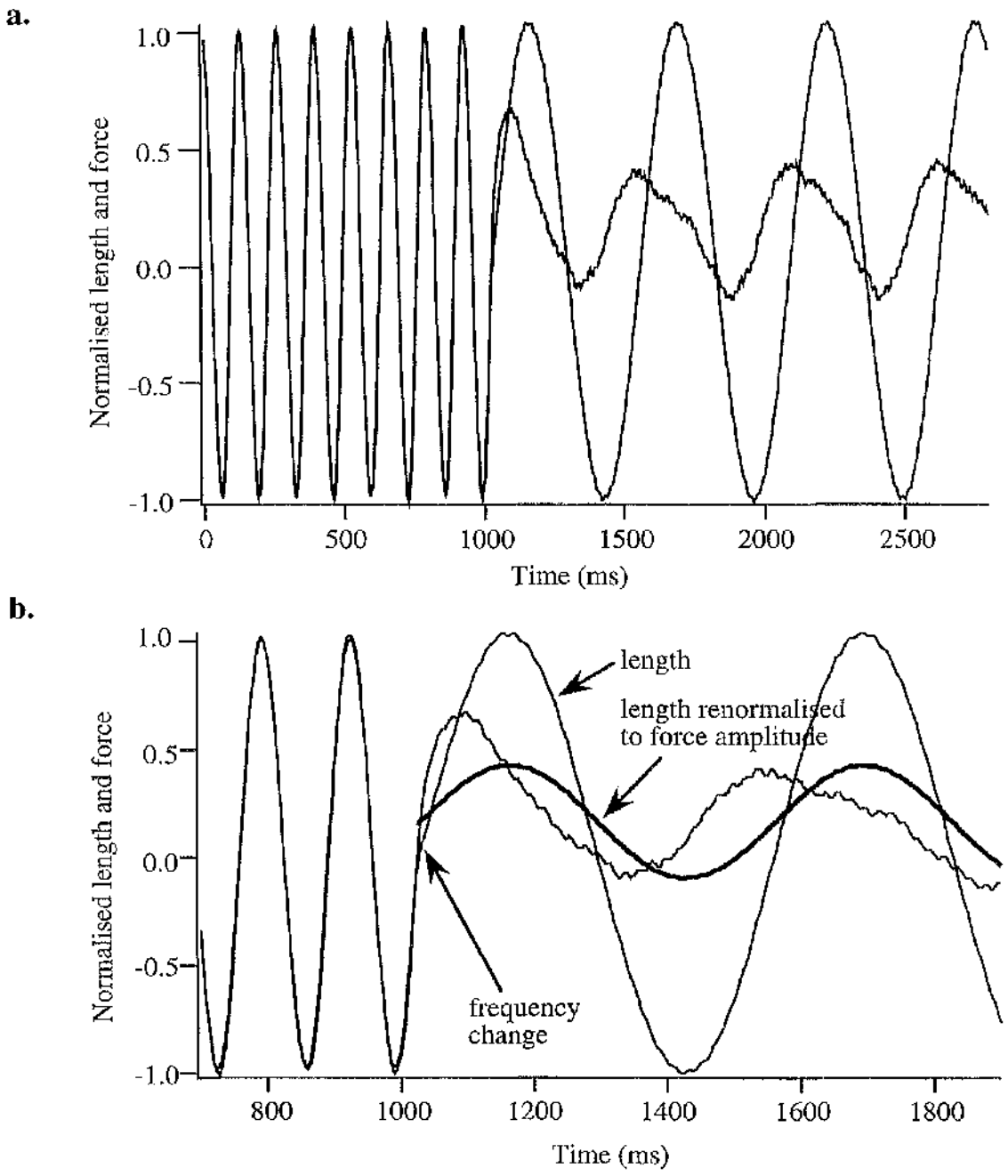

Fig. 2.4. Oscillation frequency transition between 2.5 Hz and 1.88Hz. **a.** experimental trace showing length and force vs time. **b.** close up of the frequency transition shown in trace **a.**, however, in this example the length waveform has been normalised to the force amplitude in order to calculate the phase shift. Both traces show that after a frequency change the force waveform stabilises within one cycle of the waveform.

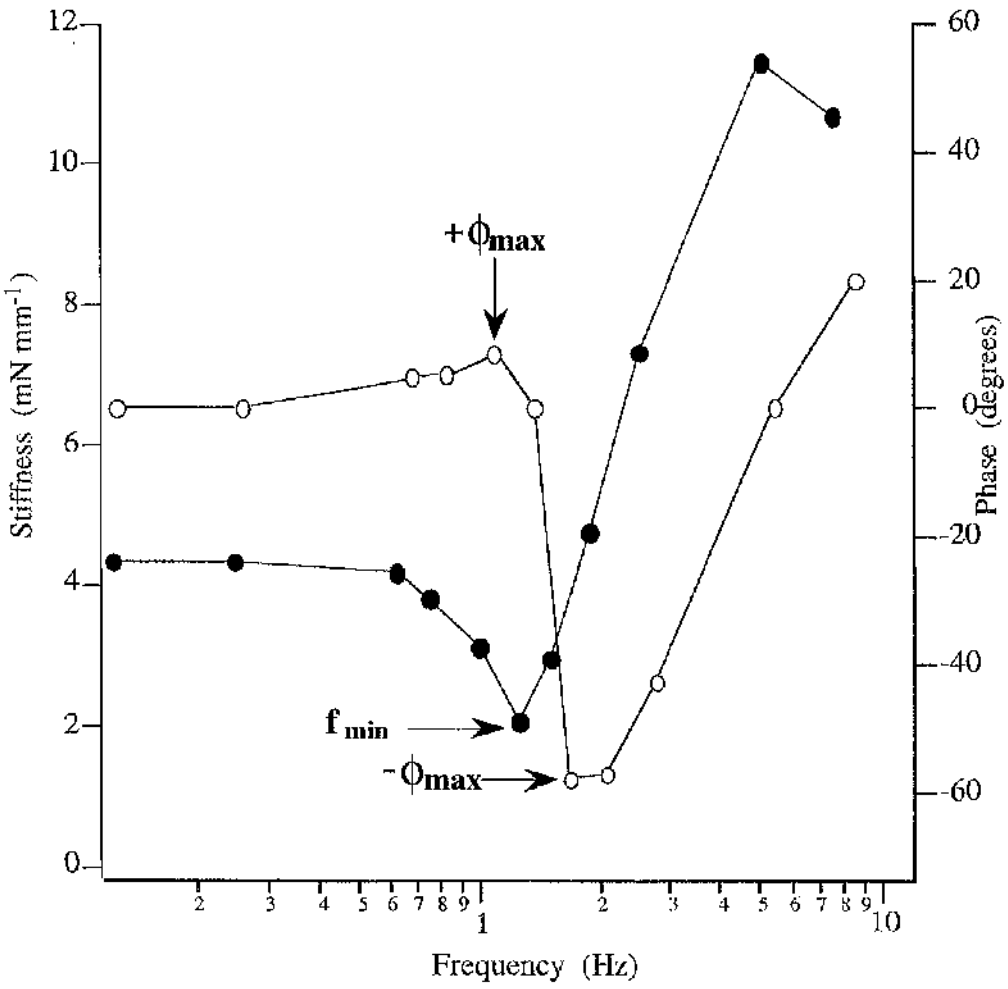

Fig. 2.5. Frequency plots of dynamic stiffness (●) and phase (○) obtained from sinusoidal perturbation of a maximally Ca-activated trabecula.

2.13.2 Phase shift

The phase relationship (ϕ) between the force and length signals was also examined. Phase shift is calculated from the time difference between the two signals which is related to cycle period and then expressed in degrees. For phase shifts of 0° and 360° the waveforms are superimposable. Figure 2.6. depicts a theoretical example of phase shift between two sinusoidal waveforms representing force and length. In this example, a 180° phase shift has been chosen to illustrate the maximal phase difference that can be observed between the two steady waveforms *i.e.* the two waveforms are fully

'out of phase'. In these experiments, the development of phase shift immediately after a frequency change, or at the start of oscillation altogether, could be observed. This confirms that phase shift was never greater than about 90°, *i.e.* the force wave never lagged or led by more than a fraction of one wavelength. The ϕ value obtained was rather arbitrarily measured at the mid-point of the rising phase of the length waveform (the 'stretch' phase). This type of analysis yielded either a positive ϕ value, indicating a phase lag of force behind length, a negative ϕ value, indicating a phase lead of force before length, or a zero ϕ value where the force and length sinusoids were in phase with one another. When plotted as a function of frequency, the phase data produced a plot broadly similar in shape to that of the dynamic stiffness data (see Fig. 2.5.).

It should be noted here that over the course of the experiments described in this thesis the number of frequencies imposed upon a trabecula was reduced, thereby shortening the period of oscillation. This allowed more interventions to be investigated within a single protocol. Having examined several different protocols, I was confident that the resultant 'profile' obtained with the shortened oscillation period did not distort the stiffness-frequency or phase-frequency plots.

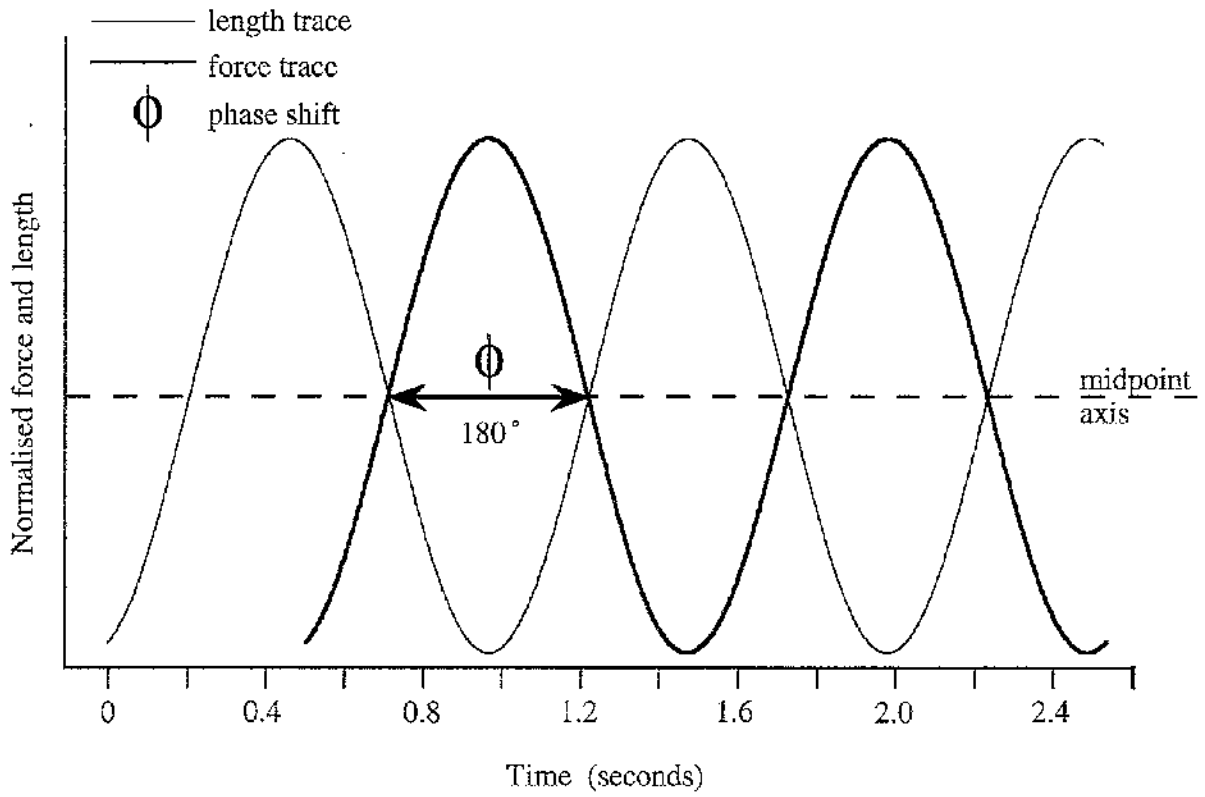

Fig. 2.6. Theoretical illustration of phase shift between length and force waveforms. Phase shift (f) is a function of time expressed in degrees (°). In the above illustration, at 1Hz, the ϕ observed between the two waveforms is 180° i.e. the two waveforms are fully out of phase.

2.13.3 Oscillatory work and power

Net oscillatory work at a given frequency, W(f) and the associated power, P(f) output of the muscle can be derived from the information revealed by both the dynamic stiffness and the phase plots (Rossmanith *et al*, 1986), and are given by

$$W(f)=2\,X(f)\sin\phi \tag{2.4}$$

$$P(f)=W(f)\,f \tag{2.5}$$

where f denotes frequency, ϕ phase and X(f) the value obtained when stiffness is normalised to the maximum force generated by the muscle. Positive values for W(f) indicate that, for that frequency, the muscle is generating net external work on the apparatus. Negative values indicate that, for that frequency, the apparatus is doing work against the muscle, or alternatively, the muscle is absorbing net oscillatory work. The frequency at which f_{min} occurs, or at which maximum work done (f_w) or maximum power (f_p) is displayed, have all been used as indicators of crossbridge kinetics (Steiger & Rüegg, 1969; Kawai & Brandt, 1980).

2.13.4 Procedure for quantifying oscillatory work and power values

This formula (2.4) given by Rossmanith *et al*, used above for calculating work and power, does not necessarily provide an accurate assessment of the capacity of the muscle to generate or absorb oscillatory work. When examining the force and length waveforms, it was noticed that the phase shift was not constant throughout a given cycle, although the pattern remained constant from one cycle to the next. Thus, the observed force waveform was not always a perfect sinusoid, as assumed by (2.4), in contrast to the imposed length waveform. This would result in an inaccuracy because of over- or under-estimation of the oscillatory work/power generating or absorbing capacity of the muscle, depending on how much the phase shift deviated from the ideal.

The ideal form is that produced by a constant phase shift throughout a cycle which yields an elliptical length vs force plot. If the phase shift is 90°, the plot describes a circle (as in Fig 2.7.). Examples of how the descending and rising phases of the waveform differed from this ideal are shown in Fig. 2.8. If they differed at all, it was observed that the phase shift on the falling phase was generally of the same sign, but smaller or larger than the phase shift on the rising phase (as in Fig. 2.8 (a)). Very occasionally, phase shift could reverse the sign between the rising and falling phase (see Fig. 2.8 (b)). The latter case produces a loop that crossed over itself (see Fig. 2.9.).

It was therefore necessary to calculate individual correction factors for all the preparations used in the work and power analysis to take account of the deviation from the ideal. This factor, which quantifies the length vs force loop assymetry (the 'loop' factor), was then used to scale the value obtained from equation 2.4 to give the final accurate value. The following procedure for determining the correction factor was used:-

i . The length signal, a perfect sinus, was duplicated and then offset by a time equal to the observed maximum ϕ value (see Fig. 2.10.), such that the midpoint of the rising phase of the two waveforms (length sinus and force) corresponded with one another.

ii . These waveforms were plotted to produce two loops *i.e.* a length vs force loop and an 'idealised phase shifted force' vs length loop, the latter of which produced an ellipse, which were then superimposed (as in Fig 2.11.).

iii . The area under these loops was calculated. The ratio between the two defines the loop factor. This factor was then multiplied by the value obtained from the previous calculation using equation (2.4) to give the final corrected value for either the work/power generated or absorbed by the preparation. The actual results generated by this method are discussed further in chapter 4.

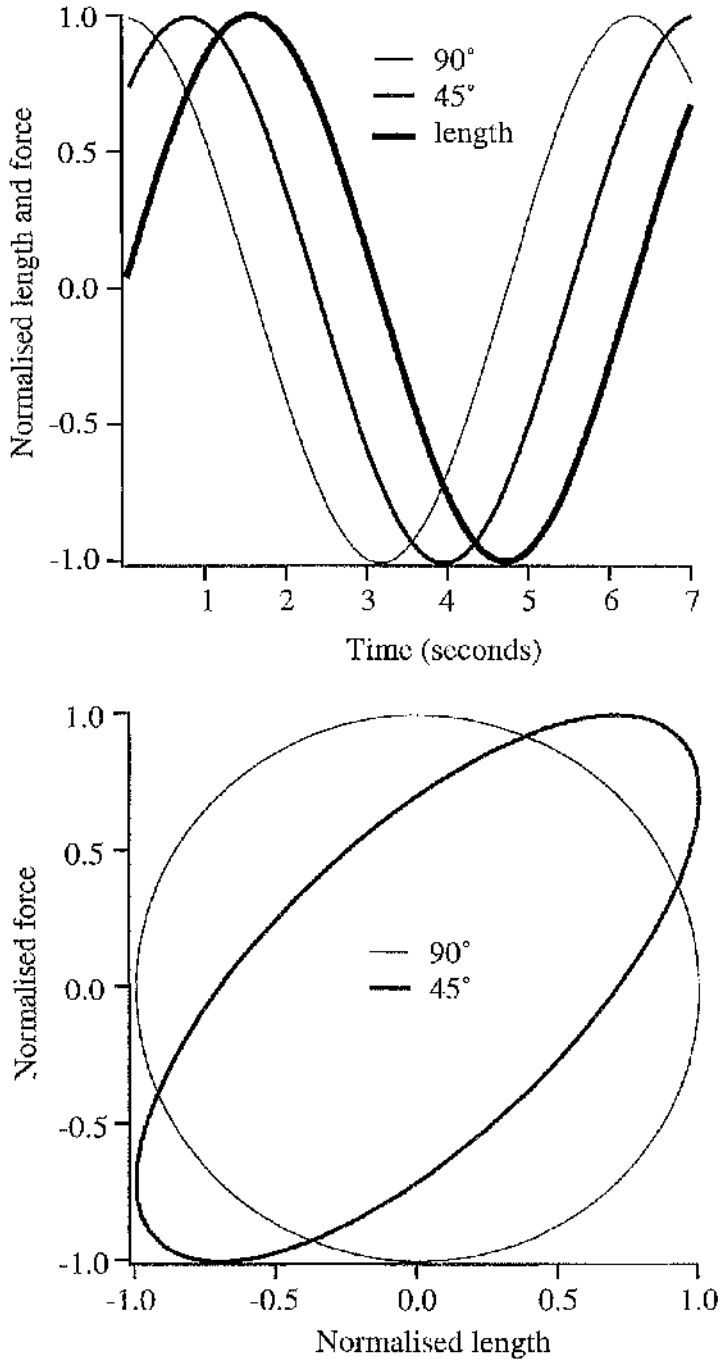

Fig. 2.7. Idealised phase shift for pure sinusoidal waves. **a.** diagrammatic representation of length and idealised force waveforms corresponding to 45° and 90° phase shifts. **b.** the corresponding force vs length plots for the waveforms shown in **a.** As described in the text, a 90° phase shift describes a circle, whereas a 45° phase shift yields an ellipse.

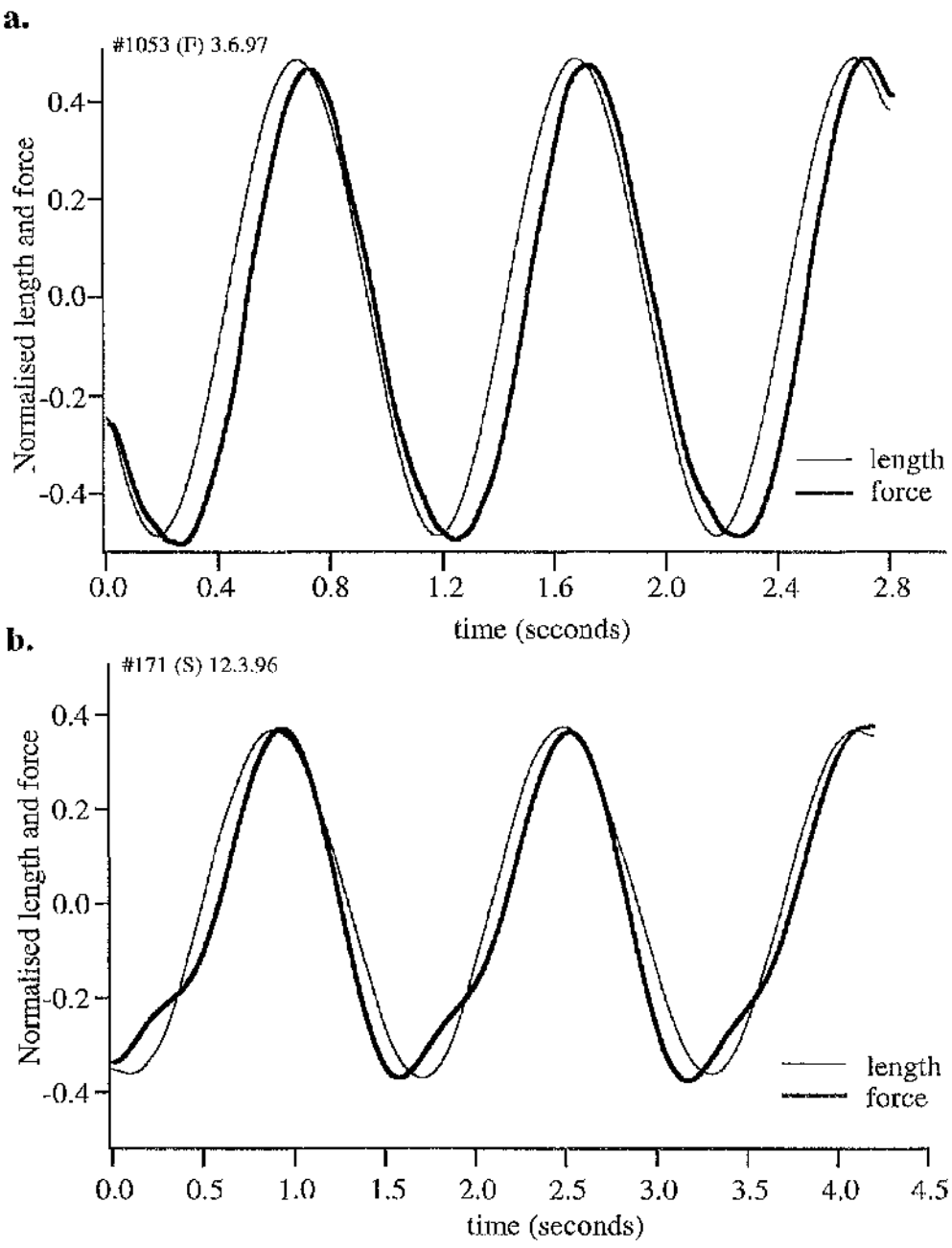

Fig. 2.8. Length and force waveforms illustrating that the phase shift observed between the waveforms on the ascending limb may differ from that observed on the descending limb. **a.** the observed phase shift between the ascending limb of the waveforms is of the same sign, but is much larger than the phase shift observed between the descending limbs. **b.** the phase shift observed between the ascending limb of the waveforms is of the opposite sign from the phase shift observed on the descending limb.

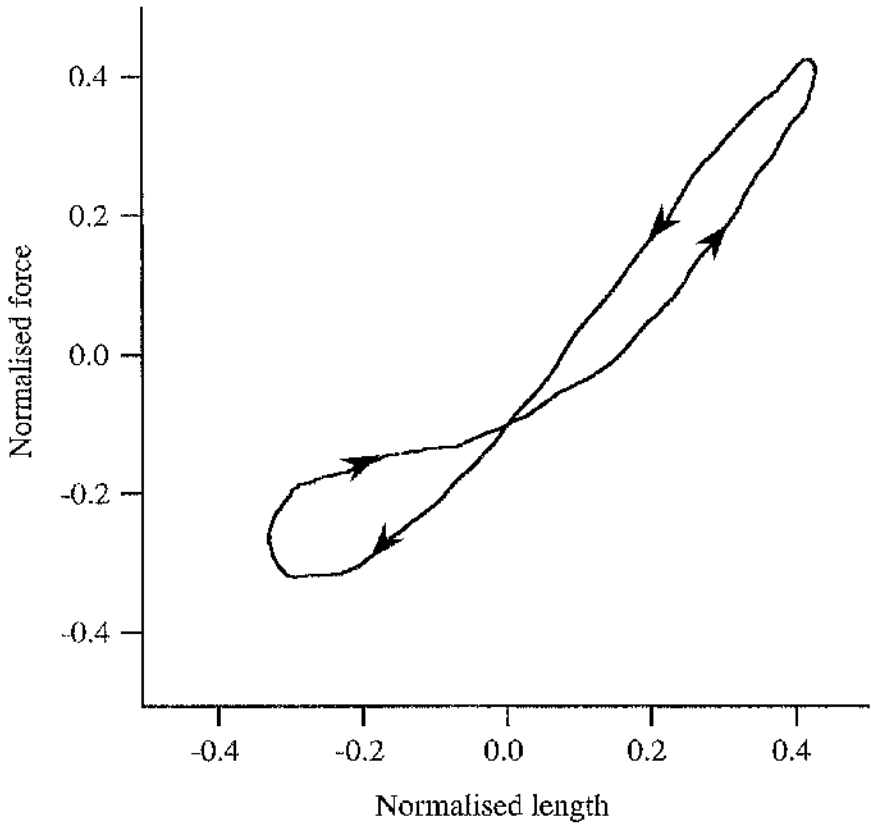

Fig. 2.9. Example of a force vs. length loop (corresponding to the waveforms shown in Fig. 2.8. b.) where the phase shift on the ascending limb of the waveform is of the opposite sign from the descending limb, therefore the loop crosses over itself.

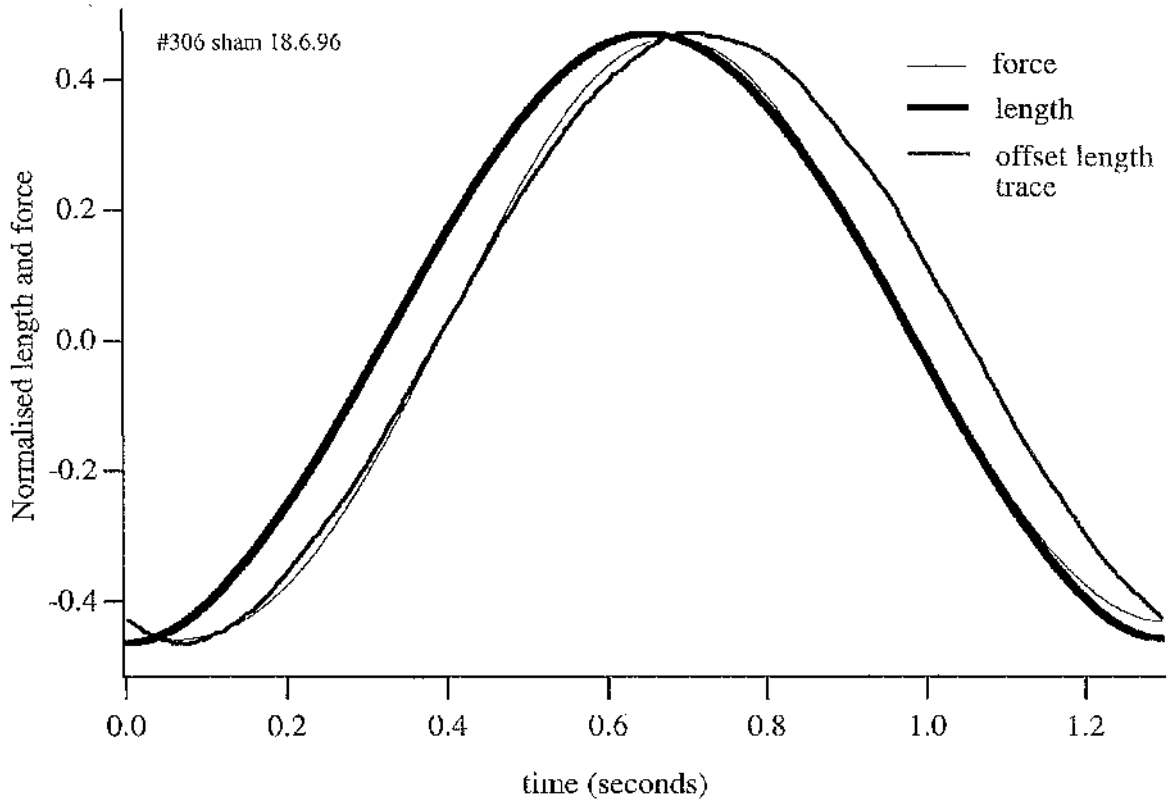

Fig. 2.10. Graph showing normalised length and force waveforms against time at 0.75 Hz. The length waveforms are perfectly sinusoidal, whereas the force waveform is slightly distorted. The length waveform that lies towards the right is a duplicate of the original length waveform, but it has been displaced in time, corresponding to that calculated to be equal to the phase shift observed at this frequency (see text for details). Hence, the rising phase of this waveform and the rising phase of the force waveform now lie upon one another as far as is possible. In this example force is lagging behind length therefore the muscle is performing oscillatory work.

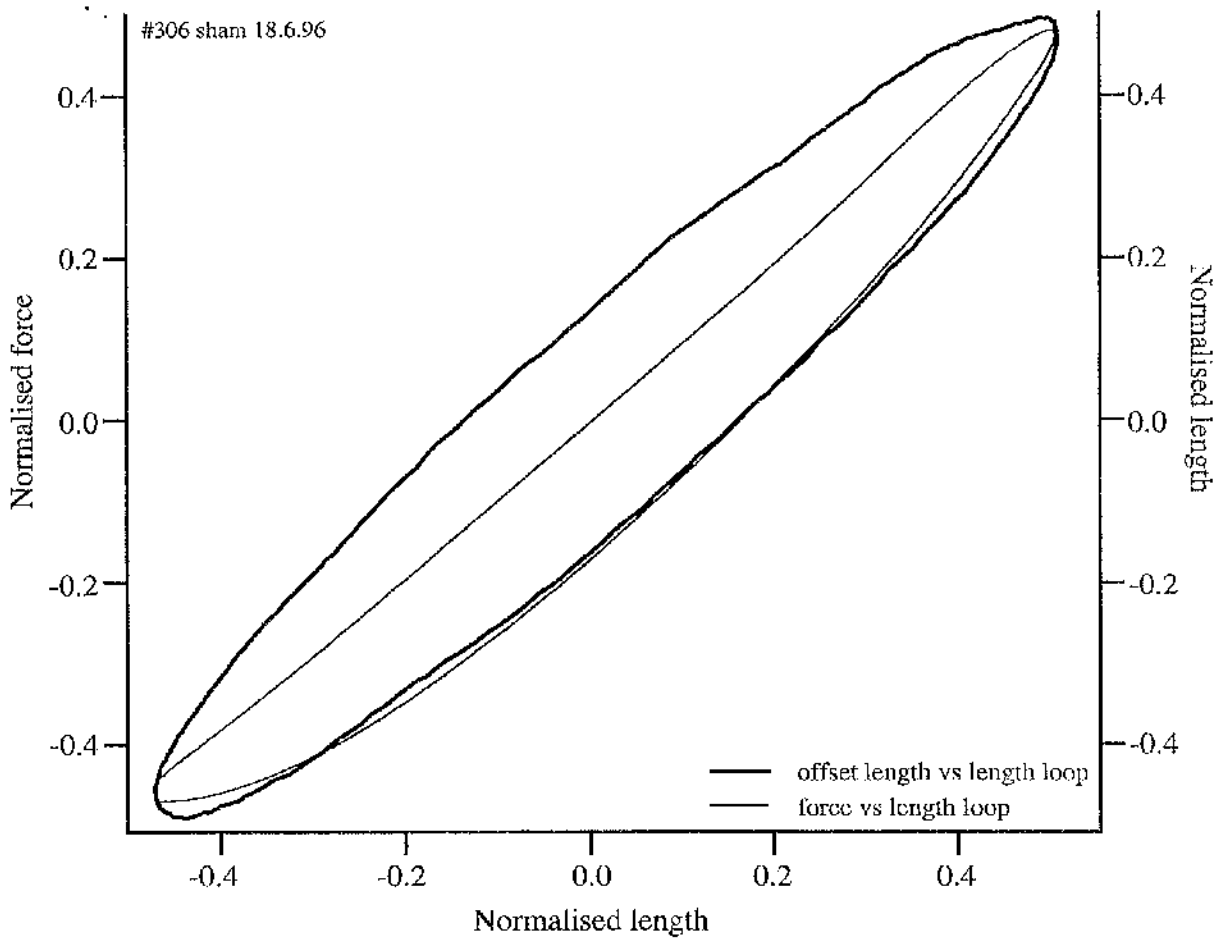

Fig. 2.11. Graph showing the length vs length loop superimposed upon the force vs length loop (corresponding to the waveforms in Fig. 2.10).Clearly the area under the two loops do differ from one another. In this example the area under the loops determines the work performed by the trabecula, since these loops correspond to those in Fig. 2.10 where there is a positive phase shift. The ratio of the area under these loops determines the correction factor used to calculate the actual work/power output for this trabecula.

2.14 Relaxation Rate Experiments

The trabeculae were mounted for isometric force measurement as previously described (methods section 2.1), and skinned in Triton X-100 for 30 minutes. The preparations were then activated in solution D, at a low [Ca^{2+}], in order to allow force to develop slowly until reaching approximately maximum force. This slow activation ensured that at any one time, the myofilaments across the entire preparation were partially activated. Since all the myofilaments are only partially activated, the preparation could be relaxed at any point during contraction without significantly influencing results, however, as mentioned above, the preparations were routinely allowed to develop 70-80% of the previously measured maximum force. While the preparations were developing force, force was recorded, as described previously, and digitised at 40 Hz. Once the preparations had developed sufficient force, the digitising rate was increased to 400 Hz, to ensure that enough data points were recorded to examine the rate of relaxation, and the preparation relaxed. This protocol was repeated for each of the solutions E-I, which differed in their [EGTA], allowing a two minute period in between each cycle of contraction and relaxation, where the preparation was immersed in solution E, (see fig 2.12.). This protocol was also repeated in a random order to examine whether the sequence of application of the solutions affected the results. The results did not significantly differ between these protocols, so the order in which they were applied was concluded to be irrelevant.

The composition of solutions used for these experiments is as follows:

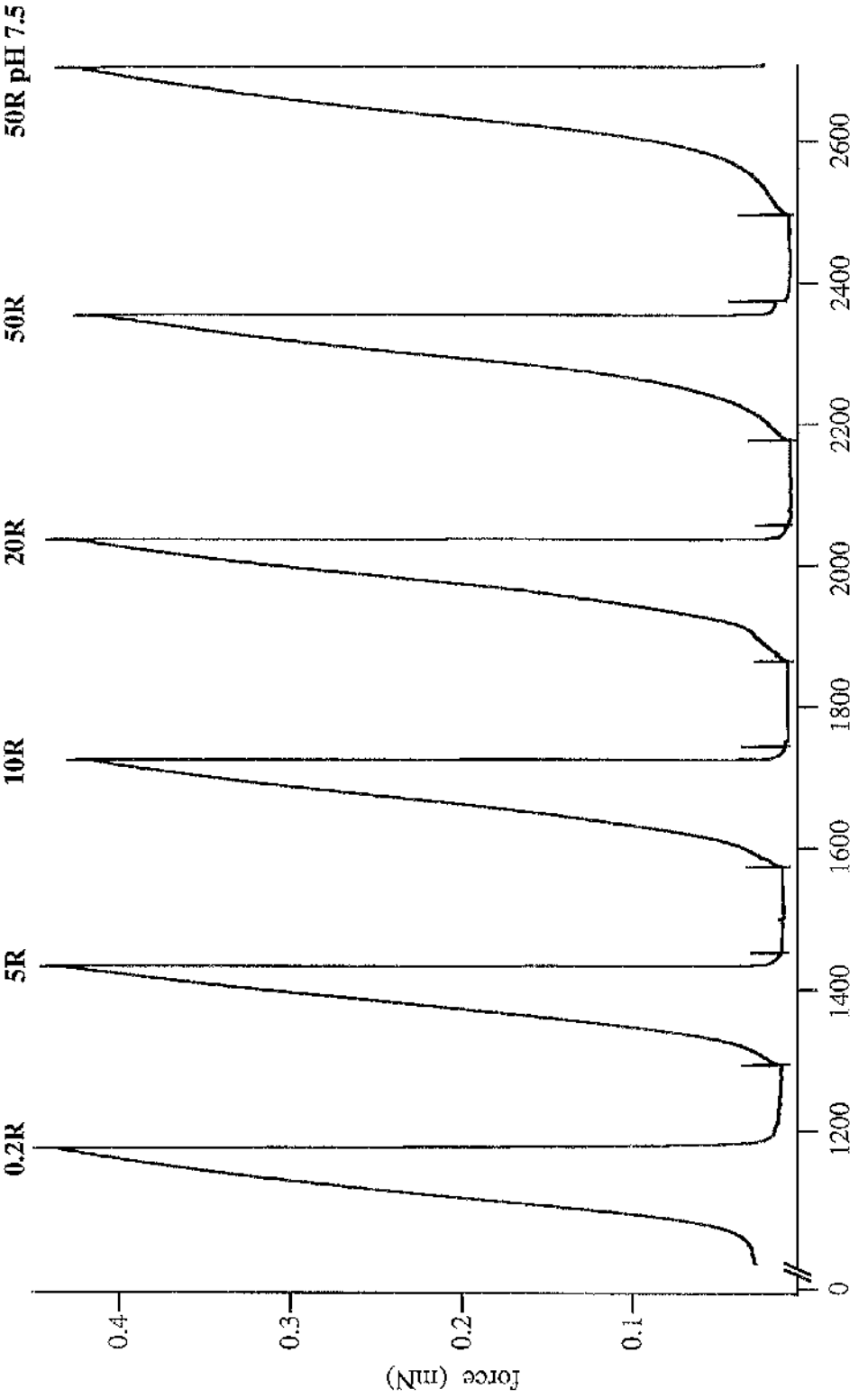

Fig. 2.12. Experimental trace showing the fast relaxation protocol (as described in methods section 2.14). A close up of one of these relaxations (5R), on an extended time scale, is shown in Fig. 2.13.

Soln.	K^+ *	*Mg* †	*Free Mg*	*ATP*	*CrP*	*Na* ‡	*EGTA*	*CaEGTA*	*Free Ca*	*HDTA*	*Hepes*
D	140	7	2.23	5	15	40	-	0.2	13.6μM	49.8	25
E	140	7	2.22	5	15	40	0.2	-	65.70	49.8¶	25
F	140	7	2.15	5	15	40	5	-	2.39	45¶	25
G	140	7	2.09	5	15	40	10	-	1.20	40¶	25
H	140	7	1.96	5	15	40	20	-	0.59	30¶	25
I	140	7	1.67	5	15	40	50	-	0.24	0	25

Table 2.3. Composition of solutions for relaxation rate experiments (in mM, except free Ca which is in nM unless otherwise stated; pH 7.0)

*, †, ‡ and ¶ as detailed previously in the text following table 2.1.

2.14.1 Curve fitting

The relaxation transients (for example see Fig. 2.13) were well fitted in all cases with a single exponential curve (see Fig. 2.14.) after the first 5-10% of force fall. Fitting was done with the program Igor Pro ver. 3.3. and the following equation:

$$y = A + B * exp^{(-k_r * t)} \tag{2.6}$$

where A is the residual force, B is the initial force value minus the residual, k_r is the rate constant for relaxation and t is time in seconds. The value of k_r obtained from each relaxation transient, for a single preparation, was then plotted against [EGTA]. The points were satisfactorily fitted with a rising exponential curve, using the same program detailed above, and the following equation:

$$y = C * [1 - exp^{(-k_E * D)}] \tag{2.7}$$

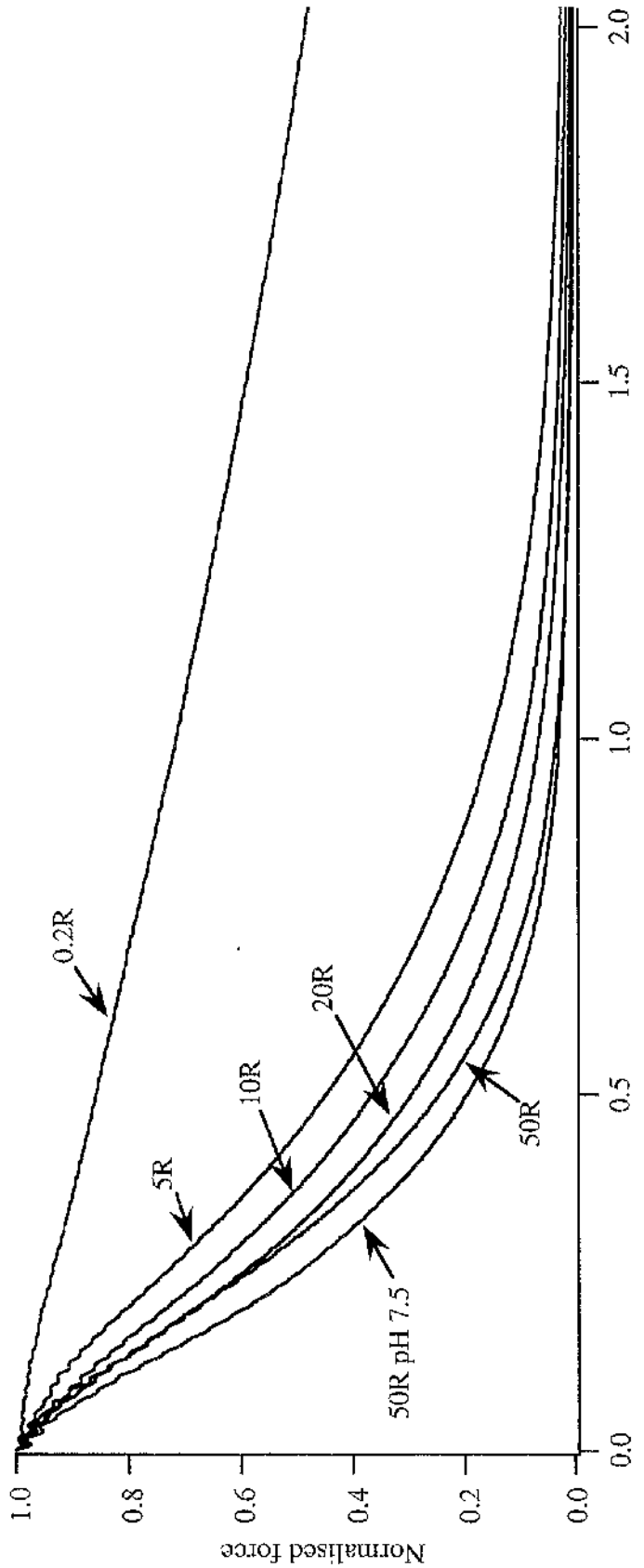

Fig. 2.13. Relaxation transients from a single run of the relaxation protocol (corresponding to Fig. 2.12.), described in section 2.14, on an extended time scale. The transients were well fitted with a single exponential curve fit in all cases (not shown in this example, see Fig. 2.14. for example of curve fitting). The time scale has been normalised to the start of the solution change that initiates relaxation, whereas force has been normalised to the force before relaxation began.

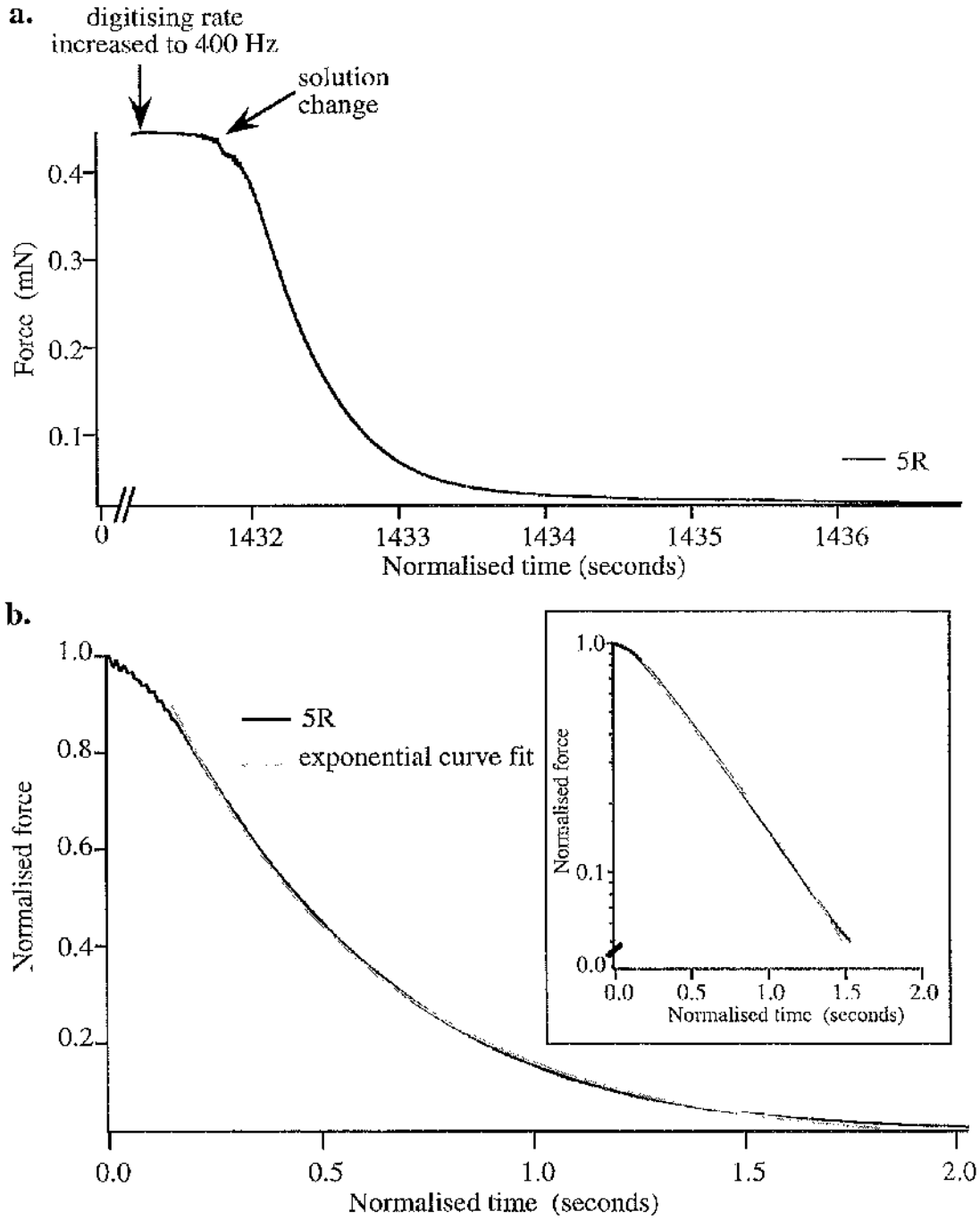

Fig. 2.14. Relaxation transients for a solution change into a 5 mM EGTA relaxing solution, shown on extended time scales (corresponding to 5R in Fig. 2.12.). **a.** Actual relaxation transient from experimental trace showing at which point the digitising rate is increased and where the solution change occurs. **b.** the same relaxation transient as in **a.**, with the corresponding single exponential curve fit, however, this time force has been normalised to the force immediately before the onset of relaxation, and time has been normalised to the onset of relaxation. Inset shows same transient and curve fit as a semi-log plot and, as expected for a single exponential process, both traces produce a straight line provided the residual is small.

where C is the offset, k_E is the rate constant for the rate of change of force at the various [EGTA] and D is the [EGTA]. Equation 2.7 calculated the maximum rate of relaxation obtained from the line of best fit, and this value was compared with the maximum rate obtained experimentally. Both the individual and mean data sets were fitted in this manner, and it was found that the mean curve and maximum rate were representative of the data set (see results chapter 5 for details).

2.15 Reactive Oxygen Species Experiments

Both the sinusoidal analysis and relaxation rate protocols were repeated after treating the preparation with reactive oxygen species (ROS). The major part of the protocols used in these experiments were very similar to those already described in the relevant sections, therefore, only the deviations from these protocols will be described here. Hypochlorous acid was prepared immediately prior to use, by adjusting NaOCl to pH 7.0 with HCl. The concentrations of HOCl quoted in this thesis refer to the concentrations of NaOCl added to the solution. Therefore at pH 7.0, the proportion of the dissociated hypochlorite anion (OCl^-) will be approximately 25% (pK_a 7.5). Hydrogen peroxide (H_2O_2) was added from a stock solution immediately before use.

2.15.1 Sinusoidal length change experiments in the presence of ROS

Preparations were mounted as described in sections 2.2. Control runs were performed (using protocol described in section 2.13) on muscle in the relaxed, Ca^{2+}-activated and rigor state. Application of the ROS hypochlorous acid (HOCl), was made to maximally activated trabeculae, once force had stabilised, as in Fig 2.15, and allowed to act for approximately 45 seconds, before the trabecula was relaxed. The effects of the ROS on maximum and resting force were apparent at this stage. The trabeculae were then subjected to ROS exposure in all of the states listed above.

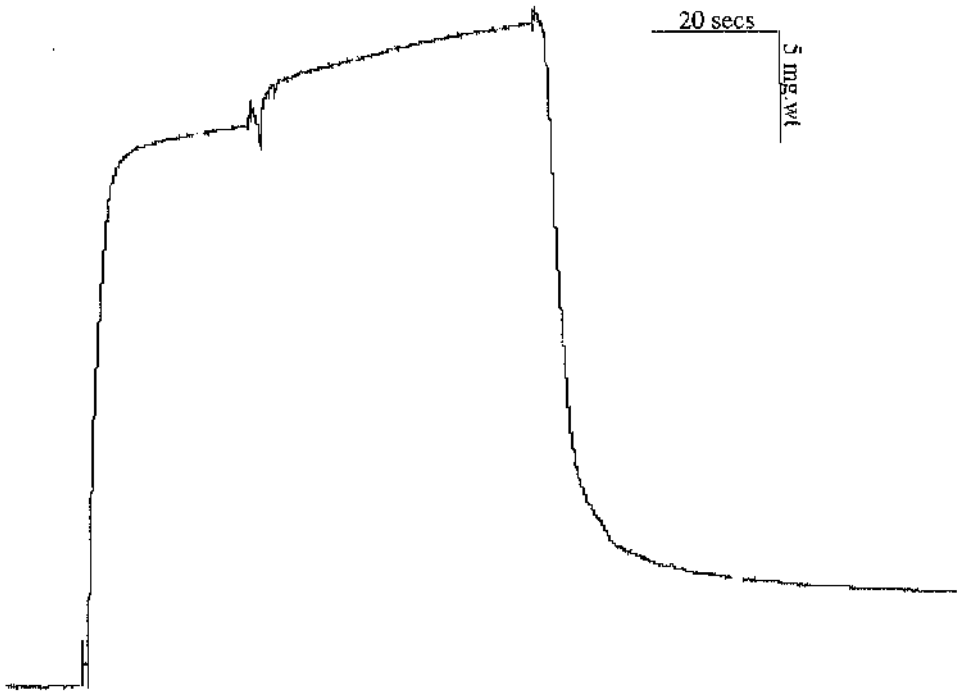

Fig. 2.15. Experimental trace showing application of HOCl. The trabecula was maximally activated (pCa 4.0) and then transferred to a similar solution containing HOCl for approximately 45 seconds. Applying HOCl increased maximum tension. After relaxing the preparation, in the absence of HOCl, resting tension failed to return to control levels. However, since resting tension increased (from nominally zero to about 17% of control in this example) the relative level of calcium-activated tension diminshed (by about 15% in this example).

2.15.2 Relaxation rate experiments performed in the presence of ROS

Preparations were mounted as described in sections 2.2, and subjected to a control run of the protocol described in section 2.14. The preparation was then maximally activated, and once force had reached a steady level the preparation was transferred to a similar solution containing the ROS. The ROS was allowed to act for approximately 45 seconds before being relaxed (as described in the previous section, and shown in Fig. 2.14). The relaxation protocol was then repeated as before.

Chapter 3

Alterations in the Contractile Properties of the Myofilaments in a Rabbit Coronary Artery Ligation Model of Left Ventricular Dysfunction

3.1 Introduction

Contractile dysfunction is one of the many symptoms observed during heart failure. The decreased contractility is characterised by a slowing of systolic and diastolic function (*i.e.* contraction and relaxation) and an overall prolongation of contraction duration. This contractile dysfunction can occur as a result of altered intracellular Ca^{2+} handling (E-C coupling), upon which much work has focused, altered energy utilisation, or as a result of changes in the properties and functioning of the contractile proteins. One of the possible factors contributing to the contractile dysfunction, at the sub-cellular level, could be alterations in crossbridge interactions. It is generally believed that the cyclic interaction of myosin crossbridges with actin is responsible for force generation and shortening in striated muscle. The crossbridges therefore, play an important role in determining the contractile status of the heart such that any alterations in crossbridge kinetics and/ or the number of cycling crossbridges could have a profound effect on the contractile activity of the heart.

Sinusoidal analysis has proved to be a useful technique for investigating crossbridge properties originally in skeletal muscle (used originally to observe oscillatory work performed in insect flight muscle: Machin and Pringle, 1959; White and Thorson, 1973), but is now widely applied to cardiac muscle. Although several groups have used variations of this technique for some time now (*e.g.* Rack, 1966; Steiger and Rüegg, 1969; Kawai, 1979) sinusoidal analysis was first rigorously described by Kawai and Brandt in 1980. Application of this technique to chemically-skinned trabeculae at rest will reveal information about the passive properties of the muscle, whereas, the same procedure in a Ca^{2+}-activated trabeculae will provide information about the dynamic properties of the muscle, such as the intrinsic crossbridge cycling rate and the number of crossbridges attached (dynamic stiffness). Slack tests (Edman, 1979) have been traditionally used to examine crossbridge kinetics. Using this technique, a sudden reduction in length is applied to an

isometrically contracting muscle and the resulting force transients are examined. The force transients to a step length change have been described in terms of four phases (Huxley and Simmons, 1973). Phase 1 represents the simultaneous change in force in the direction of the applied length change and has been more or less attributed to instant elasticity. Phase 2 corresponds to the rapid early recovery of force, thought to be due to the tensing of pre-attached crossbridges to restore force. Phase 3 represents the delayed force response in which there is a reversal of force in the direction of the applied length change, and finally phase 4 encompasses the gradual force recovery back to the original isometric force. Phases 3 and 4 are thought to be associated with crossbridge detachment and reattachment. These experiments examine the parameter V_{max}, a measure of the rate at which fully detached crossbridges cycle through several cycles to take up the slack and produce shortening. V_{max} is limited by the rate of crossbridge detachment (Edman, 1976). f_{min}, on the other hand is a measure of the mean crossbridge cycling rate, derived under isometric conditions. Another technique applying the same principles as sinusoidal analysis, but using a shorter time scale, has been favoured by other groups to investigate muscle mechanics, this technique is pseudo-random binary noise-modulated analysis, referred to as PRBN analysis (Rossmanith, 1986).

The aim of the experiments detailed in this chapter are twofold. The first part of this chapter reports the results from experiments that were performed in order to determine a suitable protocol for using the sinusoidal analysis technique on myocardial tissue. The aim of these preliminary experiments was first to establish the reproducibility of the technique and the viability of the preparations subjected to small length oscillations. This approach was particularly relevant for the free radical experiments, where an irreversible agent was tested. A time control was, therefore, required for the analysis of these results. A time control was also needed to establish whether any significant changes occurred in either f_{min} or phase shift with time rather than the frequency of oscillation, since the protocol required a significant period of time to apply the various test frequencies.

It was necessary to examine the preparation dimensions of both groups to see if they differed. This might be anticipated as a result of the remodelling of the myocardium which may have occurred within the ligated group. Additionally, so that a direct comparison of myocardial mechanics could be made, it was also necessary to examine the ability of trabeculae from both groups to generate force, and subsequently, to assess their Ca^{2+}-sensitivity and establish whether they were or were not significantly different. If all these features did not differ significantly between groups, then the interpretation of results comparing the myocardial mechanics of the two groups is much more straightforward. Indeed, any alterations in f_{min} or phase shift observed between the two groups can be directly attributable to alterations in contractile protein kinetics of the failing myocardium.

Once this was established, it was necessary to determine whether or not the choice of activation level would influence results. Some studies have reported that the degree of activation can influence crossbridge kinetics (*e.g.* Wolff *et al,* 1995). However, other studies have found that the crossbridge cycling rate is unaffected by activation level (Rossmanith *et al,* 1986; Shibata *et al,* 1987; Hajjar & Gwathmey, 1992). Any possible influences that sub-maximal activations may have on contractile protein contraction kinetics can be eliminated by maximally activating the trabeculae (*e.g.* at ~ pCa 4.0). However, it remains necessary to determine whether or not using fully activated preparations would provide adequate information to define myocardial crossbridge kinetics. To assess this, trabeculae were subjected to sinusoidal oscillation at a range of pCa values. The results from these experiments would be used to develop a suitable protocol for examining myocardial mechanics.

Another aspect of the protocol that needed to be examined was whether this technique would allow us to elucidate the properties of the myocardium at rest and in ATP withdrawal-induced rigor. As is generally agreed in the literature, both f_{min} and phase shift should be virtually independent of frequency in resting and rigor muscle (*e.g.* Hajjar and Gwathmey, 1992). Therefore, it was necessary to determine whether this protocol would confirm this. It would obviously be important to determine this in

resting muscle before proceeding with the Ca^{2+}-activated protocol, since a very large resting stiffness, in either sham or ligated hearts, would indicate that a large percentage of the preparation was not viable muscle, but rather fibrosed or connective tissue, and was therefore unsuitable for mechanical analysis. If this appeared to be the case, the results from these preparations would be included for examination of the resting properties of the muscle, however, they would not be used for the Ca^{2+}-activated protocol, as these preparations tended to deteriorate very quickly if subjected to oscillation.

The aim of the experiments in the latter part of this chapter was to examine crossbridge kinetics in a rabbit model of LVD using sinusoidal analysis. Traditionally, Edman's slack test (1979) has been used to examine crossbridge cycling rate, predominantly in skeletal muscle, but is now widely accepted for use in cardiac muscle. This technique measures the velocity at which crossbridges cycle to take up the slack induced by a length change under zero load, known as V_{max}. However, the information provided by the two techniques is different in terms of the steps in the crossbridge cycle. Sinusoidal analysis was used to determine if there were; first, any alterations in myocardial stiffness at rest, which would have an affect on the muscle's compliance, and secondly whether there were any changes in the parameter f_{min}, and hence mean crossbridge cycling rate at C_{max}. Comparing the results from the ligated model with sham-operated controls, should reflect alterations in the contractile functioning of the heart associated with LVD.

3.2 Results

Note on animals used in this study

The operative procedure used in this model produces a wide range of left ventricular dysfunction (LVD) depending on how far up or down the left marginal coronary artery the ligature was tied, because this determines the size of the infarct produced. LVD was assessed by echocardiography and the ejection fraction (%, EF) was taken as an indicator of the degree of LVD. Sometimes animals that underwent coronary ligation did not have any visible infarct and EF fraction was consequently still quite high. On the other hand, occasionally sham-operated animals showed signs of LVD, due to adhesions forming to the chest wall after surgery, or the apical tie used to manoeuvre the heart in the sham procedure produced an area of infarction. These animals showed signs of a small LVD as indicated by a fall in EF. On this basis, it was decided before analysis, that animals showing LVD in the ligated group would only be included in analysis if their EF was ≤ 50. In addition, controls would only be accepted for analysis if their EF remained sufficiently high (≥65) for them to be assessed as having normal cardiac function. All the data examined in this thesis are separated using this criterion. The ejection fraction for a healthy rabbit is ~70 % (data obtained by Dr. André Ng from the Royal Infirmary, Glasgow).

The ejection fraction of the left ventricle is one of the most commonly used indices for assessing the degree of heart failure. The ejection fraction relates stroke volume to the end-diastolic volume, and is therefore an index of left ventricular fibre shortening. It is particularly useful for evaluating the course of chronic heart disease, assuming that the preload and the afterload are approximately unchanged. However, this is known not to be the case in heart failure. Since the ejection fraction is an index of the contractile behaviour of the heart throughout systole, it is afterload-sensitive and is therefore not the most ideal index of contractility. However, although

imperfect, it remains the best index we have for assessing the degree of left ventricular dysfunction in this model.

Experiments were also performed on control animals that had not undergone any surgery and the results from these were compared with the sham operated group. Any significant differences between the results from these groups would indicate that the surgery performed on sham animals was significantly altering the data. However, we found no significant differences (data not shown) between the results from both groups. so we were confident in using the sham operated animals as a suitable control for the results presented in this thesis.

Preparation viability

Fig. 3.1 shows an experimental trace containing a series of maximal activations, during which small, sinusoidal length perturbations have been applied. The maximum force produced by the trabecula does deteriorate slowly with time, however, the f_{min} value remains stable. The frequency at which f_{min} occurs, is generally accepted to reflect the intrinsic cycling rate of the crossbridges, (see introduction and discussion). The time control indicates that the mean cycling rate of the crossbridges is unaffected by the period of time that has elapsed since the beginning of the experiment. Although the maximum force generated by the preparation does fall off slightly with time, the maximum dynamic stiffness, reflecting the number of attached crossbridges (see discussion) is conserved throughout the protocol. Previous experiments from this lab have shown that force tends to deteriorate linearly with time, therefore the amount of force produced can be corrected for a specific time, knowing the fall-off rate of force per second.

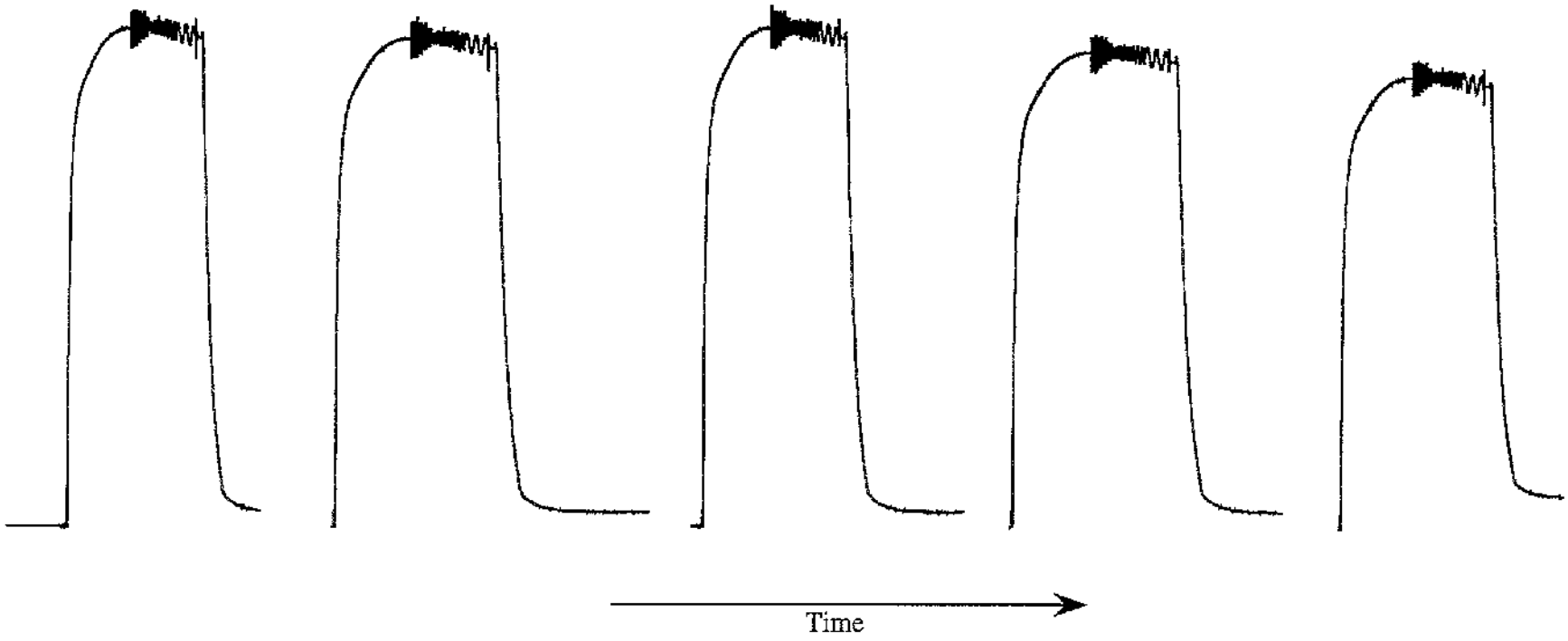

Fig. 3.1. Experimental trace showing a series of maximally Ca-activated (pCa 4.0) contractions for a single trabecula. The trabecula was bathed in a relaxing solution for 15 minutes in between each activation (0.2R solution - see Methods, section 2.5). Force is falling off slightly, however, fmin is well maintained throughout the protocol.

Preparation dimensions and ability to generate force

There was no significant difference in the cross-sectional area (0.021±0.003 vs 0.018±0.002 mm^2, p >0.05, n=28 and 26 sham and ligated respectively), or length (1.34±0.067 vs 1.54±0.084 mm, p >0.05, n=49 and 54 sham and ligated respectively) of preparations between sham and ligated animals. Similarly, there was no significant difference in the maximum force developed by preparations (1.19±1.42 vs 1.09±1.28 mN, p >0.05, sham, n=28, and ligated, n=26, respectively) in absolute terms, or when normalised for CSA (60.84±4.58 vs 61.92±6.02 mN mm^{-2}, p >0.05, sham, n=28, and ligated, n=26, respectively- see Figure 3.2). These figures lie within the range published by Allen (1983). Figure 3.3 illustrates that the maximum force produced by each trabeculae correlates with its CSA for both groups *i.e.* the larger preparations generate more force, as expected.

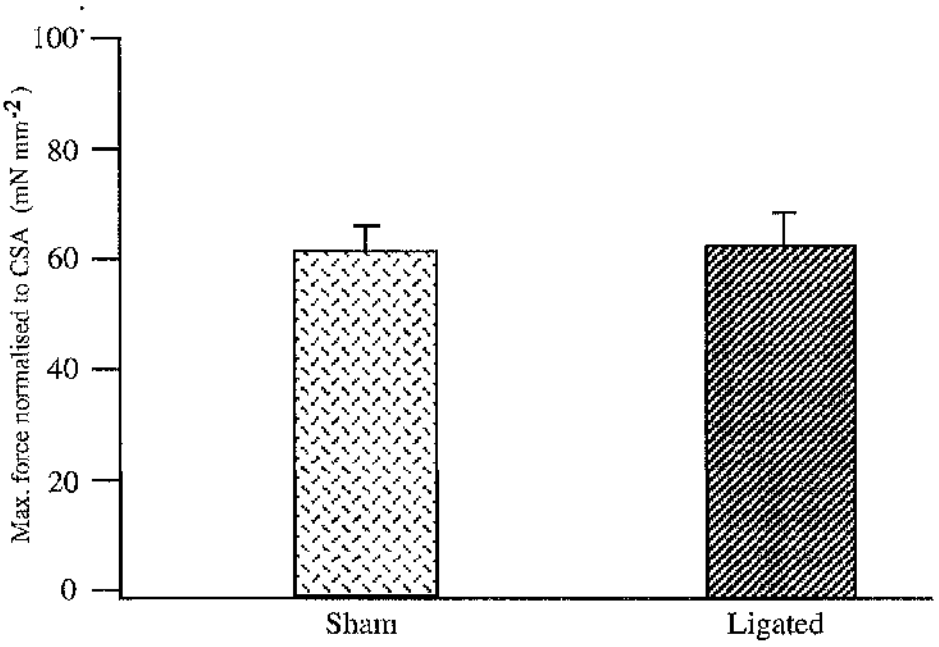

Fig. 3.2. Graph of maximum Ca-activated force (pCa 4.0) normalised to CSA for both sham and ligated groups. Mean data 60.84±4.58 (n=28) vs 61.92±6.02 $mN.mm^{-2}$ (n=26) respectively. $p > 0.05$.

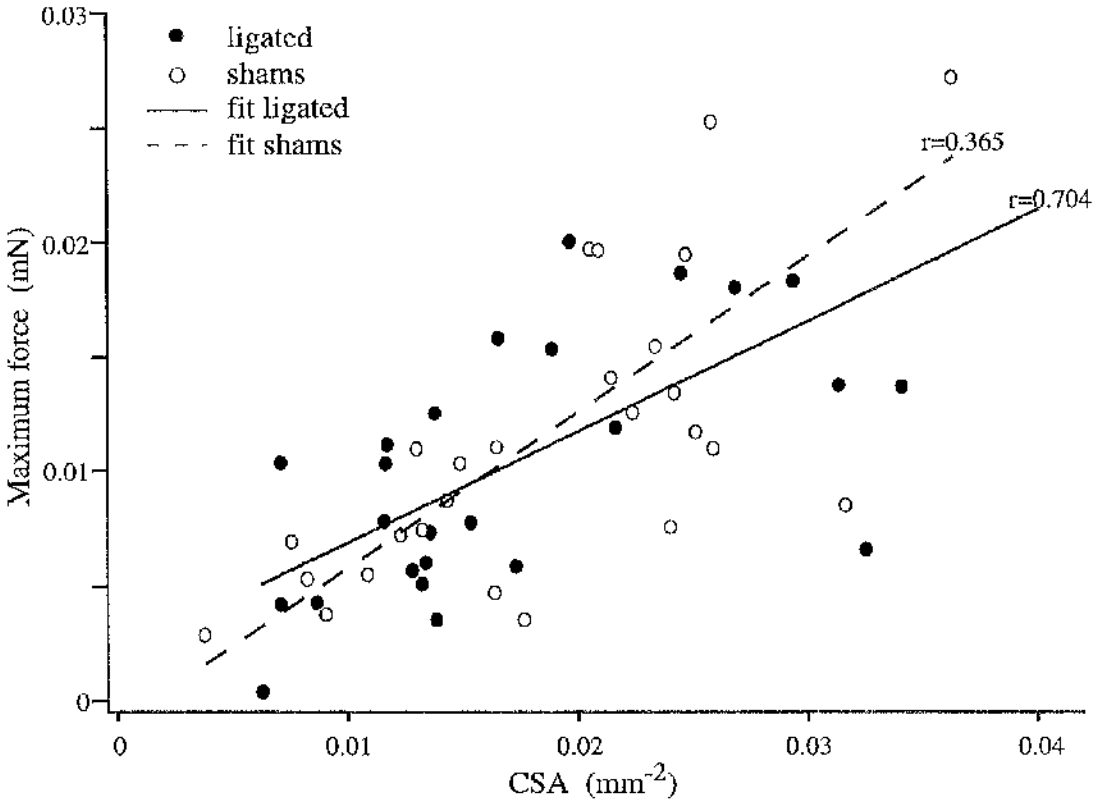

Fig 3.3. Graph of maximum force generated by trabeculae plotted against their cross sectional area for both sham (n=28) and ligated (n=26) groups. Linear regression lines for each group (- - - sham, —— ligated) are also shown on the graph.

Ca^{2+}-sensitivity

Fig 3.4 shows the pCa-force relationship for both sham (n=5) and ligated (n=6) animals. The concentrations of free Ca^{2+} used ranged between 10^{-8} M and 10^{-4} M with both groups maximally activated at pCa 4.0. Force development saturated at ~pCa 4.5 and remained maximal at pCa 4.0. As shown in Figure 3.4, there were no significant differences in Ca^{2+} sensitivity or cooperativity (steepness of the pCa-force relation) between trabeculae from control or LVD hearts, $pCa_{50\%}$ was 5.56±0.046 and 5.57±0.048, and the Hill coefficients were 3.33±0.36 and 2.82±0.33, sham and ligated respectively. The mean maximum force reached at pCa 4.0 is reported in the previous paragraph.

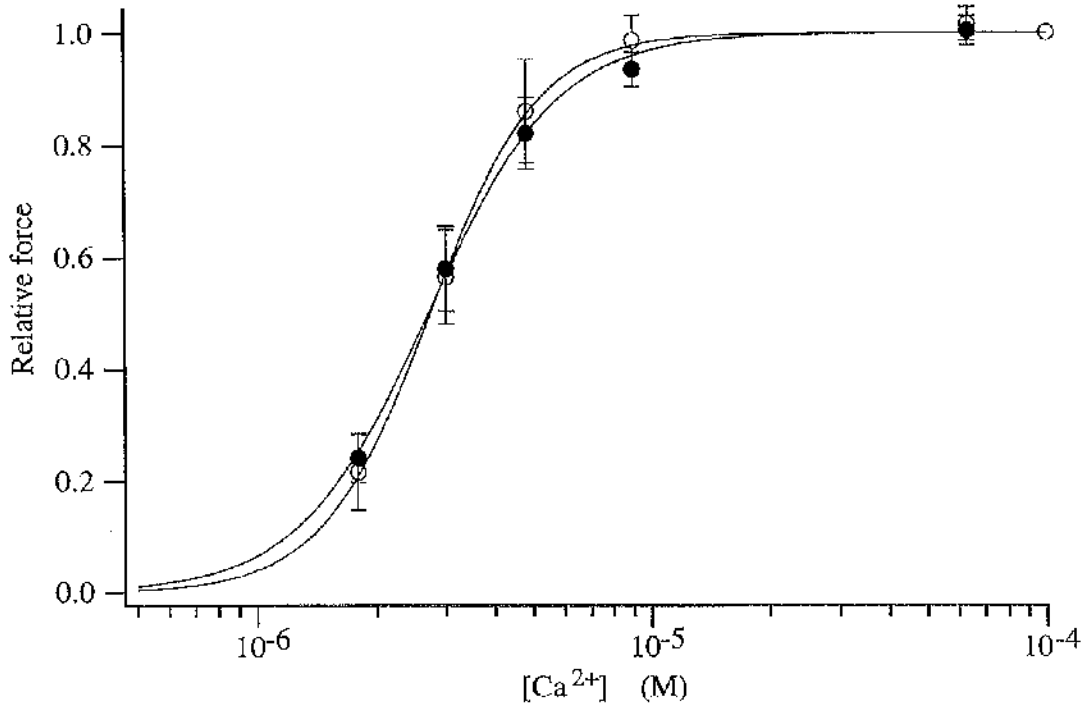

Fig. 3.4. Calcium sensitivity curve for both sham and ligated animals. The activation range for both sham (n=6) and ligated (n=5) was between $5x10^{-8}$M and 10^{-4}M. The individual data sets were fitted using the Hill equation. $[Ca^{2+}]_{50}$ was 2.75±0.03 μM and 2.78±0.03 μM, and the Hill coefficients were 3.33±0.36 and 2.82±0.33, sham and ligated respectively.

Effects of different levels of activation

Chemically skinned trabeculae were activated under controlled conditions of free$[Ca^{2+}]$, at pCa values of 5.74, 5.52, 5.31, 5.04 and 4.00. The effect of altering the free $[Ca^{2+}]$ on dynamic stiffness is shown in Figure 3.5. The plots show that even though both high and low frequency stiffness values vary with active force, the f_{min} value does not. Maximum force produced in this example was 0.49 mN and using the aforementioned pCa values, 11, 50, 75 and 96% of maximum force was attained.

In addition, Figure 3.6 shows the effects of altering the imposed length change on the frequency spectra of a preparation at rest. The imposed length change was initially 0.5% of muscle length and was then increased to 1%. The corresponding stiffness at each frequency was not significantly different when a longer length excursion was applied.

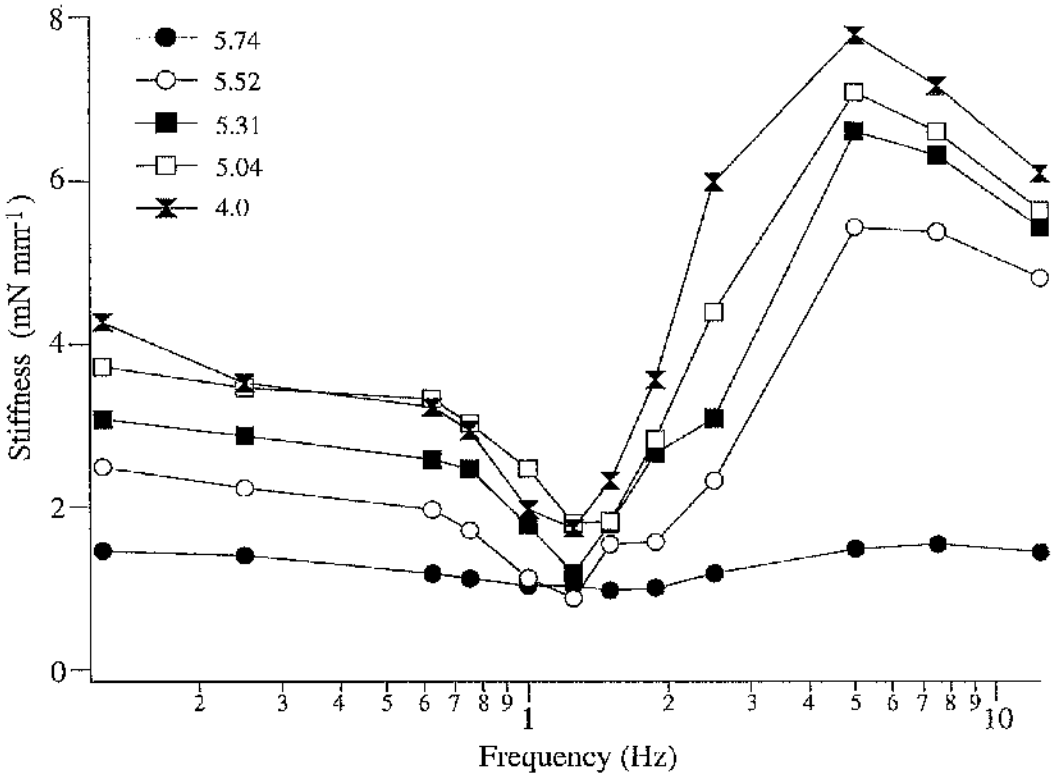

Fig. 3.5. Frequency plots of dynamic stiffness at different levels of free calcium. Maximum force produced at pCa 4.0 was 0.49 mN: at pCa values of 5.74, 5.52, 5.31, and 5.04, 11%, 50%, 75% and 96% respectively of the maximum force was attained.

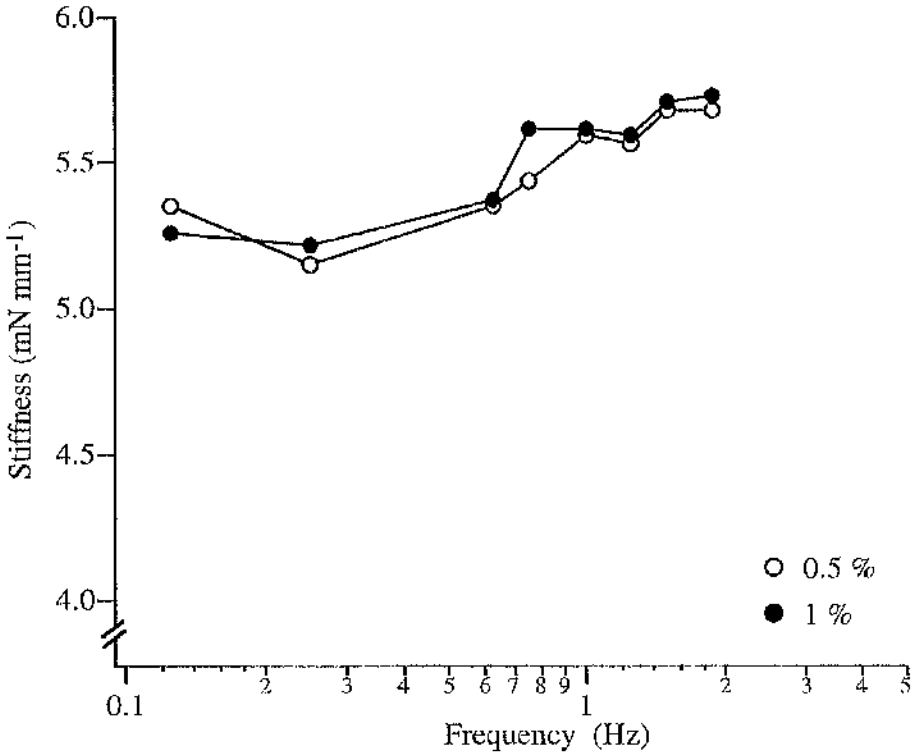

Fig. 3.6. Graph showing the effect of different length changes on stiffness from a trabecula at rest. The amplitude of oscillation was initially 0.5 % of preparation length (after sarcomere length has been set to 2.2μm) and was then increased to 1 %. The different amplitude of length excursion applied to the trabecula did not significantly alter the resting stiffness of the preparation.

Resting stiffness

Fig 3.7 shows the mean data for the stiffness obtained at rest, normalised to cross sectional area, for both sham and ligated animals. The graph shows that although the ligated preparations are slightly stiffer at all frequencies examined, the difference between the two means does not reach statistical significance (sham: 7.12±2.32 vs ligated: 7.97±1.50 mN mm^{-3}, n=25 for both).

Also shown on the chart are the mean data for two sub-divisions of the ligated group. The ligated group were further sub-divided on the basis of the f_{min} value derived experimentally for each trabecula. The first group, termed the 'slow' ligated group, contained trabeculae with an f_{min} value of ≤0.99 and the second group, termed the 'fast' ligated group, an f_{min} value of ≥1.00. The mean f_{min} value for the slow and fast ligated groups were 0.59±0.06 (n=16) and 1.26±0.09 Hz (n=9) respectively. On the basis of this subdivision, the faster ligated animals have a mean f_{min} value and resting stiffness (6.66±2.33 mN mm^{-3}) that are very similar to the mean values observed for the shams (f_{min}: 1.15±0.06 Hz, n=25). The ligated animals showing signs of more severe LVD, demonstrated by their depressed crossbridge cycling rate (which is significantly different from controls, $p<0.05$), tending to have a more pronounced increase in their resting stiffness (8.71±2.02 mN mm^{-2}) when compared with controls, however, this still fails to reach statistical significance.

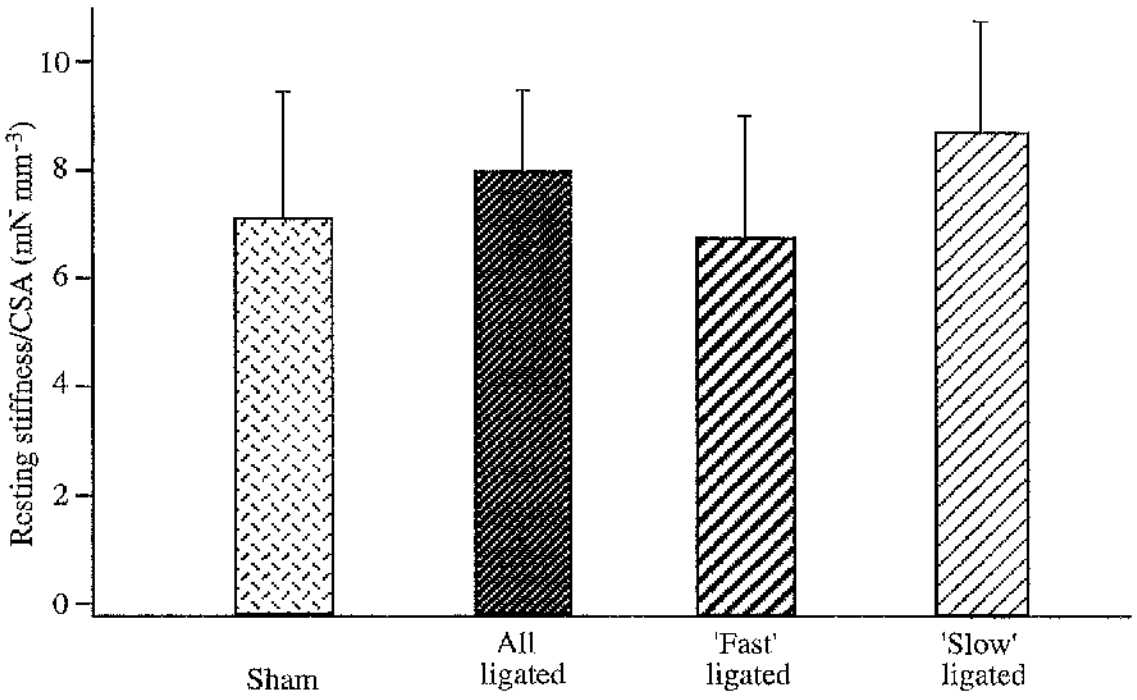

Fig. 3.7. Graph showing the mean resting stiffness results for both sham and ligated animals. Resting stiffness has been normalised to CSA. The resting stiffness is not significantly different between the two groups (sham: 7.12±2.32 vs. lig: 7.97±1.50 mN mm^{-3}, n=25 for both groups). The ligated animals have been further subdivided into 'fast' (f_{min}>1.00) and 'slow' (f_{min}<0.99). The faster ligated animals have a mean f_{min}(1.26±0.09 Hz, n=9) that is not significantly different from that of the shams (1.15±0.06, n=25), whereas the slower ligated animals have a significantly different f_{min} (0.59±0.06, n=16) from the shams. On the basis of this subdivision, the faster ligated animals have a resting stiffness that is similar to the shams (6.66±2.33 mN mm^{-3}), whereas the group of ligated animals that have shown slowing of the crossbridge cycling rate have a higher resting stiffness (8.71±2.02 mN mm^{-3}). However, this difference does not reach statistical significance. The mean f_{min} for all the ligated animals (0.83±0.08, n=25) still remains significantly different from the sham animals.

Dynamic stiffness

As length was oscillated sinusoidally, the force transients produced by the trabeculae were also approximately sinusoidal in both control and ligated animals. At low frequencies of oscillation, the amplitude of force oscillation reached a minimum at 0.91±0.07 Hz (n=15) for control trabeculae and 0.71±0.05 Hz (n=16) for LVD trabeculae ($p< 0.05$). This frequency has been termed the frequency of minimum stiffness, f_{min}, and corresponds to the point of reversal in the descending part of the stiffness-frequency curve. At frequencies beyond f_{min}, dynamic stiffness increases until reaching a plateau at ~7.5 Hz. Frequency spectra of the stiffness measurements for both sham and ligated trabeculae are shown in Figure 3.8. The stiffness spectra are not significantly different between the two groups at any of the frequencies examined. The f_{min} values here are similar to those obtianed from other studies performed at 20°C (*e.g.* Hajjar and Gwathmey, 1992), but are somewhat slower than those obtained at 37°C. f_{min} has been shown to be temperature dependent (Shibata *et al*, 1987 a,b). Layland *et al* (1995 b) have shown (at 37°C) that f_{min} and the frequency of maximum work production correspond closely to the resting heart rate of the animal. This is not the case in these experiments (at 20°C), however, at 37°C f_{min} would be anticipated to be faster and may therefore correlate with the resting heart rate of the rabbit.

Fig. 3.9 shows the relationship between active force and dynamic stiffness at a range of free $[Ca^{2+}]$s. Force has been normalised to maximum force, and high frequency stiffness (taken at 7.5 Hz) has been normalised to the maximum stiffness obtained during maximal activation. There is a close correlation (r=0.933) between the two variables. Combined data for both control (n=4) and ligated (n=4) trabeculae are shown since the correlation coefficients were not significantly different from one another.

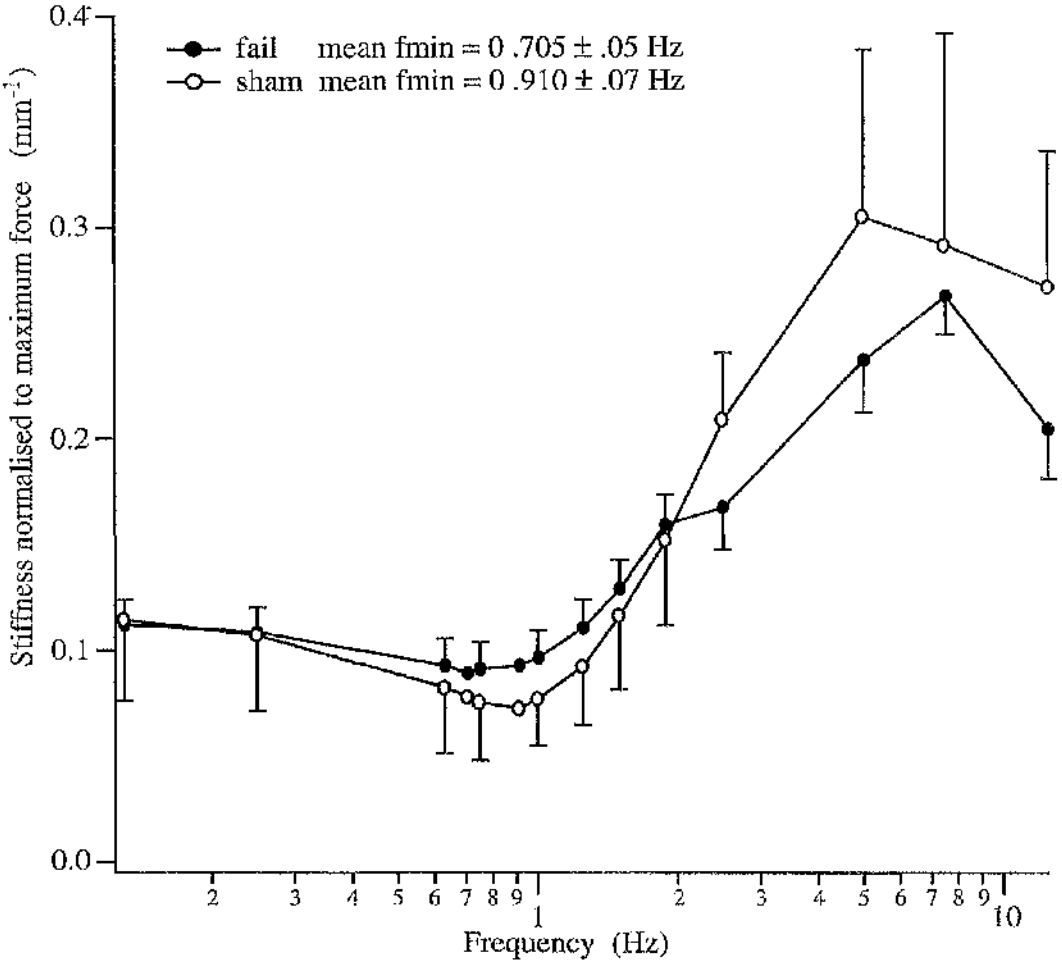

Fig. 3.8. Active stiffness, normalised to maximum force against frequency for sham and ligated groups. Data shown are mean±sem. The mean intrinsic cycling frequency of the crossbridges is significantly slower in the ligated group (as indicated by f_{min} - see text for more details) when compared with controls.

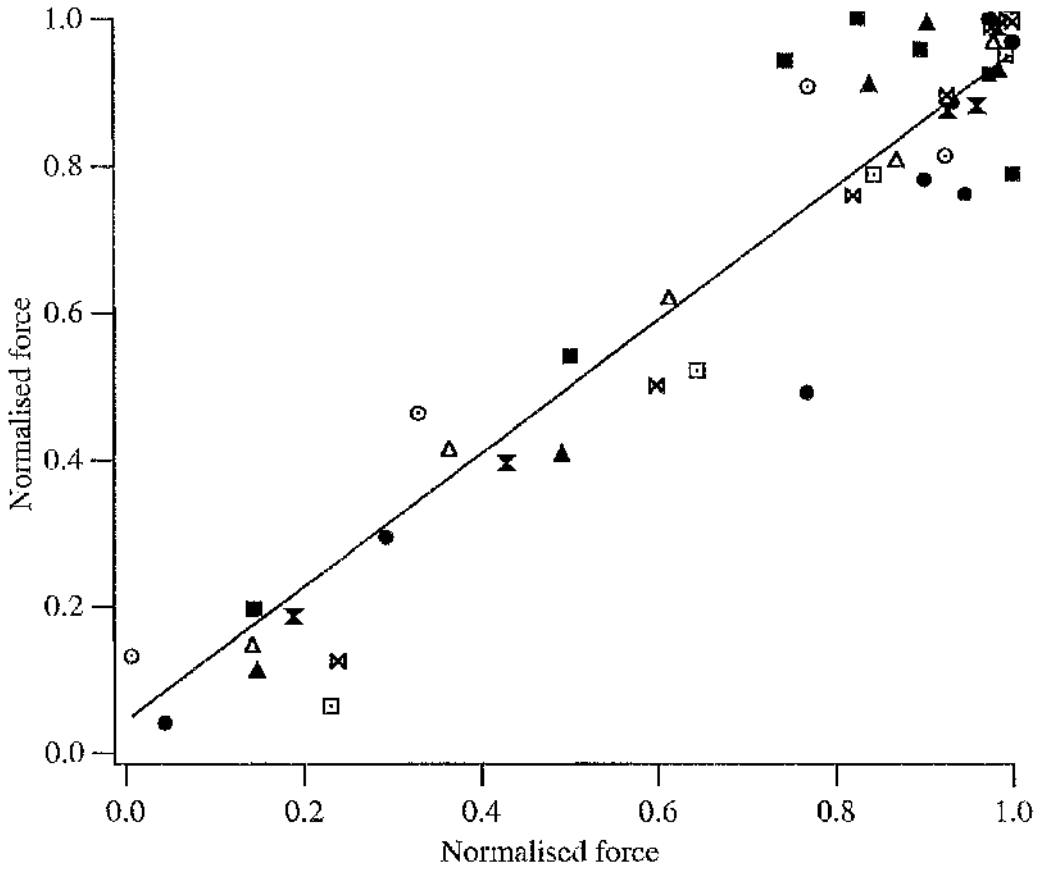

Fig. 3.9. Force-high frequency stiffness relation in control and ligated trabeculae. Open symbols, control muscles (n=4); closed symbols, ligated muscles (n=4), different symbols denote different preparations. Stiffness measurements were obtained at 7.5 Hz, over a range of pCa values (*i.e.* 5.74, 5.52, 5.31, 5.04, 4.20 and 4.0). Force was normalised to maximum (pCa 4.0) and stiffness was normalised to the maximum stiffness at 7.5 Hz obtained during maximal activation. Linear regression line is shown (—, correlation coefficient, r=0.933).

Rigor stiffness

Fig 3.10 over leaf shows the stiffness-frequency relationship for a trabecula in rigor (*i.e.* zero ATP). Fig. 3.10 shows experimental chart recording, with both length and force waveforms illustrated. Rigor stiffness is frequency-independent, as indicated by the constant amplitude of the force waveform. The force trace clearly shows the frequency-independence of rigor stiffness. The stiffness of an activated or rigor muscle reflects the number of attached crossbridges. In rigor conditions, crossbridges are permanently attached, therefore the observed stiffness should be high, as is shown in Fig. 3.10.

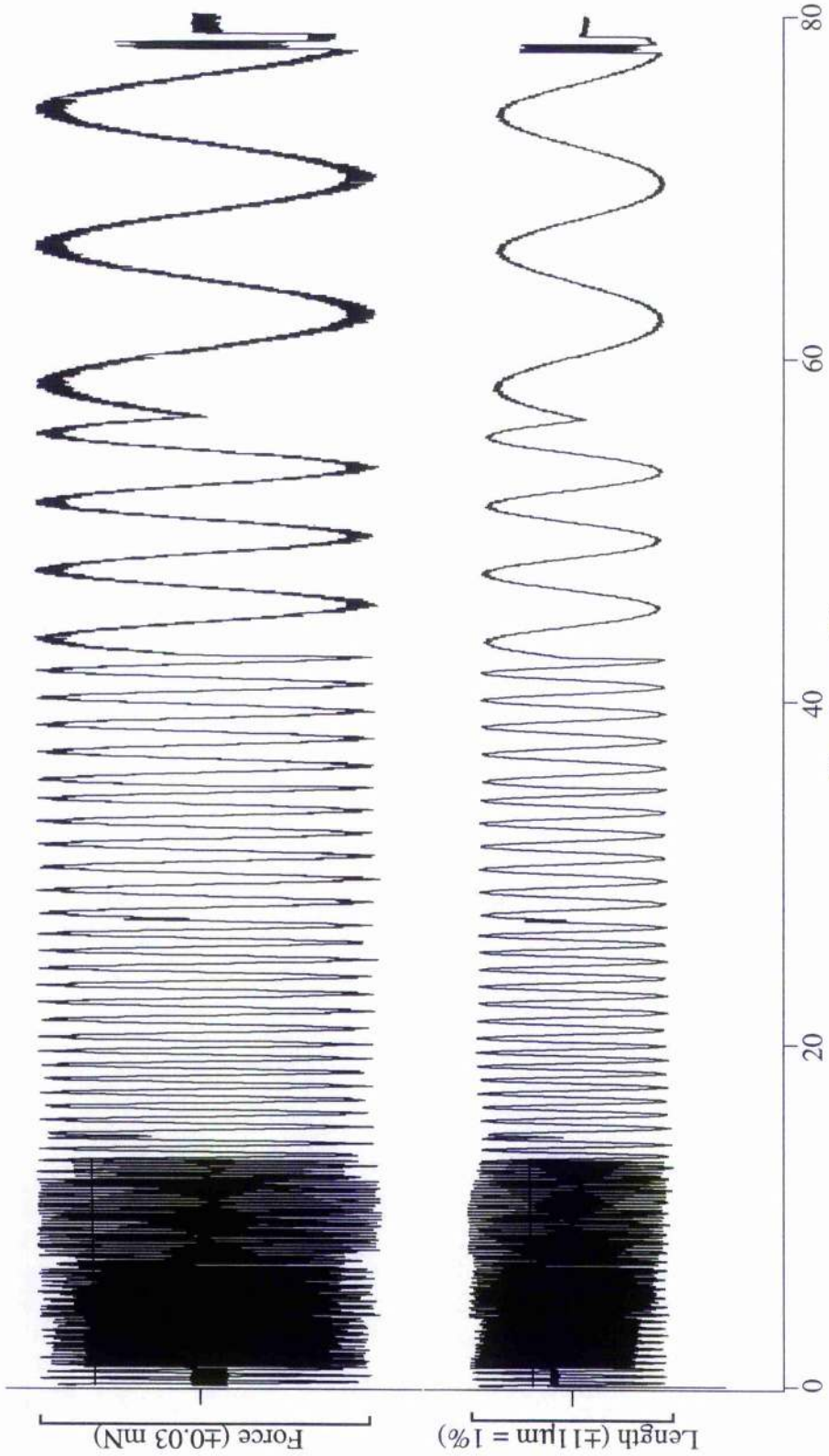

Fig. 3.10. Experimental traces showing the length and force waveforms against time for a trabecula in rigor over a range of frequencies (12.5-0.125 Hz). As with resting stiffness, rigor stiffness is frequency-independent. The stiffness of the preparation is high due to the sustained attachment of all crossbridges in the strongly attached orientation. Some aliasing distorts the trace at at the higher frequencies examined, however, this is not apparent on a much larger time scale.

	Sham	Ligated
Force/CSA ($mN\ mm^{-2}$)	60.84±4.58 (n=28)	61.92±6.02 (n=26)
Ca^{2+}-sensitivity Hill coefficient	3.33±0.36 (n=6)	2.82±0.33 (n=5)
pCa_{50}	5.56±0.046	5.57±0.048
f_{min} (Hz)	0.91±0.07 (n=25)	0.71±.05 (n=25)
Resting stiffness/CSA ($mN\ mm^{-3}$)	7.12±2.32 (n=25)	7.97±1.50 (n=25)

Table 3.1. Summary of results±sem.

3.3 Discussion

It has been well documented, using time-domain analyses of the mechanical function of papillary muscles and single cardiac fibres, that both force and V_{max} of cardiac muscle are sensitive to the level of activation by Ca^{2+} ions (*e.g.* Brutsaert *et al,* 1973: De Clerk *et al,* 1977). The number of active crossbridges during contraction is clearly influenced by Ca^{2+}, however, it is not so obvious when investigating V_{max} changes in cardiac muscle, whether these changes reflect a change in crossbridge kinetics. Sinusoidal analysis of skinned cardiac fibres allows direct measurement of any alterations of mechanical parameters that occur during activation with different levels of free Ca^{2+}. The results from this frequency-domain analysis demonstrate that increasing the level of activation with Ca^{2+} was correlated with an increase in the dynamic stiffness of the muscle, reflecting an increase in the number of active crossbridges. However, the level of activation did not affect the intrinsic cycling rate of the crossbridges. These results then suggest that altering the level of activation changes the number of active crossbridges (*i.e.* 'recruitment'), but not crossbridge kinetics.

Altering the level of activation of cardiac muscle solely by altering $[Ca^{2+}]$ does not resemble the situation *in vivo*. It is well known that *in vivo*, stretching of the myocardium, within a defined range, influences the force of contraction of the heart. More specifically, stretching of the myocardium (via increased preload) is associated with an increase in force production. This length-force relationship is considered to be the basis of the Frank-Starling law of the heart. Other studies (*e.g.* Rossmanith *et al,* 1986) have examined different levels of activation of cardiac muscle by altering the length of the preparation and then using frequency-domain analysis to examine the mechanical parameters under these conditions. They (Rossmanith *et al,*) also found that the mechanical parameters were unaffected by altering the level of activation in this way. Collectively, these results imply that only the number of active crossbridges,

rather than crossbridge kinetics, are influenced by the Frank-Starling relationship of the heart.

The aim of the experiments detailed in the latter half of this chapter was to examine alterations in mechanical parameters, such as f_{min}, in a rabbit model of LVD. The sinusoidal analysis protocol used to examine these parameters, on the basis of these findings, was carried out at maximal Ca^{2+}-activation (pCa 4.0). From the results determined in these preliminary experiments we were confident that only using maximally activated fibres to examine crossbridge kinetics, allowed us to extract the required information necessary for kinetic analysis. In addition, using maximally activated trabeculae circumvented the ambiguities associated with using sub-maximally activated preparations.

Several groups have used sinusoidal analysis and the pseudo-random binary noise-modulated perturbation (PRBN) technique to examine the kinetics of isometrically contracting cardiac muscle (*e.g.* sinusoidal analysis: Hajjar and Gwathmey, 1992; Saeki *et al,* 1991 and PRBN: Rossmanith, 1986). These groups interpreted the time course of force transients (muscle 'stiffness'-indicative of the number of attached crossbridges) in response to rapid, small amplitude length changes applied at a range of frequencies to isometrically contracting papillary muscles or trabeculae in terms of the kinetics of the active interaction of myosin with actin. These techniques produced characteristic stiffness-frequency spectra, where the amplitude of the force transients varies with the imposed frequency. More specifically of interest is the frequency of minimum stiffness (f_{min}), which reflects the frequency at which resonance exists between the mechanical cycle of the muscle during activation, and the mechanical frequency imposed on the muscle. Furthermore, it has been shown that f_{min} is similar in skinned and intact myocardium (Saeki *et al,* 1991). Support for f_{min} as a reliable indicator of the intrinsic cycling rate of active crossbridges arises from studies demonstrating that this frequency is independent of muscle length (Rossmanith *et al,* 1986) and degree of activation (Rossmanith *et al,* 1986 and results from this study), but strongly dependent on for example temperature (Shibata

et al, 1987 a,b) myosin isoform composition (Rossmanith *et al,* 1986), age (Shibata *et al,* 1987b) and pharmacological intervention (*e.g.* Hoh *et al,* 1988).

The results from this study using sinusoidal analysis have shown that the mean cycling rate of the crossbridges is significantly slower in rabbits that have undergone coronary artery ligation when compared with sham-operated controls. In human and animal models of cardiac disease states, alterations in the functional properties of the myofilaments have been reported that may reflect altered crossbridge cycling kinetics (*e.g.* Human: Hajjar and Gwathmey, 1991; Morano *et al,* 1991). In accordance with our findings, Hajjar and Gwathmey (1992) have shown that the crossbridge cycling rate is significantly reduced in human heart failure patients when compared with controls. f_{min} has been shown to correlate with the ratio of the V_1 to V_3 myosin isoforms (*e.g.* Rossmanith *et al,* 1995), becoming increasingly slowed as the amount of the V_1 isoform diminishes. Myosin isoform shifts have been well documented in association with various cardiac pathological states and the maturational status of several species. In human and adult rabbit hearts, the slow V_3 is already the predominant isoform, therefore no consistent change in isoform pattern has been reported with disease states (Schier and Adelstein, 1982; Mercadier *et al,* 1983; Litten *et al,* 1985; Eble *et al,* 1997). Although it is generally assumed that no significant isoform shift occurs in rabbits, a few studies have shown that a shift, although small, does in fact occur in adult rabbits of up to five months of age (Litten *et al,* 1985; Eble *et al,* 1997). This shift could therefore be possible in the rabbits used in this study as they are approximately 5 months of age when trabeculae are harvested and used for experimentation. Occasionally, animals were left on procedure, allowing LVD to develop for 16 weeks, however, only very few of these animals were used in any of these experiments. Other studies have demonstrated that changes in the myosin molecule independent of a change in myosin isoform population can decrease the maximum ATPase rate. In humans, mis-sense mutations in the β-MHC have been shown to account for the decreased ATPase rate observed in familial hypertrophic cardiomyopathy (Geisterfer-Lowrance *et al,* 1990; Tanigawa *et al,* 1990).

Furthermore, in a hamster model of heart failure, the loss or alteration of myosin light chains by a specific protease has been demonstrated, affecting ATPase rate, and this may also be present in human cardiomyopathies (Margossian *et al,* 1992). This idea is also discussed in chapter 5 in relation to the relaxation kinetics of trabeculae using this model.

The content of the regulatory myosin light chain (MLC_2) in human ventricles has been reported to be decreased in cardiac disease states (Margossian *et al,* 1992). In skinned cardiac muscle experiments, removal of MLC_2 has profound effects on actin-myosin interaction. An increase in sub-maximal force without a concomitant increase in maximal force generation (increased Ca^{2+}-sensitivity) and a decrease in the unloaded velocity of shortening has been demonstrated after MLC_2 removal. The decreased crossbridge cycling rate, unchanged maximal force generation and raised resting stiffness (though the latter not significantly) are consistent with a decreased MLC_2 content, however, what does not appear consistent is that no alterations in the Ca^{2+}-sensitivity of the myofilaments occurred in our LVD preparations. Therefore, loss of MLC_2 is unlikely to account for the slowed contractile mechanics observed in this model. However, regardless of the amount of MLC_2 present in the ventricles, the phosphorylation status of MLC_2 has been implicated by some authors as one of the mechanisms responsible for the decline in the contractile activity of the heart observed during failure (*e.g.* Kopp and Barany, 1979; Morano and Rüegg, 1986), though other authors dispute this (*e.g.* High and Stull, 1980; Jeacocke and England, 1980). Phosphorylation of MLC_2 increases f_{app}, the apparent rate constant for the transition of crossbridges from the non force-generating state to the force-generating state (Brenner, 1988). Therefore, phosphorylation would be expected to increase the rate of force development and also maximum Ca^{2+}-activated force. Although both increases and decreases in MLC_2 phosphorylation have been implicated in cardiac disease states, alterations in phosphorylation status are unlikely in this instance since maximum force generation was not significantly different between sham and ligated trabeculae.

Hasenfuss and colleagues (1992) reported decreased numbers of crossbridges in human heart failure, as indicated by a reduction in force dependent heat. Force dependent heat is liberated via high-energy phosphate hydrolysis during crossbridge cycling, assuming that one high-energy bond is hydrolysed per crossbridge cycle. Force dependent heat therefore directly reflects the number of force-generating crossbridges under isometric conditions. Maximum stiffness of the trabeculae (measured at 7.5 Hz and under maximal Ca^{2+}-activation at pCa 4.0) used in this study was not significantly different between control and LVD groups. If the number of crossbridges were reduced in this model, the same maximal stiffness observed between the two groups would imply that the active crossbridges were stiffer in ligated animals than in controls. However, if the numbers of crossbridges were reduced, then a corresponding decrease in maximum Ca^{2+}-activated force would be expected. This was not the case in our LVD group. Since the maximum force generated by diseased trabeculae in this study was not significantly different from controls, a reduction in the number of force-producing crossbridges seems unlikely.

Alterations in the individual force generating process of crossbridges has been described in failing hearts (*e.g.* Hasenfuss *et al*, 1992). They found that the average crossbridge force-time integral, which is thought to reflect crossbridge attachment time, was increased by ~33% in human failing myocardium. This would be in agreement with a slowing of crossbridge cycling rate as observed in this model. An increased crossbridge force-time integral can manifest two different outcomes in terms of mechanical functioning of the heart. An increased force-time integral, from an energy-economy point of view, may indeed be favourable (especially since diseased hearts have a reduced energy reserve when compared with normal hearts (Hajjar and Gwathmey, 1992)) since a greater force is generated by the muscle per unit of high energy phosphate utilised. This would allow the muscle to generate the same force as controls, as occurs in this model of heart failure. However, a less favourable outcome for the myocardium resulting from an increased crossbridge force-time integral is that a prolonged attachment time may result in decreased rates

of relaxation (as discussed in chapter 5) and therefore compromise the power development capacity of the heart.

It has been postulated that alterations in TnT isoforms may underlie the depressed myofibrillar ATPase rate which is a feature of failing myocardium (Anderson *et al,* 1991, 1992).

Chapter 4

Alterations in the Work and Power Output of Trabeculae from a Rabbit Coronary Artery Ligation Model of Left Ventricular Dysfunction

4.1 Introduction

It has been known for some time that in active striated muscle, myosin crossbridges interact cyclically with actin to transduce chemical energy stored as ATP into useful mechanical work, often referred to as chemo-mechanical transduction (Huxley, 1974; Eisenberg and Hill, 1985). The technique of sinusoidal analysis was originally developed to observe the phenomenon of oscillatory work in insect flight muscle (Machin and Pringle, 1959), but has since been utilised to study other muscle types. In these initial experiments, a muscle was stimulated at a frequency sufficient to maintain continuous activation while a sinusoidal perturbation was imposed on the muscle. The resultant force transients were recorded and analysed. It was found that at discrete frequencies of sinusoidal length perturbations, the resulting force transient lags behind the change in length (*i.e.* a phase lag), such that the muscle force at any length is higher during the shortening portion of the cycle than during lengthening. When the force transient is plotted against length, a loop is produced that rotates anti-clockwise. The area under this loop measures the work output per length cycle of the muscle. At other discrete frequencies, the force transient is observed to precede length (*i.e.* a phase lead) and in this instance, when force is plotted against length a loop that rotates clockwise is produced. The area under this loop represents negative work or the work absorbed by the muscle. Negative work is potentially available to be released by the muscle as useful work. The time that a muscle spends absorbing work, as a fraction of the normal working cycle, becomes significant if this phase is prolonged such that the muscle is unable to generate positive work. When this occurs the work absorbed that is potentially available to generate useful work is dissipated (*i.e.* it is lost since the fraction of the working cycle spent absorbing work is >1).

This technique has since been modified to examine the work output of muscle in conditions that correspond better to the 'physiological' situation, depending on the muscle being examined, and is now more commonly known as the work loop

technique (Josephson, 1985). Before the development of this technique, most studies of muscle work output were carried out on muscles shortening under constant load *i.e.* isotonic contraction and the muscle power output assessed using the product of force and shortening velocity. The work/power generating capacity of isolated cardiac muscle was originally determined in this manner (Sonnenblick, 1962). However, these experimental conditions were grossly different from the normal operating conditions observed *in vivo*, especially in the heart, where purely isotonic contractions do not occur. Another shortfall of these initial studies was that they did not take into account the work which must be put into the muscle to re-lengthen it. Sinusoidal analysis circumvents this problem, allowing both the work- generating and absorbing capacities of the muscle to be examined. Sinusoidal analysis has been employed in two different ways to examine the oscillatory work capacity of different muscle types. Sinusoidal length perturbation of Ca^{2+}-activated muscle, under isometric conditions, has been used to examine the mechanical performance of muscle (*e.g.* Kawai and Brandt, 1980; Hajjar and Gwathmey, 1992). This is in contrast to the work-loop technique described by Josephson (1985) in which the muscle is activated, at a particular point during the sinusoidal length perturbation cycle, by electrical stimulation. In skeletal muscle brief, tetanic stimulation is often applied during perturbation, however this cannot be done in cardiac muscle so the technique employs evoking a single twitch. In both cases the application of the different electrical stimulation patterns is necessary in order to resemble more closely the conditions observed *in vivo*. Using both of these sinusoidal analysis techniques, the power output of the muscle can also be measured. The rate at which mechanical work is done, *i.e.* the power output, is calculated as the product of work and the cycle frequency. *In vivo* the rate at which mechanical work is done is determined by the heart rate of the animal.

The heart behaves as a functional 'syncytium' (*i.e.* all cells within the myocardium contract with each beat). The overall force generated by the heart is increased by the combined actions of each cell. This situation is functionally very

different from how skeletal muscle operates. In skeletal muscle, force is modulated by either increasing or decreasing the numbers of functional fibres (*i.e.* by altering 'recruitment' of motor units). The very nature of the role of the heart to maintain an adequate supply of oxygen to the rest of the body, without fatigue, requires that the heart is able constantly to adapt its power output to meet the variable haemodynamic demands made by the body. Indeed, in 1950 A.V. Hill proposed that the contractile properties of muscle have evolved such that they best suit their functional requirements *in vivo*. This proposal encompassed all muscles within the body and that each of them are adapted for maximal power and efficiency in their important range of speed. In heart failure, however, the heart fails to meet the metabolic demands of the body. The compensatory mechanisms associated with the development of heart failure provoke the heart to 'work harder' *i.e.* a vicious cycle occurs where the work output of the heart is already compromised, but in order to maintain an adequate cardiac output to the rest of the body, the workload of the heart is again increased. In addition, the heart has to work against an increased peripheral resistance that is associated with heart failure requiring once again a greater work output to maintain cardiac output.

The aim of the experiments in this chapter was to use sinusoidal analysis to examine both the intrinsic work- and power- generating capacity of the myofilaments from a coronary artery ligation model of heart failure and compare this with sham operated controls. Small amplitude sinusoidal length perturbations were applied to Ca^{2+}-activated, chemically-skinned trabeculae and the resultant phase relationships between force and length transients were examined. This study thus examines the work and power 'output' of these trabeculae, as well as the ability of the muscle to absorb oscillatory work which is the net negative work region of the phase-frequency diagram.

4.2 Results

Phase shift

The procedure for calculating the oscillatory work and power produced by trabeculae using sinusoidal analysis is described in Methods (section *2.13.3 - 2.13.4*). However, before these parameters can be calculated the phase shift observed between the length and force sinusoidal waveforms must be determined.

The mean phase shift at each discrete frequency between force and length waveforms showed a strong frequency dependence analogous to that of muscle stiffness, as seen in Figure 4.1. For an individual preparation the phase shift was generally close to zero (positive, and only marginally in the LVD group) at frequencies below f_{min}, but increased slightly to a maximum at the frequency immediately below f_{min}. Just above f_{min}, the phase shift abruptly changes to negative. Phase shift gradually increases at higher frequencies, becoming positive again (see Figure 2.5). This trend is not apparent when the mean phase shift observed at each discrete frequency plotted as in Figure 4.1. The mean maximum positive phase shift values and the mean negative phase shift values are significantly lower in the ligated animals.

Fig. 4.1 shows the mean phase shift obtained at a discrete frequency of oscillation imposed on the individual trabeculae. However, the maximum phase shift value on this graph for both sham and ligated animals (positive and negative) is lower than the maximum phase shift values shown in Table 4.1. This is because the phase shift values used to calculate the figures shown in Table 4.1 were the largest phase shift values (positive and negative) obtained from an *individual* experiment regardless of the frequency at which this occurred. When the values were meaned for a particular frequency of oscillation, and since the frequency at which maximal work and power

(positive and negative) was observed varied amongst preparations, the maximal values appear different, the sem is also large as a direct result.

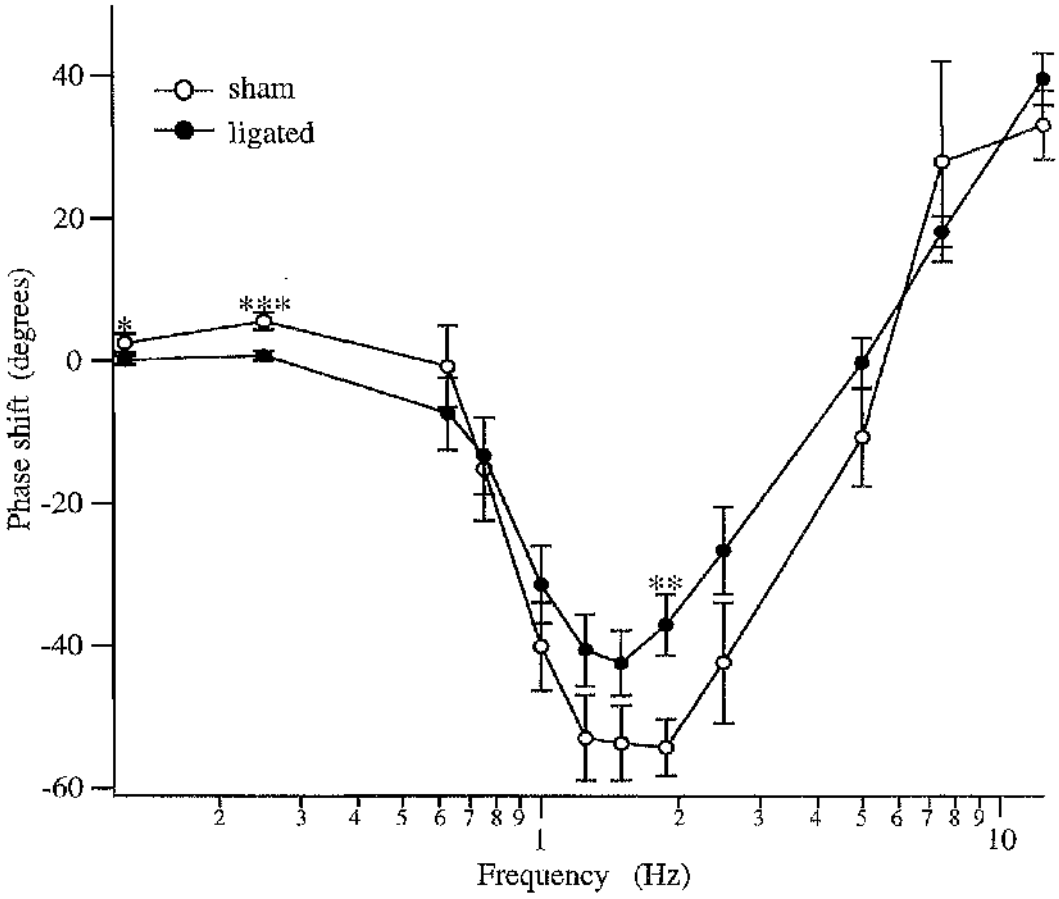

Fig. 4.1. Mean phase shift between length and force waveforms over a range of frequencies. The mean phase shift observed at all frequencies (with the exception of 0.13 Hz, *p<0.05; 1.875 Hz, ** p<0.005 and 2.5 Hz *** p<0.001), is not significantly different between the two groups. A positive phase shift occurs when length is leading force, indicative of positive work being generated. A negative phase shift occurs when length is lagging force, indicative of oscillatory work being absorbed. The maximum positive phase shift for each group, obtained by taking the mean phase shift at each discrete frequency is 5.65±1.22 and 0.68±0.05 (degrees), sham (n=22) and ligated (n=24) respectively and the mean negative phase shift is -54.23±3.93 and -42.44±4.59 (degrees).

Table 4.1 shows the maximum phase shift (positive and negative) that is derived from taking the mean of the maximum phase shifts for each preparation, regardless of the frequency at which this occurs. The maximum positive phase shift observed in the controls is significantly lower in the LVD group, as is the negative phase shift. The maximum phase shift values obtained in this manner are larger than the values obtained previously by taking the mean at each discrete frequency, however, the significance of difference between the two groups remains unchanged.

	Sham	Ligated
n	22	24
Max. positive phase shift (°)	13.58±1.02	6.74±1.06**
Max. negative phase shift (°)	-70.08±3.89	-49.88±4.89*

Table 4.1. Summary of mean phase shift data. The values in this table are obtained by taking the maximum values of phase shift (positive and negative) independent of the frequency at which this occurs. (*$p<0.01$, **$p<0.001$).

Fig. 4.2 shows examples of length vs force loops for both positive and negative work in a (a) sham and (b) ligated animal. The direction of the loop is indicated by the arrows. The area under an anti-clockwise loop represents external work, whereas the area under a clockwise rotating loop denotes negative work. It is obvious from these loops that the work absorbed by the preparation is far greater than the work generated by the preparation. This is consistently the case for all preparations examined.

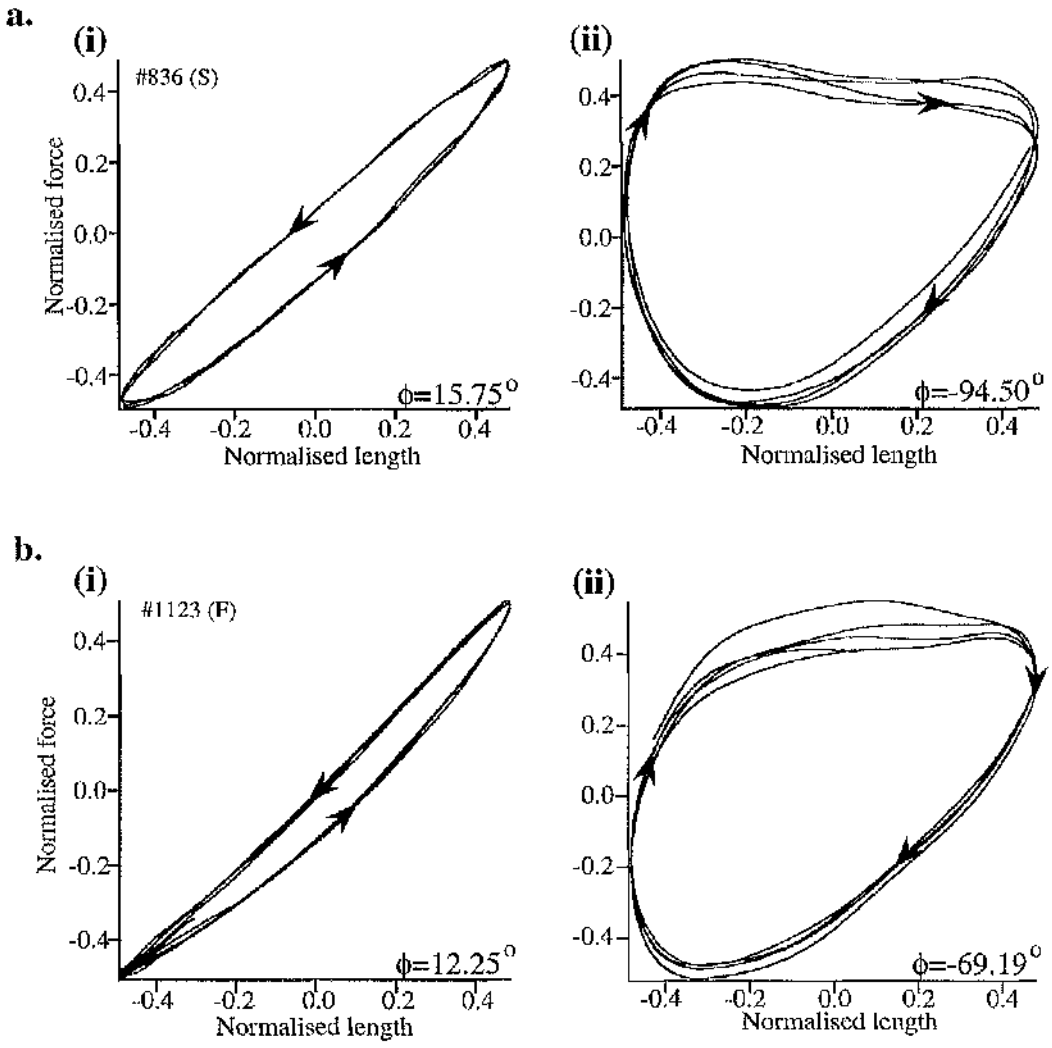

Fig. 4.2. Positive and negative work loops for a sham and a ligated animal. **a.** Examples of work loops for a sham-operated animal. The arrows denote the direction around the loop. (i) Positive work loop which rotates anti-clockwise and (ii) a negative work loop which rotates clockwise.
b. Examples of work loops for a ligated animal. (i) and (ii) are as described for the sham animal. Depending upon the direction the loop rotates, the area under the loop represents the positive or negative work performed by the animal.

Note on work and power units

The results described in the following pages concerning work and power (generated and absorbed) show no units for these parameters, derived using equations 2.4 and 2.5 (in Methods). To make comparisons between results obtained from different trabeculae, stiffness was normalised to maximum force. Therefore, a number without units was derived. Similarly, the distance each trabecula was oscillated was normalised, since this was 0.5% of preparation length in each case. For a typical preparation generating 0.60 mN, stiffness at f_{min} would be perhaps 5% *i.e.* 4.23 mN-mm^{-1}. The length change was 0.5% *i.e.* 7.5 μm for a 1.5 mm preparation. Thus, work = force x distance = $3 \cdot 10^{-6}$kg x $7.5 \cdot 10^{-6}$m = 22.5 pJ. At 1 Hz this is equivalent to 22.5 pW oscillatory power.

Work output

Fig 4.3a shows the work output of individual preparations plotted against ejection fraction and the mean values for the group. The work capacity of the trabeculae is decreased in those that are showing signs of LVD. The mean values for work output are significantly lower in the LVD animals when compared with controls. Additionally, five out of the fifteen ligated animals used in these experiments, did not generate any positive work, whereas all control animals did.

Fig 4.3b shows the relationship between the work produced by the trabeculae and their mean crossbridge cycling rate (*i.e.* their f_{min}, see Chapter 3 for description). plus the mean values for both parameters. The mean f_{min} value is significantly lower in the ligated group (work values quoted in previous paragraph).

Fig. 4.4 shows the relationship between the frequency at which maximum work is produced and f_{min}. Both groups show the same trend *i.e.* the frequency of maximum work is reduced if f_{min} is decreased. In both groups the frequency at which maximum work is produced is always fractionally slower than the frequency at which the crossbridges are cycling.

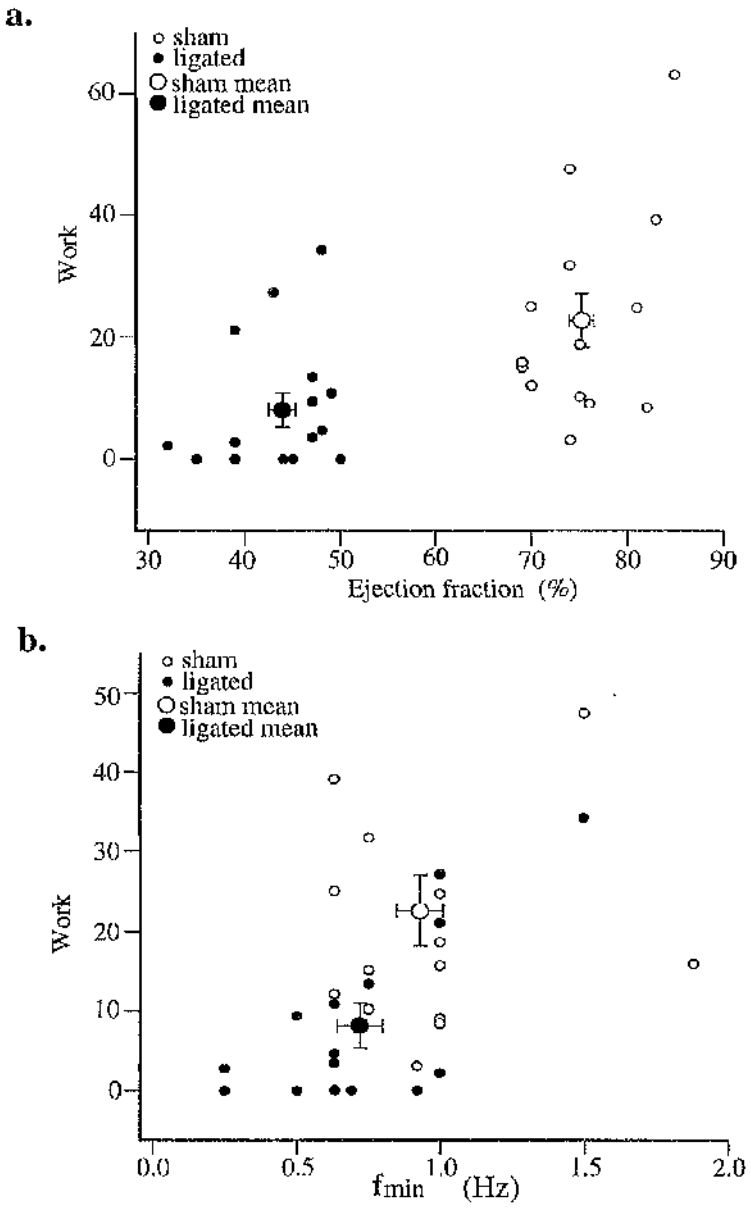

Fig. 4.3. Graph showing net positive work generated by trabeculae against **a.** EF and **b.** f_{min} for both sham (○), n=13, and ligated (●) n=15, animals. The larger open and filled circles represent the mean values±sem for both data sets. External work: 0.023±0.004 vs 0.008±0.003, sham and ligated respectively. **a.** EF: 75.24±1.29 vs 43.88±1.43 % and **b.** fmin : 0.931±.083 vs 0.719±0.081 Hz, $p<0.05$.

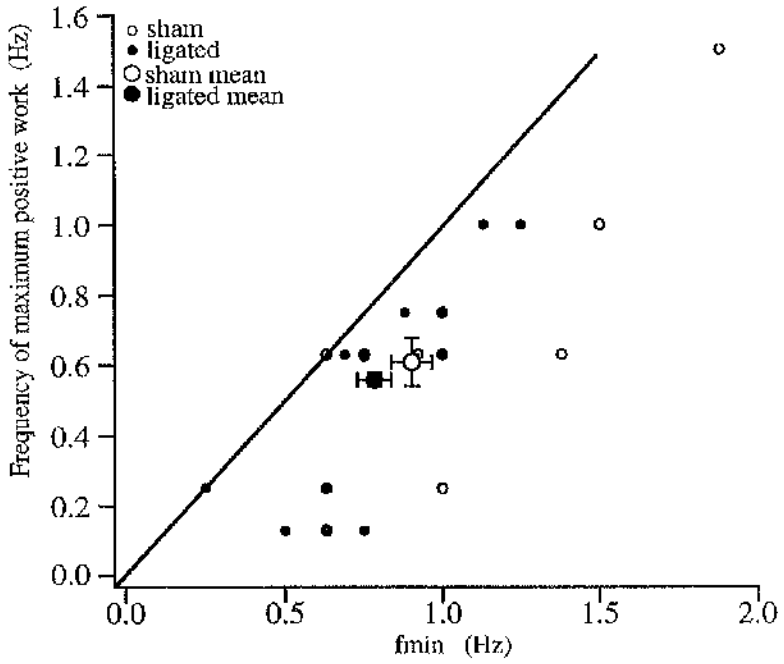

Fig. 4.4. Relationship between the frequency at which maximum work is generated and f_{min} . The larger open and filled circles represent the mean for both sham and ligated animals respectively (work freq: 0.61±0.07 vs 0.56±0.02, $p>0.05$, and f_{min} : 0.931±0.083 vs 0.719±0.081, $p<0.05$).
— denotes the line of equality.

Work absorbed

Fig. 4.5a shows the relationship between work absorbed by the preparation and the ejection fraction for that animal, together with the mean for each group. In this case the mean work absorbed by the trabeculae, although slightly lower in the ligated group, is not significantly different between control and ligated animals.

Fig. 4.5b shows how the work absorbed by the trabeculae varies with f_{min}. Again, as just described, the mean work absorbed by the control group is greater than that by the ligated animals, however, the difference does not reach statistical difference, whereas f_{min} does.

Fig 4.6 shows the relationship between the frequency at which maximum work is absorbed and the frequency at which the crossbridges are cycling for both sham and ligated animals. In both groups the mean frequency at which maximum work is absorbed is significantly faster than the mean rate at which the crossbridges are cycling ($p<0.001$).

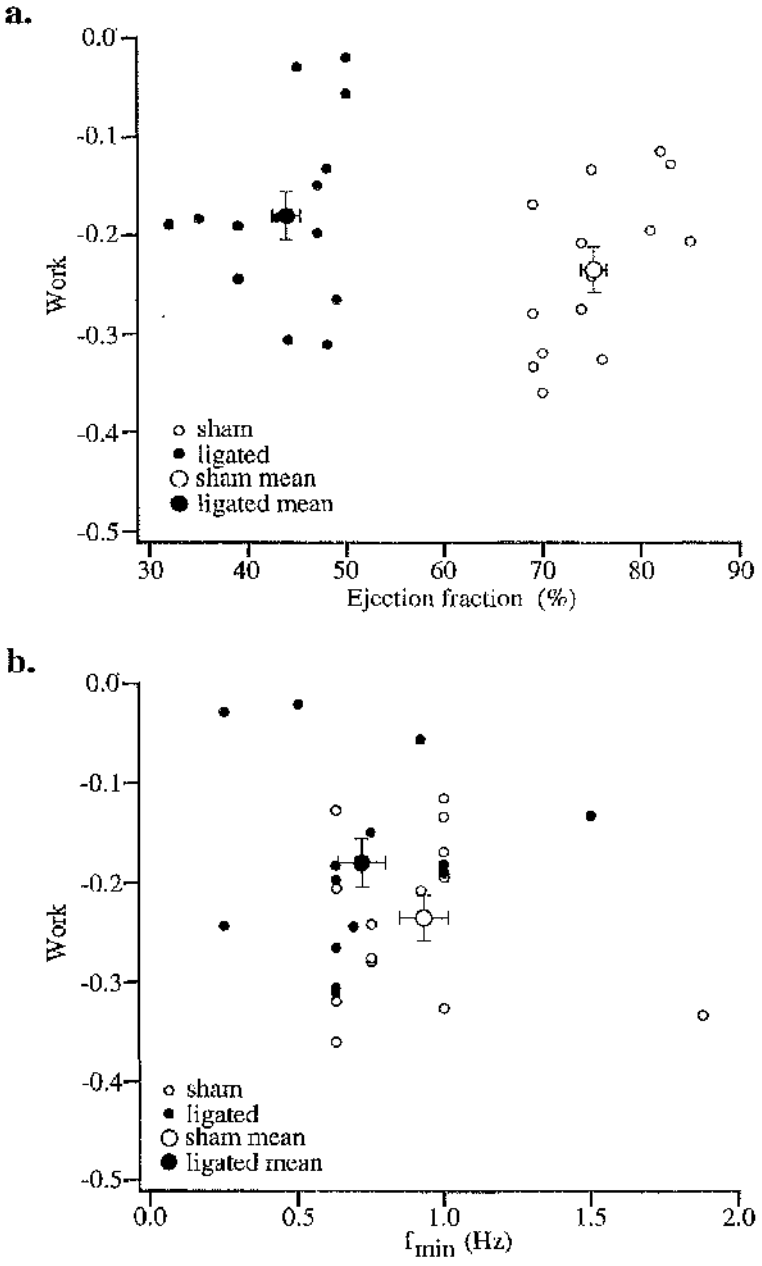

Fig. 4.5. Graph showing negative work performed against **a.** EF and **b.** f_{min} for both sham (○), n=13, and ligated (●), n=15, animals. The larger open and filled circles represent the mean values±sem for both data sets. Negative work: -0.24±0.02 vs -0.02±0.02, p>0.05, sham and ligated respectively. **a.** EF: 75.24±1.29 vs 43.88±1.43 and **b.** f_{min} : 0.93±.08 vs 0.72±0.08 Hz, p<0.05.

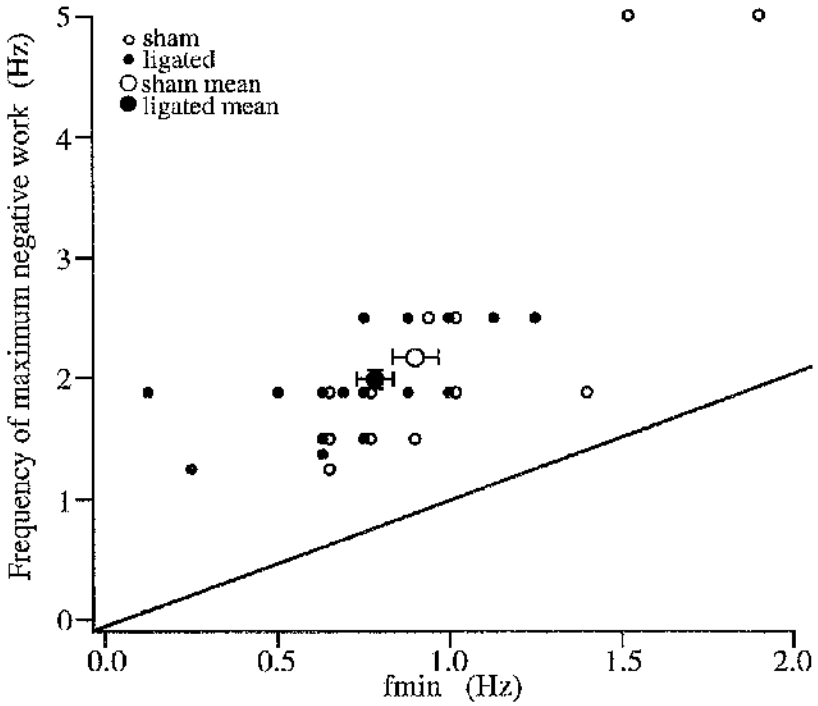

Fig. 4.6. Relationship between the frequency at which maximum work is absorbed and f_{min}. The larger open and filled circles represent the mean for both sham and ligated animals respectively (neg. power freq: 2.17±0.02 vs 1.99±0.08 $p>0.05$, and f_{min} : 0.93±0.08 vs 0.72±0.08, $p<0.05$). —— denotes the line of equality.

Power output

Power, the rate at which work is done, is calculated from the product of net work (results shown in previous paragraphs) and the frequency at which the trabecula was oscillated.

Fig. 4.7a shows the maximum power generated by individual trabeculae, from both sham and ligated animals, plotted against its ejection fraction. A reduced ejection fraction tends to be associated with a decreased maximum power generating capacity.

Fig. 4.7b shows the same power values, but this time plotted against f_{min}. Both power and f_{min} from ligated preparations were significantly lower than controls.

Fig. 4.8 shows the relationship between the frequency at which maximum power is generated and the frequency at which the crossbridges are cycling for individual trabeculae. The means for the frequency of maximum power output are not significantly different between the two groups ($p>0.05$). In both groups, the frequency at which maximum power is generated is marginally faster than the frequency at which maximum work is generated, but still slightly slower than the frequency at which the crossbridges are cycling.

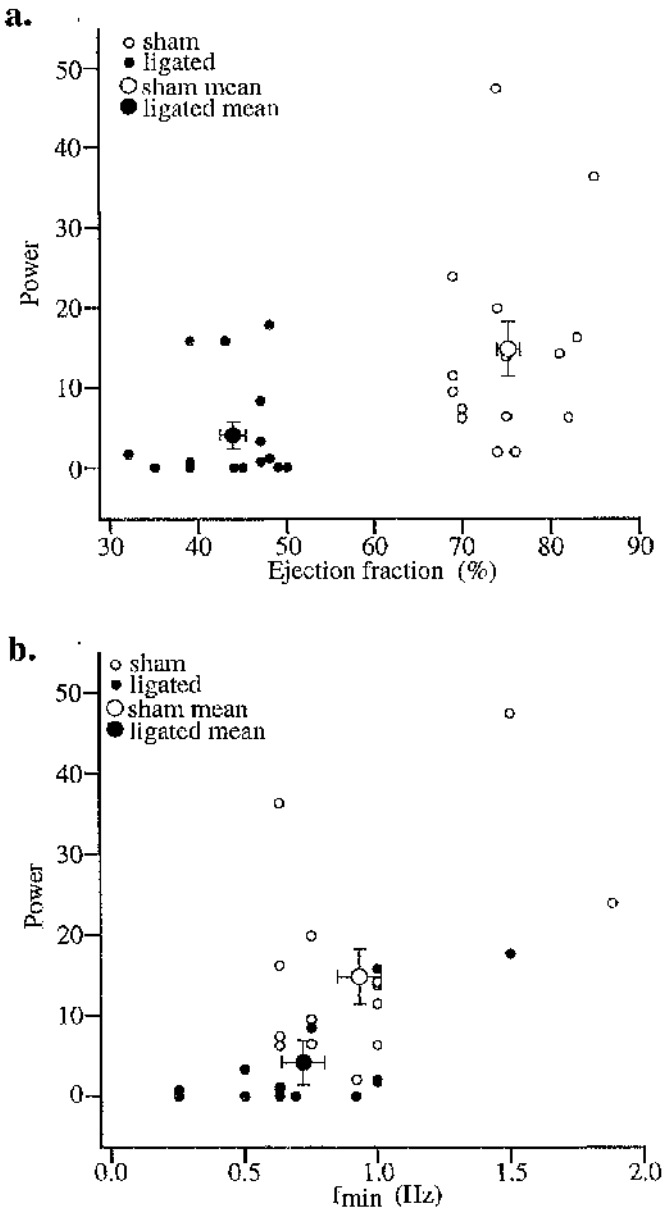

Fig. 4.7. Graph showing positive power generated by trabeculae against **a.** EF and **b.** f_{min} for both sham (○), n=15, and ligated (●), n=16, animals. The larger open and filled circles represent the mean values for both data sets. Power: 0.015±0.0034 vs 0.004±0.0017, p <0.01 sham and ligated respectively. **a.** EF: 75.24±1.29 vs 43.88±1.43 % and **b.** f_{min} : 0.93±0.08 vs 0.72±0.08, p<0.05.

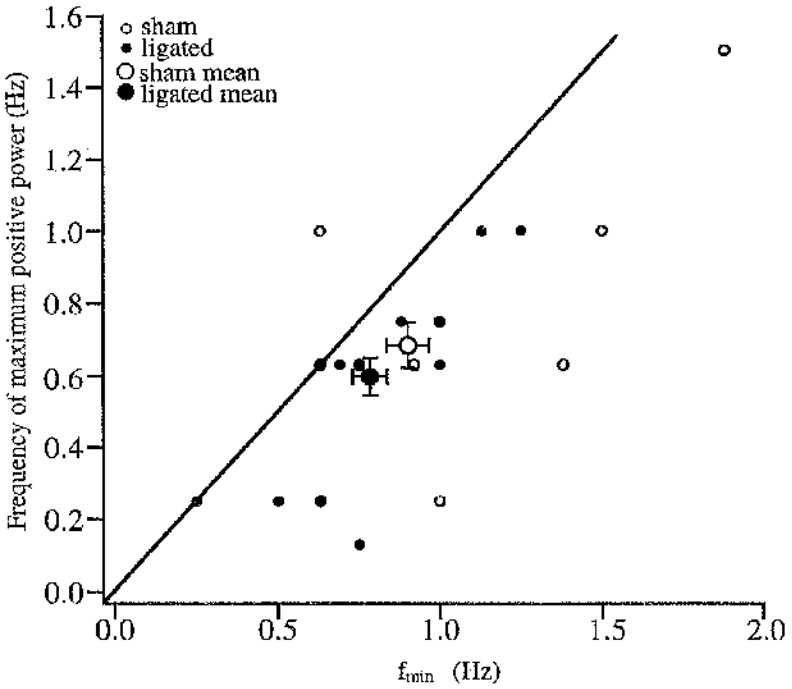

Fig. 4.8. Relationship between the frequency at which maximum power is generated and f_{min}. The larger open and filled circles represent the mean for both sham and ligated animals respectively (power freq: 0.68±0.06 vs 0.60±0.05, $p>0.05$, and f_{min} : 0.93±0.08 vs 0.72±0.08, $p<0.05$).

—— denotes the line of equality.

Power absorbed

Fig. 4.9a depicts the relationship between maximum power absorbed by individual trabeculae and their EF for both sham and ligated animals. The mean power absorbed by LVD trabeculae is significantly lower than the mean power absorbed by the control group.

Fig. 4.9b shows the same power values and the means plotted against f_{min}. The means for the two parameters are significantly different between sham and ligated animals.

Fig. 4.10 shows how the frequency of maximum negative power varies with the cycling frequency of the crossbridges. The mean frequency at which maximum power absorption occurs is not significantly different between the two groups. In both groups, the frequency at which maximal power absorption occurs is faster than the frequency of maximum work absorption, and again, this frequency is significantly higher than the mean frequency of crossbridge cycling.

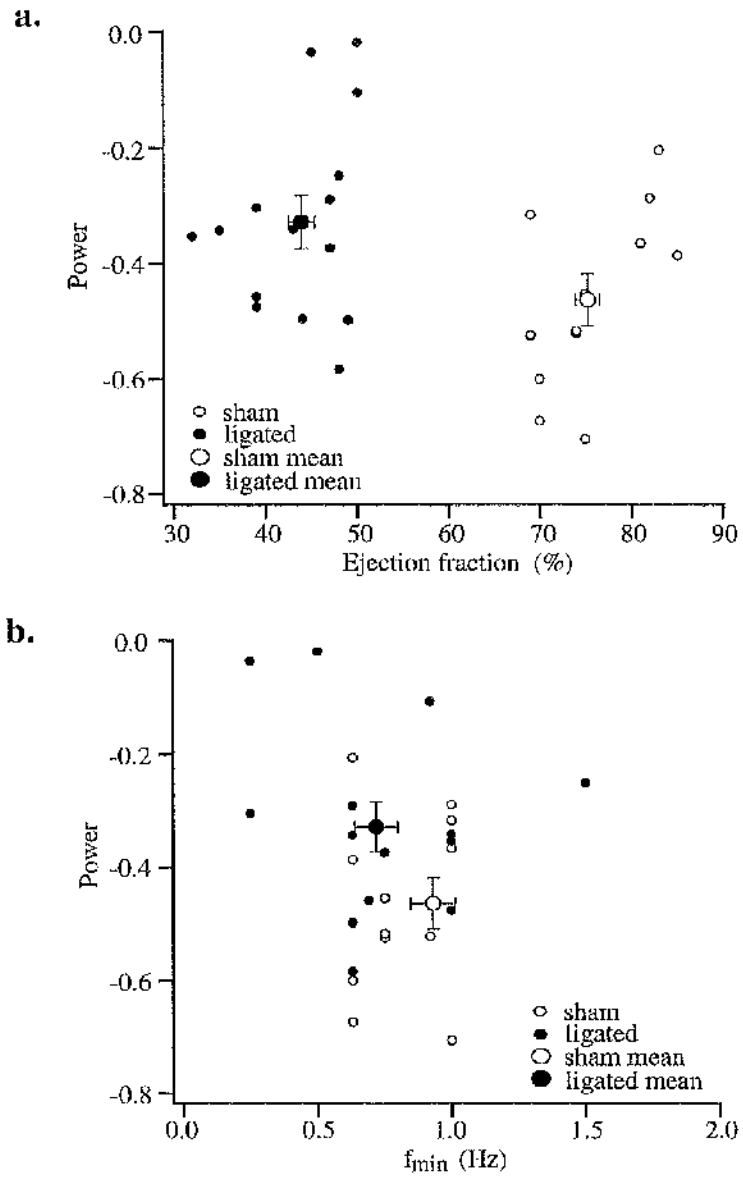

Fig. 4.9. Graph showing maximum power absorbed by trabeculae against **a.** EF and **b.** f_{min} for both sham (○), n= 13, and ligated (●), n=15, animals. The larger open and filled circles represent the mean values±sem for both data sets. Negative power: -0.51±0.06 vs -0.33±0.05, $p < 0.05$, sham and ligated respectively.
a. EF: 75.24±1.29 vs 43.88±1.43 and **b.** f_{min} : 0.93±0.08 vs 0.72±0.08, $p<0.05$.

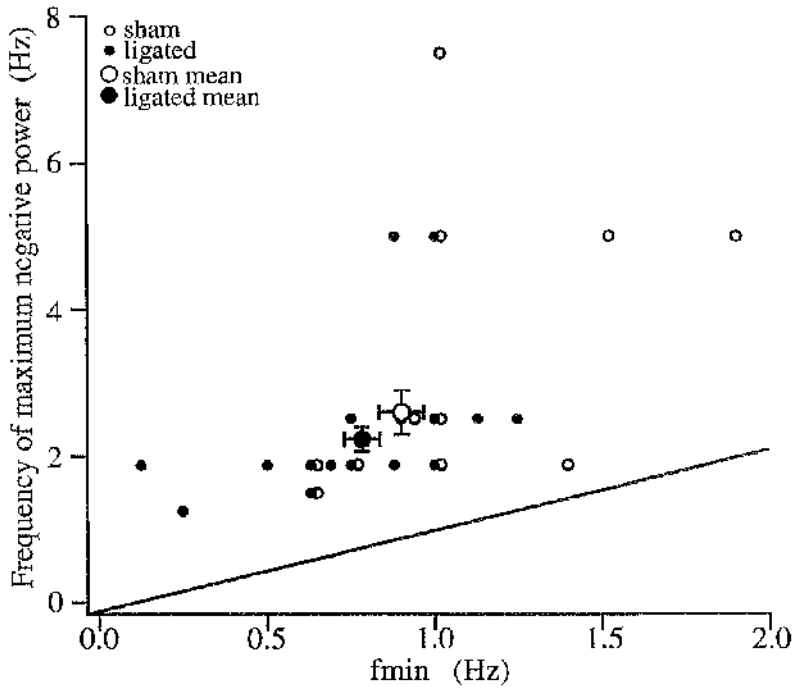

Fig. 4.10. Relationship between the frequency at which maximum power is absorbed and f_{min}. The larger open and filled circles represent the mean for both sham and ligated animals respectively (neg. power freq: 2.59±0.30 vs 2.22±0.16 $p>0.05$, and f_{min}: 0.93±0.08 vs 0.72±0.08, $p<0.05$). —— denotes the line of equality.

Loop correction

The positive and negative work and power values obtained using equations 2.4 and 2.5 in Methods section *2.13.4* were subject to correction, since the phase shift measured at a single point in the cycle was not always representative of the phase shift observed throughout an entire cycle (though maintained from one cycle to the next - see Methods *2.13.4* for examples of this). The force vs length loops thus produced were not symmetrical. A correction factor (which we have termed the 'loop correction factor') was calculated for each individual preparation and then the corresponding work and power values were multiplied by this loop factor to obtain the accurate values. The mean loop correction for each parameter is quoted for both sham and ligated animals in Table 4.2. When compared using t-tests, the loop correction factor for both positive work and power were significantly different between the two sets of animals.

The mean work and power values calculated before loop correction are shown in Table 4.3. The values in this table overestimate the actual work and power output of the trabeculae in both groups, specifically so in the ligated group.

	n	Mean max. work performed	Mean max. work absorbed	Mean max. power performed	Mean max. power absorbed
Sham	15	0.023±0.004*	-0.235±0.023	0.015±0.003*	2.59±0.30*
Loop correction		0.684±0.022*	1.054±0.012	0.678±0.022*	1.050±0.012
Ligated	16	0.008±0.003	-0.180±0.024	0.004±0.002	-0.329±0.016
Loop correction		0.368±0.024	0.991±0.011	0.314±0.024	0.992±0.045

Table 4.2 Maximum work and power results after loop correction. (significance of difference between sham and ligated groups, * $p<0.05$).

	Sham	Ligated
n	15	16
Max. +ve work±sem	0.030±0.005*	0.019±0.005
Max. -ve work±sem	-0.239±0.021	-0.209±0.032
Max. +ve power±sem	0.018±0.003*	0.012±0.005
Max. -ve power±sem	-0.606±0.103	-0.380±0.059

Table 4.3 Summary of the mean data for the work and power output of trabeculae from both sham and ligated groups before loop correction. (significance of difference between sham and ligated groups, * $p<0.05$).

Resting muscle

A muscle at rest is obviously not capable of generating external work. This can be verified by imposing sinusoidal length perturbations to a trabecula at rest. Fig 4.11a shows that the phase shift between length and force waveforms in a resting muscle. There is no phase shift observed between the two waveforms on the rising limb, however, there is a small phase lead on the descending limb. Fig. 4.11b shows the corresponding force vs length loop that is produced when the waveforms in Fig. 4.11a are plotted. As expected the loop is quite flat, but rotates in a clockwise direction, therefore a small amount of work is being absorbed by the trabecula at rest.

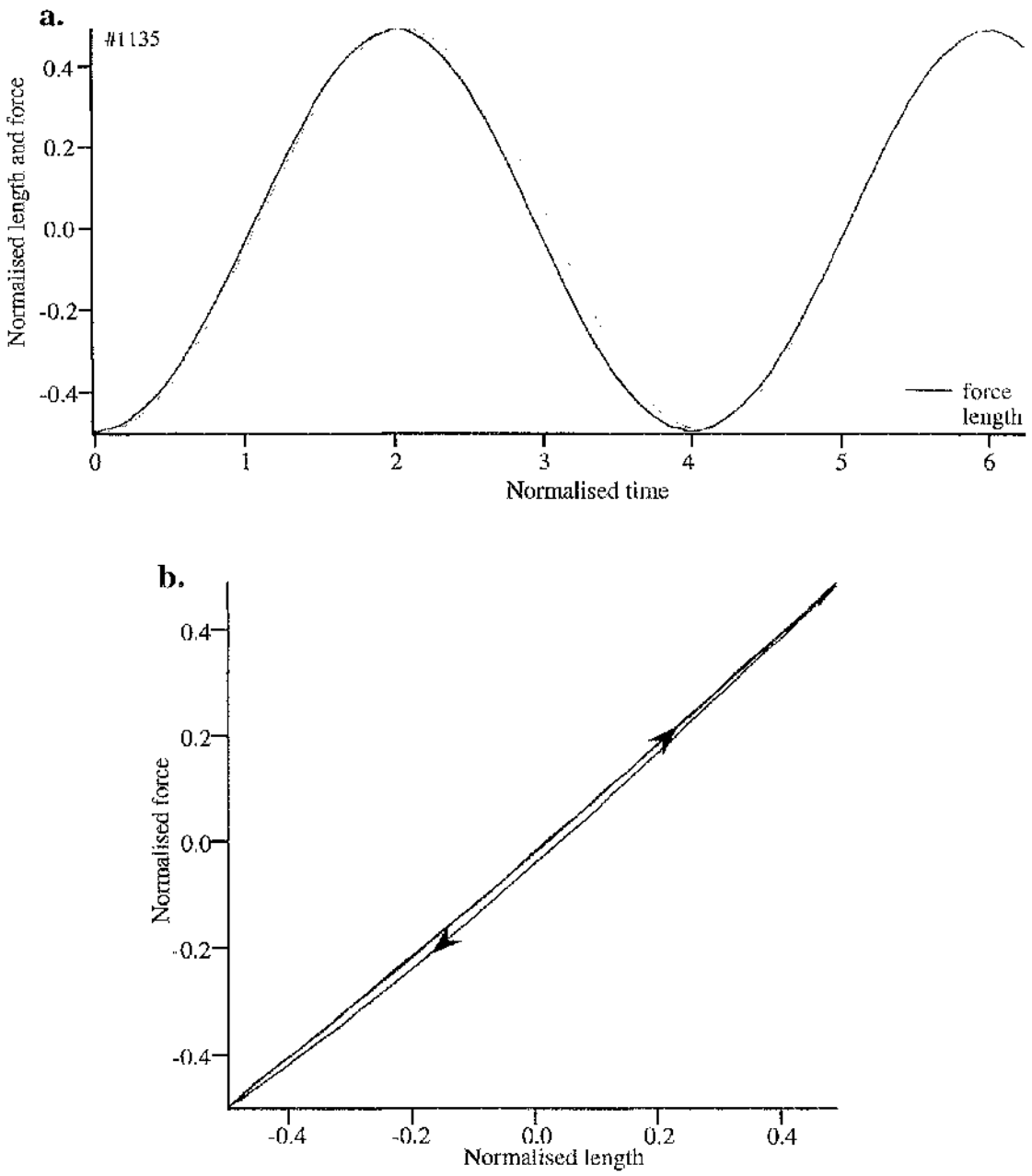

Fig. 4.11. Normalised length and force waveforms of a trabecula at rest. **a.** Sinusoidal length and force waveforms. There is no phase difference on the rising limb of the waveform, however, there is a small phase lead (indicative of work being absorbed) on the descending limb. **b.** Force vs length loop, corresponding to the waveforms in **a.** The loop rotates clockwise, therefore a small amount of work is being absorbed while the trabecula is at rest.

Rigor muscle

Fig. 4.12 shows the phase relationship between the length and force waveforms for a preparation in rigor. When rigor force is fully developed, in the absence of ATP, all the crossbridges are able to attach to, but are unable to detach from actin. Therefore, the preparation becomes very stiff (which is detected by an increase in the amplitude of the force transient produced during sinusoidal oscillation- see Chapter 3). During rigor a small phase lag is observed between the length and force waveforms (see Fig. 4.12a) therefore the trabecula is generating a small amount of external work. Correspondingly, the area within the length-force loop produced during rigor is very small (see Fig. 4.12b).

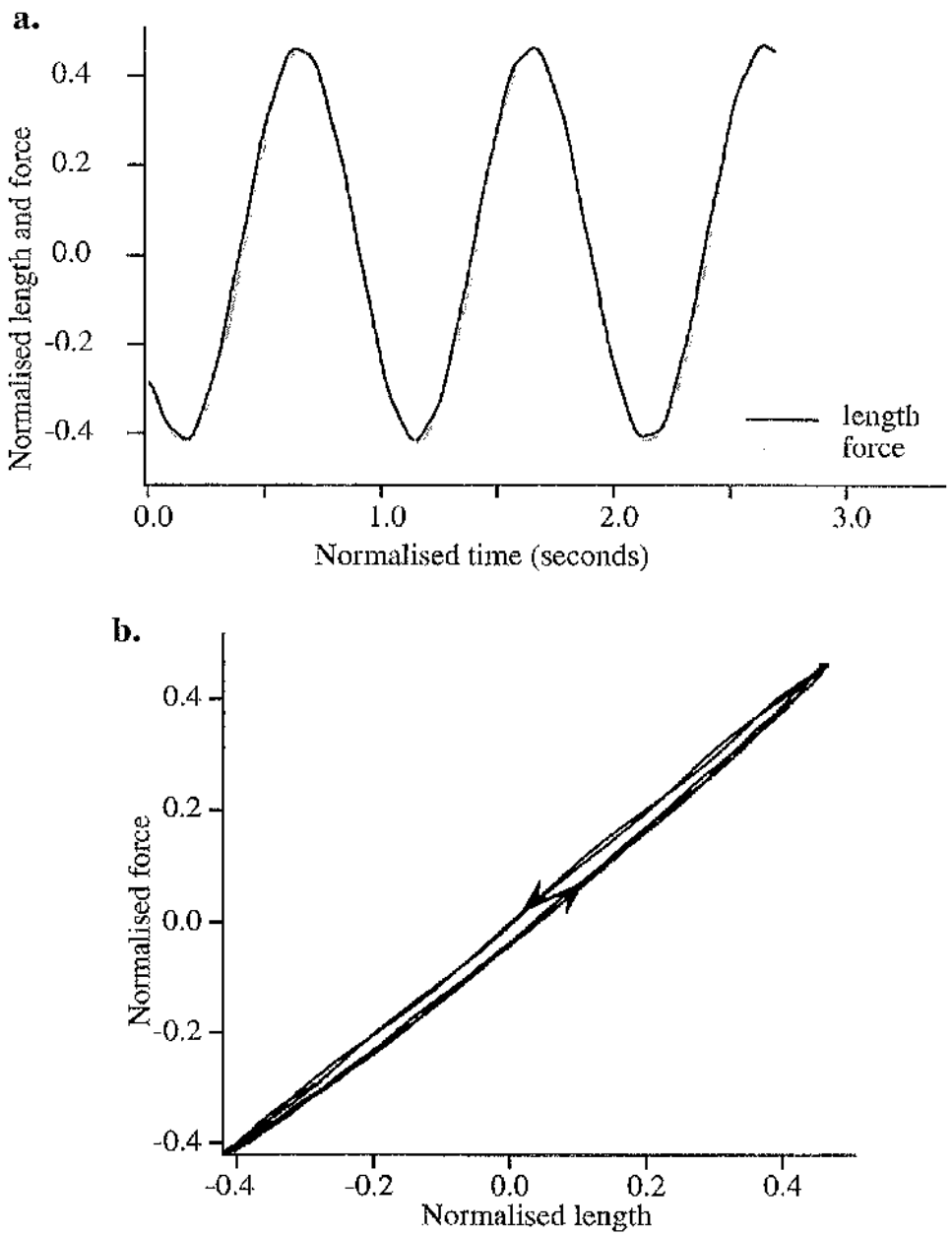

Fig. 4.12. Phase relationship between length and force waveforms for a trabecula in rigor at 1 Hz. **a.** Normalised length and force waveforms plotted against time which has been normalised to the start of oscillation. **b.** Normalised force vs length loop corresponding to the waveforms in **a.** In this example, length marginally precedes force therefore the loop rotates anti-clockwise indicative that a small amount of external work is being generated by the trabecula at this frequency.

4.3 Discussion

It is well established that the phase relationship between the length and force waveforms obtained from sinusoidally perturbed striated muscle reveals information about its mechanical properties (Thorson and White, 1969; Kawai and Brandt, 1980). Phase shift is calculated from the time difference between the sinusoidal length and (approximately sinusoidal) force waveforms, for each discrete frequency imposed upon the muscle, and then expressed as an angular delay in degrees. The phase shift between the two waveforms is frequency dependent in Ca^{2+}-activated muscle and can be either positive, when length precedes force (phase lag), or negative, when force precedes length (phase lead).

Phase shift is an important parameter in investigating muscle kinetics as it is used to calculate the (positive and negative) work and power generating capacity of the muscle. A plot of force vs length produces a loop which rotates clockwise or anti-clockwise, depending on whether the phase shift is positive or negative, the area within reflects (positive or negative) work. If no phase shift is observed between the two waveforms, the muscle is neither generating or absorbing oscillatory work and the area within the force vs length loop is zero.

In the LVD group, maximum positive and negative phase shifts are significantly reduced compared with controls. This indicates that there must also be significant alterations in the work and power generating and absorbing capacity of the muscle in the LVD group. Indeed, this is the case (see following text for more details). As shown in Methods, the phase shift between the two waveforms is quickly established after a change in frequency is imposed, tending to stabilise well within one cycle (see Fig. 2.4). Some authors (*e.g.* Rossmanith, 1986) argue that the time taken for phase shift to stabilise at each frequency is one of the drawbacks of this technique. This is their main argument in favour of using the PRBN technique to examine the kinetics of striated muscle which only requires that the perturbed system

attains steady state only once at the beginning of experimentation. However, in our analysis of phase shift, we have observed that the phase shift between the two waveforms is not necessarily constant throughout a single cycle (see Methods, Figs. 2.4, 2.8 and 2.9), but nevertheless entirely stable. Therefore, the brief periods of oscillation used in the PRBN technique will not provide an accurate assessment of the phase shift at each frequency and subsequently (positive and negative) work and power generation. Since the phase shift was not always constant throughout a single cycle, we determined a correction factor (as described in Methods, section *2.13.4*), which we termed the 'loop correction' factor. This amounts to an estimate of actual loop area relative to that anticipated for a constant phase shift value. The product of the loop correction factor and the work or power value obtained using equations 2.4 and 2.5 (in Methods, section *2.13.3*) gave an accurate value for the actual work or power generated by the trabecula at that frequency. When there was a phase lead (*i.e.* when oscillatory work/power was being absorbed), the loop correction factor was similar and close to 1 for both groups, meaning that the phase shift remained fairly constant throughout a single cycle. However, when there was a phase lag (*i.e.* when external work/power was being generated), the loop correction factor was significantly lower for the ligated group than for controls (see Table 4.2). This reveals that the loops produced for the ligated animals were less symmetrical in shape than the control loops, and consequently, the work and power values assessed using equations 2.4 and 2.5 were significantly over-estimated for the ligated animals than for the controls. It was consistently observed that the difference in the shape of the ligated loops was mainly on the shortening side of the loop, *i.e.* during concentric contraction (see Fig. 4.2a and b, panel (i), for comparison). The anti-clockwise loop for the sham is fairly symmetrical whereas the area is virtually zero under the shortening side of the loop in the ligated example.

Under resting conditions, the heart is working at sub-maximal mechanical potential (Katz, 1992). This reflects the sub-optimal myofibril length (ventricular filling) and inotropic state of the heart. Therefore, cardiac muscle has a substantial

contractile reserve which allows the myocardium to enhance its performance to meet the haemodynamic demands of the body . However, in heart failure, the myocardium has reduced scope in conditions such as exercise which require enhanced contractile performance *i.e.* an increased work and power output. The results in this chapter have shown that the ability of the myofilaments themselves under conditions of optimal activation to generate work, and thus produce power, is reduced in this model of heart failure. To understand the implications of this result the normal functioning of the heart *in vivo* should be considered.

A decreased contractility associated with heart failure has been well documented in the literature (*e.g.* Hajjar and Gwathmey, 1992; Hasenfuss *et al,* 1992; Solaro *et al,* 1993). Alterations in contractility, however, are clinically very difficult to assess accurately. The measurement of pressure-volume loops (for diagrammatic representation see Fig. 4.13) are among the best of the present approaches for the assessment of the contractile behaviour of the intact heart (Opie, 1995). Analysis of work-loops derived from sinusoidal analysis bear a striking resemblance to the pressure-volume loops derived clinically (Syme, 1993).

During the early period of contraction of the ventricle, the aortic and pulmonary valves remain closed (a, Fig. 4.13) while the mitral and tricuspid valves close, therefore the muscle is developing pressure without a corresponding change in the volume within the ventricles. This phase is known as isovolumic contraction and is analogous to isometric conditions experimentally. During isovolumic contraction the myocardium is generating force without length change and is therefore not producing external work. (There will, of course, be some local movements within the chamber walls as forces are equilibrated across the activated tissue and internal work is accomplished by the crossbridges). Once sufficient pressure has developed, the aortic and pulmonary valves open (b, Fig. 4.13), and the ejection phase begins (somewhat analogous to isotonic conditions). The rate at which the blood is ejected, once the aortic valve is opened, is influenced here by the power generating ability of the muscle rather than simply by the work generated by the muscle. The power output

of the myocardium is the rate at which the muscle is performing work and is intimately related to the heart rate of the animal (Layland *et al,* 1995a, b). At the end of the ejection phase, the heart then undergoes a phase of isovolumic relaxation after the closure of the aortic valve (c, Fig. 4.13). The mitral and tricuspid valves then open (d, Fig. 4.13) and the period of filling occurs during which there is a small change (*i.e.* increase) in first the ventricular volume and then pressure, such that lengthening occurs. Part of the resistance to filling is contributed by the active crossbridges still attached as myocardial relaxation proceeds.

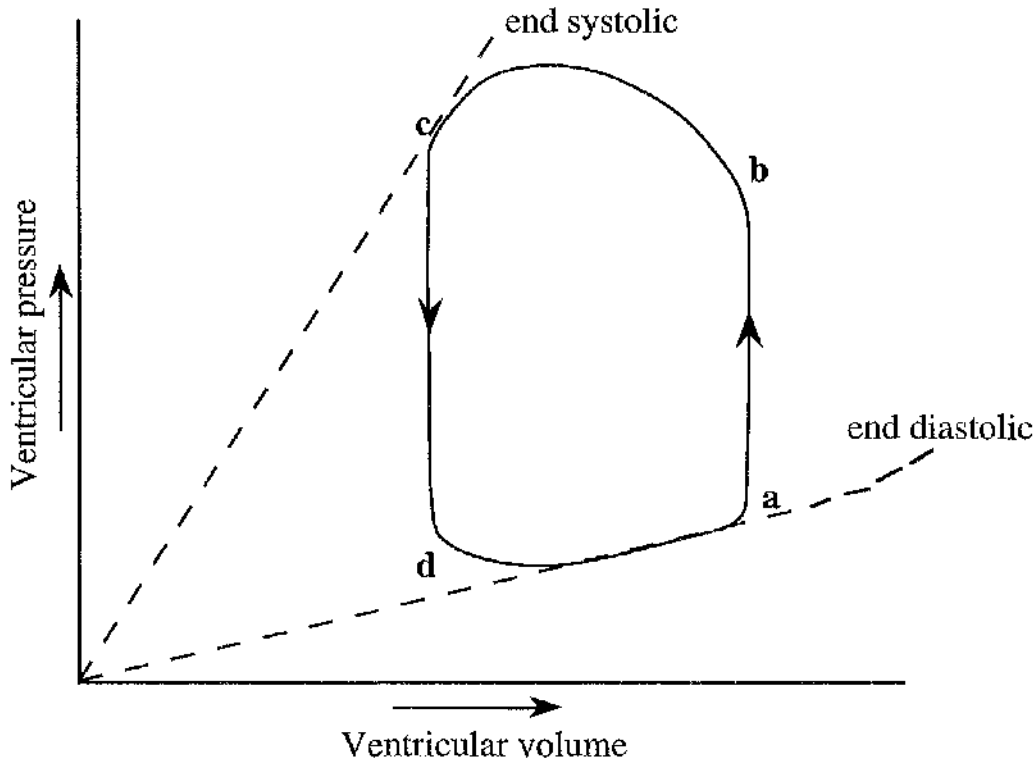

Fig. 4.13. Diagrammatic representation of pressure-volume loop.

The physiological significance of the results obtained from this study examining the work and power output of trabeculae from a rabbit coronary artery ligation model *in vitro* are best described by relating the impact of the alterations observed in these parameters on the pressure-volume characteristics of the heart *in vivo*. During isovolumic contraction, the muscle is mostly only performing internal work. The results in this study show that the ability to do work (*i.e.* shorten and generate force) in neighbouring cells is reduced in LVD. The development of

quasi-isometric force (analogous to isovolumic pressure) in the whole heart (or either ventricle) requires that the component segments both develop force and sustain it. The maximum force is set, and then maintained, by the weakest link in the mechanical chain. To develop quasi-isometric force those crossbridges (or sarcomeres, or cells, or groups of cells) that are too weak to shorten against their stronger colleagues must at least be able to resist being lengthened unduly, else force will fall. The intrinsic force production by the trabeculae is not significantly reduced in this model of LVD (see results chapter 3). However, the phase analysis here reveals that the kinetic properties (which define the ability of the muscle to produce work or power) are defective in LVD. While isometric force might be relatively unchanged, the capacity to move this force through significant distances (shortening or lengthening) is significantly reduced. Therefore, the rate of development of quasi-isometric force in the isovolumic phase can indeed be compromised even if 'true' isometric force is not. This deficit will be more prominent once ejection begins. From this point in the cycle then, there is significant shortening which will again require local adjustments which will subject some crossbridges (or sarcomeres, or cells, or groups of cells) to stretch (or at least stress) as others can shorten. With a reduced maximal work generating capacity, the diseased trabeculae would have a slowed initial phase of contraction (*i.e.* isovolumic contraction). Another facet of a reduced working capacity of the myocardium is that the time taken to produce the same amount of force as the control would be increased and, therefore, more internal work would be required to do so. If the work capacity is reduced it will take longer for sufficient pressure to build up within the ventricle in order to open the valve. This effect could somewhat be compensated for if, during the ejection phase, the myocardium was able to generate sufficient power. However, this study has shown that the myofilaments of the failing myocardium generate less power, so the rate at which the ventricle expels blood, and the amount expelled, is also compromised. These various deficits will all lead to a decreased ejection fraction, as is observed in this model. This work and power generating deficit would be exacerbated *in vivo*, since the heart would be pumping against an increased afterload,

due to the increased peripheral resistance associated with the progression of heart failure. Ultimately, this would require an increased work and power generating capacity of the myocardium in order to supply the body effectively. However, the failing heart cannot accommodate this increase and is placed under further stress.

In normal myocardium, the frequency at which maximal work output is optimal is marginally slower than the frequency at which power output is maximal. In addition, the frequency at which power output is maximal is slightly slower than the frequency at which the crossbridges are cycling. We have shown that the frequency at which maximal work and power is produced is slower in the LVD trabeculae. The results in Chapter 3 provide evidence that the crossbridges are cycling at a slower rate in the trabeculae from myocardium showing signs of LVD. The relationship between the frequency of maximal work and power output is thus maintained such that these frequencies remain close to the intrinsic cycling rate of the crossbridges. Therefore, although the frequency at which maximal work and power generation occur is reduced, it may be a consequence of the muscle adapting to stress.

Chapter 5

Alterations in Relaxation Kinetics of Trabeculae from a Rabbit Model of Left Ventricular Dysfunction Using an 'EGTA-jump' Protocol

5.1 Introduction

It is now established that CHF can develop in patients with well-preserved systolic function due to abnormalities in diastolic function. Attention paid to myocardial relaxation increased after the knowledge that this process may be affected long before contraction has become inadequate in various heart disease states (Braunwald and Ross, 1963; Hirota, 1980). Diastolic dysfunction is the major pathophysiologic mechanism in approximately 40% of patients with symptoms of CHF (Soufer *et al,* 1985; Nwasokwa, 1993; Vassen *et al,* 1996). Clinically, diastolic function is taken to include aspects of relaxation as well as resting properties of the myocardium, influenced by, for example, passive elasticity. Recognition of diastolic dysfunction in humans is crucial for appropriate therapy to be administered, particularly since CHF treatment aimed at improving systolic function may be useless, or even detrimental, in alleviating the underlying diastolic dysfunction (Lorell, 1991).

The relaxation of systolic force requires the rapid reduction of Ca^{2+} to its resting level (*i.e.* ~0.2μM). The initial removal of free Ca^{2+} occurs via uptake into the SR. The rapid fall in cytosolic Ca^{2+} then favours the dissociation of Ca^{2+} from TnC which inactivates the thin filaments. This is achieved when Tm returns to its resting position along the actin filaments, preventing further crossbridge attachment. As those active crossbridges which remain bound at this point detach, force declines. The interplay of these mechanisms determines the rate at which myocardial force declines in intact preparations.

The majority of studies examining the activation and relaxation kinetics of cardiac muscle have used isolated preparations, such as papillary muscles, trabeculae or single myocytes, rather than using the whole heart. Utilising isolated preparations such as these removes many of the complications encountered in kinetic studies using the intact heart. Assessing myocardial relaxation in the working whole heart is

complicated due to variations in the load imposed on the heart (Brutsaert *et al*, 1980) and the non-uniformity of adjacent myocardial segments (Blaustein and Gaasch, 1983; Brutsaert, 1987). Collectively, these can alter the variables used to define the lusitropic state. Indeed, in this study, and many others, chemically-skinned trabeculae have been favoured for examining the relaxation kinetics of cardiac muscle, as they allow better control of the variables just discussed. With chemically-skinned trabeculae, the SR and sarcolemma have been disrupted, therefore no intact, functional SR remains within them. This allows the examination of relaxation kinetics without the intervention of the SR, so that the rate at which the SR sequesters Ca^{2+} need no longer be considered as a possible rate-limiting factor in determining the relaxation rate. The main factor now governing the rate of decline of $[Ca^{2+}]$ is the rate and extent of binding of Ca^{2+} to the calcium buffer EGTA, which is free to diffuse between the myofilaments; the concentration of free Ca^{2+} is influenced by the release of Ca^{2+} from TnC. As mentioned previously in this thesis, the use of skinned preparations does not detract from the validity of comparing the results with those using similar, intact preparations, as Saeki and colleagues (1991) have shown that the crossbridge kinetics of skinned and intact ferret (similar isomyosin composition to the rabbit) trabeculae were not significantly different from one another.

The crossbridge cycling rate has been shown to be slower than normal in human myopathic trabeculae (Hajjar and Gwathmey, 1992), whereas the maximal force generating capacity of the trabeculae remains unchanged. With a reduced crossbridge cycling rate, the time each crossbridge spends attached to actin will be increased, assuming that the attachment time as a fraction of the cycle duration does not decrease, leading to a subsequent decrease in the rate of relaxation. This slowing of crossbridge rate may serve as a compensatory response which tends to preserve normal cardiac output in an energy efficient manner. The same decrease in crossbridge cycling rate is also observed in other species (Mercadier *et al*, 1981), however, the mechanism governing this decrease in cycling rate may not necessarily be the same.

In smaller mammals, such as the rat, the slowing of the crossbridges can be accounted for by a change in the predominant myosin isoform within the ventricles. The predominant myosin isoform found in normal rat myocardium is the V_1 type ($\alpha\alpha$-homodimer). However, with chronic overload, a shift in the predominant isoform from the V_1 to the V_3 type ($\beta\beta$-homodimer) occurs. The former of these isoforms has a faster ATPase rate (Lompre *et al,* 1979), but lower force generating capacity than the latter (Van Buren *et al,* 1995). This isoform shift is considered to be an energy-efficient adaptation to myocardial stress (Alpert and Mulieri, 1982) such that normal force can be developed at a lower ATP cost. In larger mammals such as the rabbit and human, a change in the distribution of myosin isoforms cannot account for the slowing of the intrinsic crossbridge cycling rate (Mercadier *et al,* 1983), since the predominant isoform present in normal myocardium is already of the slowest, V_3 type.

The aim of the experiments detailed in this chapter was to examine the rate of relaxation of skinned trabeculae from a rabbit model of left ventricular dysfunction, using an EGTA concentration-jump protocol ([EGTA]-jump), and compare this with sham-operated controls. We have altered the rate of relaxation by simultaneously changing both the $[Ca^{2+}]$ and the concentration of the Ca^{2+}-buffer EGTA within the solution immediately surrounding the trabecula. Chemically-skinned trabeculae have been used, such that only the myofilaments remain functionally intact. After chemical skinning, the bathing solution surrounding the preparation essentially becomes an extension of the intracellular environment. Therefore, any differences in relaxation rate observed between the two groups can be confidently attributed to alterations in the properties of the myofilament proteins themselves. The diffusion rate for a small molecule such as EGTA (or CaEGTA) is unlikely to be significantly different between ligated and normal hearts after chemical skinning. Indeed, even structures like the myofilament lattice do not form a significant diffusion barrier for small ions and molecules.

5.2 Modelling the diffusion problem during [EGTA]-jump induced relaxation

The aim in these experiments was to test whether it was possible to increase the speed of relaxation by increasing the [EGTA] gradient to the point where the rate of change of $[Ca^{2+}]$ around the myofilaments was no longer rate limiting. In that case, the time course of relaxation will be determined solely by the molecular controls over crossbridge detachment. (These controls could still include the 'off' rate for TnC, but evidence from flash photolysis experiments strongly suggests that crossbridge detachment itself is then rate limiting; see Discussion). It was assumed that the speed of change of $[Ca^{2+}]$ within the tissue would increase progressively (but not necessarily linearly) if the EGTA concentration step was increased. However, the complexities of the diffusion problem involved, of Ca-buffering, and of the highly non-linear relationship between $[Ca^{2+}]$ and force required that this assumption be tested.

We have mathematically modelled the experimental situation (a sudden change in external [EGTA]) in the following way. In order to calculate the amount of force expected at a given time during relaxation produced by lowering $[Ca^{2+}]$ with EGTA, the following assumptions and simplifications have been made:

i. each preparation is regarded as cylindrical in shape and initially equilibrated to the $0.2_{Activating}$ solution (Table 2.3, Methods).

ii. the preparation cross section is initially treated as fifty concentric annuli of equal thickness that are equally spaced across its entire radius (see Fig. 5.1).

iii. to model the effects of an 'unstirred layer', the outer annulus of the preparation (*i.e.* no. 50) was considered not to contribute to the force generation of the trabecula.

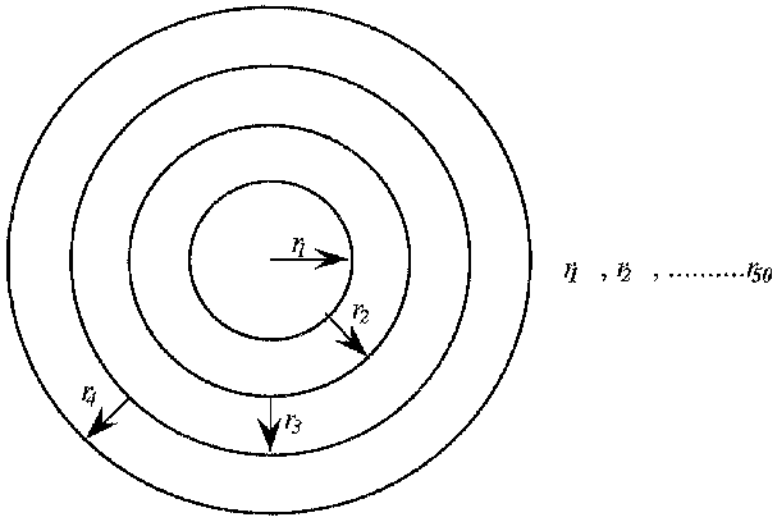

Fig. 5.1. Diagram showing the arrangement of the annuli assumed within a single trabecula. For illustrative purposes, only four annuli are shown with their respective radius (r), however, for our calculations we assumed there were fifty. ($r_0 = r_{50}$)

The solution for this condition that is required is given by (Crank (1956), equation 5.22):

$$\frac{C - C_i}{C_o - C_i} = 1 - \frac{2}{a} \sum_{n=1}^{20} \frac{e^{-D\alpha_n^2 t} J_0(r\alpha_n)}{\alpha_n J_1(a\alpha_n)} \qquad (5.1)$$

where C is the concentration (of the diffusing substance) for a particular annulus and a particular time, C_0 is the surface concentration, C_1 is the initial concentration in the cylinder, J_0 is the zero order Bessel function of the first kind, J_1 is the first order Bessel function, D is the diffusion coefficient for EGTA (cm^2s^{-1}: Kushmerick and Podolsky, 1979), t is time in seconds, α_n is the nth root of the Bessel function, r is the radius of interest and a is the outer radius of the cylinder. For stability, the first twenty roots of the Bessel functions have been taken.

By solving equation 5.1 for various times after a sudden alteration in the extracellular [EGTA], the concentration of EGTA in each annulus can be calculated. (The same calculation also predicts the fall of the [CaEGTA] as the CaEGTA species can be considered to diffuse out of the preparation.) With knowledge of the

concentration of both $EGTA_{free}$ and CaEGTA, for a given time and for each annulus, we can calculate $[Ca^{2+}]$. This was done by solving the following quadratic equation (unpublished derivation: D.J. Miller and D.G. Moisescu, 1976):

$$(Ca_{free})^2 * K + Ca_{free}(1 + K(EGTA_{total} - Ca_{total})) - Ca_{total} = 0 \qquad (5.2)$$

The initial $[Ca_{total}]$ was taken as 0.22 mM (that of CaEGTA plus 20μM, the contamination level previously determined, *e.g.* Smith and Miller, 1984). K is the $K_{apparent}$ for the interaction of EGTA and Ca under the present ionic conditions ($5 \times 10^6 M^{-1}$).

Knowing $[Ca^{2+}]$ allows calculation of the relative force for each annulus (from the Hill equation below):

$$\frac{C_x}{C_{max}} = \frac{K_{Ca}^{-h}[Ca_x]^h}{1 + K_{Ca}^{-h} + [Ca_x]^h} \qquad (5.3)$$

where h is the Hill coefficient, C_{max} is the maximum force at saturating Ca^{2+} levels, C_x is the force at a given $[Ca^{2+}]$ and K_{Ca}^{-h} is the reciprocal of the $[Ca^{2+}]$ producing half C_{max} raised to the power h (K_{app} was taken as 2.75 and 2.78×10^{-6}, and h as 3.33 and 2.82, appropriate for these preparations, sham and ligated respectively). This simplification that equation 5.3 (derived from steady-state observations) applies instantaneously has been used by other authors in similar circumstances (*e.g.* Westerblad and Allen, 1994).

The proportion of total force attributable to each annulus was assumed to be proportional to the fractional area (A) contributed by each annulus ($=r_2^2 - r_1^2 / r_0^2$, where r_2 is the outer and r_1 is the inner radius of the annulus and r_0 is the overall radius of the cylinder). Summing force calculated for all the annuli at a given time predicts the total relative force. Typically, forces for each of 10 or 20 time points spread across the total time of interest were calculated for a given relaxation condition.

The model was run in Excel 5. Graphical output showed the relative equilibration of the cross section and the relative activation of the annuli making up

the cross section. When the mathematical solution proved unstable (typically at very short times, revealed as significantly 'oscillating' (fluctuating) force predictions at the asymptotes), or where the relative force was changing very steeply, spatial resolution was increased by a factor of 10 or more (by modelling an additional 50 annuli across the region of steepest buffer or Ca^{2+} concentration change). Spurious 'negative' predicted concentrations (emerging as values of relative concentration approaching very nearly 0 or 1) were suppressed. This modelling exercise indeed predicts that the rate of relaxation would continue to increase significantly as the [EGTA] step is increased over the range of interest, if the rate of fall of Ca^{2+} were to be the rate limiting factor (see Fig. 5.2).

Since the effect of a change in pH was investigated at the highest [EGTA]-step, it was useful to model the predicted behaviour from the diffusion model. Fig. 5.3 shows the consequence of altering K_{app} by a factor of 0.5 log units (the approximate net effect of a 0.5 pH unit increase raises the affinity of EGTA by 1 log unit, but that of the muscle by only 0.5 log units (*e.g.* Smith and Miller, 1984)). As might be anticipated, for the lowest [EGTA]-step, the rate is altered (slowed), by increasing muscle Ca^{2+} affinity or speeded by lowering it. However, at the higher [EGTA]-step (100mM illustrated) very little change occurs. This is because the inward diffusion of EGTA, to an extent sufficient to control $[Ca^{2+}]$, is such a steep wave 'front' that activation switches from high to low across a few percent of its cross section. Thus the diffusion model predicts virtually no effect of a change of pH (or any other factor affecting Ca^{2+}-sensitivity) on the highest speed of relaxation.

It may be argued that a difference in preparation diameter may strongly influence the rate of trabecular relaxation. In addition, coronary artery ligation may induce alterations in myofibrillar arrangement, influencing the lattice spacing of the myofilaments, such that the diffusion coefficient for EGTA may be different between the two groups of animals. Therefore, altering both of these parameters and their effect on relaxation rate was investigated. Figure 5.4 models the effect of a different preparation diameter and diffusion coefficient on the predicted rate of relaxation. The

rate constant taken from the model (as in Figs. 5.2 and 5.3, where single exponentials are fitted) is plotted. The 'error' bars (at 150µm diameter) indicate the upper and lower estimates of rate constant from forcing the single exponential best fit to the earlier and later parts of the model relaxations, respectively. The semi-log plot reveals that a straight line fit is reasonable (against log [EGTA]), so for some other conditions examined, only the upper and lower extremes were modelled (*e.g.* here for 100µm diameter). Fig. 5.4 shows that for a given diameter, an increase in diffusion coefficient (D in equation 5.1) produces a parallel upward shift in the rate vs log [EGTA] plot. Further, the effect of a reduction in radius at a given value of D is to steepen the slope and displace upward on the Y axis, as would be expected. Increasing the number of radii regarded as modelling the 'unstirred layer' (see page 135 (iii)) allows the small delay before the onset of rapid relaxation, seen in real data, to be mimicked.

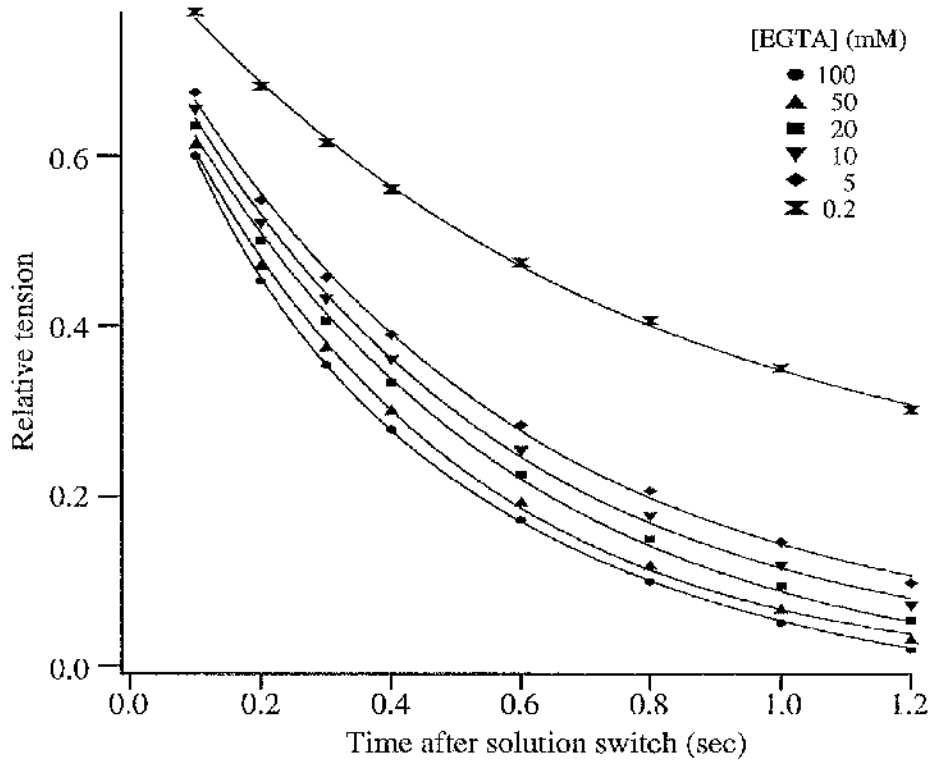

Fig. 5.2. Diffusion model predicted time courses for relaxation over a range of [EGTA]-steps from 0.2-100 mM (for a trabecula of 150 µm and a diffusion coefficient of 1 x 10^{-6} cm^2 s^{-1}). The model predicts that the rate of relaxation would continue to increase significantly as the [EGTA] step is increased over the range of interest, if the rate of fall of Ca2+ were to be the rate limiting factor.

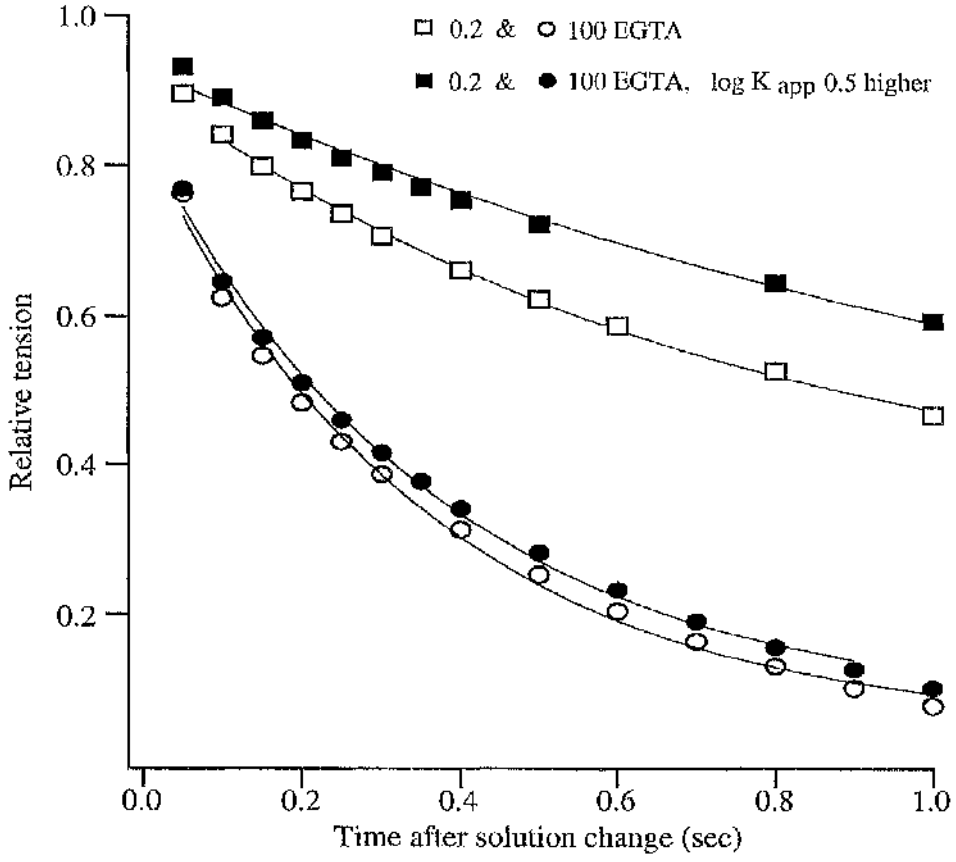

Fig. 5.3. Theoretical effect of increasing muscle Ca-affinity on relaxation time (for a trabecula of 150 μm and a diffusion coefficient of $1 \times 10^{-6} cm^2 s^{-1}$). As might be expected, altering kapp by a factor of 0.5 log units has altered (slowed) the rate of relaxation at the lowest [EGTA] step, however, this produced very little change at the higher [EGTA] step (100mM illustrated).

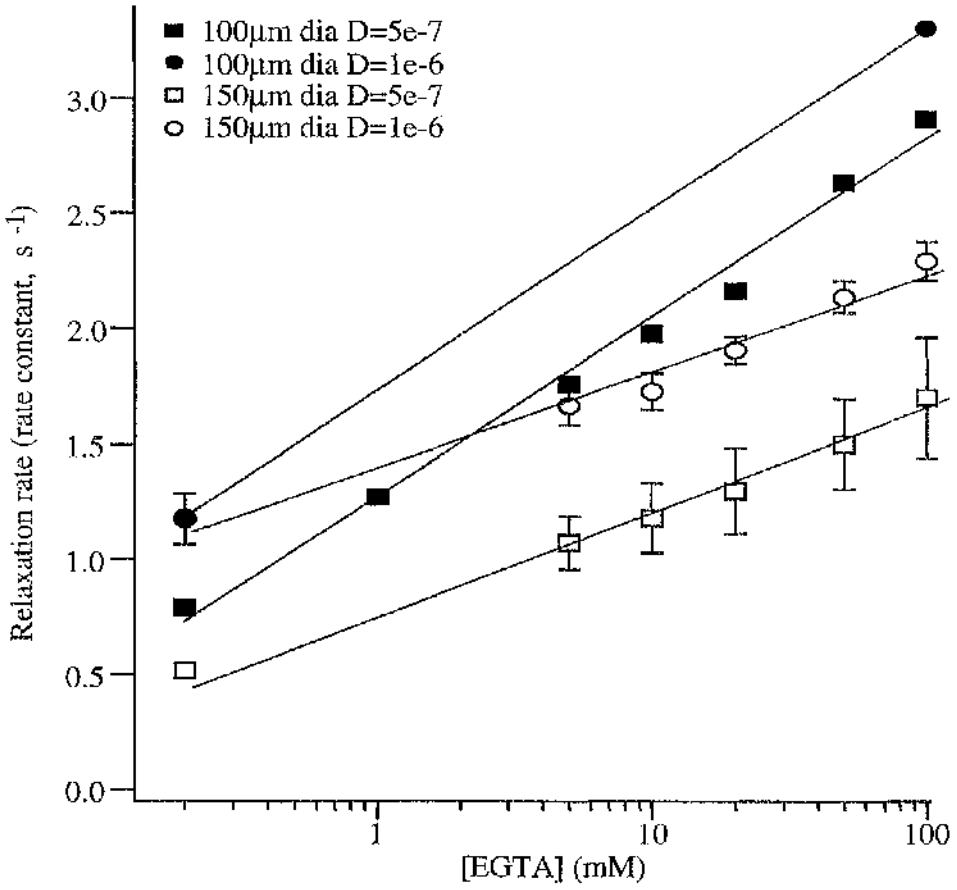

Fig. 5.4. Effect of Diffusion coefficient and diameter. This plot shows that for a given diameter, an increase in diffusion coefficient (D (cm^2 s^{-1}) in equation 5.1) produces a parallel upward shift in the rate vs log [EGTA] plot. Further, the effect of a reduction in radius at a given value of D is to steepen the slope and displace upward on the Y axis.

5.3 Results

It is important to establish the mean preparation dimensions for both groups, since a widely different diffusion distance (*i.e.* from the outside of the preparation to the centre of the preparation) between the two groups, across which EGTA must pass, would bias the results. Table 5.1 shows the mean preparation dimensions (length and minimum diameter) for both sham and ligated animals. There is no statistically significant difference between the dimensions of the two groups (length, p=0.72 and CSA, p=0.59). The minimum diameter of the preparations is used here as this represents twice the minimum distance (since the modelling process assumes the diffusion distance in terms of the *radius* of the preparation) through which the diffusing substance has to equilibrate

	n	Mean length±sem (mm)	Mean min. diameter (mm)±sem
Sham	11	0.90±0.05	0.126±0.007
Ligated	7	0.95±0.10	0.125±0.010

Table 5.1. Mean preparation dimensions for animals used in relaxation experiments.

From the force vs time plot obtained with the diffusion modelling described earlier, the experimental model predicts that the relaxation rate will continue to increase if Ca^{2+} is the only rate limiting factor in these experiments (see Fig. 5.2). Figure 5.4 shows the effect of modelling a large difference in diffusion coefficient and a change in preparation radius on predicted relaxation rates.

The first finding is that, in broad terms, the model predicts relaxation rates that correspond fairly well with those observed. The semi-log plot shows that (Fig. 5.4), for a given diameter, an increase in diffusion coefficient (D in equation 5.1) produces a parallel upward shift in the rate vs log [EGTA] plot. Further, the effect of a reduction in radius at a given value of D is to steepen the slope and displace upward on the Y axis.

The results obtained from tissues, particularly when plotted on linear axes, gave the strong impression that the rate saturates at the highest [EGTA] step. However, the slope of the theoretical relationship is also rather shallow, making it difficult to conclude with confidence that there is a departure between the theoretical and practically observed rates of relaxation. Closer inspection does show that for the failure group at least, the relevant combination of preparation dimension and plausible diffusion coefficient predicts a steeper relationship at the highest [EGTA] steps than that observed. For this group, at least, the extent of deviation between observed and modelled behaviour implies that the ligated preparations reach a region where the relaxation rate is no longer primarily determined by the rate of fall of $[Ca^{2+}]$.
Additionally, the rate of the real relaxation may be beginning to saturate in the LVD group, whereas that predicted would continue to rise. However, this is not apparent in as many preparations from the control group. Furthermore, the overall difference in relaxation rates between the sham and ligated groups is markedly different and cannot be easily explained simply in terms of diffusion (the results would imply a large difference in diffusion coefficient and diameter to account for the steepness and position of the log [EGTA] vs rate relationship). The fit is very satisfactory at lower [EGTA]-steps suggesting that where EGTA diffusion is the main factor limiting relaxation, the model is accurate.

Fig. 5.5a shows the relaxation transients obtained during a typical experiment with a sham-operated animal and 5.5b for a ligated animal. In all cases (sham and ligated) the transients were well fitted with a single exponential curve fit, indeed, the

exponential curve fits so well that it is difficult to distinguish between the original data and the curve fits.

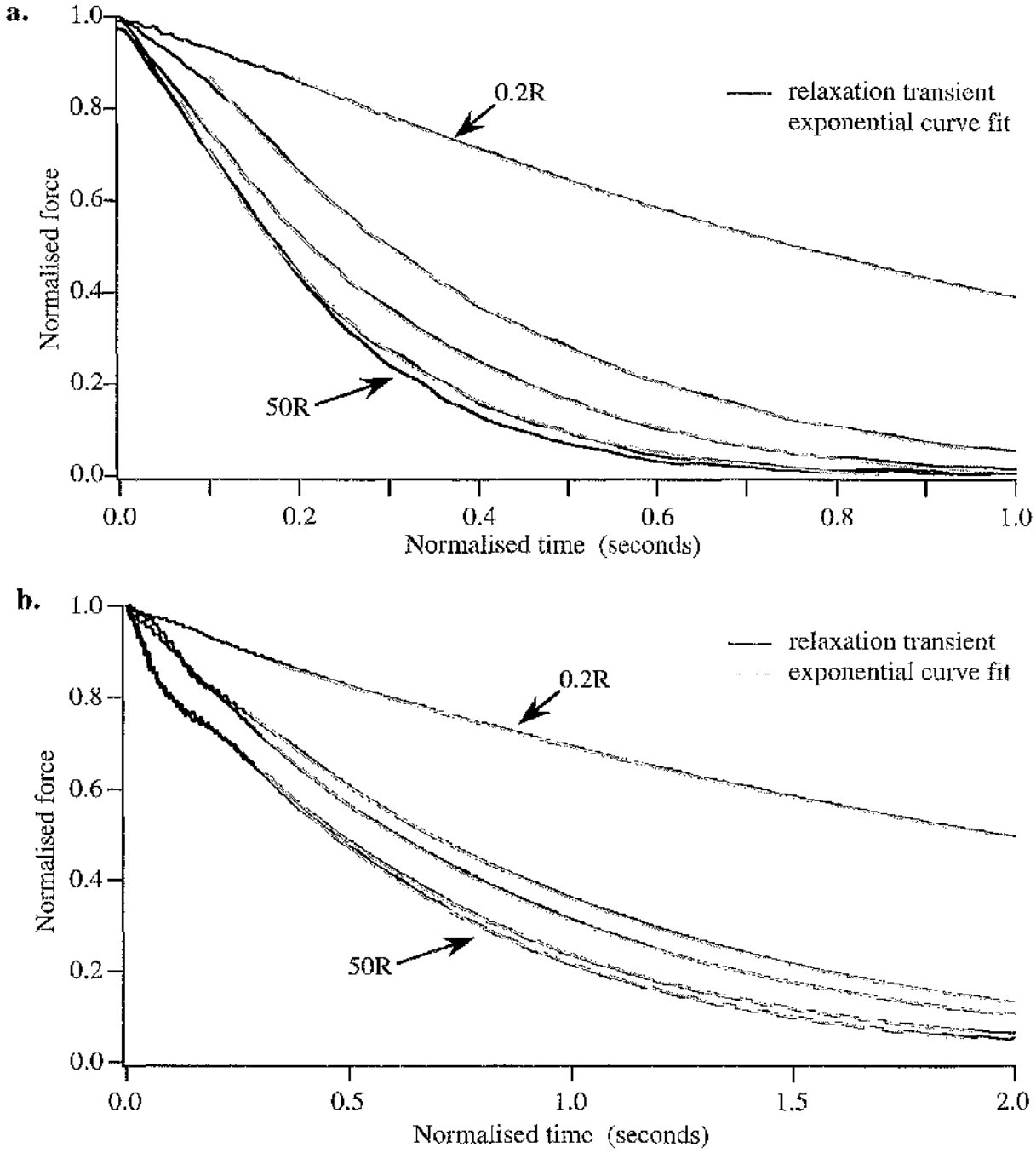

Fig. 5.5. Graph showing individual relaxation transients for a sham and ligated trabecula. **a.** relaxation transients for a sham-operated animal. **b.** relaxation transients for a ligated animal. In both **a.** and **b.** the transients obtained when relaxed in different [EGTA] solutions ranging from 0.2 - 50 mM have been fitted with a single exponential curve. In both instances, the exponential curve fits overlie the data so closely that the original data can barely be distinguished.

Fig 5.6a shows the relaxation rate constants (corresponding to the same transients illustrated in Figs. 5.5a and 5.5b), obtained from the exponential curve fitting process, for a typical single experiment using a sham-operated animal and 5.6b for a typical ligated animal. The range of rate constants derived over the range of [EGTA]-steps are well fitted with a rising exponential curve (as described in Methods, section 2.14.1). In these particular examples, the best-fit curve reaches a defined plateau whilst the diffusion-limited rate of $[Ca^{2+}]$ decline is still predicted to increase, indicating that at this [EGTA]-step some other slower intervention, other than the rate of $[Ca^{2+}]$ decline, is limiting the rate of trabecular relaxation. A similar situation was observed in the ligated animals. However, the maximal rate of relaxation was consistently slower than the rate of relaxation observed in the control group. The curve fitting procedure was repeated in this way for all experiments performed on both sham and ligated animals to obtain estimates of the asymptote indicating maximum relaxation rate. The mean rates for a given [EGTA]-step (±sem) were also plotted. The resulting curve-fits for individual experiments showed a much closer fit than that observed when the meaned data sets for both groups were plotted (compare Fig. 5.6a and b with Fig. 5.7). In addition, the mean rate for the control group does not appear to reach a clearly defined plateau, unlike the individual example shown in Fig 5.5. The mean rate for the LVD group, however, may just be reaching the point at the highest [EGTA]-step tested where the relaxation rate is just approaching its maximum and is no longer limited by the rate of change of $[Ca^{2+}]$.

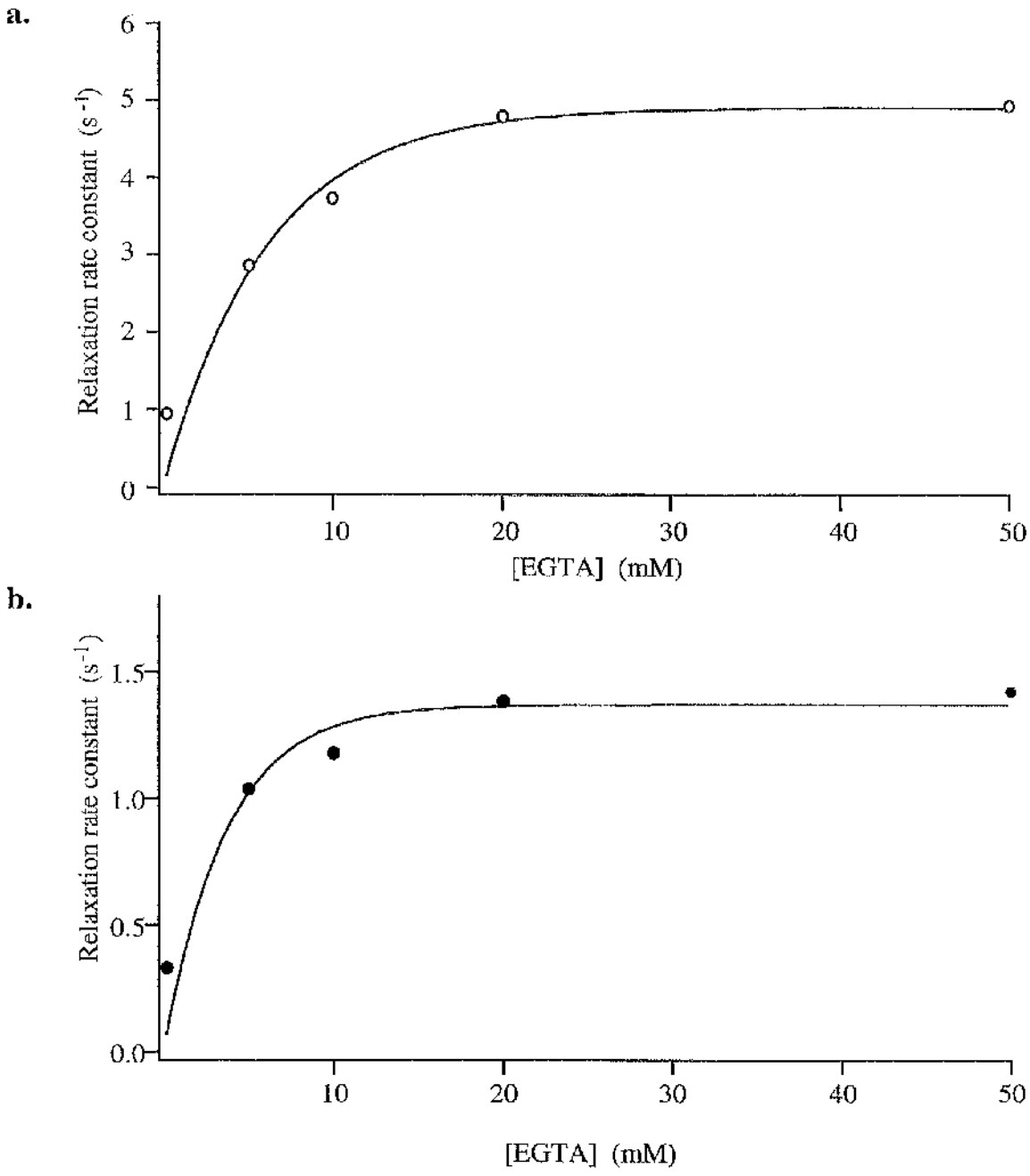

Fig. 5.6. Individual data for rates of relaxation at different [EGTA] steps. **a.** shows the individual data for a sham operated trabecula and **b.** shows the individual data for a ligated trabecula. The data set in both cases was well fitted with a rising exponential curve. From these graphs, the maximum rate of relaxation, obtained experimentally and also from the curve fitting process, is obtained. These numbers were then used to produce a graph of the mean rates (experimental and curve-fitting derived) for both groups, which is shown in Fig. 5.4.

Fig. 5.7 shows the results for the mean data sets for both sham (n=11) and ligated (n=7) animals and the corresponding rising exponential fit. The graph shows that the rate of relaxation almost reaches a plateau in the LVD group, indicating that the rate of relaxation seen at 50 mM EGTA is approaching the maximum rate of relaxation, whereas the rate of relaxation is still continuing to rise appreciably in the control group. However, it is clear that the rate of relaxation in the ligated group is significantly slower when compared with controls at all [EGTA]s used, and the rising exponential fit reaches a plateau at a significantly slower rate, indicating that the maximal rate of relaxation is decreased in this group. The curve fit shown in this figure employs the mean k_{EGTA} and $rate_{max}$ derived for the individual curve fits calculated for each preparation.

Fig. 5.8 shows a semi-log plot of the rates of relaxation at different [EGTA]-steps for two sham and ligated preparations that clearly showed a deviation from the predicted rate of relaxation at the highest [EGTA]-step examined. At this point some slower intervention, such as crossbridge kinetics, is the rate-limiting factor for relaxation. Since the rate of relaxation is beginning to saturate in some preparations indicates that we are approaching the maximal rate of relaxation which is governed by the myofilaments with this protocol.

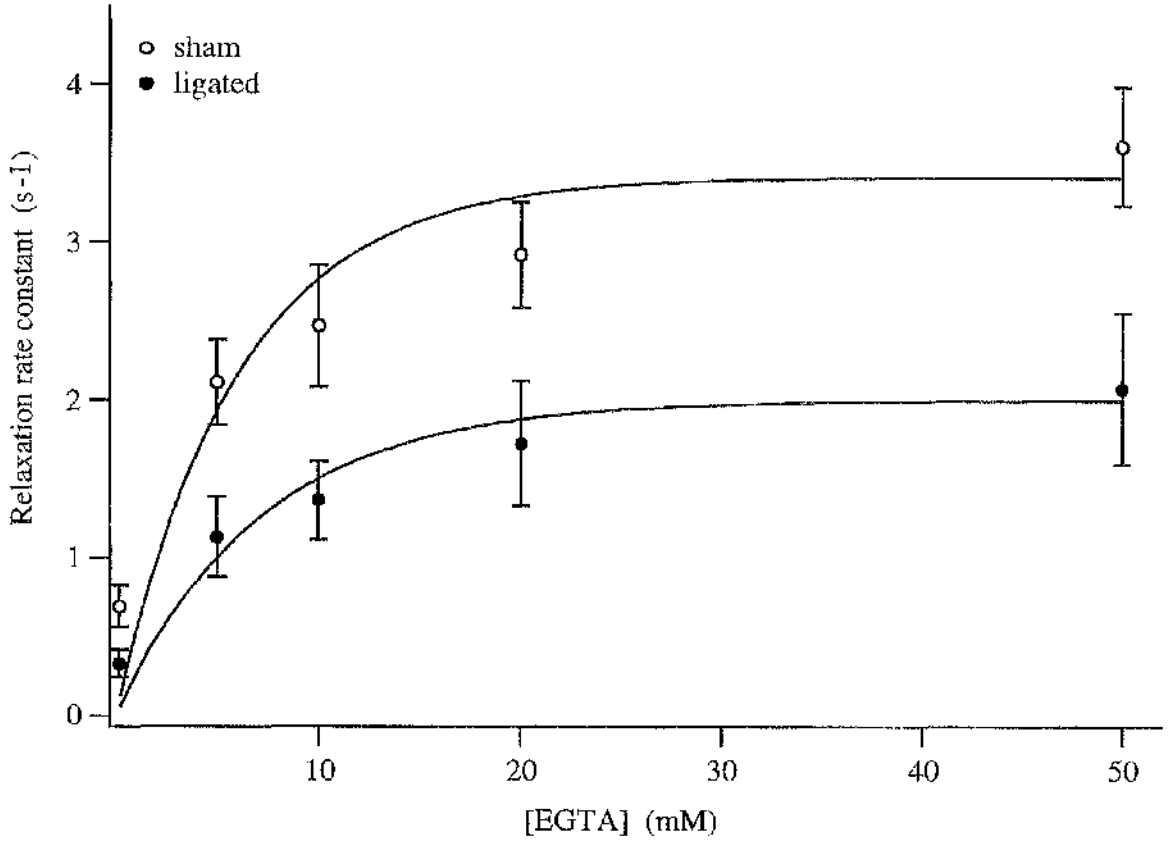

Fig. 5.7. Mean data for rates of relaxation at different [EGTA] for both sham (n=11) and ligated (n=7) animals. Each data set was fitted with a rising exponential curve and the mean fit is shown on the graph for both groups. The mean rates of relaxation between the two groups are significantly different from each other at all [EGTA], $p < 0.05$.

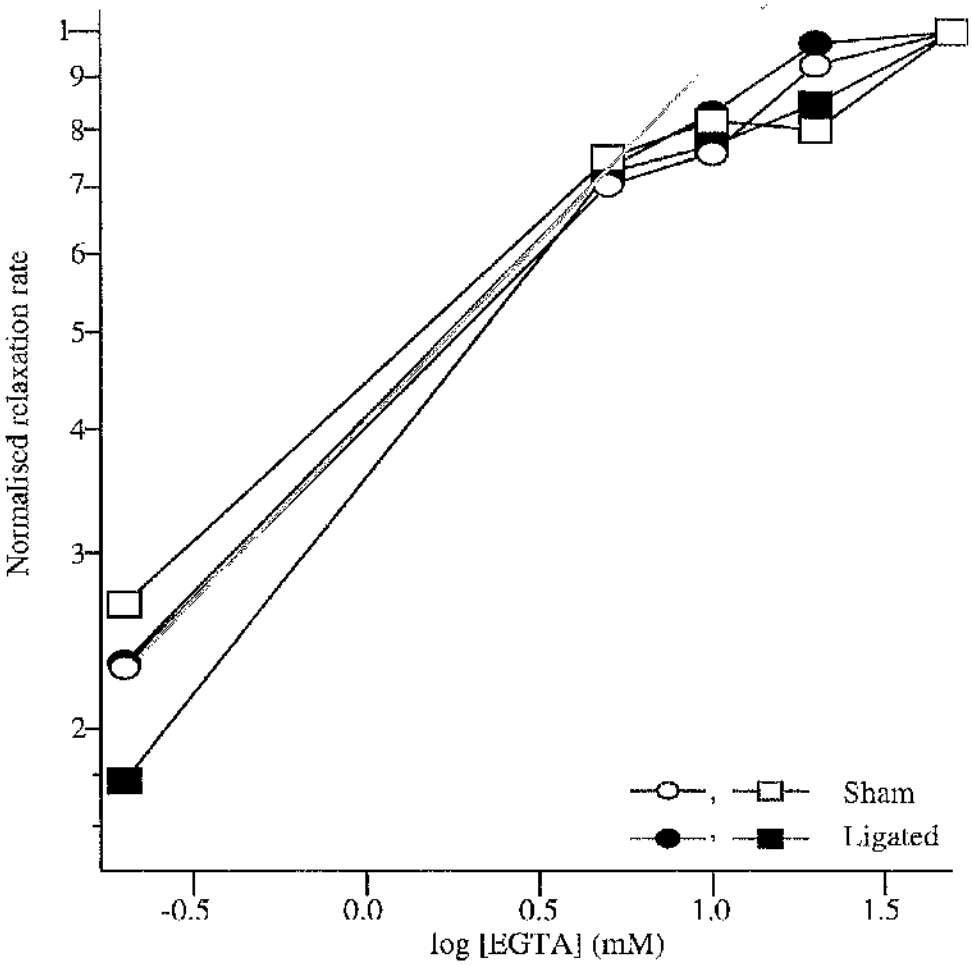

Fig. 5.8. Graph showing normalised relaxation rate against [EGTA] for two individual sham and ligated preparations. The grey line predicts the linear extrapolation of the rate predicted by the modelling exercise. It is evident in these preparations that at the highest [EGTA]-step the maximal rate of relaxation is beginning to saturate (*i.e.* deviate from that predicted). At this point the rate of fall of Ca is no longer rate-limiting.

Fig. 5.9 shows the relationship between the maximum relaxation rate and ejection fraction for both sham (n=12) and ligated (n=9) animals, with the corresponding best line of fit. With the exception of one obvious outlier amongst the ligated group, a trend is apparent showing a decrease in relaxation rate associated with a reduced ejection fraction. The n numbers shown in this graph are slightly higher than the n numbers quoted in Fig. 5.7. This is because the ejection fraction of a few of these animals were outside the criterion that was designated (and discussed in Chapter 3) at the beginning of this project for an animal to be included in the 'ligated' group for analysis. Briefly, ligated animals with an ejection fraction of ≤ 50 were regarded as showing clear LVD and were therefore included in the ligated group, whereas sham-operated animals with an ejection fraction of ≥ 65 were deemed normal and, therefore, acted as controls.

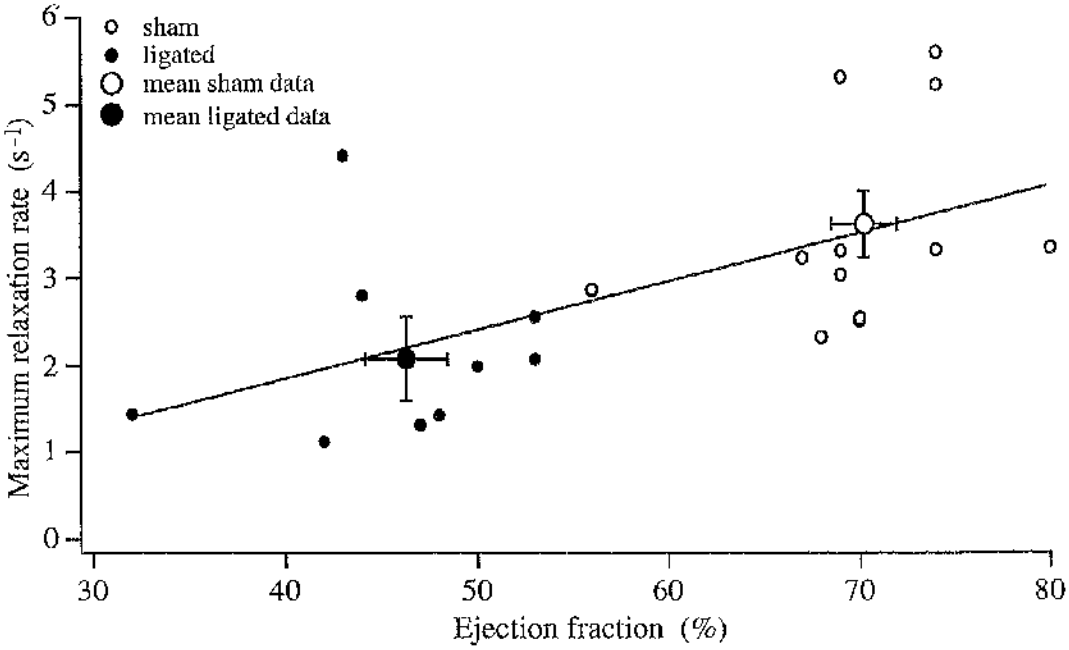

Fig. 5.9. Graph showing maximum relaxation rate against ejection fraction. Sham and ligated data are shown with the corresponding linear regression line. The larger circles represent the mean data±sem for both groups.

Table 5.2 summarises the data shown in Fig. 5.6 and 5.8 for both sham and ligated groups. In this table, both the mean maximum rate of relaxation obtained experimentally and the mean maximum rate of relaxation obtained from the curve fitting process are shown for both groups. These values were not significantly different from one another for either the sham or the ligated group, indicating that the rising exponential fit is reasonably representative of the individual data sets.

	Sham	Ligated
n	11	7
Max. rate (sec^{-1}) ±sem	3.61±0.38*	2.07±0.48
Best fit max.rate (sec^{-1})±sem	3.41±0.4*	2.00±0.46
% increase (pH 7.5)	16.94±9.49	16.36±7.12

Table 5.2: Summary of the mean data, obtained experimentally and also derived from the curve fitting process, for both sham and ligated animals. Significance of difference between sham and ligated groups is taken at the 5% level (evaluated using unpaired t-test).

Fig. 5.10 shows the effect on maximum relaxation rate when the pH of the solutions is increased from pH 7.0 to pH 7.5. The pH of the solutions was changed before the muscle was activated as well as throughout the relaxation. Both groups show a significant ($p<0.05$, statistical test performed on raw data) increase in the maximum rate of relaxation when compared with controls as the conditions are made more alkaline.

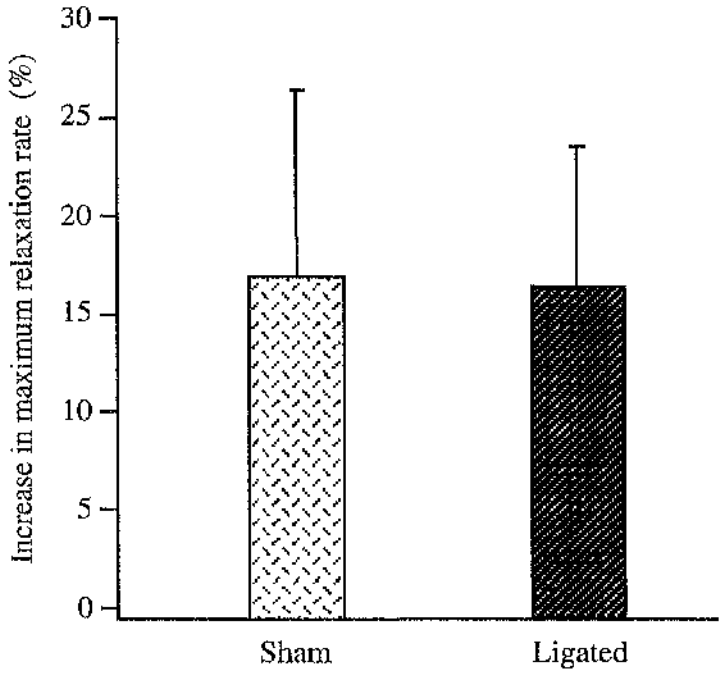

Fig. 5.10. Chart showing increase in maximum relaxation rate with an increase in pH to 7.5 expressed as a percentage of the rate at pH 7.0. Both sham and ligated animals demonstrated an increased rate of relaxation with increased pH (sham: 16.94±9.49 and ligated: 16.36±7.12 %).

5.4 Discussion

The rate of relaxation of skinned trabeculae from a rabbit model of LVD was investigated by altering the concentration of the Ca^{2+} buffer EGTA within the bathing solution. The skinning procedure ensured that any influence the SR would have had on relaxation, by resequestering Ca^{2+} or diffusion barrier provided by the sarcolemma, was eliminated. With no functional SR, the main factor controlling the uptake of free [Ca^{2+}] is the binding of the ion to available EGTA, with the rate of dissociation of Ca^{2+} from TnC influencing the level of free Ca^{2+}. We developed a model for investigating the kinetics of relaxation of skinned trabeculae using an EGTA-jump protocol, as described earlier in this chapter. This model predicts that the rate of relaxation of ventricular trabeculae will continue to increase significantly as the [EGTA]-step is increased, by accelerating the decrease of intracellular free [Ca^{2+}], if the change in [Ca^{2+}] is the rate-limiting factor (see Fig. 5.2). The results shown in this chapter demonstrate that the rate of relaxation of control trabeculae continues to increase with increasing [EGTA]-step, over the range of [EGTA]s used, whereas LVD trabeculae appear to be approaching their maximal rate of relaxation at higher concentration steps for EGTA (Figs. 5.5, 5.6 and 5.7). This result would suggest that the rate-limiting factor governing the rate of relaxation may no longer be Ca^{2+} at higher [EGTA]s in the LVD group, but most probably the crossbridge detachment rate. This is clearly not the case for the control group since the rate of relaxation is still increasing. Furthermore, the rate of relaxation in the ligated animals reached the limit at a significantly lower [EGTA]-step than the control animals, suggesting that there is an alteration in the myofilament properties of these preparations that is reducing the maximum rate of relaxation. This result cannot be easily described in terms of any likely change in diffusion properties of the diseased myocardium.

At birth, the rabbit LV contains both V_1 and V_3 isoforms, however, the V_1 isoform population then steadily declines with development. Myosin heavy chain

isoform shifts (from the V_1 isoform to the V_3 isoform) associated with hypertrophy and failure have been well documented in small mammals such as the rat (*e.g.* Mercadier *et al*, 1981). In larger mammals, including rabbits and humans, the predominant isoform is generally accepted to be the V_3 isoform, therefore no significant isoform shift is thought to occur with hypertrophy and failure, that could account for the observed alterations in contractile and relaxation kinetics. However, a few studies (Litten *et al*, 1985; Eble *et al*, 1997) have shown that there is a proportion of the V_1 isoform remaining within normal rabbit myocardium, that is not present after the development of left ventricular hypertrophy or failure (Eble *et al*, 1997). Eble and colleagues (1997) found that in normal rabbit myocardium ~22% of the total MHC content was of the V_1 isoform, and that this disappeared entirely when rabbits were allowed to develop LVD through chronic ventricular pacing. In addition, Litten *et al* (1985) found that even at five months, adult rabbit myocardium still expressed a proportion of the V_1 isoform. The rabbits used in this study were operated on at approximately two months of age, and then allowed to develop LVD for eight weeks post-ligation. Therefore, it is feasible that there is a small amount of the V_1 isoform remaining within the myocardium of the control rabbits used in this study, that may have shifted towards the V_3 isoform in the ligated group. This may indeed make an additional, small contribution (though unlikely to be solely responsible) to the slowing of the relaxation kinetics observed in this model.

Other alterations within the thick filament, such as the phosphorylation states of the regulatory myosin light chain (MLC_2) may be involved, and indeed some studies have related alterations in the phosphorylation status of MLC_2 to the contractile abnormalities that are observed in cardiac muscle under pathological conditions (*e.g.* Morano *et al*, 1988; Liu *et al*, 1995). Studies by Patel and colleagues (1998) examining the role of MLC_2 phosphorylation have shown that slowing of relaxation is associated with increased MLC_2 phosphorylation. Phosphorylation of MLC_2 has been shown to increase the probability of attachment of crossbridges as well as the rate constant for the transition of crossbridges from the weakly-bound,

non-force-generating states to the strongly-bound, force-generating states (termed f_{app}: Brenner, 1988). The outcome of this is, therefore, an increased ability of the muscle to generate force (Metzger *et al,* 1989; Sweeney and Stull, 1990; Sweeney *et al,* 1993). Once the crossbridges are in a strongly bound, force-generating state, the tendency of further crossbridges to attach, due to the high rate constant of attachment relative to detachment, will tend to keep the proportion of bound crossbridges high, even after Ca^{2+} has begun falling. This crossbridge-induced activation will thereby slow relaxation. However, alterations in MLC_2 phosphorylation are unlikely to contribute to the slowing of relaxation kinetics in this instance. With increased MLC_2 phosphorylation, maximal force production would be expected to increase (Metzger *et al,* 1989; Sweeney and Stull, 1990) however, the maximal force generation of the ligated group trabeculae used in this study did not significantly differ from that of the control group (as discussed in Chapter 3). Nevertheless, alterations in the phosphorylation status of MLC_2 have been reported in some animal models of heart failure (*e.g.* Liu *et al,* 1995). These authors observed a decreased level of MLC_2 phosphorylation in the failing left ventricle of rats (after induction of experimental myocardial infarction), but also a significantly increased level of MLC_2 phosphorylation in the right ventricle and septum.

Whether any alterations in the essential MLC (MLC_1), associated with cardiac pathological abnormalities, occurs remains to be elucidated. However, Morano and colleagues (1995) have established that the interaction of MLC_1 with actin modulates crossbridge kinetics by increasing the detachment rate. Therefore, any interference with this interaction has the potential to influence the relaxation kinetics of cardiac muscle.

The rate at which relaxation occurs in skinned preparations can be limited by factors other than alterations in myosin isoform population or altered phosphorylation status, such as the rate of Ca^{2+} release from TnC (*i.e.* the Ca^{2+} 'off' rate, denoted by k_{off}), the rate of conformational changes before actomyosin dissociation, or by the crossbridge detachment rate from actin (denoted by k_{det}). The results from the

experiments in this chapter begin to suggest that it is the last of these processes that may become rate-limiting in the ligated group at higher [EGTA]s in this model of LVD. To strengthen this conjecture, there are lines of evidence, derived from different studies, indicating that the rate of Ca^{2+} dissociation from TnC is not the rate-limiting step in myocardial relaxation. The affinity of TnC for Ca^{2+} ($k_{Ca} \approx 4 \times 10^5$ mol L^{-1}: Palmer and Kentish, 1994; Dong *et al,* 1996) and the apparent rate constant for Ca^{2+} binding to TnC (k_{on}, 1.4×10^8 mol L^{-1} s^{-1}: Dong *et al,* 1996) have previously been measured. Using these figures, the rate of detachment of Ca^{2+} from TnC should be $\approx$ 350 s^{-1} (*i.e.* $k_{off} \approx k_{on} / k_{Ca}$) which is substantially faster that the maximum rate observed in these experiments or in others using flash photolysis. Further evidence against Ca^{2+} being the rate-limiting factor in myocardial relaxation was published recently by Palmer and Kentish (1997). They were looking at the effects of caffeine and CGP 48506 on the rate of relaxation of rat skinned trabeculae after photolysis of the photosensitive, Ca^{2+}-chelator diazo-2. Previous studies (Palmer and Kentish 1994; Powers and Solaro, 1995) had established that caffeine did not alter the affinity of isolated TnC for Ca^{2+} and therefore, if k_{off} was the rate-limiting factor in myocardial relaxation, they predicted that caffeine should have no effect on the rate of relaxation. In fact this was not the case and caffeine actually increased the rate of relaxation in these experiments, suggesting once again that Ca^{2+} dissociation from TnC is not rate-limiting. Results from the same study strengthen the hypothesis that Ca^{2+} is not the rate-limiting factor in myocardial relaxation. Relaxation in the presence of CGP 48506 and EMD 57033, produced extremely similar relaxation transients (Lee *et al* 1996; Palmer and Kentish, 1997). Previous Studies had determined the mechanism of action of EMD 57033 (Solaro *et al,* 1993) and it was determined that EMD 57033 acted directly on the crossbridges without altering Ca^{2+} binding to TnC. Therefore, to explain the similar relaxation transients, they (Palmer and Kentish) proposed a similar mechanism for CGP 48506.

The effect of an increase in pH by half a log unit was to significantly increase the maximal rate of relaxation in both groups, and to a similar extent in both. Fig. 5.3

models the expected effect that pH would have on relaxation rate if maximal relaxation was limited by diffusion. The models predicts no effect of pH at the highest [EGTA]-step examined. However, Fig. 5.10 clearly shows that pH increased the maximal rate of relaxation, therefore this effect can be attributed to a direct action on the myofilaments. Since the effect of a change in pH cannot be attributed to EGTA diffusion but the myofilaments, it reinforces the conclusion that, at the highest [EGTA]-step used, the crossbridge detachment process has indeed become rate-limiting.

Finally, it has been well documented that the production of oxygen-derived free radicals and ROS is associated with the development of CHF (*e.g.* Braunwald and Kloner, 1982). This then presents another mechanism whereby the rate of relaxation of the trabeculae with LVD, could be slowed. Results presented later in this thesis have determined that the myocardium from control and ligated animals is susceptible to oxidant damage. Exposure to ROS in these experiments resulted in a more prominent slowing of the relaxation transient (post-exposure) in the sham-operated controls than in the ligated animals. Therefore, the possibility that the myocardium from the ligated group has already been 'pre-exposed' to small amounts of ROS, impairing their rate of relaxation, cannot be ruled out.

The finding that the relaxation of both sham and ligated trabecular preparations are best fitted with a single exponential phase suggests that relaxation is governed by a single rate-limiting process. This is in contrast to other studies using myocardium from different species (*e.g.* guinea pig, Johns *et al,* 1997; cat, Parmley & Sonnenblick, 1969; dog, Tamiya *et al,* 1995), as well as those in skeletal muscle (*e.g.* Simnett *et al,* 1993) which have found that the relaxation transients were best fitted with double exponential fits, although none of these studies offer an explanation as to why there could be two separate rate-limiting processes. Johns *et al* employed the technique of laser flash photolysis of the photo-labile 'caged' Ca^{2+} chelator diazo-2, as did Palmer and Kentish (1997), to induce rapid relaxation. The former of these groups performed experiments at 12˚C (and were flashed in air) whereas the

latter were carried out at room temperature (as in this study). The average maximum rate of relaxation observed in this study for both groups (sham: $\approx 3.5\ s^{-1}$, ligated: $\approx 2.0\ s^{-1}$) was slower than the 'fast' phase of relaxation, but still faster than the 'slow' phase of relaxation that was obtained in these other studies using double exponential curve fits. Interestingly, Palmer and Kentish (1997) refer to unpublished data of theirs describing the relaxation rates of guinea pig trabeculae using the same flash photolysis protocol as for the rat. They found that the control maximum relaxation rates of rat trabeculae are approximately six times faster than that of the guinea pig. The relaxation rates of the guinea pig, which is of a similar isomyosin composition as the rabbit, would therefore compare very well with the values obtained for the control animals in this study using the [EGTA]-jump protocol. A criticism of the technique of Johns *et al* could be that only a part of the preparation is 'flashed' to induce relaxation (this is to avoid the laser beam contacting the aluminium clips used to secure the trabecula). Therefore the central part of the trabecula is flashed, inducing relaxation, whereas the preparations ends are not, which would thus presumably still be generating force at this point.

The implications of the results described in this chapter *in vivo* cannot be fully determined from these experiments. In the intact system, the role of the SR in removing Ca^{2+} from the cytosol must also be considered. To date it has not been established which of the two systems (SR and the myofilaments) has the greater control. If the SR is functioning normally, the rate at which it resequesters Ca^{2+} may be fast enough such that the crossbridges are indeed the rate-limiting factor for relaxation. However, if the SR is not functioning properly, as may occur in disease states, then the rate of Ca^{2+} sequestration by the SR may in fact be slowed to such an extent that the crossbridges can 'keep up' and are no longer rate-limiting. The findings from this study do not allow us to resolve this uncertainty. Other studies from this lab have already shown that SR function is in fact altered in this model (*e.g.* Denvir *et al*, 1996), so there may be a different rate-limiting factor for relaxation at different parts of relaxation *in vivo* in this particular model (*e.g.* crossbridges are rate-limiting first,

(if initially Ca^{2+} falls fast) and then the SR (if the rate of fall of Ca^{2+} slows down)). However, the finding that the maximum rate of relaxation of trabeculae from animals with signs of LVD is significantly reduced, when compared with sham-operated controls in skinned cardiac muscle, suggests that there are alterations at the level of the myofilaments. More specifically, these experiments have shown that there are alterations in the properties of the myofilaments of the diseased myocardium that cannot be accounted for by a simple myosin isoform shift, as is seen in smaller mammals.

Chapter 6

Effects of Reactive Oxygen Species on Myofilament Properties in a Rabbit Coronary Artery Ligation Model of Left Ventricular Dysfunction

6.1 Introduction

Experimental studies have demonstrated that survival after a myocardial infarction is inversely related to infarct size (Geltman *et al*, 1979) and that early reperfusion limits infarct size (Reimer *et al*, 1977). However, although reperfusion halts the progression of ischaemic injury, it predisposes the heart to post-ischaemic contractile dysfunction and might contribute to chronic heart failure (CHF) with its attendant morbidity and mortality (Braunwald and Kloner, 1982). Reactive oxygen species (ROS) have been postulated to contribute to the depression of contractile function observed during reperfusion, and in CHF, and can mediate the process of lipid peroxidation (the peroxidative degradation of lipids, often polyunsaturated fatty acids present in biomembranes) which compromises normal membrane function in the myocyte.

Knowledge of the action of ROS on the contractile proteins and the SR is important. Hypochlorous acid (HOCl) is produced during the 'chronic' response to ischaemia with or without reperfusion (*i.e.* upon neutrophil activation and infiltration occurring as part of the inflammatory response). Previous investigations in this laboratory have shown the effects of ROS on the myofilaments and SR in normal cardiac muscle. Both the myofilaments and the SR proved sensitive to HOCl: significant reductions in force occur during and after exposure to pathophysiologically relevant concentrations of HOCl (1-50μM) despite an increase in resting force and myofilament Ca-sensitivity (MacFarlane and Miller, 1994). Caffeine-induced Ca-release from the SR is diminished after exposure to HOCl besides an increase in spontaneous SR Ca-release (MacFarlane *et al*, 1994). The exact mode of action of HOCl on the myofilaments remains to be elucidated, but the previous results have afforded some insight. In our experimental protocols we applied HOCl in the Ca^{2+}-activated state. In addition, previous studies in this laboratory have applied HOCl in the resting and rigor states as well as the Ca^{2+}-activated state. These studies

showed that HOCl produced significant effects independently of the protocol of application. A rise in resting force was associated with HOCl exposure which exhibited features consistent with the formation of permanently attached rigor-like crossbridges.

The preceding discussion demonstrates that ROS can contribute to the depression of contractility observed in the reperfused myocardium. There is evidence to suggest that patients with CHF have an increased level of ROS activity and a decreased level of endogenous antioxidants (McMurray *et al*, 1990, Halliwell, 1991), suggesting that 'failed' myocardium will be more susceptible to ROS damage. 'Failing' myocardium exhibits a decrease in the rate of both the rise and fall of the force transient. The basis of this effect could be abnormal SR function and/or modification of the contractile proteins (*e.g.* both SR Ca-ATPase and myofibrillar ATPase activities appear to be depressed in 'failed' myocardium; Dhalla *et al*, 1994). Therefore, it is important to characterise the effects of ROS applied exogenously to 'failing' myocardium and compare them with the responses observed in normal tissues. The results reported in the previous chapters in this thesis demonstrate abnormalities in both the contractile and relaxation properties of the myocardium in this model of LVD. Therefore, with the current interest in ROS and their contribution to the development of CHF, it would seem appropriate to examine whether exposure to ROS in the sham-operated group, in this instance HOCl, produced alterations in mechanical functioning similar to the alterations observed in the animals with signs of developing CHF.

6.2 Results

Force, resting force and Ca^{2+}-sensitivity

Experiments examining the effects of exposure to HOCl on force, resting force and Ca^{2+}-sensitivity have previously been carried out in this lab and the results published (MacFarlane and Miller, 1994). Briefly, a short exposure of a maximally Ca^{2+}-activated trabecula to HOCl resulted in an immediate increase in maximal force. After relaxing the preparation, with HOCl now absent, resting force was sustained above control levels. The Ca^{2+}-sensitive force developed by preparations in subsequent activations was, therefore, reduced. The effects of HOCl exposure, described previously (MacFarlane and Miller, 1994), were an increase in resting force that had rigor-like properties, but which was insensitive to ATP, and an increase in myofilament Ca^{2+}-sensitivity. In addition a similar exposure to the HOCl increased the Ca^{2+}-sensitivity of the preparation.

Paired t-tests, performed on the raw data, were used to analyse the results throughout this chapter. Significance of difference was again taken at the 5% level.

fmin

Fig. 6.1 shows the reduction in the mean cycling rate of the crossbridges after exposure to HOCl, expressed as a percentage of control, for both sham and ligated animals. In both groups exposure to the HOCl causes a decrease in the intrinsic cycling rate of the crossbridges (as f_{min}). However, the reduction in mean cycling rate is significantly greater in the sham-operated control group when compared with the ligated animals.

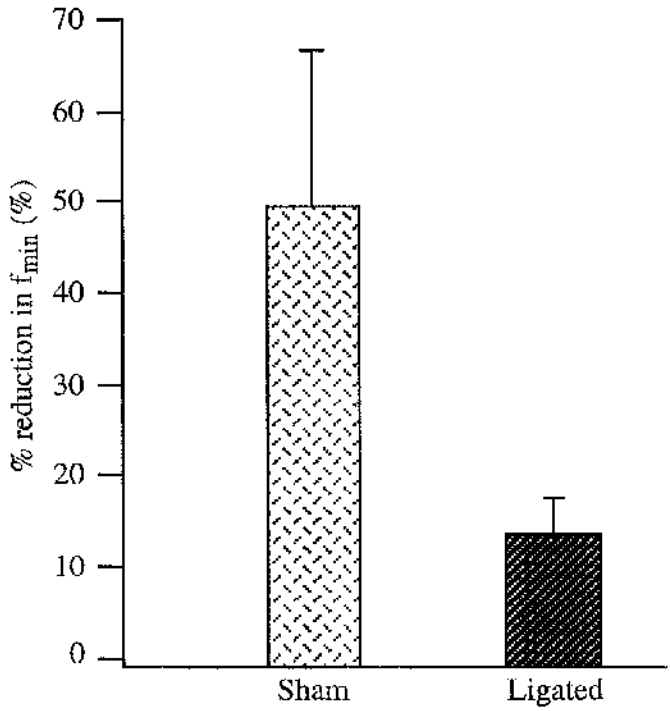

Fig. 6.1. Graph of percentage reduction in f_{min} after exposure to HOCl (n=4 for both groups). In both groups, f_{min} is significantly decreased from control values ($p<0.05$). The observed reduction in f_{min} is significantly greater in the control group.

Stiffness

Fig. 6.2 shows the alterations in myocardial Ca^{2+}-activated stiffness over a range of frequencies after exposure to HOCl, for both sham and ligated animals.

Fig. 6.2a shows myocardial stiffness values at a range of frequencies both pre- and post-HOCl exposure for the sham-operated controls. At all frequencies examined, HOCl exposure resulted in an increase in dynamic stiffness. For individual preparations, this increase in stiffness is significant. However, the mean increase in stiffness at a particular frequency for each group is not due to the large error bars.

Fig 6.2b shows a similar plot to 6.2a, but for the ligated animals. With the exception of the highest frequency examined, HOCl exposure caused an increase in myocardial stiffness. However, the increase in stiffness was less pronounced than for the sham-operated controls.

Fig. 6.3 shows the effect of HOCl exposure on myocardial stiffness (same results as shown in Figs. 6.2a and b) expressed as a percentage increase of control values for both sham and ligated animals.

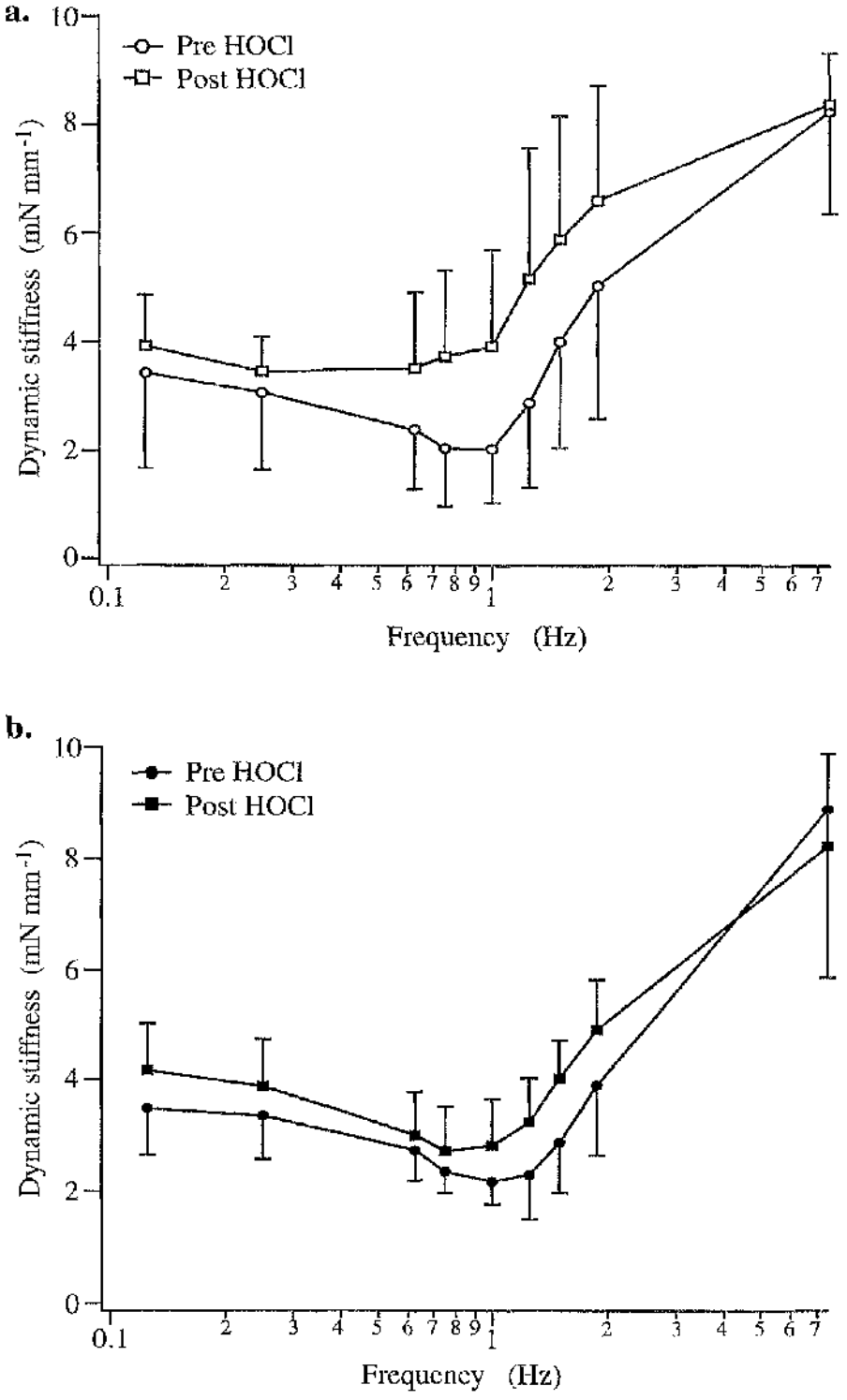

Fig. 6.2. The effect of HOCl exposure on Ca-activated stiffness for **a.** sham and **b.** ligated animals. n=4 for both groups. Exposure to HOCl increased myocardial stiffness in both sham and ligated animals, however, the shams were more susceptible to ROS damage.

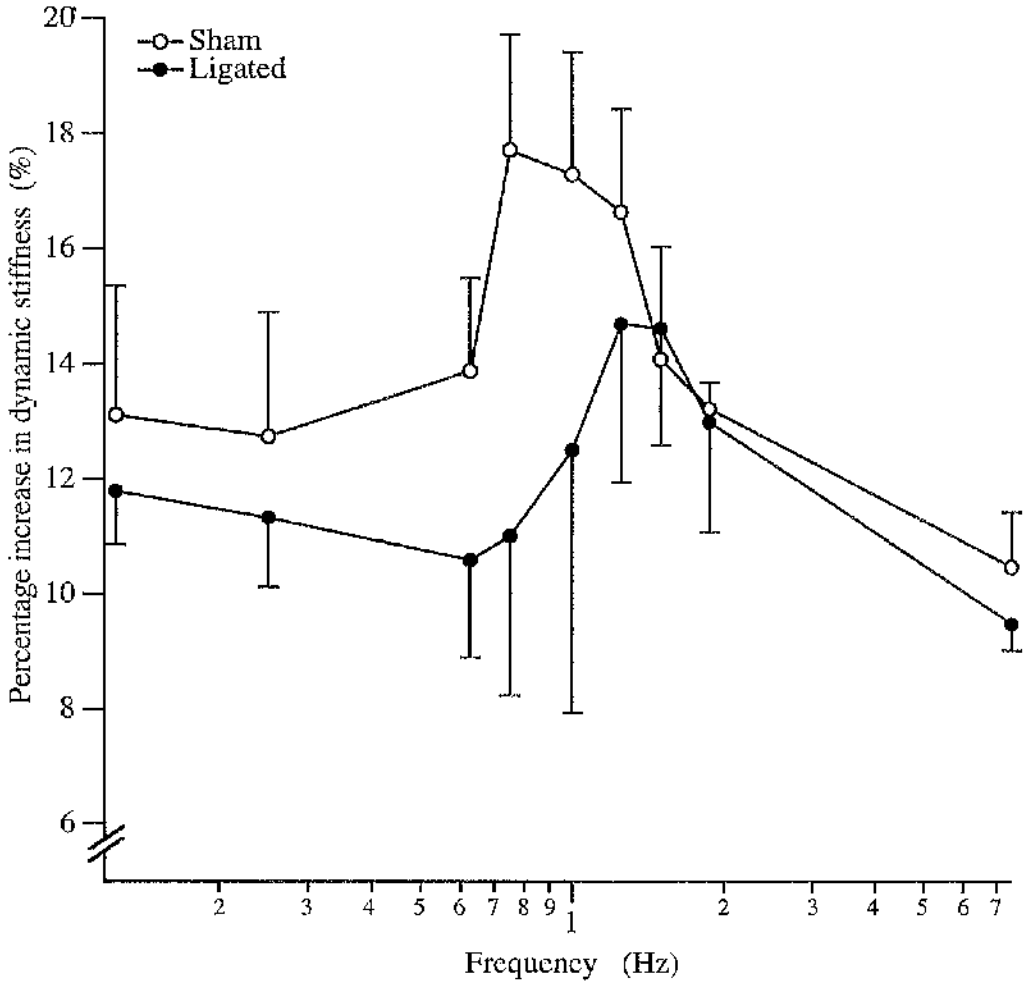

Fig. 6.3. Effect of HOCl exposure on Ca-activated stiffness, expressed as a percentage increase from control values. n=4 for both groups. An increase in myocardial stiffness is observed at all frequencies examined with the control preparations being more susceptible to ROS damage than the ligated animals. A larger increase in stiffness is observed at the frequencies closely associated with the mean frequency at which the crossbridges are cycling.

Resting stiffness

Fig. 6.4 shows the effect of HOCl exposure on resting stiffness for both sham (a) and ligated (b) animals. Resting stiffness was slightly higher in the ligated group pre-HOCl exposure. In both groups, HOCl exposure, resulted in an increased resting stiffness. This increase in resting stiffness was proportionately larger in the control group when compared with the ligated animals.

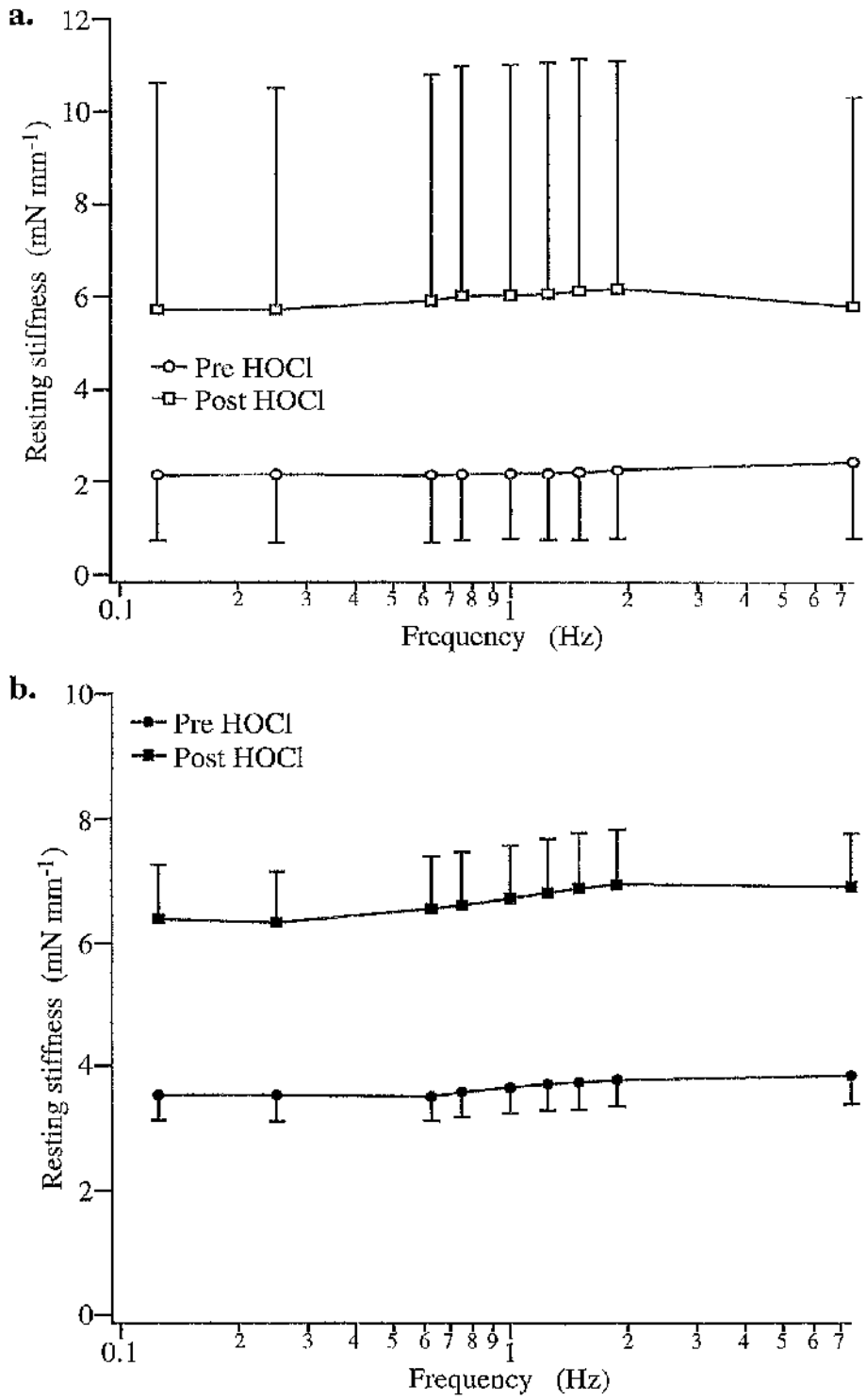

Fig. 6.4. Effect of HOCl exposure on resting myocardial stiffness for both **a.** sham and **b.** ligated animals. n=4 for both groups. Resting stiffness pre ROS exposure was slightly higher in the LVD animals when compared with controls. Exposure to the ROS increased resting stiffness in both groups, but to a greater extent in the controls.

Phase shift

Fig. 6.5 shows the effect of HOCl exposure on the positive and negative phase relationship in both sham and ligated animals. Results are expressed as a percentage of control phase shift values. In both groups, exposure to HOCl resulted in a decrease in both the maximum positive and negative phase shift values. A similar relative reduction was observed for both groups (values are summarised in Table 6.1), however, in absolute terms the reduction is greater for the control group since these preparations obviously start at a higher phase shift value.

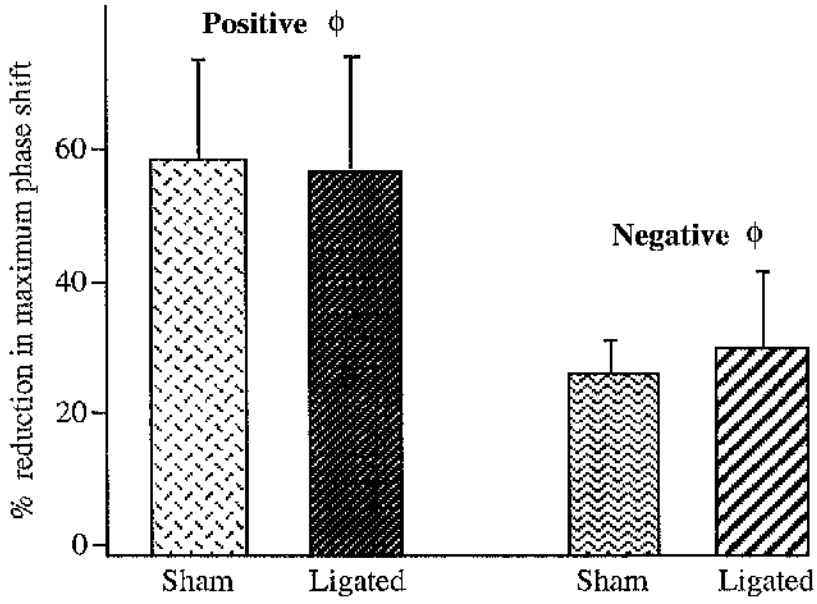

Fig. 6.5. Graph showing the reduction (%) in maximum positive and negative phase shift after exposure to HOCl for both sham (n=4) and ligated (n=4) animals.

Work/power

Fig. 6.6 shows the effect of HOCl exposure on both positive and negative work generation for both sham and ligated animals. Results are expressed as a percentage of control. Both positive and negative work were significantly reduced from control values in both groups of animals. In relative terms, positive work is reduced by a similar extent in both groups, but in absolute terms the control group is affected to a greater extent.

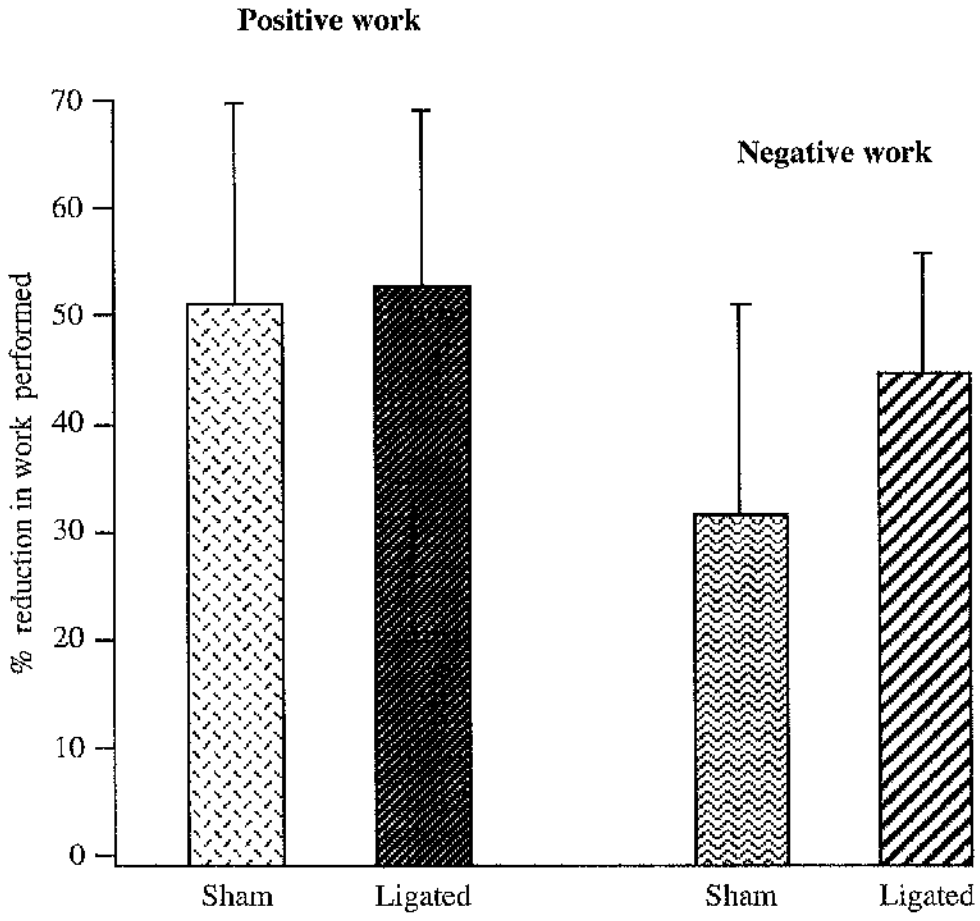

Fig. 6.6. Graph showing the percentage reduction in maximum positive and negative work production after exposure to HOCl for both sham (n=4) and ligated (n=4) animals.

Fig. 6.7 shows the effect of HOCl exposure on the positive and negative power generation of trabeculae from both sham and ligated animals. Results are expressed as a percentage of control. There is a significant reduction in positive and negative power generation when compared with control values in both animal groups.

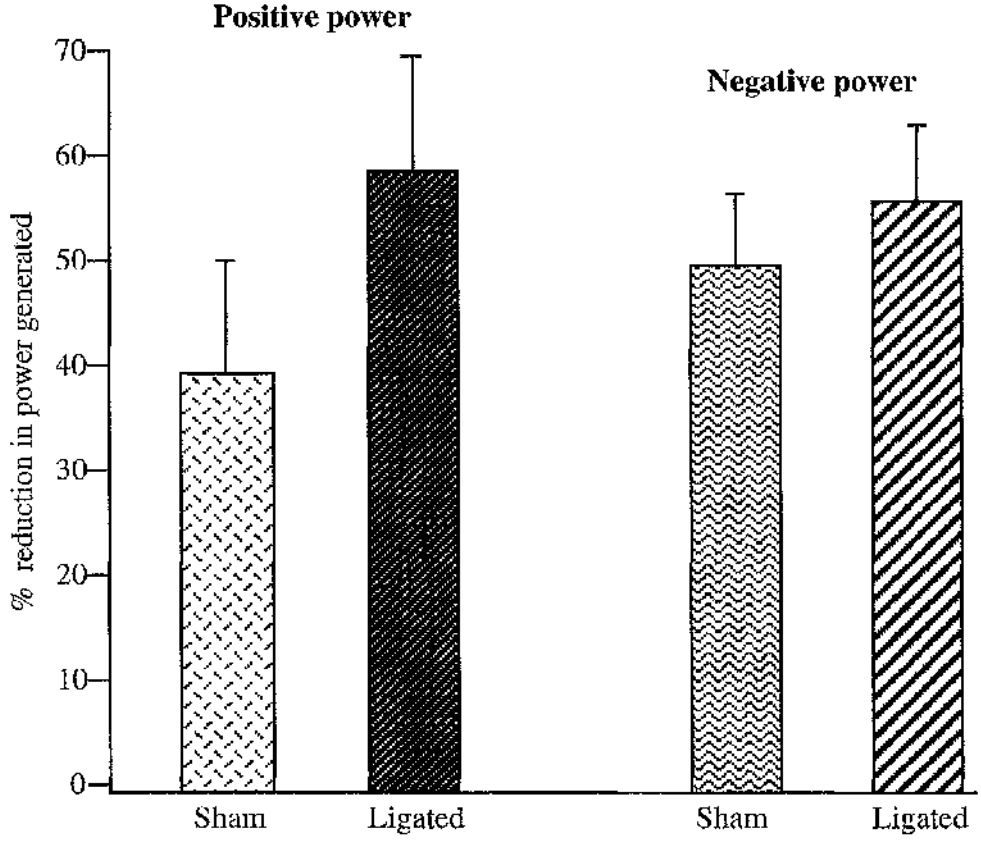

Fig. 6.7. Graph showing the percentage reduction in maximum positive and negative power generation after exposure to HOCl for both sham (n=4) and ligated (n=4) animals.

Fig. 6.8 shows an example of the phase relationship and positive and negative work loops for a sham operated animal under control conditions *i.e.* pre-HOCl exposure. The maximum positive and negative phase shift values shown in panel **a** correspond to the positive and negative work loops depicted below in panels **b** and **c** respectively.

Fig. 6.9 shows the effect of HOCl exposure on all of the parameters described above. Comparing Figs. 6.8 and 6.9 it is obvious that exposure to the ROS has significantly ($p<0.05$) decreased the maximum positive and negative phase shift values shown in panel **a** as, as well as decreasing the frequency at which these occurred. In addition the area under both positive and negative work loops (depicted in panels **b** and **c**) has been significantly reduced.

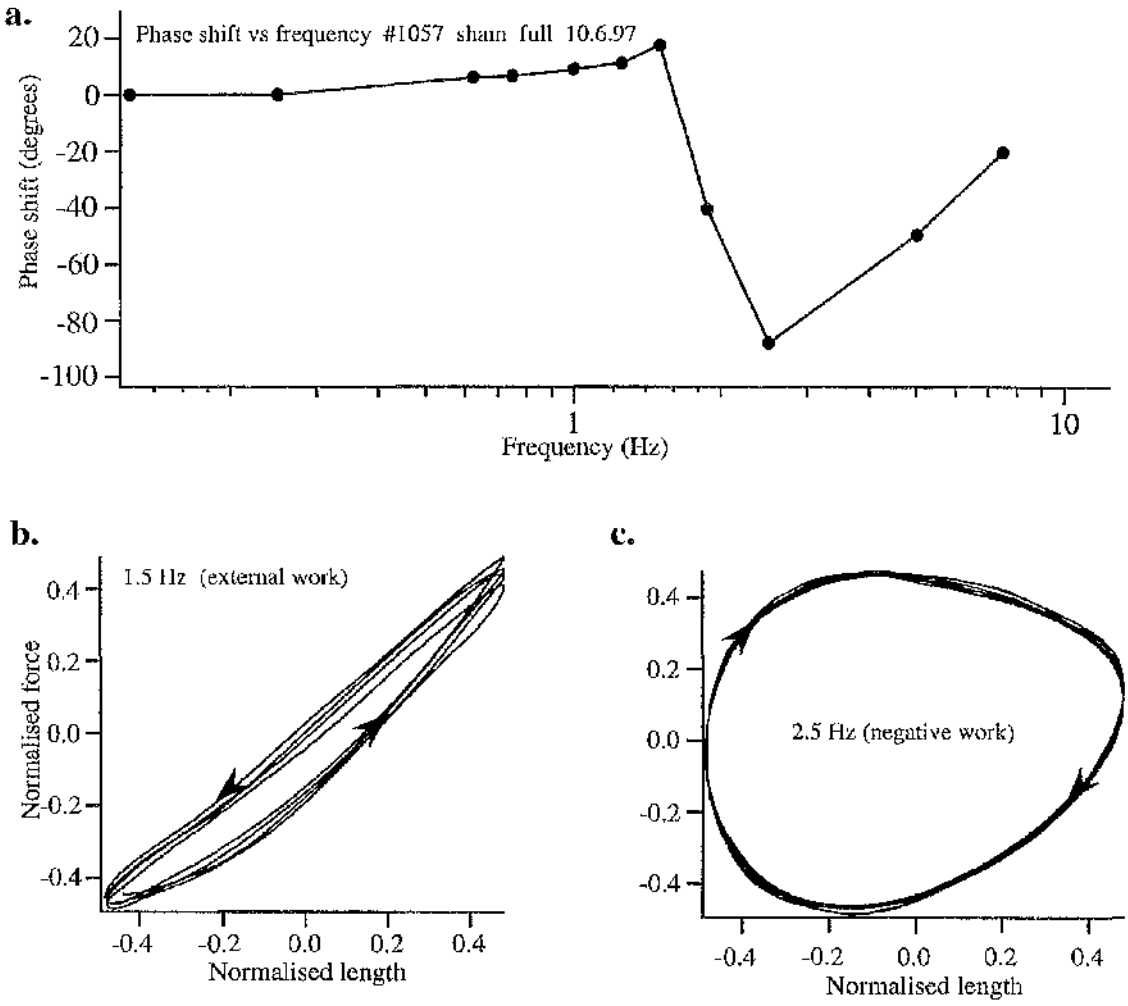

Fig. 6.8. Phase relationship and work loops for a sham operated animal pre-HOCl exposure. **a.** shows the phase-frequency relationship under control conditions. **b.** shows the force-length loop, which rotates anti-clockwise, hence the area within the loop represents external work generated by the trabecula. **c.** shows the force-length loop, which rotates clockwise, hence the area within the loop represents the negative work performed by the trabecula.

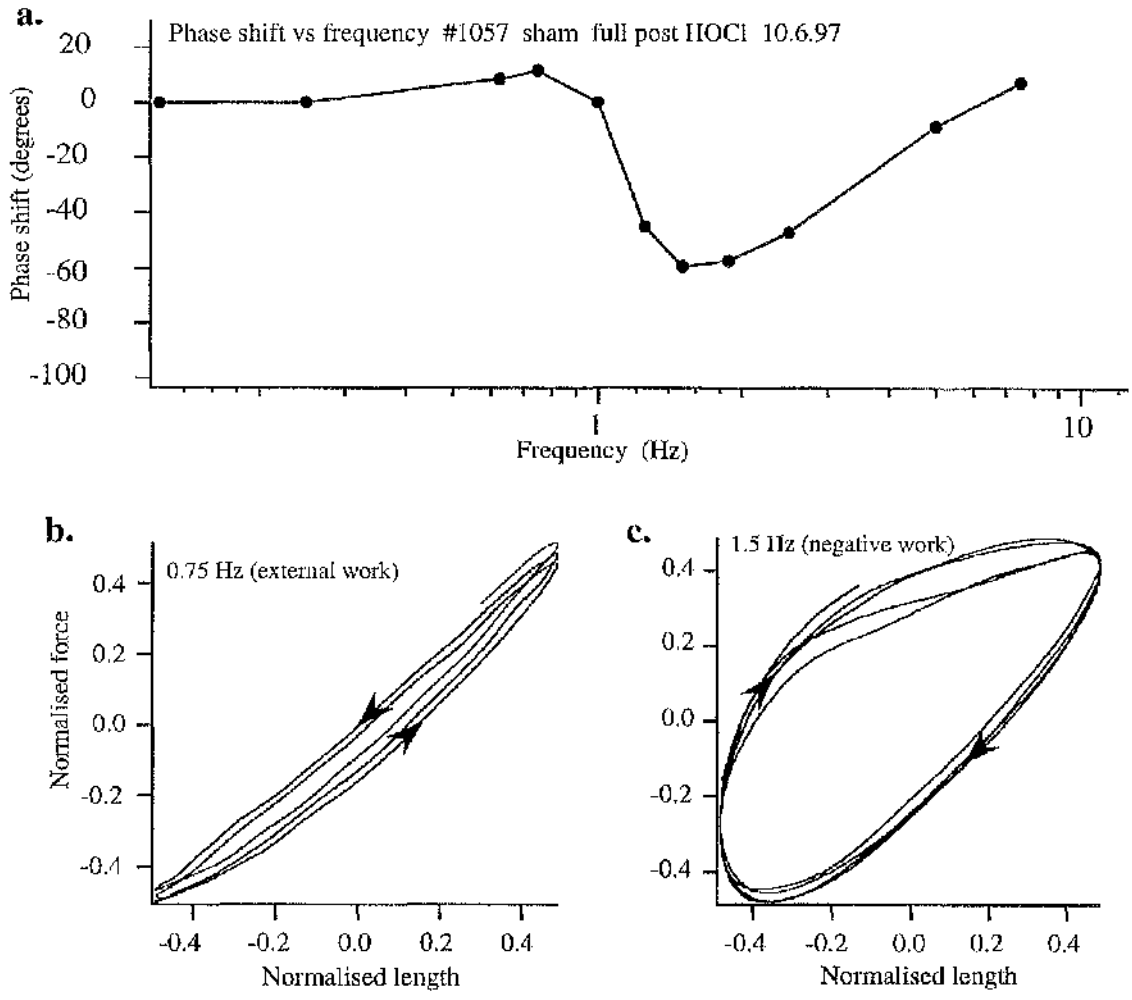

Fig. 6.9. Phase relationship and work loops for the same sham operated animal in Fig. 6.8 post-HOCl exposure. **a.** shows the phase-frequency relationship after HOCl exposure. **b.** shows the force-length loop produced after HOCl exposure. The loop rotates anti-clockwise, hence the area within the loop represents external work generated by the trabecula. **c.** shows the force-length loop produced after HOCl exposure. The loop rotates clockwise therefore the area within the loop represents the negative work performed by the trabecula. HOCl exposure reduced the maximum positive and negative phase shift values, reduced the area under the anti-clockwise and clockwise work loops and decreased the frequency at which all of these parameters were observed.

Fig. 6.10 shows an example of the phase relationship and positive and negative work loops for a ligated animal under control conditions *i.e.* pre-HOCl exposure. The maximum positive and negative phase shift values shown in panel **a** correspond to the positive and negative work loops depicted below in panels **b** and **c** respectively.

Fig. 6.11 shows the effect of HOCl exposure on all of the parameters described above. The effect of HOCl exposure is similar to that of the control animal. Comparing Figs. 6.10 and 6.11 it is obvious that exposure to the ROS has significantly decreased the maximum positive and negative phase shift values shown in panel **a** as, as well as decreasing the frequency at which these occurred. In addition the area under both positive and negative work loops (depicted in panels **b** and **c**) has been significantly reduced.

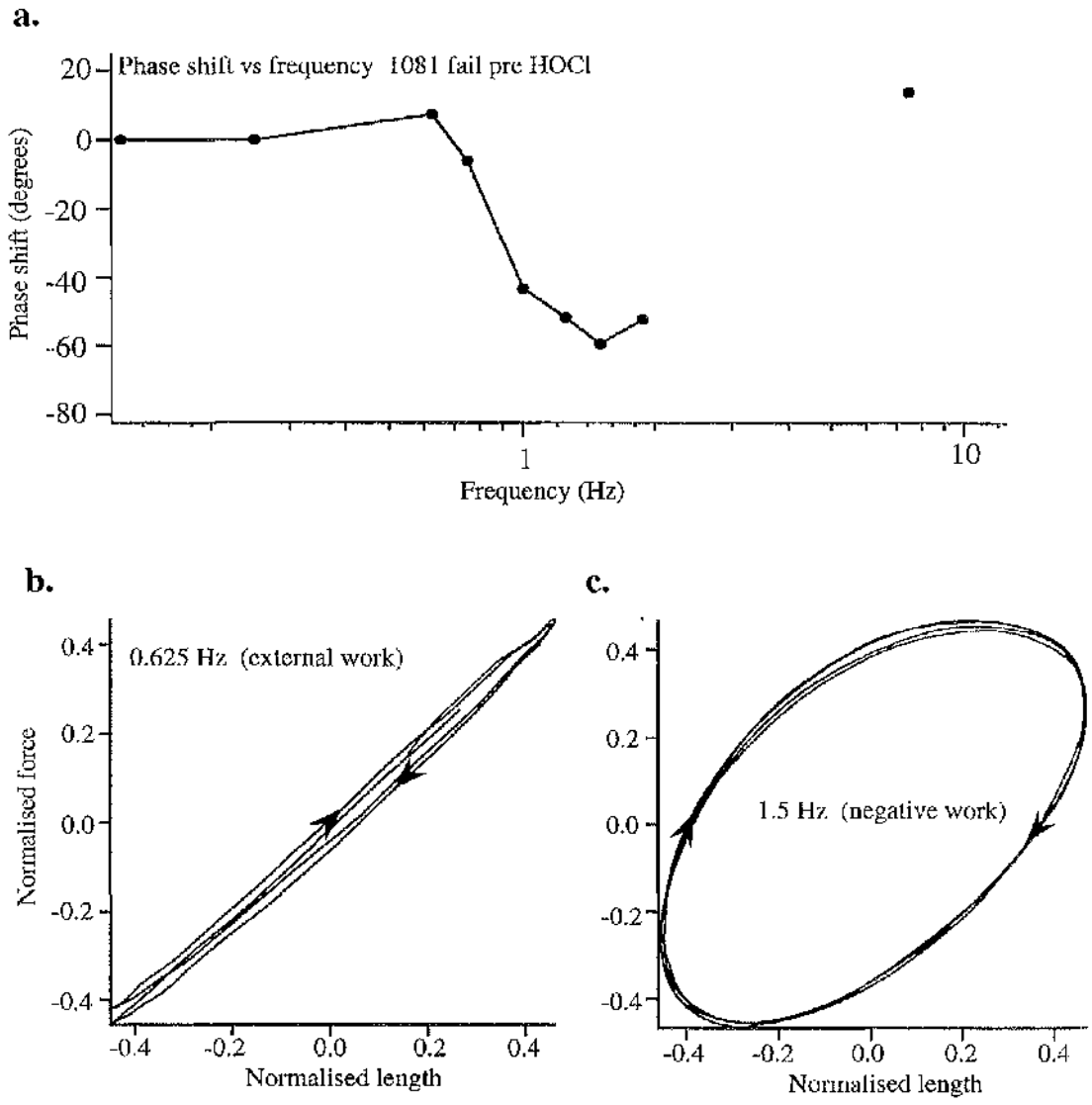

Fig. 6.10. Phase relationship and work loops for a ligated animal pre-HOCl exposure. **a.** shows the phase-frequency relationship under control conditions. **b.** shows the force-length loop, which rotates anti-clockwise, hence the area within the loop represents external work generated by the trabecula. **c.** shows the force-length loop, which rotates clockwise, hence the area within the loop represents the negative work performed by the trabecula.

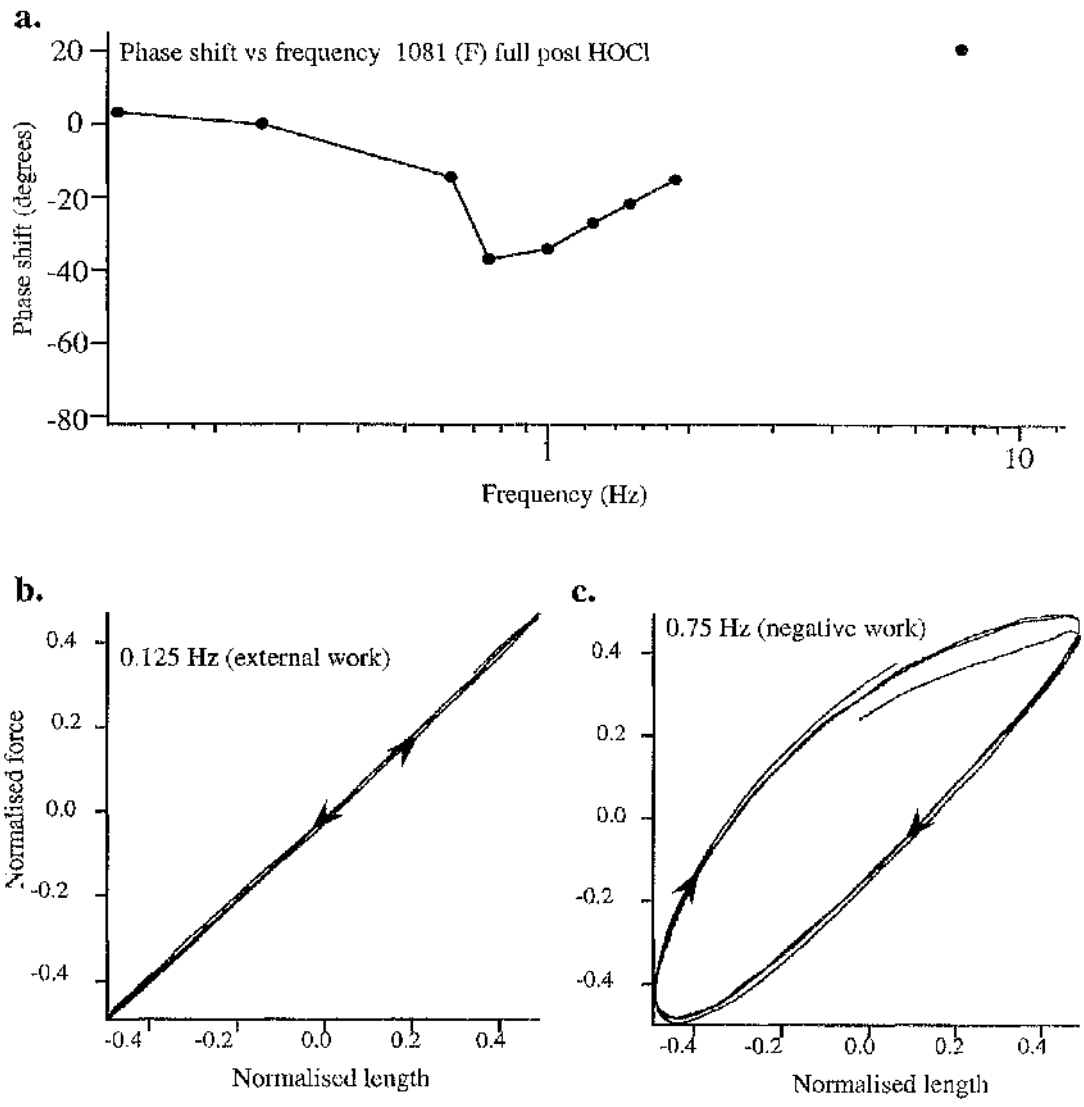

Fig. 6.11. Phase relationship and work loops for the same ligated animal as in Fig. 6.10 post-HOCl exposure. **a.** shows the phase-frequency relationship after HOCl exposure. **b.** shows the force-length loop produced after HOCl exposure. The loop rotates anti-clockwise, hence the area within the loop represents external work generated by the trabecula. **c.** shows the force-length loop produced after HOCl exposure. The loop rotates clockwise, therefore the area within the loop represents the negative work performed by the trabecula. HOCl exposure reduced the maximum positive and negative phase shift values, reduced the area under the anti-clockwise and clockwise work loops and decreased the frequency at which all of these parameters were observed.

Table 6.1 summarises the results shown in Figs. 6.5-6.7. All results are expressed as a percentage reduction from control values obtained pre-HOCl exposure.

Table 6.2 summarises the effects of HOCl exposure on the frequency at which maximum positive and negative work/power is generated for both sham and ligated trabeculae. In both groups, the frequency at which all of these parameters occurred was reduced by a similar extent.

	n	Max. positive phase shift %±sem	Max. negative phase shift %±sem	Max. positive work %±sem	Max. negative work %±sem	Max. positive power %±sem	Max. negative power %±sem
Sham	4	58.44±14.76	25.84±4.98	51.48±18.67	31.64±19.52	39.20±10.84	49.44±6.87
Ligated	4	56.87±16.88	29.74±11.47	52.86±16.22	44.61±11.18	58.57±10.98	55.60±7.30

Table 6.1. Summary data for the reduction in maximum positive and negative phase shift, work- and power-generation, expressed as a percentage of control.

	n	Freq max. positive phase shift %±sem	Freq max. negative phase shift %±sem	Freq max. positive work %±sem	Freq max. negative work %±sem	Freq max. positive power %±sem	Freq max. negative power %±sem
Sham	4	25.56±7.41	25.67±9.39	22.97±3.76	24.23±8.42	23.67±3.84	24.01±7.99
Ligated	4	23.67±8.49	22.22±8.76	20.25±7.79	22.51±8.01	20.98±8.03	23.12±8.40

Table 6.2. Summary data for the reduction in frequency of maximum positive and negative phase shift, work- and power-generation, expressed as a percentage of control.

Relaxation rate

Fig. 6.12 shows the effect of HOCl exposure on the maximum relaxation rate (achieved at 50mM EGTA) of both sham and ligated trabeculae, expressed as a percentage of control. In both groups the maximum relaxation rate is significantly reduced from control rates. The relaxation rate of the sham-operated controls was reduced to a greater extent when compared with the ligated group.

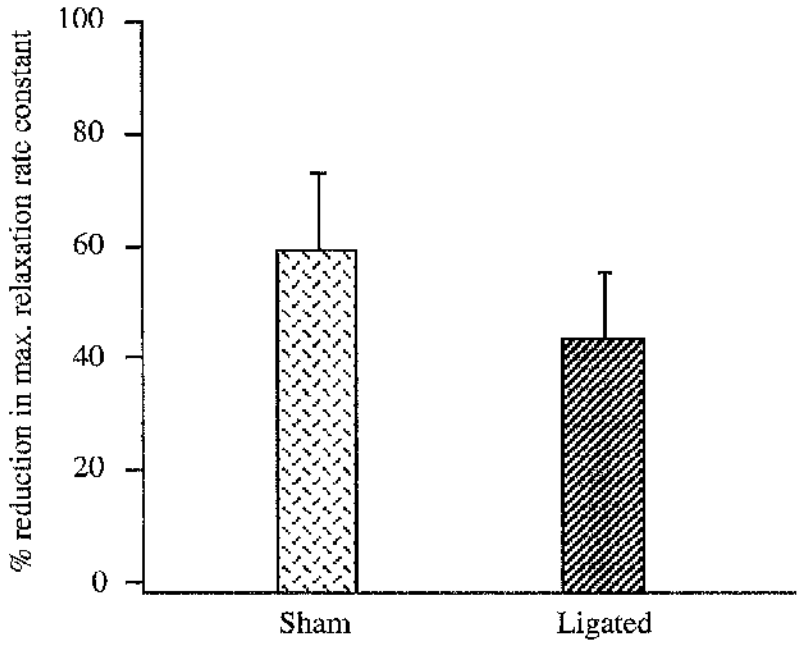

Fig. 6.12. Graph showing the percentage reduction±sem in the maximum relaxation rate constant after treatment with HOCl for both sham (n=4) and ligated (n=4) groups.

6.3 Discussion

It is well established in the literature that reactive oxygen species can affect myocardial function (*e.g.* MacFarlane and Miller, 1992, 1994; Mekhfi *et al,* 1996). The sites of action for such species are thought to include the sarcolemma, intracellular membrane systems such as the SR and the contractile proteins themselves. HOCl is produced by activated neutrophils which can infiltrate the myocardium during prolonged periods of ischaemia or infarction, hence the significance of the experiments detailed in this chapter. HOCl is generated by lymphocytes outside of the myocyte and therefore is unlikely to reach the contractile proteins directly. Nevertheless, since HOCl is a weak acid, at physiological pH, and after an ischaemic episode (where pH falls causing acidosis), a greater proportion of the species will be undissociated and, therefore, able to permeate membranes. The intracellular concentration of HOCl produced by activated neutrophils has not yet been established. Previous studies in this lab (MacFarlane and Miller, 1994) have shown that the effects of HOCl exposure are both time- and concentration-dependent. Therefore, it is not unreasonable to assume that sustained neutrophil activation *in vivo* could produce some of the effects described earlier in this thesis. Previous studies have suggested that HOCl-induced effects on myocardial contractile function are consistent with an effect on permanently attached rigor-like crossbridges (*e.g.* MacFarlane and Miller, 1994).

The results presented in this chapter demonstrate that exposure to the HOCl has deleterious effects at all stages of myocardial mechanical functioning in both sham and ligated groups. However, although similarly affected (*i.e.* qualitatively), the extent of the induced mechanical alterations was different between the two groups (*i.e.* quantitatively). The intrinsic rate of crossbridge cycling (as indicated by f_{min}) was significantly reduced in both groups, but to a greater extent in the sham-operated controls after HOCl exposure. As described previously in this thesis, the rabbit

ventricle at birth is predominantly comprised of the fast V_1 isoform. However, the relative amount of this isoform decreases dramatically as development continues such that the adult ventricle is mainly comprised of the slow V_3 isoform. In smaller mammals cardiac disease states induce a relative change in the ratio of these two different isoforms such that the V_3 isoform becomes predominant. This would produce a decrease in the energy cost of myocardial function, reflecting an adaptation to the stress imposed upon the myocardium during the development of CHF. Since the rabbit ventricle is already predominantly V_3, further slowing would not be expected to any great degree, however, the results presented in Chapter 3 clearly show that slowing has occurred in this model. Alterations in the function of myosin can occur by mechanisms other than a change in the MHC population. Exposure to the HOCl, as shown in this chapter, also produces a small slowing in f_{min} in the ligated group. Therefore it is not unreasonable to postulate that ROS exposure could contribute to the slowing of the crossbridges in this model. Furthermore, the ligated animals are affected to a (significantly) lesser extent than the control group, consistent with the hypothesis that these tissues were pre-exposed to the ROS *in vivo*.

Myocardial stiffness over a range of different frequencies was also affected by HOCl exposure in both groups. The percentage increase in myocardial stiffness at each discrete frequency of oscillation was, with the exception of 1.5 Hz, greater in the control group (see Fig. 6.5 for comparison). In this group of experiments, pre-HOCl exposure myocardial stiffness was not significantly different between the two groups. However, HOCl has its most pronounced effect on the control group when compared with ligated animals at the lower frequencies (*i.e.* <1.25 Hz, where the LVD myocardium is initially stiffer (but not significantly)). Resting stiffness was similarly affected. Pre-HOCl exposure, myocardial stiffness was proportionately higher in the LVD, but not significantly (as in the larger experimental group in Chapter 3 results), over the entire frequency range examined. In addition, at all frequencies examined, the resting stiffness in the control group was increased to a greater extent by HOCl exposure. As with the previous results in this chapter, these results could still imply a

pre-exposure to the HOCl in the *in vivo* situation since the alterations to the mechanical functioning of the sham animals resemble those of the ligated animals in the transition to CHF.

However, when examining the phase shift and (positive and negative) work and power alterations after HOCl exposure, the results deviate from that expected if pre-exposure had occurred in the ligated group. Phase shift is similarly reduced in both groups (in relative terms) after HOCl exposure, as is positive work. However, as mentioned previously in this chapter, the reduction in phase shift and positive work in absolute terms is greater for the control group since these preparations obviously start at a higher phase shift value and positive work level. Thus, HOCl keeps on reducing function even when function is already compromised (as in the ligated group). The alterations seen in positive power and negative work/power are difficult to explain in terms of pre-exposure to the ROS. These latter parameters are slightly more reduced in the ligated group this time unlike the other parameters, though not to any significant extent due to the large error bars. However, the reduction in the frequency at which these parameters occur is reduced to the same extent in both groups. This would still fit in with the pre-exposure theory as these alterations mimic the results described in Chapter 4 with respect to the relationship between f_{min} and the frequency of maximum positive work and power.

Finally, HOCl exposure significantly reduced the maximum rate of myocardial relaxation in both groups, but to a greater extent in the controls. It has been reported (Mekhfi *et al*, 1996) that HOCl acts by inhibiting myofibrillar creatine kinase (CK). HOCl does this by oxidation of essential sulphydryl groups located on CK which induces inactivation of the enzyme and therefore a decrease in the local ATP to ADP ratio. Inhibition of CK leads to a slowing of the 'off' rate of crossbridges and thus a prolonged duty ratio. This would fit well with the results described in Chapter 5. Although our modelling exercise did not allow us to predict confidently that the rate of crossbridge detachment was the main rate-limiting factor for relaxation at the highest [EGTA]-steps examined, the results and those cited in the literature do

suggest that this is most probably the case. A slowing of the crossbridge detachment rate would similarly increase the duty ratio of the crossbridges as occurs with HOCl exposure. Therefore, these latter results also seem to suggest that pre-exposure to the ROS (whose production was induced following coronary artery ligation in the LVD group) may be a plausible explanation for the mechanical alterations described in this chapter as well as one of the many possible alterations that may occur *in vivo* in this experimental model with the development of CHF.

Chapter 7

Conclusions

Heart failure is characterised by abnormalities of systolic and diastolic function. While there are changes in the Ca^{2+}-handling of failing myocardium that can account for some of the observed contractile abnormalities, there is evidence to suggest that myofilament alterations also have a profound influence as failure proceeds. The coronary artery ligation model was chosen to study heart failure (or LVD) because of its clinical relevance to the human condition. This procedure produces a well defined region of infarcted tissue which induces ventricular remodelling as is seen in the human. Like man, the rabbit heart is mainly comprised of the slow, V_3 myosin isoform. The main purpose of contraction is to obtain maximal work from the energy of ATP hydrolysis in order to optimise the efficiency of contraction, whereas that of relaxation is to remove force, or permit relengthening, as quickly as possible. All of these aspects were investigated. The results presented in this thesis demonstrate that this model does indeed have clear contractile abnormalities (both systolic and diastolic) at the level of the myofilaments when compared with sham-operated controls.

Systolic abnormalities were elucidated using the technique of sinusoidal analysis. This technique allowed the examination of crossbridge kinetics *in vitro* using chemically-skinned trabeculae, such that the 'intracellular' environment could be directly controlled. Crossbridge cycling rate (indicated by f_{min}) was significantly reduced in LVD animals (0.910±0.07 vs 0.705±0.05 Hz) , when compared with controls, in this model. Maximal force generation, however, remained similar to that of the control group, despite slowed crossbridge cycling kinetics. This has been seen in other models of hypertrophy in other species such as the rat and human (rat: Mayoux *et al,* 1994 and human: Hajjar and Gwathmey, 1992). Maximal force (per unit cross sectional area) generated by trabeculae in this study is similar to that reported for other species such as rat and guinea pig.

Sinusoidal analysis also allowed the positive and negative work and power generating capacity of the LVD myocardium to be investigated, and compare this

with controls. The results presented clearly show that the diseased myocardium has a significantly decreased capacity to generate both work and power (both in relative force units for a 0.5% length change (see page 109); positive work: 0.023±0.004 vs 0.008±0.003 and power (work per second): 0.015±0.003 vs 0.004±0.002), placing the heart under stress. The stress placed upon the heart by its inadequacy to produce sufficient work and power will become increasingly more significant as the disease progresses.

Coronary artery ligation has been demonstrated here to produce clear diastolic abnormalities as well as systolic. Using an 'EGTA-jump' protocol, which rapidly and simultaneously changes both the $[Ca^{2+}]$ and the concentration of the Ca^{2+}-buffer EGTA within the solution immediately surrounding the trabecula, the kinetics of relaxation were investigated. Rabbits with LVD had a significantly reduced maximal rate of relaxation when compared with sham-operated controls (3.61±0.38 vs 2.07±0.48 sec^{-1}). Our diffusion modelling exercise predicted that the rate of relaxation would continue to increase at higher [EGTA]-steps, however, this was not what was observed in a significant fraction of the preparations examined. Therefore, a slowed crossbridge detachment rate (*i.e.* g_{app}: Brenner, 1988) would seem the most likely rate-limiting factor for relaxation in this model of LVD. Since the relaxation transients were well fitted with a single exponential curve fit, we can assume that there is a single, simple rate-limiting factor consistent with crossbridge detachment. However, these results only apply to cardiac muscle in isolation, and can not be attributed to the situation *in vivo*, where the SR and its rate of re-sequestration of intracellular Ca^{2+} must also be taken into account. A reduced rate of relaxation will compromise diastolic filling as some cells will still be relengthening after contraction has commenced, providing resistance to ventricular filling. Ultimately, a decreased relaxation rate via a slowing of crossbridge dissociation, as is postulated here, will decrease filling time which is detrimental in heart failure.

During steady-state force production under isometric conditions, a fraction of the active crossbridge population is attached to actin in the strongly-bound,

force-generating state and a fraction is in the weakly-bound, non force-generating state. The apparent rate constant for the transition from the weakly-bound to the strongly-bound state is known as f_{app} (Brenner, 1988), and the rate constant for the transition in the opposite direction is known as g_{app}. Isometric force is proportional to the fraction of crossbridges at any one time in the strongly-bound, force-generating state and is determined by the ratio:

$$force = k_1 \frac{f_{app}}{f_{app} + g_{app}}$$

assuming that the number of crossbridges and the force per crossbridge remain constant. ATPase activity during steady-state, isometric contraction is proportional to:

$$ATPase = k_2 \frac{f_{app} \times g_{app}}{f_{app} + g_{app}}$$

(where k_1 and k_2 are proportionality constants). Therefore, by re-arranging the above two equations, the relation between ATPase and isometric force equals g_{app}. *i.e.*

$$\frac{ATPase}{force} = \frac{k_2}{k_1} \bullet g_{app}$$

A decreased relaxation rate can be accounted for by a decreased g_{app}. This would lead to an increase in the duty ratio (described in Introduction, section 1.9) of the crossbridges. Maximal force is unaltered in this model, therefore, there must be a reduced ATPase activity. This decreased ATPase activity must be due to other myofibrillar alterations other than a simple myosin isoform shift, since the rabbit is already predominantly V_3. Such a change would confer an adaptive advantage on the LVD heart since the ATP 'cost' of force production is thereby reduced.

A decreased susceptibility to hypochlorite anion exposure has been demonstrated in the LVD when compared with controls in this study. Increased production of ROS is one of the detrimental features associated with the progression of heart failure. 'Pre-exposure' of the myofilaments to ROS during the development of LVD may account for this decreased susceptibility. ROS exposure is shown to decrease the intrinsic cycling rate of the crossbridges, decrease the work and power

generating capacity and decrease maximal rate of relaxation in trabeculae from both sham and ligated animals. With the exception of the relative work and power generating capacity of the myocardium, in which both groups are similarly affected, the control animals are more susceptible to damage through hypochlorite anion exposure. More interestingly, however, the alterations in mechanical functioning demonstrated by the control animals after hypochlorite anion exposure (again with the exception of no apparent decrease in maximal force generation - see results Chapter 3), resemble the alterations in mechanical functioning that occurs in the myocardium of LVD animals after coronary artery ligation.

Chapter 8

References

AL-HILLAWI, E., BHANDARI, D.G., TRAYER, H.R. & TRAYER, I.P. (1995) The Effects of Phosphorylation of cardiac Troponin I on its Interactions with Actin and Cardiac Troponin C. *European Journal Biochemistry*, **228**, 962-970.

ALLEN, D.G. (1983) The use of isolated cardiac muscle preparations. *Cardiovascular Physiology*, **P310**, 1-21.

ALPERT, N.R. & MULIERI, L.A. (1982) Increased myothermal economy of isometric force generation in compensated cardiac hypertrophy induced by pulmonary artery constriction in the rabbit. *Circulation Research*, **50**, 491-500.

ANDERSON, P.A.W., GREIG, A., MARK, T.M., MALOUF, N.N., OAKELEY, A.E., UNGERLEIDER, R.M., ALLEN, P.D. & KAY, A.B. (1995) Molecular basis of human cardiac troponin T isoforms expressed in the developing, adult and failing heart. *Circulation Research*, **76**, 681-686.

ANDERSON, P.A.W., MALOUF, N.N., OAKELEY, A.E., PAGANI, E.D. & ALLEN, P.D. (1992) Troponin T isoforms expression in the normal and failing human left ventricle: a correlation with myofibrillar ATPase activity. *Basic Research in Cardiology*, **87**, 117-127.

ANDERSON, P.A.W., MALOUF, N.N., OAKELEY, A.E., PAGANI, E.D. & ALLEN, P.D. (1991) Troponin-T isoform expression in humans - a comparison among normal and failing adult heart, fetal heart, and adult and fetal skeletal-muscle. *Circulation Research*, **69**, 1226-1233.

ANDERSON, P.A. MANRING, A., ARENTZEN, C.E., RANKIN, J.S. & JOHNSON, E.A. (1977) Pressure-induced hypertrophy of cat right ventricle. An evaluation with the force-interval relationship. *Circualtion Research*, **41**, 582-588.

ANDERSON, P.A.W. & OAKELEY, A.E. (1989) Immunological identification of five troponin T Isoforms reveals an elaborate maturational troponin T profile in rabbit myocardium. *Circulation Research*, **65**, 1087-1093.

ANSON, M., GEEVES, M.A., KURZAWA, S.E. & MANSTEIN, D.J. (1996) Myosin motors with artificial lever arms. *EMBO Journal*, **15**, 6069-6074.

ASHLEY, C. C. & MOISESCU, D. G. (1977) Effect of changing the composition of the bathing solutions upon the isometric tension-pCa relation in bundles of crustacean myofibrils. *Journal of Physiology* , **270**, 627-652

BABU, A., SCORDILIS, S.P., SONNENBLICK, E.H. & GULATI, J. (1987) The control of myocardial contraction with skeletal fast muscle Troponin C. *Journal of Biological Chemistry*, **262**, 5815-5822.

BACKX, P.H., GAO, W-D., AZAN-BACKX, M.D. & MARBAN, E. (1994) Mechanism of force inhibition by 2,3-butanedione monoxime in rat cardiac muscle: Roles of $[Ca^{2+}]i$ and cross-bridge kinetics. *Journal of Physiology*, **476**, 487-500.

BIANCHI, C.P. (1968) Pharmacological actions on excitation-contraction coupling in striated muscle. *Federation Proceedings* , **27**, 126-131.

BING, O.H.L. (1994) Hypothesis: Apoptosis may be a mechanism for the transition to heart failure with chronic pressure overload. *Journal of Molecular and Cellular Cardiology*, **26**, 943-948.

BLAUSTEIN, A.S. & GAASCH, W.H. (1983) Myocardial relaxation. Effects of beta-adrenergic tone and synchrony on LV relaxation rate. *American Journal of Physiology,* **244,** H417-H422.

BLOCK, S.M., GOLDSTEIN, L.S.B., SCHNAPP, B.J. (1990) Bead movement by single kinesin molecules studied with optical tweezers. *Nature,* **348,** 348-352.

BODOR, G.S., OAKELEY, A.E., ALLEN, P.D., CRIMMINS, D.L., LADENSON, J.H. & ANDERSON, P.A.W. (1997) Troponin I Phosphorylation in the Normal and Failing Adult Human Heart. *Circulation*, **96**, 1495-1500.

BOHELER, K.R., CARRIER, L., de la BASTIE, D., ALLEN, P.D., KOMAJDA, M., MERCADIER, J-J. & SCHWARTZ, K. (1991) Skeletal Actin mRNA Increases in the Human Heart during Ontogenic Development and is the Major Isoform of Control and Failing Adult Hearts. *Journal of Clinical Investigations*, **88**, 323-330.

BOLUYT, M.O., O'NEILL, L., MEREDITH, A.L., BING, O.H.L., BROOKS, W.W., CONRAD, C.H., CROW, M.T. & LAKATTA, E.G. (1994) Alterations in Cardiac Gene Expression During the Transition from Stable Hypertrophy to Heart Failure: Marked upregulation of genes encoding extracellular matrix components. *Circulation* Research, **75**, 23-32.

BRADY, A.J. (1968) Active state in cardiac muscle. *Physiological reviews*, **48**, 570-600.

BRADY, A.J. (1991) Mechanical Properties of Isolated Cardiac Myocytes. *Physiological Reviews*, **71**, 413-428.

BRAUNWALD, E. & KLONER, R.A. (1982) The stunned myocardium - prolonged, post-ischaemic ventricular dysfunction. *Circulation*, **66**, 1146-1149.

BRAUNWALD, E. & ROSS, J. Jr. (1963) The ventricular end-diastolic pressure: appraisal of its value in the recognition of ventricular failure in man (editorial). *American Journal of Medicine*, **34**, 147-150.

BRENNER, B. (1988) Effect of Ca^{2+} on cross-bridge turnover kinetics in skinned single rabbit psoas fibers: implications for regulation of muscle contraction. *Proceedings of the National Academy of Sciences USA,* **85**, 2365-2369.

BRUTSAERT,D. L. (1987) Nonuniformity: a physiologic modulator of contraction and relaxation of the normal heart. *Journal of American College of Cardiology*, **9**, 341-348.

BRUTSAERT, D.L., CLAES, V.A. & GOETHALS, M.A. (1973) Effect of calcium on force-velocity-length relations of heart muscle of the cat. *Circulation Research*, **32**, 385-392.

BRUTSAERT, D.L., HOUSMANS, P.R. & GOETHALS, M.A. (1980) Dual control of relaxation. Its role in the ventricular function in the mammalian heart. *Circulation Research*, **47**, 637-652.

CARABELLO, B.A., MEE, R., COLLINS, J.J., KLONER, R.A., LEVIN, D. & GROSSMAN, W. (1981) Contractile function in chronic gradually developing sub-coronary aortic-stenosis. *American Journal of Physiology*, **240**, H80-H86.

CARVER, W., NAGPAL, M.L., NACHTIGAL, M., BORG, T.K. & TERRACIO, L. (1991) Collagen express in mechanically stimulated cardiac fibroblasts. *Circulation Research*, **69**, 116-122.

CHIEN, K.R., KNOWLTON, K.U., ZHU, H. & CHIEN, S. (1991) Regulation of cardiac gene expression during myocardial growth and hypertrophy: molecular studies of an adaptive physiologic response. *FASEB*, **5**, 3037-3046.

CONNELLY, C., VOGEL, W.M., HERNANDEZ, Y.M. & APSTEIN, C.S. (1982) Movement of necrotic wave-front after coronary-artery occlusion in rabbit. *American Journal of Physiology*, **243**, H682-H690.

CONRAD, C.H., BROOKS, W.W., SENS, S., ROBINSON, K.G. & BING, O.H.L. (1990) Increased collagen content may contribute to increased myocardial stiffness and heart failure in the spontaneously hypertensive rat. *Journal of the American College of Cardiology*, **15**, 48A.

COOPER, G., TOMANEK, R.J., EHRHARDT, J.C. & MARCUS, M.L. (1981) Chronic progressive pressure overload of the cat right ventricle. *Circulation Research*, **48**, 488-497.

CRANK, J. (1956) Chapter 5. In The Mathematics of Diffusion. Oxford University Press.

De WINKEL, M.E.M., BLANGE, T. & TREIJTEL, B.W. (1993) The complex Young's modulus of skeletal muscle fibre segments in the high frequency range determined from frequency transients. *Journal of Muscle Research and Cell Motility*, **14**, 302-310.

DENVIR, M.A., MacFARLANE, N.G., MILLER, D.J. & COBBE, S.M. (1996) Enhanced SR function in saponin-treated ventricular trabeculae from rabbits with heart failure. *American Journal of Physiology*, **271**, H850-H859.

DILLMANN, W.H. (1980) Diabetes mellitus induces changes in cardiac myosin of the rat. *Diabetes*, **29**, 579-582.

DILLON, P.F. & MURPHY, R.A. (1982) High force development and cross-bridge attachment in smooth muscle from swine carotid arteries. *Circulation Research*, **50**, 799-804.

DONG, W.J., CHANDRA, M., XING, J., SOLARO, R.J. & CHEUNG, H. (1997) Fluorescence studies of the N-terminal segment of cardiac troponin I. *Biochemistry*, **36**, 6745-6753.

DONG, W.J., ROSENFELD, S.S., WANG, C.K., GORDON, A.M. & CHEUNG, H.C. (1996) Kinetic studies of calcium binding to the regulatory site of troponin C from cardiac muscle. *Journal of Biological Chemistry*, **271**, 688-694.

DOSREMEDIOS, C.G. & MOENS, P.D.J. (1995) Actin and the actomyosin interface - a review. *Biochemica and Biophysica Acta*, **1228**, 99-124.

EBASHI, S. & ENDOH, M. (1968) Calcium ion and muscle contraction. *Progress in Biophysics and Molecular Biology*, **18**, 125-183.

EBLE, D.M., WALKER, J.D., MUKERJEE, R., SAMAREL, A.M. & SPINALE, F.G. (1997) Myosin heavy chain synthesis is increased in a rabbit model of heart failure. *American Journal of Physiology*, **272**, H969-H978.

EDMAN, K.A.P. (1979) The velocity of unloaded shortening and its relation to sarcomere length and isometric force in vertebrate muscle fibers. *Journal of Physiology*, **291**, 143-159.

EISENBERG, E. & GREENE, L.E. (1980) The relation of muscle biochemistry to muscle physiology. *Annual Reviews in Physiology*, **42**, 293-309.

EISENBERG, E. & HILL, T.L. (1985) Muscle contraction and free energy transduction in biological systems. *Science*, **227**, 999-1006.

EPSTEIN, N., ZHU, W.S., CUDA, G., SELLERS, J., CYRAN, F., COHN, G. & FANANAPAZIR, L. (1992) Mutant message and myosin protein in skeletal-muscle of hypertrophic cardiomyopathy patients with distinct mutations in the beta-myosin heavy-chain gene. *Circulation*, **86**, 229.

ERIKSSON, H. (1995) Heart Failure: a growing public health problem. *Journal of Internal Medicine*, **237**, 135-141.

EVERETT, A.W., CLARK, W.A., CHIZZONITE, R.A. & ZAK, R. (1982) Change in synthesis of alpha- and beta-myosin heavy chains in rabbit heart after treatment with thyroid hormone. *Journal of Biological Chemistry*, **258**, 2421-2425.

FABIATO, A. & FABIATO, F. (1976) Dependence of calcium release, tension generation and restoring forces on sarcomere length in skinned cardiac cells. *European Journal of Cardiology*, **4**, 13-27.

FARAH, C.S. & REINACH, F.C. (1995) The troponin complex and regulation of muscle contraction. *FASEB Journal*, **9**, 755-767.

FELDMAN, A.M., WEINBERG, E.O., RAY, P.E. & LORELL, B.H. (1993) Selective changes in cardiac gene-expression during compensated hypertrophy and the transition to cardiac decompensation in rats with chronic aortic banding. *Circulation Research*, **73**, 184-192.

FERENCZI, M.A., HOMSHER, E. & TRENTHAM, D.R. (1984) The kinetics of magnesium adenosine triphosphate cleavage in skinned muscle fibres of rabbit. *Journal of Physiology*, **352**, 575-599.

FINER, J.T., SIMMONS, R.M. & SPUDICH, J.A. (1994) Single myosin molecule mechanics: piconewton forces and nanometre steps. *Nature*, **368**, 113-119.

FLINK, I.L., RADER, J.H., BANERJEE, S.K. & MORKIN, E. (1979) Atrial and ventricular cardiac myosins contain different heavy chain species. *FEBS Letters*, **94**, 125-130.

FLORES, N.A., DAVIES, R.L., PENNY, W.J. & SHERIDAN, D.J. (1984) Coronary microangiography in the guinea pig, rabbit and ferret. *International Journal of Cardiology*, **6**, 459-471.

FORD, L.E., HUXLEY, A.F. & SIMMONS, R.M. (1977) Tension responses to sudden length change in stimulated frog muscle fibres near slack length. *Journal of Physiology*, **269**, 441-515.

FRYER, M.W., NEERING, I.R. & STEPHENSON, D.G. (1988) Effects of 2,3-butanedione monoxime on the contractile activation properties of fast- and slow-twitch rat muscle fibre. *Journal of Physiology*, **407**, 53-75.

FURST, D.O., OSBORN, M., NAVE, R. & WEBER, K. (1988) The organisation of titin filaments in the half-sarcomere revealed by monoclonal antibodies in immunoelectron microscopy: a map of ten nonrepetitive epitopes starting at the Z-line extend close to the M-line. *Journal of Cellular Biology*, **106**, 1563-15752.

GEEVES, M.A., GOODY, R.S. AND GUTFREUND, H. (1984) Kinetics of Acto-S1 Interaction as a Guide to a Model for the Crossbridge Cycle. *Journal of Muscle Research and Cell Motility*, **5**, 351-361.

GEISTERFER-LOWRANCE, A.A.T., KASS, S., TANIGAWA, G., VOSBERG, H-P., McKENNA, W., SEIDMAN, J.G. & SEIDMAN, C.E. (1990) A molecular basis for familial hypertrophic cardiomyopathy: a β-cardiac myosin heavy chain gene missense mutation. *Cell*, **62**, 999-1006.

GELTMAN, E.M., EHSANI, A.A., CAMPBELL, M.K., SCHECHTMAN, K., ROBERTS, R. & SOBEL, B.E. (1979) The influence of location and extent of myocardial infarction on long-term ventricular dysrythmia and mortality. *Circulation*, **60**, 805-814.

GERTZ, E.W. (1973) Animal model of human disease. Myocardial failure, muscular dystrophy. *American Journal of Pathology*, **70**, 151-154.

GHALI, J.K., COOPER, R. & FORD, E. (1990) Trends in hospitalisation rates for heart failure in the United States, 1973-1986. Evidence for increasing population prevalence. *Archives of Internal Medicine*, **150**, 769-773.

GILLUM, R.F. (1993) Epidemiology of heart failure in the United States. *American Heart Journal*, **126**, 1042-1047.

GRANZIER, H.L. & IRVING, T.C. (1995) Passive Tension in Cardiac Muscle: Contribution of Collagen, Titin, Microtubules and Intermediate Filaments. *Biophysical Journal*, **68**, 1027-1044.

GRANZIER, H.L.M. & WANG, K. (1993) Passive tension and stiffness of vertebrate skeletal muscle and insect flight muscles: contribution of weak cross-bridges and elastic filaments. *Biophysical Journal*, **65**, 2141-2159.

GREASER, M.L. & GERGELY, J. (1971) Reconstitution of troponin activity from three protein components. *Journal of Biological Chemistry*, **246**, 4226-4233.

GUILFORD, W.H., DUPUIS, D.E., KENNEDY, G., WU, J.R., PATLACK, J.B. & WARSHAW, D.M. (1997) Smooth muscle and skeletal muscle myosins produce similar unitary forces and displacements in the laser trap. *Biophysical Journal*, **72**, 1006-1021.

GULATI, J., AKELLA, A.B., NIKOLIC, S.D., STARC, V. & SIRI, F. (1994) Shift in contractile regulatory protein subunits troponin T and troponin I in cardiac hypertrophy. *Biochemical and Biophysical Research Communications*, **202**, 384-390.

GUNNING, P., PONTE, P., BLAU, H. & KEDES, L. (1983) α-skeletal and α-cardiac actin genes are co-expressed in adult human skeletal muscle and heart. *FASEB Journal*, **5**, 3064-3070.

GWATHMEY, J.K., HAJJAR, R.J. & SOLARO, R.J. (1991) Contractile deactivation and uncoupling of crossbridges: effects of 2,3-butanedione monoxime on mammalian myocardium. *Circulation Research*, **69**, 1280-1292.

HAJJAR, R.J. & GWATHMEY, J.K. (1992) Cross-bridge dynamics in human ventricular myocardium. Regulation of contractility in the failing heart. *Circulation*, **86**, 1819-1826.

HAJJAR, R.J., GWATHMEY, J.K., BRIGGS, G.M. & MORGAN, J.P. (1988) Differential Effect of DPI 210-106 on the Sensitivity of the Myofilaments to Ca2+ in Intact and Skinned Trabeculae from Control and Myopathic Human Hearts. *Journal of Clinical Investigations*, **82**, 1578-1584.

HALLIWELL, B. (1991) Reactive oxygen species in living systems- source, biochemistry and role in human disease. *American Journal of Medicine*, **91**, 14S-22S.

HARRINGTON, W.F. (1971) A mechanochemical mechanism for muscle contraction. *Proceedings of the National Academy of Sciences USA*, **68**, 685-689.

HARRINGTON, W.F. (1979) On the origin of the contractile force in skeletal muscle. *Proceedings of the National Academy of Sciences USA*, **76**, 5066-5070.

HARRIS, D.E. & WARSHAW, D.M. (1993) Smooth and skeletal muscle actin are mechanically indistinguishable in the *in vitro* motility assay. *Circulation Research*, **72**, 219-224.

HARRISON, S.M., LAMONT, C., & MILLER, D.J. (1988) Hysteresis and the length dependence of calcium sensitivity in cardiac muscle. *Journal of Physiology* **401**, 117-145.

HASENFUSS, G., MULIERI, L.A., LEAVITT, B.J., ALLEN, P.D., HAEBERLE, J.R. & ALPERT, N. R. (1992) Alteration of Contractile Function and Excitation-contraction Coupling in Dilated Cardiomyopathy. *Circulation Research*, **70**, 1225-1232.

HASENFUSS, G., REINECKE, H., STUDER, R., MEYER, M., PIESKE, B., HOLTZ, J., HOLUBARSCH, C., POSIVAL, H., JUST, H. & DREXLER, H. (1994) Relation between myocardial function and expression of sarcoplasmic reticulum Ca^{2+}-ATPase in failing and non-failing human myocardium. *Circulation Research*, **75**, 434-442.

HERZBERG, O. & JAMES, M.N.G. (1988) Refined crystal structure of troponin C from turkey skeletal muscle at 2.0 Å resolution. *Journal of Molecular Biology*, **203**, 761-779.

HIGH, C. & STULL, J. (1980) Phosphorylation of myosin in perfused rabbit and rat hearts. *American Journal of Physiology*, **239**, H756-H764.

HILL, A.V. (1950) The dimensions of animals and their muscular dynamics. *Scientific Progress*, **38**, 209-230.

HILL, M.F. & SINGAL, P.K. (1996) Anti-oxidant and oxidative stress changes in heart failure subsequent to myocardial infarction in rats. *American Journal of Pathology*, **148**, 291-300.

HIROTA, Y. (1980) A clinical study of left ventricular relaxation. *Circulation*, **62**, 756-763.

HOH, J.F.Y. & EGERTON, L.J. (1979) Action of tri-iodothyronine on the synthesis of rat ventricular myosin isoenzymes. *FEBS Letters*, **101**, 143-148.

HOH, J.F.Y. , McGRATH, P.A. & HALE, P.T. (1978) Electrophoretic analysis of multiple forms of rat cardiac myosin: Effects of hypophysectomy and thyroxine replacement. *Journal of Molecular and Cellular Cardiology*, **10**, 1053-1076.

HOH, J.F.Y., ROSSMANITH, G.H., KWAN, L.J. & HAMILTON, A.M. (1988) Adrenaline Increases the Rate of Cycling of Crossbridges in Rat Cardiac Muscles as Measured by Pseudo-Random Binary Noise-Modulated Perturbation Analysis. *Circulation Research*, **62**, 452-461.

HOH, J.F.Y., YEOH, G.P.S., THOMAS, M.A.W. & HIGGENBOTTOM, L. (1979) Structural differences in the heavy chains of rat ventricular myosin isoenzymes. *FEBS Letters*, **97**, 330-334.

HOLMES, K.C., POPP, D., GEBHARDT, W. & KABSCH, W. (1990) Atomic model of the actin filament. *Nature*, **347**, 685-689.

HOWARD, J. (1997) Molecular motors: structural adaptations to cellular functions. *Nature*, **389**, 561-567.

HUXLEY, A.F. (1974) Muscular contraction. *Journal of Physiology*, **243**, 1-43.

HUXLEY, A.F. & SIMMONS, R.M. (1973) Mechanical transients and the origin of muscular force. *Cold Spring Harbour Symposia in Quantitative Biology*, **37**, 661-668.

HUXLEY, A.F. (1992) A fine time for contractual alterations. *Nature*, **357**, 110.

HUXLEY, H.E. (1957) The double array of filaments in cross-striated muscle. *Journal of Biophysical and Biochemical Cytology*, **3**, 631-648.

HUXLEY, H.E. (1969) The mechanism of muscular contraction. *Science*, **164**, 1356-1366.

HUXLEY, H.E. (1973) Structural changes in the actin- and myosin-containing filaments during contraction. *Cold Spring Harbour Symposium for Quantitative Biology*, **37**, 361-376.

HUXLEY, H.E. (1975) The structural basis of contraction and regulation in skeletal muscle. *Acta Anatomica Nipponica*, **50**, 310-325.

HUXLEY, H.E. & KRESS, M. (1985) Crossbridge behaviour during muscle contraction. *Journal of Muscle Research and Cell Motility*, **6**, 153-162.

HUXLEY, H.E. & SIMMONS, R.M. (1971) Proposed mechanism for force generation in striated muscle. *Nature*, **233**, 533-538.

HUXLEY, H.E., SIMMONS, R.M., FARUQI, A.R., KRESS, M., BORDAS, J. & KOCH, M.H.J. (1983) Changes in the X-ray reflections from contracting muscle during rapid mechanical transients and their structural implications. *Journal of Molecular Biology*, **169**, 469-506.

IRVING, M., St CLAIRE ALLEN, T., SABIDO-DAVID, C., CRAIK, J.S., BRANDMEIER, B., KENDRICK-JONES, J., CORRIE, J.E.T., TRENTHAM, D.R. & GOLDMAN, Y.E. (1995) Tilting of the light-chain region of myosin during step length changes and active force generation in skeletal muscle. *Nature*, **375**, 688-691.

ISHIJIMA, A., KOJIMA, H., HIGUCHI, H., HARADA, Y., FUNATSU, T. & YANAGIDA, T. (1996) Multiple- and single-molecule analysis of the actomyosin motor by nanometre-piconewton manipulation with a microneedle: unitary steps and forces. *Biophysical Journal*, **70**, 383-400.

JEACOCKE, S. & ENGLAND, P. (1980) Phosphorylation of myosin light chains in perfused rabbit heart. *Journal of Biochemistry*, **188**, 763-768.

JOHNS, E.C., SIMNETT, S.J., MULLIGAN, I.P. & ASHLEY, C.C. (1997) Troponin I phosphorylation does not increase the rate of relaxation following laser flash photolysis of diazo-2 in guinea-pig skinned trabeculae. *Pflugers Archives*, **433**, 842-844.

JOHNSON, J.D., CHARLTON, S.C. & POTTER, J.D. (1979) A fluorescence stopped flow analysis of Ca^{2+}-exchange with troponin C. *Journal of Biological Chemistry*, **254**, 3497-3502.

JOHNSON, J.D., COLLINS, J.H., ROBERTSON, S.P. & POETTER, J.D. (1980) A fluorescent probe study of Ca^{2+} binding to the Ca^{2+} specific sites of cardiac troponin and troponin C. *Journal of Biological Chemistry*, **255**, 9635-9640.

JOHNSON, J.D., NAKKULA, R.J., VASULKA, C. & SMILLIE, L.B. (1994) Modulation of Ca2+ exchange with the Ca2+–specific regulatory sites of troponin. *Journal of Biological Chemistry*, **269**, 8919-8123.

JONTES, J.D., WILSON-KUBALEK, E.M. & MILLIGAN, R.A. (1995) The brush border myosin-I tail swings through a 32° arc upon ADP release. *Nature*, **378**, 751-753.

JOSEPHSON, R.K. (1985) Mechanical power output from striated muscle during cyclic contraction. *Journal of Experimental Biology*, **114**, 493-512.

JUNG, D.W.G., BLANGE, T., De GRAAF, H. & TREIJTEL, B.W. (1988) Elastic properties of relaxed, activated and rigor muscle fibres measured with microsecond time resolution. *Biophysical Journal*, **54**, 897-908.

KABSCH, W., MANNHERTZ, H.G., SUCK, D., PAI, E.F. & HOLMES, K.C. (1990) Atomic structure of the actin DNase complex. *Nature*, **347**, 37-44.

KAGIYA, T., HORI, M., IWAKURA, K., IWAI, K., WATANABE, Y., UCHIDA, S., YOSHIDA, H., KITABATAKE, A., INOUE, M. & KAMADA, T. (1991) Role of Increased α_1-Adrenergic Activity in Cardiomyopathic Syrian Hamsters. *American Journal of Physiology*, **260**, H80-H88.

KATZ, A.M. (1990) Cardiomyopathy of overload. A major determinant of prognosis in congestive heart. *New England Journal of Medicine*, **332**, 100-110.

KAWAI, M. (1979) Effect of MgATP on cross-bridge kinetics in chemically-skinned rabbit psoas fibers as measured by sinusoidal analysis technique. In Cross-bridge Mechanism in Muscle Contraction, edited by Sugi, H. and Pollack,G.H. 149-169.

KAWAI, M & BRANDT, P W (1980) Sinusoidal analysis: a high resolution method for correlating biochemical reactions with physiological processes in activated skeletal muscles of rabbit, frog and crayfish. *Journal of Muscle Research & Cell Motility*, **1**, 279-303.

KAWAI, M. & HALVORSON, H.R. (1991) Two step mechanism of phosphate release and the mechanism of force generation in chemically skinned fibres of rabbit psoas muscle *Biophysical Journal*, **59**, 329-342.

KAWAI, M. & ZHAO, Y. (1993) Crossbridge Scheme and Force per Crossbridge State in Skinned Rabbit Psoas Muscle Fibres. *Biophysical Journal*, **65**, 638-651.

KISHINO, A. & YANAGIDA, T. (1988) Force measurements by micromanipulation of a single actin filament by glass needles. *Nature*, **334**, 74-76.

KOPP, S. & BARANY, M. (1979) Phosphorylation of the 19 000 dalton light chain of myosin in perfused rat heart under the influence of negative and positive inotropic agents. *Journal of Biological Chemistry*, **254**, 12007-12012.

KOVANEN, V., SUOMINEN, H. & HEIKKINEN, E. (1984) Mechanical properties of fast and slow skeletal muscles with special reference to collagen and endurance training. *Journal of Biomechanics*, **17**, 725-735.

KRON, S.J. & SPUDICH, J.A. (1986) Fluorescent actin filaments move on myosin fixed to a glass surface. *Proceedings of the National Academy of Sciences USA*, **83**, 6272-6276.

KRUDY, G., KLEERKOPER, Q., GUO, X., HOWARTH, J.W., SOLARO, R.J. & ROSEVEAR, P.R. (1994) NMR studies delineating spatial relationships within the cardiac troponin I-troponin C complex. *Journal of Biological Chemistry*, **269**, 23731-23735.

KUSHMERICK, M.J. & PODOLSKY, R.J. (1979) Ionic mobility in muscle cells. *Science*, **166**, 1297-1298.

LABEIT, S. & KOLMERER, B. (1995) Titins: giant proteins in charge of muscle ultrastructure and elasticity. *Science*, **270**, 293-296.

LABEIT, S., KOLMERER, B. & LINKE, W.A. (1997) The Giant Protein Titin: Emerging Roles in Physiology and Pathophysiology. *Circulation Research*, **80**, 290-294.

LANDESBERG, A., MARKHASIN, V.S., BEYAR, R. & SIDEMAN, S. (1996) Effect of cellular inhomogeneity on cardiac tissue mechanics based on intracellular control mechanisms. *American Journal of Physiology*, **270**, H1101-H1114.

LAYLAND, J., YOUNG, I.S. & ALTRINGHAM, J.D. (1995a) The length dependence of work production in rat papillary muscle in vitro. *Journal of Experimental Biology*, **198**, 2491-2499.

LAYLAND, J., YOUNG, I.S. & ALTRINGHAM, J.D. (1995b) The effect of cycle frequency on the power output of rat papillary muscles in vitro. *Journal of Experimental Biology*, **198**, 1035-1043.

LEHRER, S.S. & MORRIS, E.P. (1982) Dual effects of tropomyosin and troponin-tropomyosin on actomyosin subfragment-1 ATPase. *Journal of Biological Chemistry*, **257**, 8073-8080.

LEIBLER, S. & HUSE, D. (1993) Porters versus rowers: a unified stochastic model of motor proteins. *Journal of Cellular Biology*, **121**, 1357-1368.

LI, Z.H., BING, O.H.L., LONG, X.L., ROBINSON, K.G. & LAKATTA, E.G. (1997) Increased cardiomyocyte apoptosis during the transition to heart failure in the spontaneously hypertensive rat. *American Journal of Physiology*, **272**, H2313-H2319.

LINDPAINTNER, K. & GANTEN, D. (1991) The cardiac renin-angiotensin system- a synopsis of current experimental and clinical data. *News in Physiological Sciences*, **6**, 227-232.

LINKE, W.A., POPOV, V.I. & POLLACK, G.H. (1994) Passive and active tension in single cardiac myofibrils. *Biophysical Journal*, **67**, 782-792.

LITTEN, R.Z., MARTIN, B.J., BUCHTHAL, R.H., NAGAI, R., LOW, R.B. & ALPERT, N.R. (1985) Heterogeneity of myosin isozyme content of rabbit heart. *Circulation Research*, **57**, 406-414.

LIU, Y., SHAO, Q. & DHALLA, N.S. (1995) Myosin Light Chain Phosphorylation in Cardiac Hypertrophy and Failure due to Myocardial Infarction. *Journal of Molecular and Cellular Cardiology*, **27**, 2613-2621.

LOMPRE, A.M., NADL-GINARD, B. & MAHDAVI, V. (1984) Expression of the cardiac ventricular alpha- and beta-myosin heavy chain is developmentally and hormonally regulated. *Journal of Biological Chemistry*, **259**, 6437-6446.

LOMPRE, A., SCHWARTZ, K., d'ALBIS, A., LACOMBE, G., VANTHIEM, N. & SWYNGHEDAUW, B. (1979) Myosin isoenzyme redistribution in chronic heart overload. *Nature*, **282**, 105-107.

LORELL, B.H. (1991) Significance of diastolic dysfunction of the heart. *Annual Reviews in Medicine*, **42**, 411-436.

LUTZ, J.E. (1988) An XII century description of congestive heart failure. *American Journal of Cardiology*, **61**, 494-495.

MacFARLANE, N.G. & MILLER, D.J. (1994) Effects of reactive oxygen species hypochlorous acid and hydrogen peroxide on force production and calcium sensitivity of rat cardiac myofilaments. *Pflügers Archives*, **428**, 561-568.

MacFARLANE, N.G., MILLER, D.J., SMITH, G.L. & STEELE, D.S. (1994) Effects of oxygen-derived free radicals and reactive oxygen species in cardiac myofibrils. *Cardiovascular Research*, **28**, 1647-1652.

MACHIN, K.E. & PRINGLE, J.W.S. (1959) The Physiology of insect flight muscle. II. The mechanical properties of a beetle flight muscle. *Proceedings of the Royal Society*, series B, **151**, 204-225.

MARGOSSIAN, S.S., WHITE, H.D., CAULFIELD, J.B., NORTON, P., TAYLOR, S. & SLAYTOR, H.S. (1992) Light chain 2 profile and activity of human ventricular myosin during dilated cardiomyopathy: Identification of a causal agent for impaired myocardial function. *Circulation*, **85**, 1720-1733.

MARON, B.J. (1988) Right ventricular cardiomyopathy - another cause of sudden-death in the young. *New England Journal of Medicine*, **318**, 178-180.

MARUYAMA, K. (1994) Connectin, an elastic protein of striated muscle. *Biophysical Chemistry*, **50**, 73-85.

MAXWELL, M.P., HEARSE, D.J. & YELLON, D.M. (1987) Species variation in the coronary collateral circulation during regional myocardial ischaemia: a critical determinant of the rate of evolution and extent of myocardial infarction. *Cardiovascular Research*, **21**, 737-746.

MAYOUX, E., COUTRY, N., LECHENE, P., MAROTTE, F., HOFFMANN, C. VENTURA-CLAPIER, R. (1994) Effects of acidosis and alkalosis on mechanical properties of hypertrophied rat heart fiber bundles. *American Jornal of Physiology*, **266**, H2051-H2060.

McMURRAY, J., McLAY, J., CHOPRA, M., BRIDGES, A. & BELCH, J.J.F. (1990) Evidence for enhanced free radical activity in chronic congestive heart failure secondary to coronary artery disease. *American Journal of Cardiology*, **65**, 1261-1262.

McMURRAY, J., HART, W. & RHODES, G. (1993) An evaluation of the cost of heart failure to the National Health Service in the United Kingdom. *British Journal of Medical Economics*, **6**, 99-110.

McMURRAY, J., McDONAGH, T., MORRISON, C.E. & DARGIE, H.J. (1993) Trends in hospitalisation for heart failure in Scotland. *European Heart Journal*, **14**, 1158-1162.

McMURRAY, J., McLAY, J., CHOPRA, M., BRIDGES, A. & BELCH, J.J.F. (1990) Evidence for enhanced free radical activity in chronic congestive heart failure secondary to coronary artery disease. *American Journal of Cardiology*, **65**, 1261-1262.

MEHTA, A.D., FIBER, J.T. & SPUDICH, J.A. (1997) Detection of single molecule interactions using correlated thermal diffusion. *Proceedings of the National Academy of Sciences USA*, **94**, 7927-7931.

MEKHFI, H., VEKSLER, V., MATEO, P., MAUPOIL, V., ROCHETTE, L. & VENTURA-CLAPIER, R. (1996) Creatine Kinase is the Main Target of Reactive Oxygen Species in Cardiac Myofibrils. *Circulation Research*, **78**, 1016-1027.

MERCADIER, J.J., LOMPRE, A.M., WISNEWSKI, C., SAMUEL, J.L., BERCOVICI, J., SWYNGHEDAUW, B. & SCHWARTZ, K. (1981) Myosin isoenzyme changes in several models of rat cardiac hypertrophy. *Circulation Research*, **49**, 525-532.

MERCADIER, J.J., BOUVERET, P., GORZA, L., SCHIAFFINO, S., CLARK, W.A., ZAK, R., SWYNGHEDAUW, B. & SCHWARTZ, K. (1983) Myosin Isoenzymes in Normal and Hypertrophied Human Ventricular Myocardium. *Circulation Research*, **53**, 52-62.

METTLER, F.P., YOUNG, D.M. & WARD, J.M. (1977) Adriamycin-induced cardiotoxicity (cardiomyopathy and congestive heart failure) in rats. *Cancer Research*, **37**, 2705-2713.

METZGER, J.M., GREASER, M.L. & MOSS, R.L. (1989) Variations in cross-bridge attachment rate and tension with phosphorylation of myosin in mammalian skinned skeletal muscle fibers. *Journal of General Physiology*, **93**, 855-883.

MILLER, C.J., CHEUNG, P., WHITE, P. & REISLER, E. (1995) Actins view of actomyosin interface. *Biophysical Journal*, **68**, Suppl. S50-S54.

MILLER, D. J. (1975) Diffusion delays and the rate of contracture development in frog heart muscle. *Pflügers Archives*, **359**, R23

MILLER, D. J., ELDER, H. Y. & SMITH, G. L. (1985) Ultrastructural and X-ray microprobe analysis of EGTA- and detergent treated heart muscle. *Journal of Muscle Research & Cell Motility*, **6**, 525-540.

MILLER, D. J. & SMITH, G. L. (1984) EGTA purity and the buffering of calcium ions in physiological solutions. *American Journal of Physiology* , **246**, C160-166.

MOISESCU, D. G. (1976) Kinetics of reaction in calcium activated skinned muscle fibres. *Nature*, **262**, 610-613

MOLLOY, J.E., BURNS, J.E., KENDRICK-JONES, J., TREAGER, R.T. & WHITE, D.C.S. (1995) Force and movement produced by a single myosin head. *Nature*, **378**, 209-212.

MORANO, I., RITTER, O., BONZ, A., TIMER, T., VAHL, C.F. & MICHEL, G. (1995) Myosin Light Chain-Actin Interaction Regulates Cardiac Contractility. *Circulation Research*, **76**, 720-725.

MORANO, I. & RÜEGG, J.C. (1986) Calcium sensitivity of myofilaments in cardiac muscle - effect of myosin phosphorylation. *Basic Research in Cardiology*, **81**, 17-23.

MORANO, I., LENGSFELD, M., GANTEN, U., GANTEN, D. & RUEGG, J.C. (1988) Chronic hypertension changes myosin isoenzyme pattern and decreases myosin phosphorylation in the rat heart. *Journal of Molecular and Cellular Cardiology*, **20**, 875-886.

MORGAN, H., GORDON, E., KITA, Y., CHUA, B., RUSSO, L., PETERSON, C., McDERMOTT, P. & WATSON, P. (1987) Biochemical mechanisms of cardiac hypertrophy. *Annual Reviews in Physiology*, **49**, 533-543.

MOSS, R.L., LAUER, M.R., GIULIAN, G.G. & GREASER, M.L. (1986) Altered Ca^{2+}-dependence of tension development in skinned skeletal muscle fibers following modification of troponin by partial substitution with cardiac TnC. *Journal of Biological Chemistry*, **261**, 6096-6099.

NAKAO, K., YASUE, H., FUJIMOTO, K., JOUGASAKI, M., YAMAMOTO, H., HITOSHI, Y., TAKATSU, K. & MIYAMOTO, E. (1992) Increased expression and regional differences of atrial myosin light chain-1 in human ventricles with old myocardial infarction. *Circulation*, **86**, 1727-1737.

NG, G.A., COBBE, S.M. & SMITH, G.L. (1998) Non-uniform prolongation of intracellular Ca^{2+} transients recorded from the epicardial surface of isolated hearts from rabbits with heart failure. *Cardiovascular Research*, **37**, 489-502.

NWASOKWA, O.N. (1993) A model of the time course of myocardial dynamics: use in characterisation of relaxation and evaluation of its indices. *Cardiovascular Research*, **27**, 1510-1521.

OPIE, L.H. (1995) Regulation of Myocardial Contractility. *Journal of Cardiovascular Pharmacology*, **26**, S1-S9.

PALMER, S. & KENTISH, J.C. (1994) The role of troponin C in modulating the Ca^{2+} sensitivity of mammalian skinned cardiac and skeletal muscle fibres. *Journal of Physiology*, **491**, 162P.

PALMER, S. & KENTISH, J.C. (1997) Differential Effects of the Ca2+ Sensitisers Caffeine and CGP 48506 on the Relaxation Rate of Rat Skinned Cardiac Trabeculae. *Circulation Research*, **80**, 682-687.

PARMACEK, M.S. & LEIDEN, J.M. (1991) Structure, function and regulation of troponin-C. *Circulation*, **84**, 991-1003.

PARMLEY, W.W. & SONNENBLICK, E.H. (1969) Relation between mechanics of contraction and relaxation in mammalian cardiac muscle. *American Journal of Physiology*, **216**, 1084-1091.

PARRY, D.A.D. & SQUIRE, J.M. (1973) Structural role of tropomyosin in muscle regulation: analysis of the X-ray diffraction patterns from relaxed and contracting muscles. *Journal of Molecular Biology*, **75**, 33-55.

PATEL, J.R., DIFFEE, G.M., HUANG, X.O. & MOSS, R.L. (1998) Phosphorylation of Myosin Regulatory Light Chain Eliminates Force-dependent Changes in Relaxation Rates in Skeletal Muscle. *Biophysical Journal*, **74**, 360-368.

PERRY, S.V., COLE, H.A., HEAD, J.F. & WILSON, F.J. (1972) Localisation and mode of action of the inhibitory protein component of the troponin complex. *Cold Spring Harbour Symposia of Quantitative Biology*, **37**, 251-262.

PFEFFER, M.A. & BRAUNWALD, E. (**1991**) Ventricular remodelling after myocardial infarction- experimental observations and clinical implications. *Circulation*, **81**, 1161-1172.

POETTER, K., JIANG, H., HASSANZADEH, S., MASTER, S.R., CHANG, A., DALAKIS, M.C., RAYMENT, I., SELLERS, J.R., FANAPAZIR, L. & EPSTEIN, N.D. (1996) Mutations in either the essential or regulatory light chains of myosin are associated with a rare myopathy in human heart and skeletal muscle. *Nature Genetics*, **13**, 63-69.

POOLE-WILSON, P.A. (1985) Heart Failure. *Medicine International*, **2**, 866-871.

POTTER, J.D. & GERGELY, J. (1974) Troponin, tropomyosin, and actin interactions in the Ca^{2+}-regulation of muscle contraction. *Biochemistry*, **13**, 2697-2703.

POWERS, F.M. & SOLARO, R.J. (1995) Caffeine alters cardiac myofilament activity and regulation independently of Ca^{2+} binding to troponin-C. *American Journal of Physiology*, **268**, C1348-C1353.

POULEUR, H., ROUSSEAU, M.F., VAN EYLL, C., MELIN, J., YOUNGBLOOD, M. & YUSUF, S. (1993) Cardiac Mechanics During Development of Heart Failure. *Circulation*, **87**, IV14 - IV 20.

PYE, M.P., BLACK, M. & COBBE, S.M. (1996) Comparison of *in vivo* and *in vitro* Haemodynamic Function in Experimental Heart Failure: Use of echocardiography. *Cardiovascular Research*, **31**, 873-881.

RACK, P.M.H. (1966) The behaviour of a mammalian muscle during sinusoidal stretching. *Journal of Physiology*, **183**, 1-14.

RAYMENT, I., HOLDEN, H.M., WHITTAKER, M., YOHN, C.B., LORENZ, M., HOLMES, K.C. & MILLIGAN, R.A. (1993) Structure of the actin-myosin complex and its implications for muscle-contraction. *Science*, **261**, 58-65.

REEDY, M.C., HOLMES, K.C. & TREGEAR, R.T. (1965) Induced changes in orientation of the cross-bridges of glycerinated insect flight muscle. *Journal of Molecular Biology*, **204**, 1276-1280.

REIMER, K.A., LOWE, J.E., RASMUSSEN, M.M. & JENNINGS, R.B. (1977) The wave front phenomenon of ischaemic cell death. I. Myocardial infarct size versus duration of coronary occlusion in dog. *Circulation*, **56**, 786-794.

ROBERTSON, S.P., JOHNSON, J.D., HOLROYDE, M.J., KRANIAS, E.G., POTTER, J.D. & SOLARO, R. (1982) The effect of troponin-I phosphorylation on the calcium binding properties of the Ca-regulatory site of bovine cardiac troponin. *Journal of Biological Chemistry*, **257**, 260-263.

ROSSMANITH, G.H. (1986) Tension responses of muscle to n-step pseudo-random length reversals: a frequency domain representation. *Journal of Muscle Research and Cell Motility*, **7**, 299-306.

ROSSMANITH, G.H., HAMILTON, A.M. & HOH, J.F.Y. (1995) Influence of Myosin Isoforms on Tension Cost and Crossbridge Kinetics in Skinned Rat Cardiac Muscle. *Clinical and Experimental Pharmacology and Physiology*, **22**, 423-429.

ROSSMANITH, G.H., HOH, J.F.Y., KIRMAN, A. & KWAN, L.J. (1986) Influence of V1 and V3 isomyosins on the mechanical behaviour of rat papillary muscle as studied by pseudo-random binary noise modulated length perturbations. *Journal of Muscle research & Cell Motility*, **7**, 307-319.

SAEKI, Y., KATO, C., TOTSUKA, T. & YANAGISAWA, K. (1987) Mechanical properties and ATPase activity in glycerinated cardiac muscle of hyperthyroid rabbit. *Pflugers Archives*, **408**, 578-583.

SAEKI, Y, KAWAI, M, ZHAO, Y. (1991) Comparison of crossbridge dynamics between intact and skinned ferret right ventricles. *Circulation Research*, **68**, 772-781.

SAMUELS, J., RAPPAPORT, L., MERCADIER, J., LOMPRE, A.M., SARTORE, S., TRIBAN, C., SCHIAFFINO, S. & SCHWARTZ, K. (1983) Distribution of myosin isozymes within single cardiac cells. *Circulation Research*, **52**, 200-209.

SAVAGE, R.M., WAGNER, G.S., IDEKER, R.E., PODOLSKY, S.A. & HACKEL, D.B. (1977) Correlation of post mortem anatomic findings with electrocardiographic changes in patients with myocardial infarction: retrospective study of patients with typical anterior and posterior infarcts. *Circulation*, **55**, 279-285.

SAVAGE, M.P., KROLEWSKI, A.S., KENIAN, G.G., LEBEIS, M.P., CHRISTLIEB, A.R. & LEWIS, S.M. (1988) Acute myocardial infarction in diabetes mellitus and significance of congestive heart failure as a prognostic factor. *American Journal of Cardiology*, **62**, 665-669.

SCHAPER, J. & SCHAPER, W. (1983) Ultrastructural correlates of reduced cardiac-function in human-heart disease. *European Heart Journal*, **4**, 35-42.

SHEETZ, M.P. & SPUDICH, J.A. (1983) Movement of myosin-coated fluorescent beads on actin cables in vitro. *Nature*, **303**, 31-35.

SHEETZ, M.P., CHASAN, R. & SPUDICH, J.A. (1984) ATP-dependent movement of myosin *in vitro* - characterization of a quantitative assay. *Journal of Cell Biology*, **99**, 1867-1871.

SCHIER, J.J. & ADELSTEIN, R.S. (1982) Structural and enzymatic comparison of human cardiac muscle myosin isolated from infants, adults, and patients with hypertrophic cardiomyopathy. *Journal of Clinical Investigations*, **69**, 816-825.

SCHOLZ, D., DIENER, W. & SCHAPER, J. (1994) Altered nucleus/cytoplasm relationship and degenerative structural changes in human dilated cardiomyopathy. *Cardioscience*, **5**, 127-138.

SCHUTT, C.E., MYSLIK, J.C., ROZYCKI, M.D., GOOSNESEKERE, N.C. & LINDBERG, U. (1993) The structure of crystalline profilin-β-actin. *Nature*, **365**, 810-816.

SCHWARTZ, K., de la BASTIE, D., BOUVERET, P., OLIVIERO, P., ALONSO, S & BUCKINGHAM, M. (1986) α-Skeletal muscle actin mRNAs accumulate in hypertrophied adult rat hearts. *Circulation Research*, **59**, 551-555.

SCHWARTZ, K., CARRIER, L., GUICHENEY, P. & KOMAJDA, M. (1995) Molecular basis of familial cardiomyopathies. *Circulation*, **91**, 532-540.

SCHWINGER, R.H.G., BOHM, M., KOCH, A., SCHMIDT, U., MORANO, I., EISSNER, H-J., UBERFUHR, P., REICHART, B. & ERDMANN, E. (1994) The Failing Human Heart is Unable to use the Frank-Starling Mechanism. *Circulation Research*, **74**, 959-969.

SELLERS, J.R. & GOODSON, H.V. (1995) Motor Proteins 2. Myosin. *Protein Profile*, **2**, 1323-1423.

SHIBATA, T., HUNTER, W.C. & SAGAWA, K. (1987b) Dynamic stiffness of barium-contractured cardiac muscles with different speeds of contraction. *Circulation Research*, **60**, 770-779.

SHIBATA, T., HUNTER, W.C., YANG, A. & SAGAWA, K. (1987a) Dynamic stiffness measured in central segment of excised rabbit papillary muscles during barium contraction. *Circulation Research*, **60**, 756-769.

SIMNETT, S.J., LIPSCOMB, S., ASHLEY, C.C. & MULLIGAN, I.P. (1993) The effect of EMD 57033, a novel cardiotonic agent, on the relaxation of skinned cardiac and skeletal muscle produced by photolysis of diazo-2, a caged calcium chelator. *Pflugers Archives*, **425**, 175-177.

SMITH, F. H. (1969) Double refracting interference microscope.

SMITH, G.L. & MILLER, D.J. (1985). Potentiometric measurements of stoichiometric and apparent affinity constants of EGTA for protons and divalent ions including calcium. *Biochimica et Biophysica Acta*, **839**, 287-299.

SMITH, H.J. & NUTTAL, A. (1985) Experimental models of heart failure. *Cardiovascular Research*, **19**, 181-186.

SMITH, G.L. & MILLER, D.J. (1994). EGTA purity and the buffering of calcium-ions in physiological solutions. *American Journal of Physiology*, **246**, C160-C166.

SOLARO, R.J. (1993) Modulation of activation of cardiac filaments. In: Allen D. A. G, Lee J. A., eds. Modulation of Cardiac Calcium Sensitivity. Oxford, Oxford University Press. 160-177.

SOLARO, R.J., MOIR, A.G.J. & PERRY, S.V. (1976) Phosphorylation of troponin-I and the inotropic effect of adrenaline in the perfused rabbit heart. *Nature*, **262**, 615-616.

SOLARO, R.J., POWERS, F.M., GAO, L. & GWATHMEY, J.K. (1993) Control of Myofilament Activation in Heart Failure. *Circulation*, **87**, [suppl. VII], VII38-VII43.

SONNENBLICK, E.H. (1962) Force-velocity relations in mammalian heart muscle. *American Journal of Physiology*, **202**, 931-939.

SORDAHL. L.A., WOOD, W.G. & SCHWARTZ, A. (1970) Production of cardiac hypertrophy and failure in rabbits with Ameroid clips. *Journal of Molecular and Cellular Cardiology*, **1**, 341-344.

SOUFER, R., WOHLGELERNTER, D., VITA, N.A., AMUCHESTEGUI, M., SOSTMAN, H.D., BERGER, H.J. & ZARET, B.L. (1985) Intact systolic left ventricular function in clinical congestive heart failure. *American Journal of Cardiology*, 55, 1032-1036.

SPANN, J.F., BUCCINO, R.A. & SONNENBLICK, E.H. (1967) Production of right ventricular hypertrophy with and with out congestive heart failure in the cat. *Proceedings of the Society for Experimental and Biological Medicine*, **125**, 522-524.

SPUDICH, J.A. (1994) How molecular motors work. *Nature*, **372**, 515-518.

STEIGER, G.J. (1971) Stretch activation and myogenic oscillation of isolated contractile structures of heart muscle. *Pflugers Archives*, **330**, 347-361.

STEIGER, G.J. & RÜEGG, J.C. (1969) Energetics and 'efficiency' in the isolated contractile machinery of insect fibrillar muscle at various frequencies of oscillation. *Pflügers Archives*, **307**, 1-21.

STEIN, L.A., SCHWARTZ. Jr., R.P., CHOCK, P.B. & EISENBERG, E. (1979) Mechanism of actomyosin adenosine triphosphatase. Evidence that adenosine 5'-triphosphate hydrolysis can occur without dissociation of the actomyosin complex. *Biochemistry*, **18**, 3895-3909.

SVOBODA, K., SCHMIDT, C.F., SCHNAPP, B.J. & BLOCK, S.M. (1993) Direct observation of kinesin stepping by optical trapping interferometry. *Nature*, **365**, 721-727.

SWEENEY, H.L. & STULL, J.T. (1990) Alteration of Crossbridge Kinetics by Myosin Light Chain Phosphorylation in Rabbit Skeletal Muscle: implications for Regulation of Actin-myosin Interaction. *Proceedings of the National Academy of Science USA*, **87**, 414-418.

SWYNGHEDAUW, B. (1986) Developmental and Functional Adaptation of Contractile Proteins in Cardiac and Skeletal Muscles. *Physiological Reviews*, **66**, 710-771.

SYME, D.A. (1993) Influence of extent of muscle shortening and heart rate on work from frog heart trabeculae. *American Journal of Physiology*, **265**, R310-R319.

SZENT-GYORGYI, A.G. (1953) Meromyosins, the subunits of myosin. *Archives of Biochemistry and Biophysics*, **42**, 305-320.

TAMIYA, K., BEPPU, T. & ISHIHARA, K. (1995) Double-exponential curve fitting of isometric relaxation: a new measure for myocardial lusitropism. *American Journal of Physiology*, **269**, H393-H406.

TANIGAWA, G., JARCHO, J.A., KASS, S.D., SOLOMON, H-P & SEIDMAN, J.G. (1990) A molecular basis for familial hypertrophic cardiomyopathy: An α/β cardiac myosin heavy chain hybrid gene. *Cell*, **62**, 91-98.

TANOKURA, M., TAWADA, Y., ONO, A. & OHTSUKI, I. (1983) Chymotryptic subfragments of troponin T from rabbit skeleton muscle. Interaction with tropomyosin, troponin I and troponin C. *Journal of Biochemistry*, **93**, 331-337.

TAYLOR, E.W. (1979) Mechanism of actomyosin ATPase and the problem of muscular contraction. *Critical Reviews in Biochemistry*, **6**, 103-164.

THORSON, J. & WHITE, D.C. (1969) Distributed representations for actin-myosin interaction in the oscillatory contraction of muscle. *Biophysical Journal*, **9**, 360-390.

TOBACMAN, L.S. & LEE, R. (1987) Isolation and functional comparison of bovine cardiac troponin T isoforms. *Journal of Biological Chemistry*, **262**, 4059-4064.

TOYOSHIMA, Y.Y., KRON, S.J., McNALLY, E.M., NIEBLING, K.R., TOYOSHIMA, C. & SPUDICH, J.A. (1987) Myosin subfragment-1 is sufficient to move actin filamnets *in vitro*. *Nature*, **328**, 536-539.

TRINICK, J. (1996) Cytoskeleton: titin as a scaffold and spring. *Current Biology*, **6**, 258-260.

TROMBITAS, K., GREASER, M.L. & POLLACK, G.H. (1997) Interaction between titin and thin filaments in intact cardiac muscle. *Journal of Muscle Research and Cell Motility*, **18**, 345-351.

TSEIN, R.W. (1973) Cyclic AMP and contractile activity in the heart. *Advances in Cyclic Nucleotide Research*, **8**, 363-420.

UYEDA, T.Q.P., ABRAMSON, P.D. & SPUDICH, J.A. (1996) The neck region of the myosin motor domain acts as a lever arm to generate movement. *Proceedings of the National Academy of Sciences USA*, **93**, 4459-4464.

UYEDA, T.Q.P., KRON, S.J. & SPUDICH, J.A. (1990) Myosin step size: estimation from slow sliding movement of actin over low densities of heavy meromyosin. *Journal of Molecular Biology*, **214**, 699-710.

van EERD, J-P. & TAKAHASHI, K. (1975) The biological importance of each amino acid sequence of bovine cardiac troponin C. Comparison with rabbit skeletal troponin C. *Biochemical and Biophysical Research Communications*, **64**, 122-127.

Van BUREN, P., HARRIS, D.E., ALPERT, N.R. & WARSHAW, D.M. (1995) Cardiac V1 and V3 myosins differ in their hydrolytic and mechanical activities *in vitro*. *Circulation Research*, **77**, 439-444.

VASSEN, R.S., BENJAMIN, E.J. & LEVY, D. (1996) Congestive heart failure with normal left ventricular systolic function. *Archives of International Medicine*, **156**, 146-157.

VELAZ, L., HEMRIC, M.E., BENSON, C.E. & CHALOVICH, J.M. (1989) The binding of caldesmon to actin and its effect on the ATPase activity of soluble myosin subfragments in the presence and absence of tropomyosin. *Journal of Biological Chemistry*, **264**, 9602-9610.

WARSHAW, D. & TRYBUS, K. (1990) Smooth-muscle myosin crossbridge interactions modulate actin filament sliding velocity *in vitro*. *Journal of Muscle Research and Cell Motility*, **11**, 431.

WATTANAPERMPOOL, J., GUO, X. & SOLARO, R.J. (1995) The unique amino-terminal peptide of cardiac troponin I regulates myofibrillar activity only when it is phosphorylated. *Journal of Cellular Cardiology*, **27**, 1383-1391.

WEBER, K.T. & BRILLA, C.G. (1991) Pathological hypertrophy and cardiac interstitium: fibrosis and renin-angiotensin-aldosterone system. *Circulation*, **83**, 1849-1865.

WESTERBLAD, H. & ALLEN, D.G. (1994) Relaxation, [Ca2+](i) and [Mg2+](i) during prolonged tetanic stimulation of intact, single fibers from mouse skeletal-muscle. *Journal of Physiology*, **480**, 31-43.

WHITE, D.C.S., & THORSON, J. (1973) The kinetics of muscle contraction. *Progress in Biophysics and Molecular Biology*, **27**, 173-255.

WHITE, D.C.S. & THORSON, J. (1973) The kinetics of muscle contraction. *Progress in Biophysics and Molecular Biology*, **27**, 173-225.

WHITTAKER, M., WILSON-KUBALEK, E.M., SMITH, J.E., FAUST, L., MILLIGAN, R.A. & SWEENEY, H.L. (1995) Smooth muscle myosin moves 35 Å upon ADP release. *Nature*, **378**, 748-751.

WOLFF, M.R., McDONALD, K.S. & MOSS, R.L. (1995) Rate of Tension Development in Cardiac Muscle Varies with Level of Activator Ca^{2+}. *Circulation Research*, **76**, 154-160.

WOLFF, M.R., WHITESELL, L.F. & MOSS, R.L. (**1995**) Ca^{2+} Sensitivity of Isometric Tension is Increased in Canine Experimental Heart Failure. *Circulation Research*, **76**, 781-789.

WOMBLE, J.R., HADDOX, M.K. & RUSSELL, D.H. (1979) Epinephrine elevation in plasma parallels canine cardiac hypertrophy. *Life Sciences*, **19**, 1951-1957.

WYSE, R.K., WELHAM, K.C., JONES, M., SILOVE, E.D. & de LEVAL, M.R. (1983) Hemodynamics, regional myocardial bloodflow, and sarcoplasmic reticulum calcium uptake in right ventricular hypertrophy and failure. *Advances in Myocardiology*, **4**, 97-105.

YANAGIDA, T., ARATA, T. & OOSAWA, F. (1985) Sliding distance of actin filament induced by a myosin crossbridge during one ATP hydrolysis cycle *Nature*, **316**, 366-369.

YANO, M., YAMAMOTO, Y. & SHIMIZU, H. (1982) An actomyosin motor. *Nature*, **299**, 557-559.

ZHANG, R., ZHAO, J., MANDVENO, A. & POTTER, J.D. (1995) Cardiac Troponin I Phosphorylation Increases the Rate of cardiac Muscle Relaxation. *Circulation Research*, **76**, 1028-1035.

ZHAO, Y. & KAWAI, M. (1993) The Effect of Lattice Spacing Change on Crossbridge kinetics in Chemically-Skinned Rabbit Psoas Muscle fibres. *Biophysical Journal*, **64**, 197-210.

ZOT, H.G. & POTTER, J.D. (1982) A structural role for the Ca^{2+}-Mg^{2+} sites on troponin C in the regulation of muscle contraction: preparation and properties of troponin C depleted myofibrils. *Journal of Biological Chemistry*, **257**, 7678-7683.